

Sulfonium Salts for the Synthesis of PET Tracers

A dissertation presented by
Klaudia Aleksandra Cybulska

In partial fulfilment of the requirements for the award of the degree of

DOCTOR OF PHILOSOPHY
at
UNIVERSITY COLLEGE LONDON

Declaration

I, Klaudia Aleksandra Cybulska, confirm that the work presented in this thesis is my own. Where information has been derived from other sources, I confirm that this has been indicated in the thesis.

.....

Abstract

Positron Emission Tomography (PET) is a non-invasive medical imaging technique, which allows for quantification of biochemical processes *in vivo* by employing positron-emitting radiopharmaceuticals. Fluorine-18 is the most widely used radionuclide due to its favourable physical properties. Despite impressive technological advancements and large investments in PET instrumentation, its full medical potential has not been realised. The lack of broadly applicable, versatile and robust ^{18}F -labelling strategies hampers development of PET tracers.

This work describes development and optimisation of dibenzothiophene sulfonium salts as leaving groups for efficient [^{18}F]fluorination of aromatic molecules. A novel ring-closing reaction for sulfonium salt formation is described, which allows access to structurally diverse *N*-heterocyclic scaffolds, such as indoles, imidazoles and pyridines. Insights into the cyclisation mechanism and factors which orchestrate reactivity of the system are provided. A scope of common pharmacological motifs was selected to demonstrate the potential of dibenzothiophene sulfonium salts for accessing drug-like molecules.

The presented strategy was exploited to simplify and enhance radiosynthesis of a tracer for the imaging for the mGluR5 receptor, [^{18}F]FPEB. A concise and practical approach is presented, which afforded the radiolabelled product in a high radiochemical yield, offering evident advantages over existing strategies. Synthesis of a sulfonium salt precursor to a novel tracer for the imaging of aldosterone-producing adenomas is described. Radiolabelling proceeded in an excellent RCY, allowing biological evaluation *in vivo*.

The results of this work constitute a major advancement in the field of PET chemistry,

rendering dibenzothiophene sulfonium salt as one of the most attractive strategies for ^{18}F -labelling in the multitude of novel approaches. The research has the potential to provide tools for early preclinical imaging and ultimately, might lead to development of new tracers for improving patient care.

Acknowledgements

I would like to dedicate this thesis to my parents. I would like to thank them for making it possible for me to pursue higher education in a foreign country and in a foreign language. Thank you for all the support you have given me throughout these long 8 years. I would like to thank my boyfriend Nitin, for being there for me and putting up with my moods towards the end of writing this thesis. To my laboratory partner in crime, Yi - thanks for endless conversations and shenanigans and just for being there when I needed support. I would like to thank Vincent, one of the most talented chemists I have met, for letting me use his tapless chromatography column, teaching me how not to co-elute and for being awesome. A big thank you to Dr Abil Aliev for his help with NMR - the NMR department at UCL is truly fantastic. Within the Årstad group, a big thank you to Thibault, who is an amazing chemist and whose advice and help were always priceless. I am sorry if I pestered you too much! I would also like to thank Kerstin, who supervised me in my first year, for teaching me radiochemistry. Finally, I would like to thank Prof Erik Årstad, my supervisor, for his guidance, advice, patience and incredible wisdom.

Contents

Declaration	1
Abstract	2
Acknowledgements	4
Abbreviations	9
1 Radiolabelling with Fluorine-18 for Positron Emission Tomography	13
1.1 Introduction to Positron Emission Tomography	13
1.1.1 Principles of PET	13
1.1.2 Radiolabelling with ^{18}F	15
1.1.3 Nomenclature for Radiochemistry	18
1.1.4 ^{18}F -Radiochemistry: Analytical Techniques	19
2 Strategies for ^{18}F-Labelling	24
2.1 ^{18}F -Labelling of Aliphatic Molecules	24
2.2 ^{18}F -Labelling of Aryls: Traditional Approach	25
2.2.1 Electrophilic Aromatic Substitution	26
2.2.2 Nucleophilic Aromatic Substitution	27
2.2.3 Indirect Labelling via Prosthetic Groups	30
2.3 ^{18}F -Labelling of Aryls: Recent Advances	30
2.3.1 Metal-Free ^{18}F -Chemistry	31
2.3.2 Metal-Mediated ^{18}F -Chemistry	41
2.4 Summary Review of ^{18}F -Labelling Strategies for Aryls	47
3 Sulfonium Salts as ^{18}F-Labelling Precursors	51
3.1 Triarylsulfonium Salts	51
3.2 New Generation Dibenzothiophene Sulfonium Salts	53

4	Project Description: Aims and Objectives	57
5	Synthesis of Dibenzothiophene Sulfonium Salt Precursor to [¹⁸F]FPEB: Proof-of-Concept	59
5.1	[¹⁸ F]FPEB: PET Tracer for Imaging of mGluR5 Receptor	59
5.1.1	Synthesis of Sulfonium Salt Precursor to [¹⁸ F]FPEB	63
5.2	Conclusion	69
6	Insights into Mechanism of Sulfonium Salt Formation	71
6.1	Putative Mechanism of Sulfonium Salt Formation	71
6.2	Early Mechanistic Study with NMR Spectroscopy	72
6.2.1	NCS/TfOH System for Cyclisation: Formation of Superelectrophilic Species	73
6.3	Design of Model Compound to Investigate Cyclisation Mechanism . .	76
6.3.1	Expansion of Scope of Cyclisation Reagents: Acids	77
6.3.2	Expansion of Scope of Cyclisation Reagents: Hypochlorites . . .	79
6.3.3	Expansion of Scope of Cyclisation Reagents: Alternative Chlorine Sources	84
6.4	Conclusion	84
7	Expansion of Structural Scope of Sulfonium Salts for ¹⁸F-Labeling	86
7.1	¹⁸ F-AMT: PET Tracer for Imaging Tryptophan Metabolism	86
7.2	Synthesis of Sulfonium Salt with Indole Moiety	93
7.3	Radiotracers with Pyridyl Moiety	95
7.4	Synthesis of Sulfonium Salts with 2-Pyridyl Moiety	100
7.5	Synthesis of Sulfonium Salt with 3-Pyridyl Moiety	103
7.6	Conclusion	110
8	Applications of Dibenzothiophene Sulfonium Salts: PET Tracer 1	114
8.1	Towards Novel Tracer for Imaging of Aldosterone-Producing Adenomas	114
8.1.1	Aldosterone-Producing Adenomas	114
8.1.2	PET Imaging of Aldosterone-Producing Adenomas	116
8.1.3	Synthesis of Imidazole-Based Dibenzothiophene Sulfonium Salt Precursor to Novel PET Tracer Candidate	124

8.2	Conclusion	139
9	Applications of Dibenzothiophene Sulfonium Salts: PET Tracer 2	140
9.1	Synthesis of Dibenzothiophene Sulfonium Salt Based on Aldosterone Synthase Inhibitor	140
9.1.1	Selection of Novel PET Tracer Candidate for Imaging of APAs .	140
9.1.2	Synthesis of 3-Pyridyl-Based Dibenzothiophene Sulfonium Salt Precursor to Novel PET Tracer	142
9.2	Radiolabelling of Novel PET Tracer Candidate	146
9.3	Preliminary Biological Evaluation of Novel PET Tracer Candidate .	147
9.4	Conclusion	148
10	Conclusion	149
11	General Procedures	152
11.1	General Procedures: Synthetic Chemistry	152
11.2	General Procedures: Radiochemistry	153
12	Radiolabelling	154
12.1	Preparation of Tracer 74	154
12.1.1	Calculation of Specific Activity of Tracer 74	156
12.2	Preparation of 3-[¹⁸ F]fluoropyridine	157
12.3	Preparation of Tracer 59	158
13	Characterisation of Synthesised Compounds	160
13.1	Synthetic Route Towards Sulfonium Salt 7 (Chapter 5)	160
13.2	Synthetic Route Towards Sulfonium Salt 14 (Chapter 6)	167
13.3	Synthetic Route Towards Sulfonium Salt 18 (Chapter 6)	171
13.4	Synthetic Route Towards Sulfonium Salt 27 (Chapter 7)	176
13.5	Synthetic Route Towards Sulfonium Salt 32 (Chapter 7)	181
13.6	Synthetic Route Towards Sulfonium Salt 37 (Chapter 7)	183
13.7	Synthetic Route Towards Sulfonium Salt 48 (Chapter 8)	186
13.8	Synthetic Route Towards Sulfonium Salt 53 (Chapter 8)	190
13.9	Synthetic Route Towards Sulfonium Salt 58 (Chapter 8)	194
13.10	Synthetic Route Towards Sulfonium Salt 64 (Chapter 8)	198

13.11 Synthetic Route Towards Sulfonium Salt 83 (Chapter 9)	205
13.12 Compounds 81 , 78 and 80 (Chapter 9)	214
13.13 <i>N</i> -Chlorosulfonamides as Reagents for Cyclisation	217
13.14 Miscellaneous Compounds	220
13.15 Calibration Curve for Sulfonium Salt 7	221

Abbreviations

2D	Two-dimensional
AIBN	Azobisisobutyronitrile
AMT	α -methyl-L-tryptophan
APA	Aldosterone producing adenoma
AVS	Adrenal vein sampling
Bq	Becquerel
CDCl₃	Deuterated chloroform
Ci	Curie
CI	Chemical ionisation
CNS	Central nervous system
CT	Computer Tomography
CYP11B1	11 β -Hydroxylase
CYP11B2	Aldosterone synthase
dba	Dibenzylideneacetone
d.c.	Decay-corrected
DCE	Dichloroethane
DCM	Dichloromethane
dec	Decomposition

DFT	Density functional theory
DIPEA	<i>N,N</i> -Diisopropylethylamine
DMF	Dimethylformamide
DMSO	Dimethyl sulfoxide
DPEphos	Bis[(2-diphenylphosphino)phenyl] ether
E	Electrophile
EI	Electron ionisation
EOS	End of synthesis
equiv.	Equivalent
ESI	Electrospray ionisation
[¹⁸F]FDG	2-[¹⁸ F]Fluoro-2-deoxy-D-glucose
GMP	Good Manufacturing Practice
h	Hours
HATU	1-[Bis(dimethylamino)methylene]-1 <i>H</i> -1,2,3-triazolo[4,5- <i>b</i>]pyridinium 3-oxid hexafluorophosphate
HMDS	Hexamethyldisilazane
HOBt	1-Hydroxybenzotriazole hydrate
HPLC	High performance liquid chromatography
HRMS	High-resolution mass spectrometry
IDO	Indoleamine 2,3-dioxygenase
K₂₂₂	Kryptofix 222
LC-MS	Liquid chromatography mass spectrometry
M	Molarity

mGlu5	Metabotropic glutamate receptor subtype 5
mp	Melting point
MPO	Myeloperoxidase
MRI	Magnetic Resonance Imaging
MTO	Metomidate
N	Normality
NBS	<i>N</i> -Bromosuccinimide
n.d.c.	Non-decay-corrected
NIS	<i>N</i> -Iodosuccinimide
NCS	<i>N</i> -Chlorosuccinimide
NMR	Nuclear magnetic resonance
Nu	Nucleophile
<i>o</i>	<i>Ortho</i>
<i>p</i>	<i>Para</i>
Palau'Chlor[®]	2-Chloro-1,3-bis(methoxycarbonyl)guanidine
<i>p</i>-TSA	<i>Para</i> -toluenesulfonic acid
PE	Petroleum ether
Pd/C	Palladium on carbon
PET	Positron Emission Tomography
PA	Primary hyperaldosteronism
PK	Pharmacokinetics
ppm	Parts per million
Py	Pyridine

RAAS	Renin-angiotensin-aldosterone system
RCC	Radiochemical conversion
RCY	Radiochemical yield
rt	Room temperature
SA	Specific activity
SAR	Structure-activity relationship
S_N2	Nucleophilic substitution
S_NAr	Nucleophilic aromatic substitution
SUV	Standardised uptake value
TBAF	Tetrabutylammonium fluoride
TEAB	Triethylammonium bicarbonate
TEMPO	2,2,6,6-Tetramethylpiperidine 1-oxyl
<i>t</i>	<i>Tert</i>
TCCA	Trichloroisocyanuric acid
TFA	Trifluoroacetic acid
TfOH	Triflic acid
TLC	Thin layer chromatography
TMS	Trimethylsilyl
Trp	Tryptophan
Ts	Tosyl
Xantphos	4,5-Bis(diphenylphosphino)-9,9-dimethylxanthene

1 | Radiolabelling with Fluorine-18 for Positron Emission Tomography

1.1 Introduction to Positron Emission Tomography

Positron Emission Tomography (PET) is a non-invasive medical imaging technique which relies on the use of radiolabelled tracers to quantify biochemical and physiological processes *in vivo*. PET allows for tracking molecular events before they develop into anatomical abnormalities. It is used in early-stage diagnosis, as guidance for surgical procedures and in research, where it can provide insights into the pharmacokinetics of novel therapeutics and drug target interactions¹².

1.1.1 Principles of PET

PET tracers are biologically active molecules labelled with a positron emitter, which decays spontaneously via β^+ emission, releasing a positron. This positively-charged particle is the antimatter of an electron. The distance it travels is proportional to its kinetic energy, falling in the range of a few millimetres. Encounter with an electron in the surrounding tissue results in an annihilation event, in which two anti-parallel high-energy photons (511 keV) are produced. Simultaneous detection of these energy quanta allows to construct a PET image. The number of individual annihilation events is proportional to the signal-to-noise ratio²³. This is simplistically illustrated in Figure 1.1, using [¹⁸F]FDG, one of the most important PET radiopharmaceuticals.

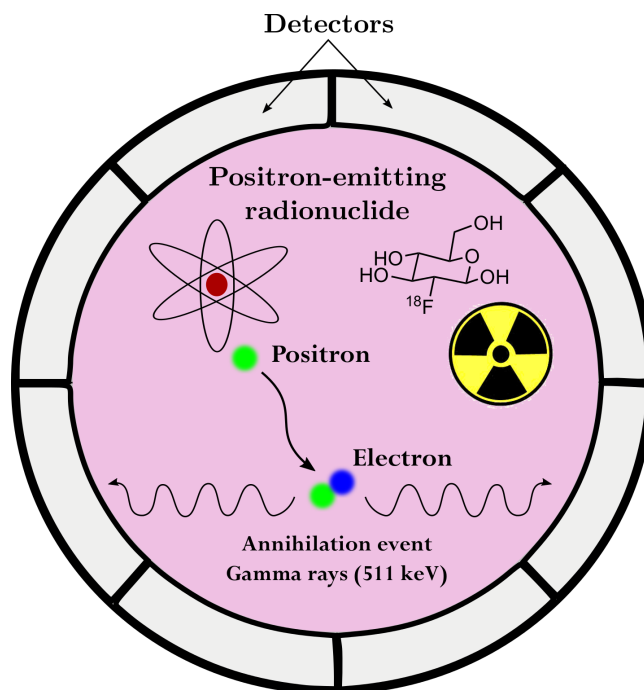


Figure 1.1: Simplified illustration of the principles of PET imaging using $[^{18}\text{F}]\text{FDG}$, an ^{18}F -labelled glucose analogue. $[^{18}\text{F}]\text{FDG}$ is a PET tracer, which enables imaging of glucose metabolism *in vivo*.

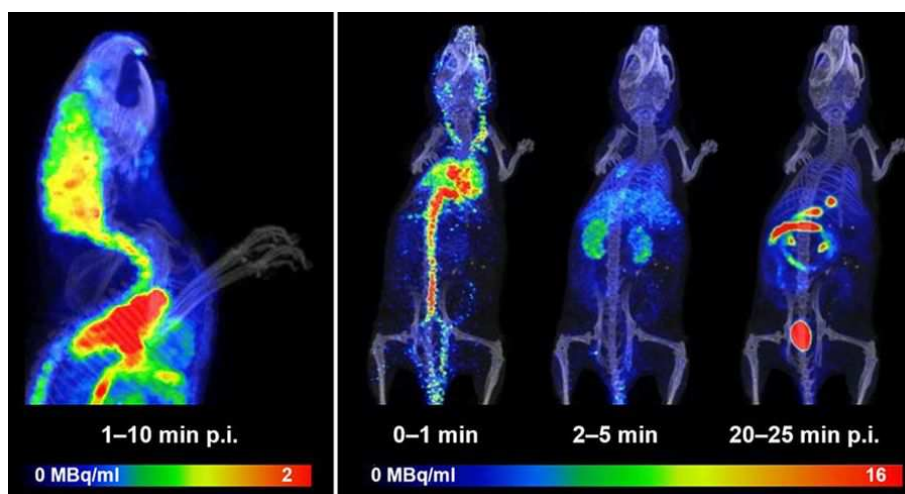


Figure 1.2: A PET-CT image of a mouse⁴.

A typical PET image is a grayscale or colour-coded map of time-dependent distribution of radioactivity in the body. With technological advancements in the field of multimodal imaging, it is now possible to superimpose biochemical information obtained in a PET scan onto functional anatomical detail, provided by, for instance MRI (Magnetic Resonance Imaging) or Computer Tomography (CT). PET-CT imaging, a union of PET and CT modalities, is now routinely used in preclinical

and clinical imaging for the evaluation of novel PET tracers, as well as diagnosis of various pathologies, including cancer³. An example of a mouse PET-CT image is shown in Figure 1.2.

Conveniently, several positron emitters are isotopes of atoms found abundantly in biologically active molecules. They are produced in cyclotron facilities by bombardment of the appropriate radionuclide with a beam of protons or deuterons. Carbon-11, oxygen-15 and nitrogen-13 are short-lived radionuclides which have been used in PET imaging, enabling study and visualisation of biochemical processes without disrupting normal bioactivity. Fluorine-18 is by far the most widely used positron emitter for clinical applications (Section 1.1.2). The main focus of UCL Radiochemistry lies in designing efficient methods of ¹⁸F-incorporation for the synthesis of ¹⁸F-radiotracers. Half-lives and nuclear reactions for production of the aforementioned radionuclides are shown in Table 1.1.

Table 1.1: Positron emitters commonly used in PET radiopharmaceuticals, with their half-lives and nuclear reactions. Based on Miller and co-workers².

Positron emitter	Half-life (min) ²	Nuclear reaction	Product	Decay product
¹⁵ O	2.04	¹⁵ N(<i>d</i> , <i>n</i>) ¹⁵ O	[¹⁵ O]O ₂	¹⁵ N
¹³ N	9.97	¹⁶ O(<i>p</i> , <i>α</i>) ¹³ N	[¹³ N]NO _x or [¹³ N]NH ₃	¹³ C
¹¹ C	20.4	¹⁴ N(<i>p</i> , <i>α</i>) ¹¹ C	[¹¹ C]CO ₂ or [¹¹ C]CH ₄	¹¹ B
¹⁸ F	110	¹⁸ O(<i>p</i> , <i>n</i>) ¹⁸ F	[¹⁸ F]fluoride or [¹⁸ F]F ₂	¹⁸ O
		²⁰ Ne(<i>d</i> , <i>α</i>) ¹⁸ F	[¹⁸ F]F ₂	¹⁸ O

1.1.2 Radiolabelling with ¹⁸F

Properties of ¹⁸F

Fluorine-18 possesses the most favourable decay properties among other positron emitters. Its half-life (110 min) is: 1) short enough to allow convenient radiolabelling and 2) long enough for the tracer to accumulate in target tissue. The use of fluorine-18 is not limited to centres located in close proximity to a cyclotron, making it more available than other radionuclides (Table 1.1). The low positron energy of fluorine-18 (0.635 MeV) translates to high resolution PET images⁵. In addition, positron emission accounts for 97% of its decay profile, yielding a stable oxygen

isotope, ^{18}O , which can be metabolised without biological consequences⁶.

Organofluorine compounds are generally not found in nature. Recent decades, however, have witnessed an increase in the number of fluorinated therapeutics⁷. In 2010 O'Hagan estimated that at least 20% of drugs on the market contained a fluorine atom⁸. In 2016 Zhou *et al.* predicted this number to have increased to 30%⁹. The importance of fluorine in contemporary medicinal chemistry is ascribed to its unique chemical properties. Fluorine is the most electronegative element in the periodic table. Consequently, the carbon-fluorine bond is highly polarised and metabolically stable^{10,11}. Its van der Waals radius is only slightly larger than that of hydrogen (1.35 Å versus 1.20 Å), allowing fluoride substitution without severe steric repercussions^{11,12}. Incorporation of fluorine impacts hydrophobicity of drug-like molecules. Replacement in aliphatic molecules decreases their lipophilic character. The opposite effect is observed for aromatic compounds. It is therefore possible to refine membrane permeability properties and solubility of biologically active molecules¹³.

Fluorine substitution has found uses in pharmaceuticals, agrochemicals and PET chemistry, in line with advancements in the field of PET imaging. One of the most remarkable bioisosteric replacement by a fluorine-18 atom gave rise to an important PET tracer, [^{18}F]FDG (Figure 1.3).

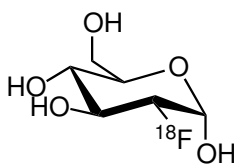


Figure 1.3: 2- ^{18}F Fluoro-2-deoxy-D-glucose or [^{18}F]FDG.

2- ^{18}F Fluoro-2-deoxy-D-glucose is undoubtedly one of the gold standard PET tracers. [^{18}F]FDG has been used to image glucose metabolism in various disease states, *e.g.* cancer: 1) melanoma¹⁴, 2) breast cancer¹⁵ and 3) colorectal cancer¹⁶. It has also been used to diagnose various forms of neurodegeneration, such as Alzheimer's¹⁷ and Parkinson's disease¹⁸. Its mode of action relies on the substitution of the 2-hydroxyl moiety by fluorine-18. After injection, the tracer is transported into cells, where it undergoes phosphorylation by the hexokinase enzyme to form [^{18}F]FDG-

phosphate. However, unlike for regular glucose, this metabolite cannot participate in further glycolysis. Consequently, it is accumulated in cells, enabling its visualisation by PET. It is therefore possible to assess the activity of glucose transporters and hexokinase, which provide a reflection of glucose metabolism in various pathologies¹². Remarkably, imaging of glucose activity by isotopic substitution with carbon-11 would not be as efficient. Although an excellent diagnostic tool for early stage cancer detection and mapping response to therapy, [¹⁸F]FDG lacks specificity to distinguish between tumour types. Accumulation can also occur in areas of usually-enhanced metabolic activity, such as inflammations, myocardium and the urinary tract¹⁹.

Preparation and Considerations of ¹⁸F

Production of radionuclides, as mentioned in Section 1.1.1, is performed in a cyclotron. Depending on further use, fluorine-18 can be provided in aqueous or gaseous form. This is done through irradiation of heavy water, [¹⁸O]H₂O, or oxygen gas, [¹⁸O]O₂, respectively (Table 1.1)¹⁰.

Water-bound [¹⁸F]fluoride cannot usually be used directly in radiolabelling. The anion is strongly bound to water molecules by a hydrogen bonding network, which inhibits its nucleophilicity and ability to participate in most chemical transformations. To restore its reactivity, water is azeotropically evaporated with acetonitrile under a stream of inert gas. A mild base, such as potassium carbonate or bicarbonate, is added to neutralise any remaining hydrofluoric acid. Complexation of the potassium cation with a macrocyclic phase-transfer reagent, *e.g.* Kryptofix 222 (K₂₂₂), leaves [¹⁸F]fluoride "naked" and highly nucleophilic (Figure 1.4). An alternative ¹⁸F-source, ¹⁸F-tetrabutylammonium fluoride ([¹⁸F]TBAF), can be prepared by elution with tetrabutylammonium bicarbonate². Radiolabelling can also be performed using [¹⁸F]F₂ but it is usually transformed into less cumbersome reagents (Section 2.2.1).

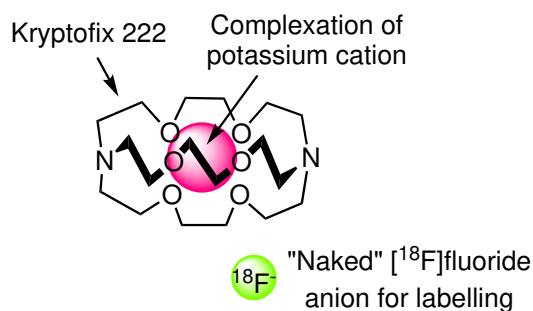


Figure 1.4: Trapping of potassium cations by Kryptofix 222, leaving behind highly reactive [¹⁸F]fluoride anions for radiolabelling. Adapted from Miller and co-workers².

1.1.3 Nomenclature for Radiochemistry

Efficiency of ¹⁸F-labelling is expressed in terms of radiochemical yield (RCY). It is a function of the chemical yield of a reaction and radioactive decay². RCY is obtained by dividing the amount of radioactivity remaining in the sample after purification by the initial value at the beginning of radiosynthesis. RCY can be reported with decay correction in order to account for the loss of radioactivity during manipulations.

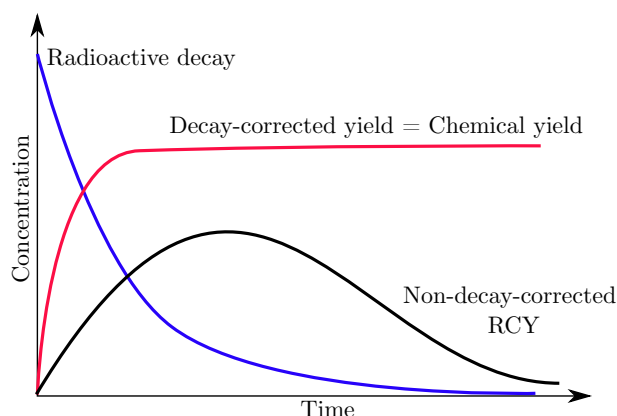


Figure 1.5: Radiochemical yield is a function of the chemical yield (red) and radioactive decay (blue). Decay- and non-decay-corrected RCYs are also shown.

Radioactivity is measured in becquerels (Bq), where 1 Bq is equal to one radioactive decay per second. Radiosyntheses for clinical uses usually start with GBq quantities, whereas for preclinical and clinical injections, MBqs of activity are used. Historically, radioactivity was expressed in curies (Ci), where 1 Ci corresponds to 3.7×10^{10} Bq. Quantities used for PET imaging are usually reported in the micro and millicurie range²⁰.

Specific activity (SA) is defined as radioactivity per unit mass of a radiotracer and it is reported in GBq per micromol. The theoretical value of SA is calculated using the following formula:

$$SA = (\ln 2/t_{1/2})N \quad (1.1)$$

where $t_{1/2}$ is half-life of the radionuclide (*e.g.* 110 min for fluorine-18) and N is the number of fluorine-18 atoms in the sample. This value is never reached because of isotopic dilution with fluorine-19 atoms. High specific activity is desired to achieve a good signal-to-noise ratio. Low specific activity results not only in target saturation (binding sites, *etc.*) but also presents a toxicity hazard²¹.

1.1.4 ¹⁸F-Radiochemistry: Analytical Techniques

This section gives a brief introduction to modern instrumental chromatography techniques used to confirm the identity of ¹⁸F-labelled compounds by UCL Radiochemistry.

Unlike non-radioactive drug-like compounds synthesised in research laboratories, identity of PET radiopharmaceuticals cannot be confirmed using standard NMR spectroscopic techniques. This is because: 1) tracers are synthesised in subnanomolar quantities which cannot be detected by the inherently insensitive NMR spectroscopy and 2) ¹⁸F-labelled samples must be appropriately shielded. For RCY and SA calculations, precise radioactivity measurements are required. Confirmation of product identity and quality control for chromophores are performed routinely using high-performance liquid chromatography (HPLC) with an integrated radioactivity detection system, known collectively as radio-HPLC. Detectors used by UCL Radiochemistry are scintillation-based. Emitted radioactivity hits the scintillation crystal and interacts with its atoms, exciting them to higher molecular orbitals, which leads to emission of light. Light is then converted into electrical energy and consequently, a signal on the detector output^{22 23}.

All radiolabelled compounds prepared and described in this thesis are aromatic molecules and all analytical work was performed using radio-HPLC. Non-radioactive

compounds were analysed using NMR spectroscopy and/or HPLC/LC-MS.

High-Performance Liquid Chromatography

High-Performance Liquid Chromatography is a modern analytical technique used to separate chemical mixtures into their constituents. Designed on the foundations of traditional liquid chromatography, HPLC employs significantly smaller sorbent particles (5 to 250 μm) to increase the surface area available for interaction and achieve the maximum resolving power. It is a powerful and versatile technique and a gold standard purification method in pharmaceutical industry and research^{24,25}. The key components are outlined in Figure 1.6.

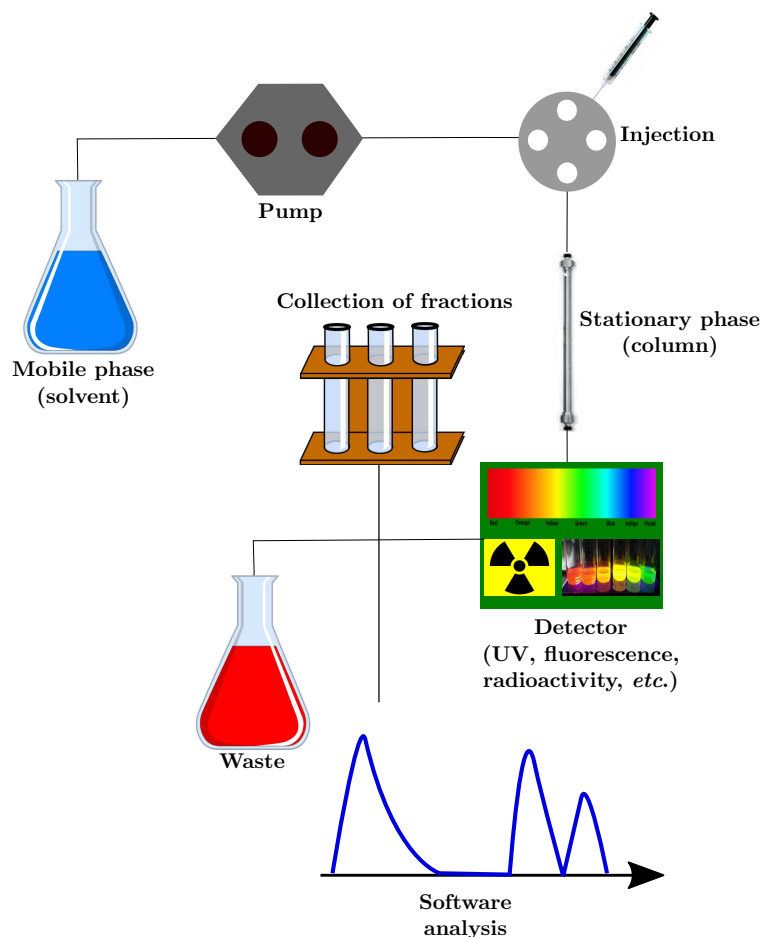


Figure 1.6: Schematic illustration of HPLC principles.

HPLC uses a wide range of separation methodologies, however, those pertinent to this work are: normal and reverse-phase. In the traditional normal-phase mode, the stationary phase is hydrophilic (silica- or alumina-based). Strong interaction with

hydrophilic analytes causes the lipophilic ones to elute more rapidly. The mobile phase is usually significantly less polar than the packing material in the column. Typical solvents include ethyl acetate and hexanes. In the reverse-phase, the opposite phenomenon occurs, however, the stationary phase is non-polar and usually contains silica with adsorbed long alkyl chains (8 and 18 carbons). Significantly more polar solvents are required, *e.g.* water, methanol and acetonitrile. Reverse-phase HPLC is commonly used in pharmaceutical research.

Parameters of the column packing material are selected to provide the highest separating power. Several factors contribute to the strength of interactions between the stationary phase and components of the mixture. These include: 1) type of particle backbone, *e.g.* silica, alumina, 2) bonded material, *e.g.* C-8 or C-18 alkyl chains, 3) particle size and surface area for resolution, as well as 4) column dimensions.

For certain compounds, adjustments of pH of the mobile phase must be made to ensure good resolution. When pH of the solvent carrier is equal to the pK_a of the compound, it will exist as both its protonated and neutral form, resulting in two peaks. Trifluoroacetic acid is a common additive in reverse-phase HPLC which rectifies this problem²⁶. Elution can be performed in two modes: gradient and isocratic. Gradient elution relies on a changing composition of the solvent mixture to achieve separation, whereas in the isocratic mode a single solvent percentage is used from the outset and throughout. There are several detection types available, depending on the nature of compound, including UV (specific wavelengths can be set), fluorescence and radioactivity, *etc.*

Radio-HPLC Chromatography analysis of reaction mixtures is performed on a radio-HPLC, which is equipped with a gamma-ray detector. Preparative and semi-preparative radio-HPLC machines are used in radiopharmaceutical production for preclinical and clinical applications^{27 28}.

Identification of the radiolabelled product is performed by co-elution with its non-radioactive reference compound (Figure 1.7). Comparison of the radioactive and UV traces allows to indirectly infer identity of the radioactive compound. Specific

activity calculations are performed using a calibration curve, based on concentrations of the non-radioactive analogue and the area under the peak corresponding to the radiolabelled compound on the UV trace. This is usually close to the limit of quantification of the machine. The amount of the [^{19}F]fluorinated product can be established using its molar mass and concentration (calibration curve), while for the [^{18}F]fluorinated product a radioactivity detector is needed.

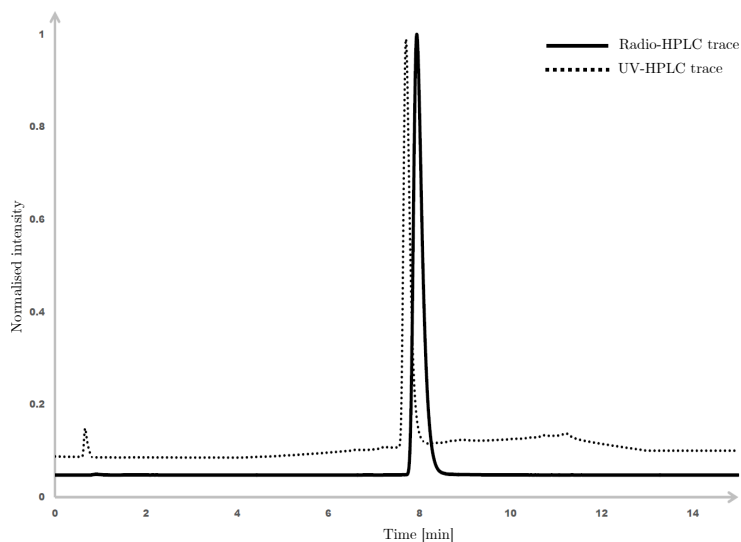


Figure 1.7: Co-injection of the radioactive trace corresponding to the [^{18}F]fluorinated product with the UV trace of its ^{19}F -analogue on radio-HPLC. Note the small delay due to the sequential use of radioactivity and UV detectors.

Liquid Chromatography Mass Spectrometry

Liquid chromatography mass spectrometry (LC-MS) is a union of HPLC and mass spectrometry instrumentation that provides analysis, identification and purification options for reaction mixtures. Research presented in this thesis relied on the use of LC-MS to confirm the mass of reaction intermediates.

In an LC-MS sequence, after HPLC separation (Figure 1.6), the components are passed through an ion source which produces various gaseous ionised species. These are then arranged according to their mass to charge ratio (m/z). Superimposition onto the HPLC trace allows to identify the masses of resolved peaks²⁹.

There are several ionisation sources available in mass spectrometry, the most common

one being Electrospray Ionisation (ESI). Strong electric field is applied to transfer ions in the solution into the gaseous phase. Large charge droplets are formed and evaporation of solvent results in the release of ions due to strong repulsion forces³⁰.

2 | Strategies for ^{18}F -Labelling

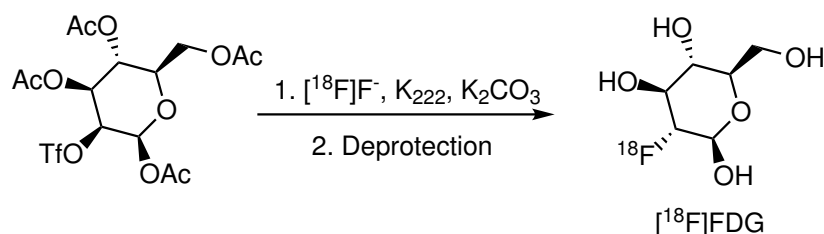
PET imaging is interdisciplinary. Its success is proportional to the degree of collaboration between different fields. Engineers and computer scientists work towards improving PET sensitivity by designing better detectors and image reconstruction algorithms. Biologists and clinicians perform biological studies, while chemists and radiochemists design PET tracers and efficient routes for radionuclide incorporation. Despite major advancements in PET chemistry, certain tracers cannot be radiosynthesised efficiently or prepared according to Good Manufacturing Practice (GMP) standards. For widespread clinical use, production of PET tracers must be scalable to quantities > 200 MBq. Radiopharmaceuticals must exhibit high specific activity values, as well as pass quality control tests for the presence of impurities, such as metallic residues³¹.

The quest for practical, efficient and scalable [^{18}F]fluorination is ongoing. The main challenge lies in C-F bond formation, which imposes severe synthetic restrictions. Extensive reviews of ^{18}F -labelling strategies have been published, with the most recent by Preshlock⁶ and van der Born³², giving an overview of the most prominent late-stage direct [^{18}F]fluorinations. This chapter gives an outlook of the most recent and/or interesting approaches to ^{18}F -labelling, with the main focus on aromatic molecules.

2.1 ^{18}F -Labelling of Aliphatic Molecules

There are several approaches to ^{18}F -incorporation into aliphatic molecules, with the most prominent utilising nucleophilic [^{18}F]fluoride in an $\text{S}_{\text{N}}2$ substitution reaction. Gold standard radiopharmaceuticals, such as [^{18}F]FDG and [^{18}F]FMISO (imaging of hypoxia), are prepared using this method. Similarly to other nucleophilic transformations, a good leaving group is required. Tosylate offers a favourable combination

of stability and reactivity but triflate and mesylate are also used. Halides are less favoured. Facility of substitution increases with decreasing steric bulk of the substrate, so [^{18}F]fluoride attack is most efficient at primary benzylic positions¹⁰. Reactions proceed in polar aprotic solvents, *e.g.* DMF, DMSO and MeCN, and usually require moderate heat.



Scheme 2.1: Nucleophilic aliphatic [^{18}F]fluorination proceeds via the S_N2 mechanism. [^{18}F]FDG is radiosynthesised using this strategy³³.

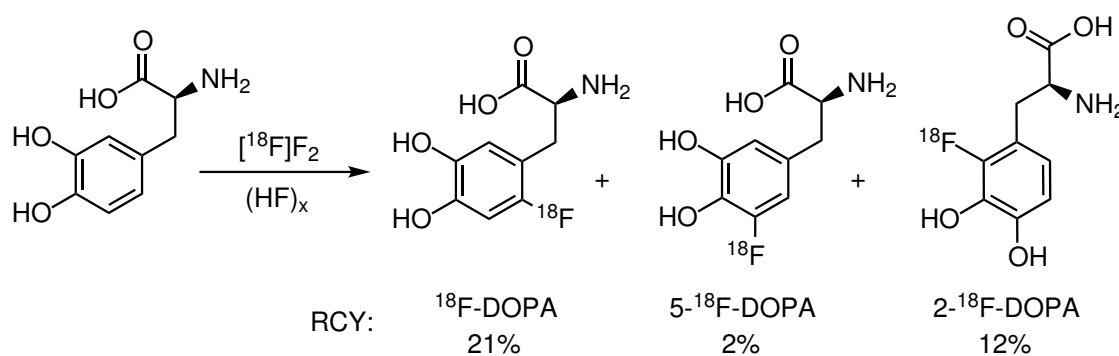
2.2 ^{18}F -Labelling of Aryls: Traditional Approach

Aromatic rings are vastly abundant in biological molecules, *e.g.* as ligands. Incorporation of arenes into drug molecules increases their metabolic stability, in comparison with unsaturated hydrocarbons. It can also induce strong interactions with proteins through π - π stacking, hydrogen bonding and stabilisation of functional groups^{34,35}.

PET radiopharmaceuticals, like therapeutics, interact with specific targets *in vivo*. They can be [^{18}F]fluorinated analogues of biologically active molecules or drugs. Direct late-stage labelling of aromatic molecules is desired, however as already mentioned, C-F bond formation is troublesome, and even more so aromatic fluorination. A multitude of impressive ^{18}F -labelling strategies have been published in the last decade. One of the main problems of fluorine-18 chemistry is, however, the lack of broadly applicable, practical and robust methods which could be adapted to GMP environments. Consequently, in order to utilise the enormous potential of PET and the ever-increasing pool of bioactive molecules, practical and elegant [^{18}F]fluorination methods need to be developed.

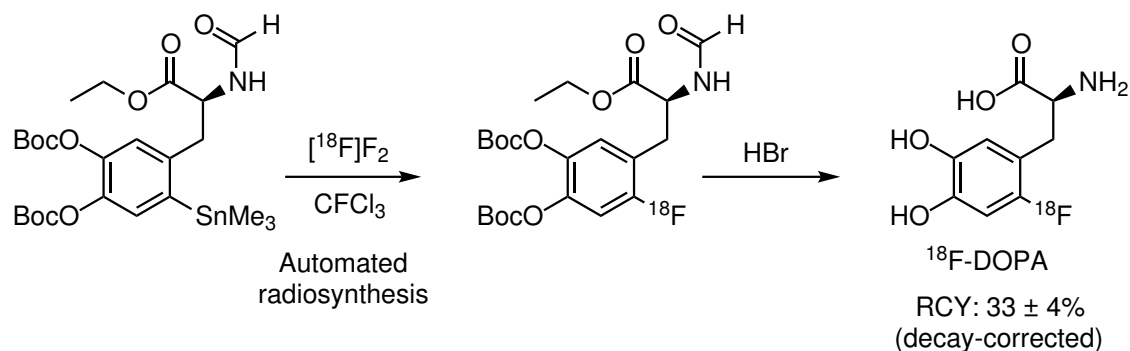
2.2.1 Electrophilic Aromatic Substitution

A review of [^{18}F]fluorination techniques for aromatic systems would not be complete without a brief introduction to electrophilic aromatic substitution. Historically, it was a common strategy for radiosynthesis of electron-rich and electron-neutral aromatic systems, including important PET radiopharmaceuticals, such as ^{18}F -DOPA (Scheme 2.2). The use of electrophilic [^{18}F]fluorination of PET tracers is currently outdated and replaced by technologies employing nucleophilic [^{18}F]fluoride.



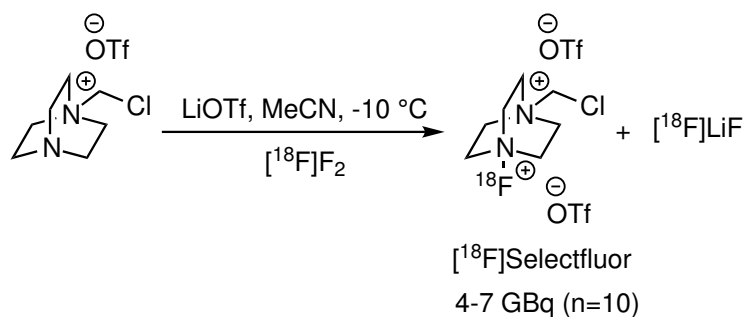
Scheme 2.2: Electrophilic [^{18}F]fluorination with [^{18}F]F₂ gas for the radiosynthesis of ^{18}F -DOPA. Two regioisomers, 2- and 5- ^{18}F -DOPA, are also formed³⁶.

Traditionally, electrophilic aromatic substitution was achieved with highly reactive [^{18}F]F₂ gas as a source of fluorine-18. Fluorine gas is a strong oxidant, has a high reaction heat and produces corrosive hydrofluoric acid in aqueous solutions. Its reactivity is challenging to temper and radiosyntheses often exhibit poor regioselectivity. A good example of this is the historic clinical production of ^{18}F -DOPA in Schemes 2.2 and 2.3³⁷. [^{18}F]F₂ is produced in a carrier-added way, resulting in low specific activity. During electrophilic [^{18}F]fluorination, only one fluorine-18 atom is incorporated into the tracer scaffold, limiting the theoretical RCY to 50%¹⁰. As a result, PET radiochemists were prompted to optimise reaction conditions and precursor substitution pattern, as well as design novel and mild electrophilic [^{18}F]fluorine sources. To enhance regioselectivity of ^{18}F -DOPA manufacture, the precursor can be decorated with an organometallic substituent, such as SnMe₃, GeMe₃ or SiMe₃, and subsequent electrophilic demetallation affords the [^{18}F]fluorinated product. Until the emergence of efficient and better yielding radiolabelling with nucleophilic [^{18}F]fluoride, fluorodestannylation long served as a clinical production route of ^{18}F -DOPA (Scheme 2.3)³⁸.



Scheme 2.3: Electrophilic aromatic [^{18}F]fluorination of the organotin precursor was a common radiosynthetic route to clinical ^{18}F -DOPA. The strategy was optimised for automation by de Vries and co-workers³⁹.

Milder electrophilic [^{18}F]fluorine sources include xenon difluoride (^{18}F] XeF_2), acetyl hypofluorite and a recent invention by the Gouverneur group, [^{18}F]Selectfluor (Scheme 2.4)^{40 41 42}. Its cumbersome preparation limits its widespread use¹⁰. As these reagents still do not provide enough regioselectivity and require complicated purification procedures, the search for mild, specific and efficient radiosynthetic routes for the labelling of electron-rich and electron-neutral aromatic scaffolds is still ongoing.

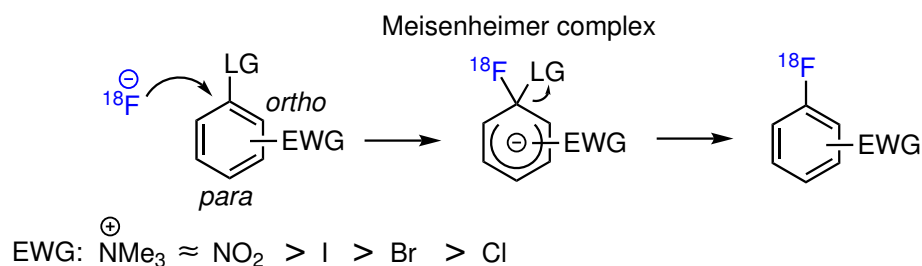


Scheme 2.4: Radiosynthesis of [^{18}F]Selectfluor, a milder electrophilic alternative to [^{18}F]fluorine gas⁴³.

2.2.2 Nucleophilic Aromatic Substitution

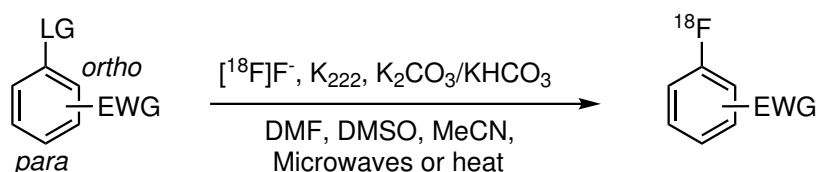
Nucleophilic aromatic substitution is routinely used to incorporate fluorine-18 into aromatic molecules. Radiolabelling is performed with [^{18}F]fluoride. This poses restrictions on the type of aromatic scaffolds which can be labelled efficiently. Radiolabelling proceeds in high RCYs for aromatics decorated with strongly electron-withdrawing substituents, such as trimethylammonium or nitro groups, located *ortho* or *para* to the leaving group (Scheme 2.5). Nucleophilic attack at these positions leads to the

formation of a negatively charged Meisenheimer complex, which is best stabilised by substituents capable of accepting electron density¹⁰⁴⁴.



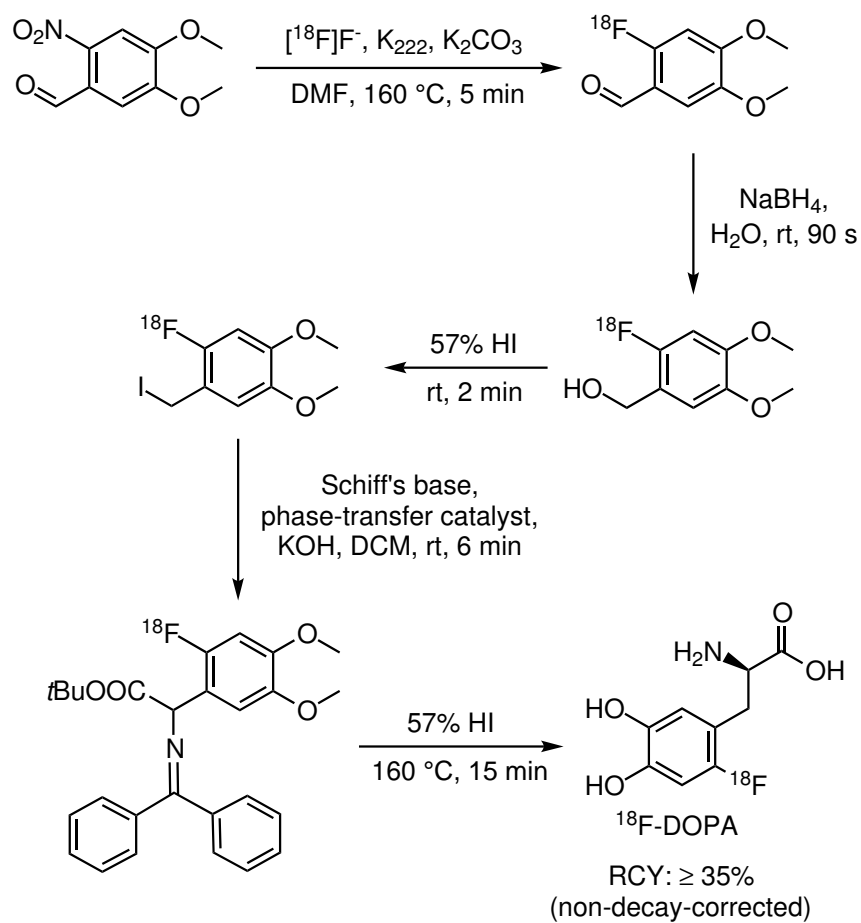
Scheme 2.5: Nucleophilic aromatic substitution with [¹⁸F]fluoride occurs via a Meisenheimer complex, stabilised by electron-deficient substituents in the *ortho*- or *para*-positions.

Typical radiolabelling using nucleophilic [¹⁸F]fluoride requires a polar aprotic solvent, such as DMF, DMSO or MeCN, thermal activation (> 100 °C) or microwaves, a phase-transfer catalyst, *e.g.* Kryptofix 222, and a mild base (Scheme 2.6).



Scheme 2.6: Typical nucleophilic aromatic [¹⁸F]fluorination of activated aromatic systems.

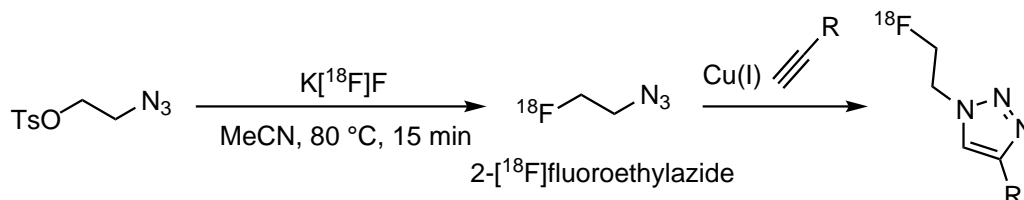
Perhaps the most prominent example of nucleophilic aromatic [¹⁸F]fluorination is the GMP radiosynthesis of ¹⁸F-DOPA. To date, this is the most efficient strategy for clinical production of this tracer. The precursor, 6-nitroveratraldehyde, is substituted by [¹⁸F]fluoride in the presence of K₂₂₂ and K₂CO₃. Reduction of the carbonyl moiety with NaBH₄ is followed by iodination, and the resulting [¹⁸F]fluorinated benzyl iodide reacts with a Schiff's base and a chiral catalyst to afford ¹⁸F-DOPA in at least 35% non-decay-corrected RCY. This route is shown in Scheme 2.7.



Scheme 2.7: Radiosynthesis of ^{18}F -DOPA performed in GMP laboratories. The first step is a nucleophilic aromatic substitution using $[^{18}\text{F}]$ fluoride with NO_2 as a leaving group.

2.2.3 Indirect Labelling via Prosthetic Groups

In radiochemistry, a prosthetic group is a bifunctional labelling agent incorporated into molecules of interest to act as an ^{18}F -tag⁴⁵. It is a common way of labelling aromatic molecules which, for various reasons, cannot be decorated with fluorine-18 directly. The use of prosthetic groups is not always ideal, as they might interfere with biological activity of PET tracers. Radiosynthesis of biomolecules, such as peptides and proteins, relies largely on indirect ^{18}F -incorporation, as their temperature- and base-sensitive nature often precludes the use of ^{18}F fluoride². Fortunately, installation of prosthetic groups is normally performed under mild conditions. An arsenal of such entities is now available to radiochemists as a result of concerted efforts to increase the pool of biologically active molecules for PET imaging. Attachment usually occurs via the NH_2 - or SH -moieties⁴⁵. New generation reagents can be installed using mild and elegant solutions such as "click reactions". A remarkable example is 2- ^{18}F fluoroethylazide, developed by Glaser and Årstad, which enables formation of ^{18}F -labelled 1,2,3-triazoles using Cu(I) -catalysed Huisgen cycloadditions (Scheme 2.8)⁴⁶.



Scheme 2.8: 2- ^{18}F Fluoroethylazide is a versatile prosthetic group, which can be used to label biologically active molecules. It reacts with terminal alkynes in elegant "click transformations"⁴⁶.

2.3 ^{18}F -Labelling of Aryls: Recent Advances

The ongoing search for milder and high yielding radiolabelling strategies has led to ground-breaking advances, particularly in last few years. Focus has been placed on engineering versatile precursors for practical and regioselective ^{18}F -labelling of electron-neutral and electron-rich aromatics. Particularly favoured are routes which avoid the use of highly reactive and low specific activity gaseous species, toxic metals, such as tin, or lengthy multi-step procedures. Although an impressive repertoire of

strategies is available, the majority cannot be readily adapted to automated GMP radiosynthesis.

This section provides a brief overview of the most recent and attractive radiosynthetic avenues for labelling of non-activated and deactivated aryls with nucleophilic [^{18}F]fluoride. Such transformations can be achieved using hypervalent iodine(III) species, sulfur-based precursors or metal-assisted reductive elimination.

2.3.1 Metal-Free ^{18}F -Chemistry

This section discusses recent advances in [^{18}F]fluorination of aromatic systems employing metal-free precursors.

Diaryliodonium Salts: Chemistry

Diaryliodonium salts (Figure 2.1) have been used in synthetic transformations for decades. The "soft" nature of the iodine(III) core makes it a good leaving group and its electron-poor character renders it prone to nucleophilic attack⁴⁷.

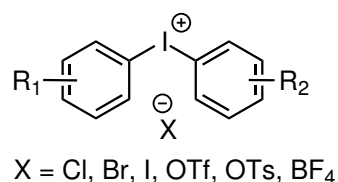
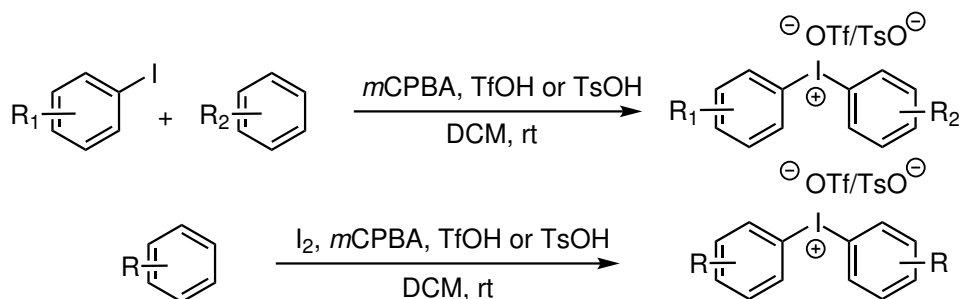


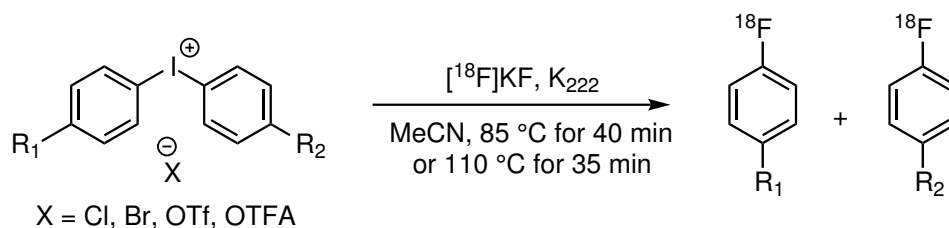
Figure 2.1: A functionalised diaryliodonium salt.



Scheme 2.9: Efficient and practical iodonium salt formation using *m*CPBA⁴⁸.

To date, there exist several synthetic routes to diaryliodonium salts. However, it was the recent work of Olofson *et al.* which has given access to structurally sophisticated variants⁴⁸. Asymmetrical diaryliodonium salts can be prepared from the corresponding aryls in the presence of *m*CPBA and TfOH or TsOH in dichloromethane at room temperature. For symmetrical analogues, molecular iodine is required (Scheme 2.9)⁴⁹. For more challenging regiospecific syntheses, arylboronic acids can be employed⁵⁰. A broad scope of diaryliodonium salts has been prepared using the aforementioned strategies.

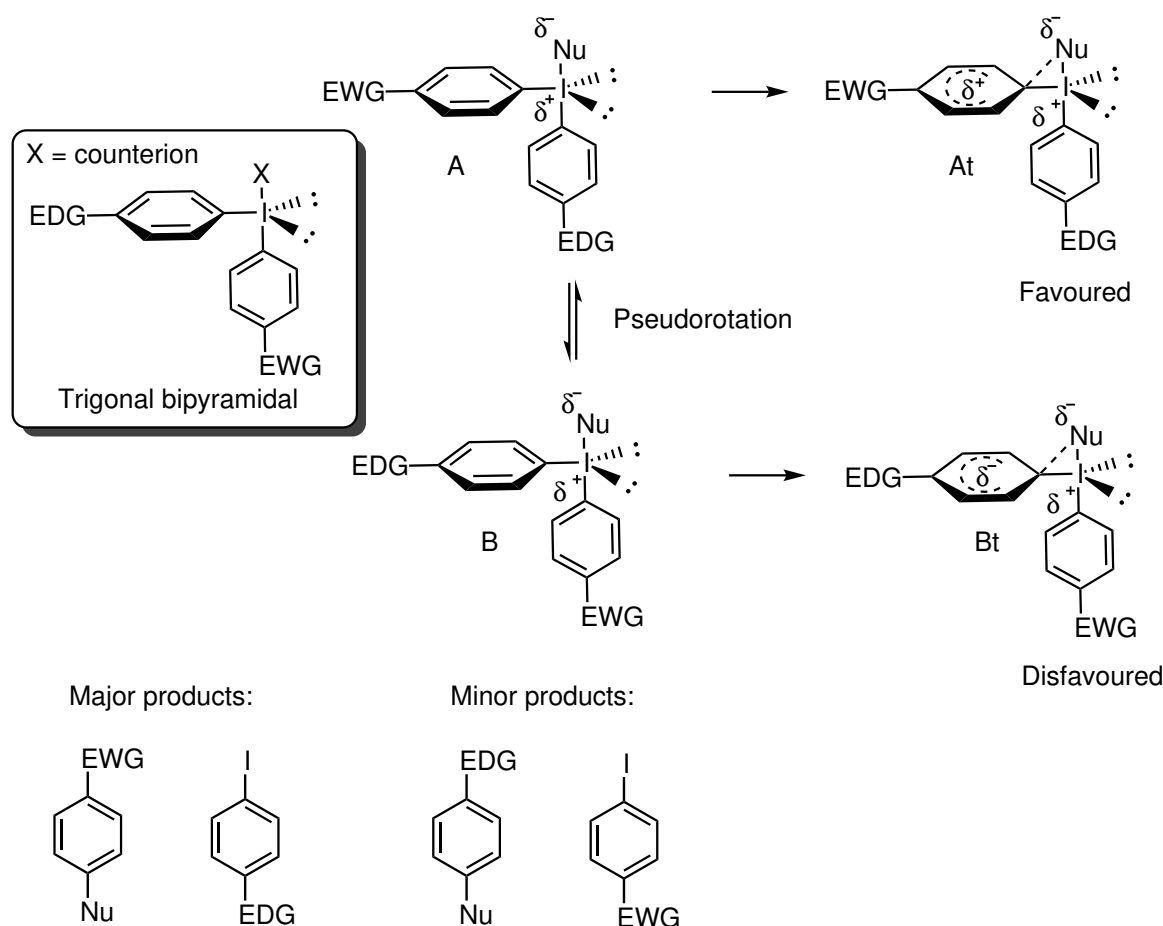
Among the wide range of nucleophilic species that react with diaryliodonium salts are thiols, thioethers, amines and phenoxides⁵¹. This methodology was expanded by Pike and Aigbirhio, who realised the potential of diaryliodonium chemistry for direct ¹⁸F-functionalisation of arenes in mid-1990s⁵². Asymmetrical precursors decorated with electron-rich methoxy and methyl substituents reacted in excellent radiochemical yields. The most remarkable example features formation of [¹⁸F]fluoroanisole from 4-methoxydiphenyliodonium bromide in 88% decay-corrected RCY. While the triflate counterion remained most explored, labelling also proceeded in the presence of chloride, bromide and trifluoroacetate. The generic radiolabelling reaction of [¹⁸F]fluoride is shown in Scheme 2.10.



Scheme 2.10: Labelling of functionalised diaryliodonium salts with [¹⁸F]fluoride in MeCN, described by Pike and Aigbirhio⁵².

Reactivity towards nucleophiles is governed by the molecular geometry exhibited by diaryliodonium salts. Trigonal bipyramidal arrangement of substituents (Scheme 2.11) is commonly found in hypervalent iodine species, however conventional depiction with the 109° bond angle (Figure 2.1) prevails⁴⁸. The degree of dissociation between the counterion and the iodine(III) centre depends on the strength of the solvent interaction.

Generic reaction of an asymmetrical diaryliodonium salt with a nucleophile is presented in Scheme 2.11. Firstly, an exchange occurs between the counterion and the nucleophile, the latter occupying the axial position. Pseudorotation around the iodine core gives rise to two intermediates, A and B. The corresponding transition state A_t is favoured and nucleophilic substitution occurs preferentially at the *ipso*-carbon of the more electron-withdrawing ring. This pattern can, however, be overridden when one of the aryl rings possesses an *ortho*-substituent. T-shaped geometry forces the more sterically hindered aryl to occupy the spacious equatorial position, leading to nucleophilic substitution *ortho* to the substituent, even if it is more electron-rich by nature^{10 53}. This selectivity is referred to as the *ortho*-effect.



Scheme 2.11: Reactivity of asymmetrical diaryliodonium salts towards nucleophiles. Adapted from Yusubov and co-workers⁵³.

Chun *et al.* reported that in certain instances, radioactive product distribution cannot be explained in terms of the *ortho*-effect and substituent bulk⁵⁴. The fact that

[^{18}F]fluoride incorporation on the methoxy-decorated ring of (2-methoxyphenyl)phenyl iodonium tosylate did not occur, brought Chun and co-workers to the conclusion that other factors could perhaps influence the fate of the nucleophilic attack, *e.g.* lipophilicity and electronics.

[^{18}F]Fluorinations of asymmetrical diaryliodonium salts performed by Gail *et al.* confirmed the observations made by Chun *et al.* RCY increased with the number of methyl substituents on the aryl ring, which cannot be explained solely by ring electronics⁵⁵. Figure 2.2 illustrates the *ortho*-effect observed in ^{18}F -labelling experiments.

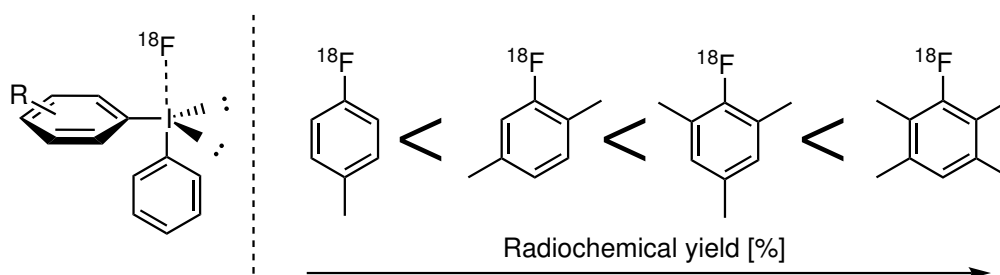
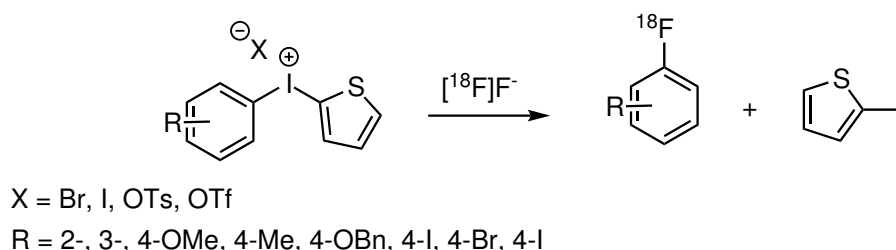


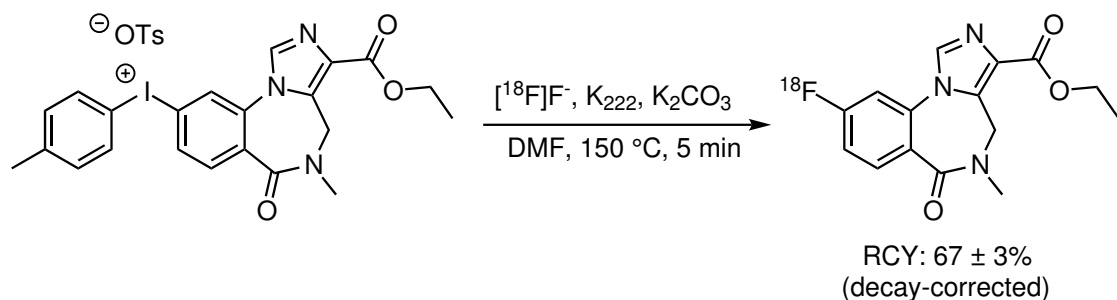
Figure 2.2: The *ortho*-effect was observed during radiolabelling of asymmetrical diaryliodonium salts by Gail and co-workers⁵⁵. Adapted from Coenen⁵⁶.

Ross *et al.* investigated nucleophilic ^{18}F -labelling of heteroaromatic diaryliodonium salts with a selection of counterions and substituents⁵⁷. A thiophene ring was selected to represent an electron-deficient arene, while the phenyl ring was decorated with electron-rich methoxy and benzyl substituents or halides (Scheme 2.12).



Scheme 2.12: ^{18}F -Labelling of heteroaromatic diaryliodonium salts to investigate the influence of substituents and counterions on RCY, was performed by Ross and co-workers⁵⁷.

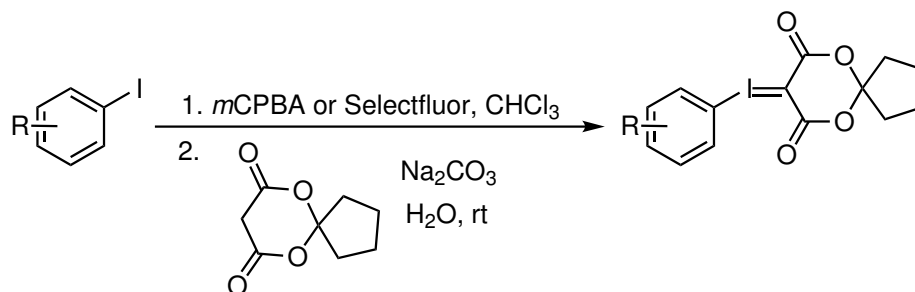
As postulated earlier, *ortho*-substituted diaryliodonium salts exhibited higher RCYs, furthering evidence towards the *ortho*-effect. While 2-[^{18}F]fluoroanisole was accessed



Scheme 2.14: Application of diaryliodonium salts: radiosynthesis of [^{18}F]flumazenil⁶⁰.

Chemistry of Iodonium Ylides

Iodonium ylides, like diaryliodonium salts, belong to the family of hypervalent iodine(III) precursors for ^{18}F -labelling. These spirocyclic reagents were designed by Rotstein *et al.* to address photostability and decomposition issues of diaryliodonium salts, and to provide stabilisation for non-activated substrates during ^{18}F -incorporation⁶². After an exhaustive optimisation process, a stable spiroiodine(III) was identified, which proved reactive towards [^{18}F]fluoride (Scheme 2.15).



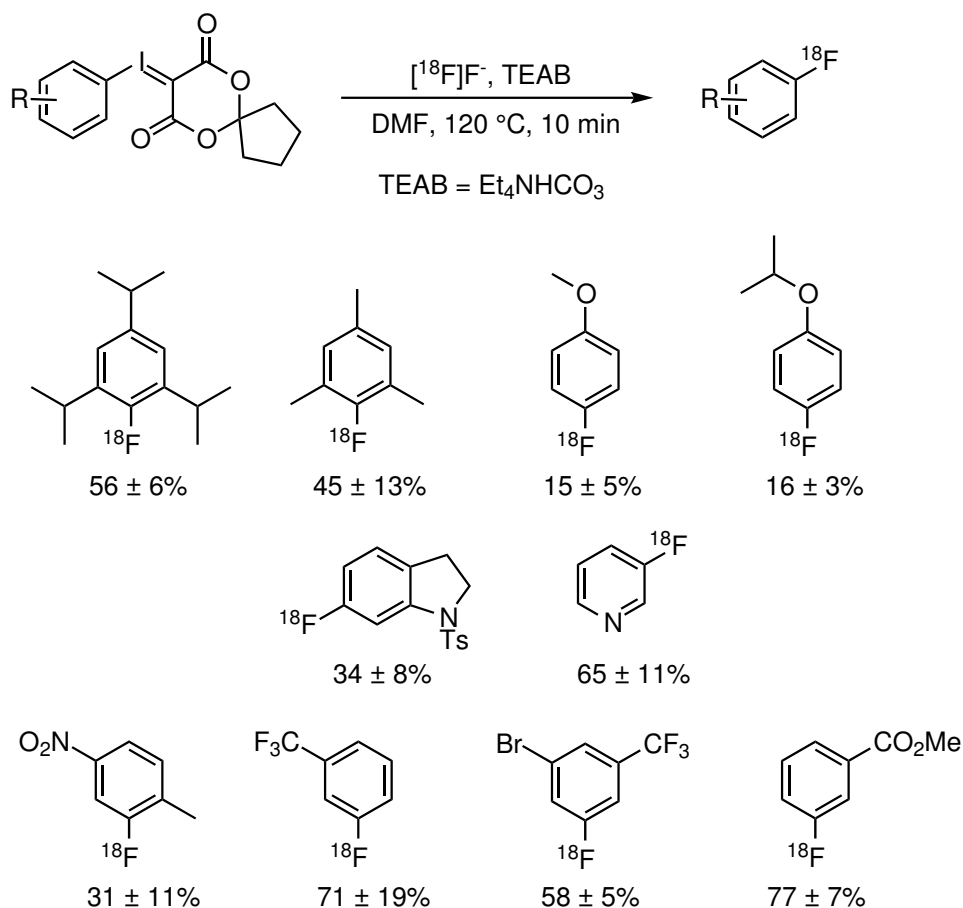
Scheme 2.15: One-pot synthesis of an optimised spirocyclic iodonium ylide precursor for ^{18}F -labelling, developed by Rotstein and co-workers⁶².

Iodonium ylides can be accessed from the corresponding aryl iodide in a convenient one-pot oxidation with *m*CPBA or Selectfluor, the spirocyclic ligand and sodium carbonate at room temperature (Scheme 2.15). Selectfluor is a strong oxidant, commonly employed in preparation of hypervalent iodine species from arenes⁶³. The range of precursor which can be accessed using this method is therefore limited to oxidation-resistant moieties.

Complementary routes were designed for substrates prone to oxidation, such as

quinolines and indoles⁶². The former can be afforded by *N*-protonation, followed by treatment with Oxone[®]. Indole-based substrates require prior *N*-Boc protection. Oxidation to the corresponding iodonium ylides proceeds in the presence of dimethyldioxirane (DMDO) in acidic media.

The substrate scope for ¹⁸F-labelling included non-activated aromatic moieties, decorated with *iso*-propyl, methyl, methoxy and *iso*-propanoxy substituents in the *ortho*-position. Enhanced RCYs were obtained for hindered alkyl-substitution patterns. The *N*-tosyl-protected 6-[¹⁸F]fluoroindoline was accessed in 34 ± 8% RCY, while incorporation at the 3-position on the pyridine afforded the corresponding [¹⁸F]fluorinated product in 65 ± 11% RCY. Labelling of non-activated *meta*-substituted arenes proceeded with good to excellent RCYs. Representative examples from Rotstein's scope study are shown in Scheme 2.16.

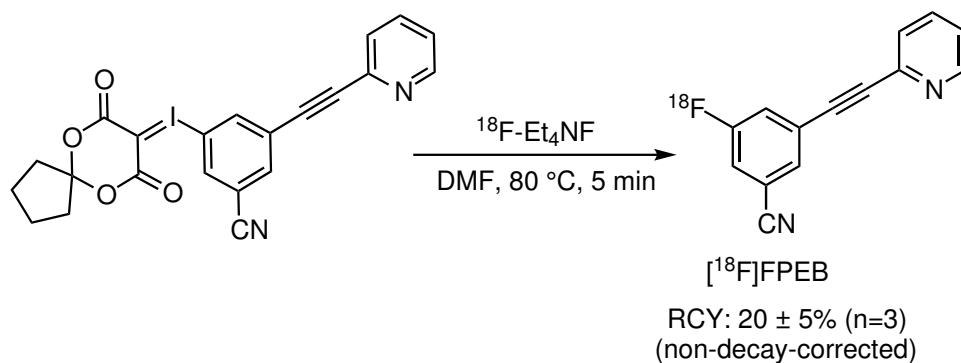


Scheme 2.16: Radiolabelling of structurally diverse aryls using iodonium ylides as precursors, performed by Rotstein and co-workers⁶². Analytical RCYs were established using radio-TLC and radio-HPLC.

Rotstein and co-workers also presented a mechanistic interpretation of iodonium ylide reactivity towards [^{18}F]fluoride⁶⁴. Using *in silico* methods and NMR spectroscopy, the authors were able to compare the reactivity of iodonium ylides versus diaryliodonium salts in radiolabelling and to explain the excellent regioselectivity of ^{18}F -incorporation at the aryl rather than the spirocyclic auxiliary. It was hypothesised that the transition state involving coordination of the nucleophile to the hypervalent iodine centre, and subsequent reductive elimination to form the [^{18}F]fluorinated aryl, has a lower activation energy, due to the stabilising effect of the auxiliary. The latter also plays a key role in enhancing thermal stability of the precursor during high temperature radiolabelling, often required for electron-rich scaffolds. As expected, iodonium ylides decorated with electron-deficient substituents, such as NO_2 or CN , can be labelled even at ambient temperatures. It was postulated that reductive elimination is likely to be the rate-determining step, with the activation barrier lower for electron-poor substrates, in line with radiosynthetic findings. Through the design of stable iodonium ylides for [^{18}F]fluorination of functionalised drug-like molecules, Rotstein *et al.* addressed the issues associated with iodonium salts precursors, such as decomposition and lower radioefficiency for deactivated aromatics.

Applications of Iodonium Ylides to PET Tracers

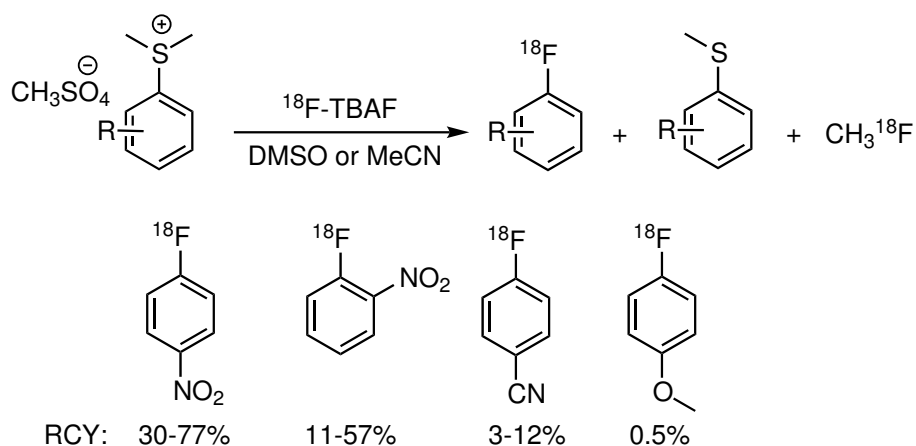
Several PET tracers have been prepared using the iodonium ylide strategy since its emergence in 2015. Stephenson *et al.* validated practicality of the method on [^{18}F]FPEB, a tracer for the imaging of the mGluR5 receptor (Chapter 5)⁶⁵. The iodonium ylide precursor to [^{18}F]FPEB was synthesised in 40% yield over 6 steps. With optimisation of the labelling conditions, Stephenson *et al.* arrived at the combination of [^{18}F]fluoride and tetraethylammonium carbonate in DMF at 80 °C for 5 min, to give [^{18}F]FPEB in $49 \pm 6\%$ RCY, as determined by radio-TLC. A high radioactivity scale radiosynthesis for clinical use afforded the tracer in 20% non-decay-corrected (n.d.c) RCY at the end of synthesis (Scheme 2.17).



Scheme 2.17: Clinical-scale radiosynthesis of [^{18}F]FPEB, starting from the iodonium ylide precursor, developed by Stephenson and co-workers⁶⁵.

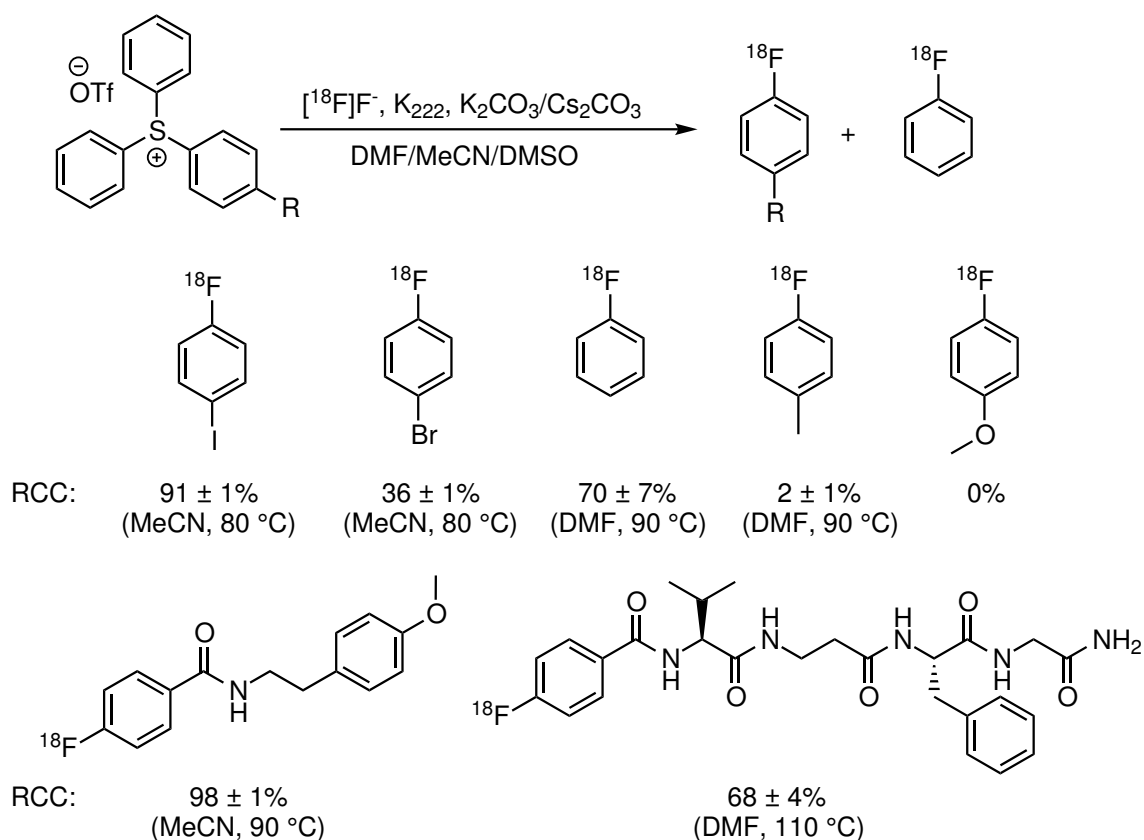
Labelling with Sulfonium Salts

Sulfonium salts have long been considered as promising precursors for ^{18}F -labelling, owing to their excellent leaving group character in nucleophilic substitution reactions⁶⁶. In the late 1980s, Maeda *et al.* reported successful ^{18}F -incorporation into aromatic molecules using aryldimethylsulfonium mesylates⁶⁷. The scope was limited to aryls activated by the strongly electron-deficient nitro group in the *ortho*- or *para*-position, which reacted with ^{18}F -TBAF in 11-77% RCYs (n.d.c). Low yields were reported for *p*-nitrile substitution and no reaction was observed for *p*-aniline (Scheme 2.18). One of the drawbacks of this strategy is facile formation of methyl [^{18}F]fluoride and demethylation of the precursor to the corresponding sulfide.



Scheme 2.18: Labelling of aryldimethylsulfonium salts with ^{18}F -TBAF, performed by Maeda and co-workers⁶⁷.

Nearly 30 years later, Mu *et al.* developed a radiolabelling protocol employing triarylsulfonium triflate salts, in response to the growing demand for alternative strategies to access non-activated and deactivated [^{18}F]fluoroaryls⁶⁸. The authors explored the influence of *para*-substitution by non-activating and deactivating groups on the RCY. A generic radiolabelling reaction of triarylsulfonium salts and the scope investigated by Mu *et al.* are shown in Scheme 2.19. High radiochemical conversions (RCCs) were reported for [^{18}F]fluoride substitution of an aryl iodide: 1) 90-91% in MeCN, 2) 62-81% in DMF and 3) 48-61% in DMSO. Regioselectivity issues were experienced, with the highest percentage of side products in DMF reactions. Decent conversion was also observed for an aryl bromide, consistent with its less activating nature, as noted from Hammett constants (σ : *p*-Br = 0.232, *p*-I = 0.276). [^{18}F]Fluorobenzene formation from triphenylsulfonium triflate proceeded in $70 \pm 7\%$ RCC in DMF, dropping to $48 \pm 3\%$ in MeCN. By-product formation was favoured for electron-donating substituents. Simple peptide scaffolds were also prepared.



Scheme 2.19: [^{18}F]Fluorination of triarylsulfonium salts, performed by Mu and co-workers⁶⁸. The scope and radiolabelling conversions are shown.

Mu *et al.* performed density functional theory (DFT) calculations to gain more understanding into the fate of sulfonium salt precursors decorated with substituents of varied activating properties. Having assumed a nucleophilic substitution pathway, the authors compared energies of the transition states arising from [^{18}F]fluoride attack at the *ipso*-position of the substituted ring or the phenyls. Activation barrier for incorporation into an electron-rich ring is higher than for [^{18}F]fluorobenzene formation. It decreases with increasing electron-withdrawing character of the *para*-substituent.

Although triarylsulfonium salts demonstrate great potential, there are synthetic limitations associated with this strategy, such as harsh reagents and reaction conditions. In addition, demonstration of applications to more sophisticated drug-like scaffolds is required.

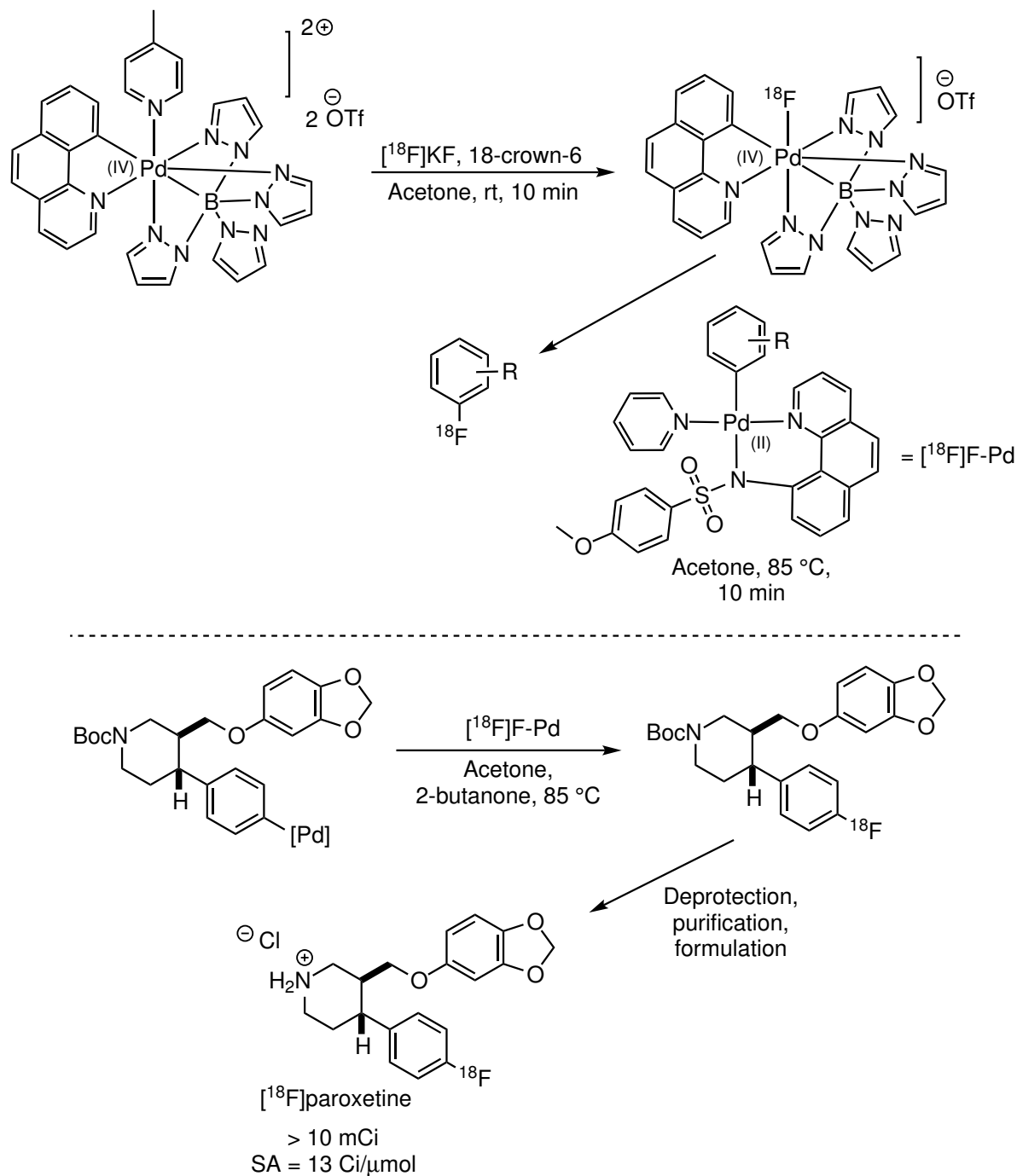
2.3.2 Metal-Mediated ^{18}F -Chemistry

Transition metals have been used widely in [^{18}F]fluorination strategies, owing to their ability to promote carbon-heteroatom bond formation. Palladium- and copper-mediated radiosyntheses have been particularly explored. Although favoured in organic chemistry, metal-catalysis poses health hazards in drug synthesis, and is best avoided for the synthesis of molecules for biomedical purposes, if at all possible¹². This section briefly highlights the most important advances in the area of metal-mediated radiofluorination.

Palladium-Mediated ^{18}F -Chemistry

Palladium involvement in [^{18}F]fluorination has been studied by various researchers in the field, with the generally accepted pathway relying on a Pd(II)/Pd(IV) catalytic cycle⁶. Lee *et al.* proposed a high-oxidation state Pd(IV) complex as a source of electrophilic [^{18}F]fluorine⁶⁹. The uniqueness of this strategy lies in the convenient *in situ* formation of the oxidative palladium- ^{18}F -complex, in which the ^{18}F -species behaves as an electrophile. Reductive elimination results in the release of the [^{18}F]fluorinated product. Starting with nucleophilic [^{18}F]fluoride, it is therefore possible to induce umpolung and access electron-rich [^{18}F]fluorinated aryls without

the use of fluorine gas carrier and consequently, without compromising on specific activity. This strategy requires anhydrous conditions due to the sensitive nature of the Pd core. Radiosynthesis using the palladium(IV)- ^{18}F -complex is shown in Scheme 2.20 (top).

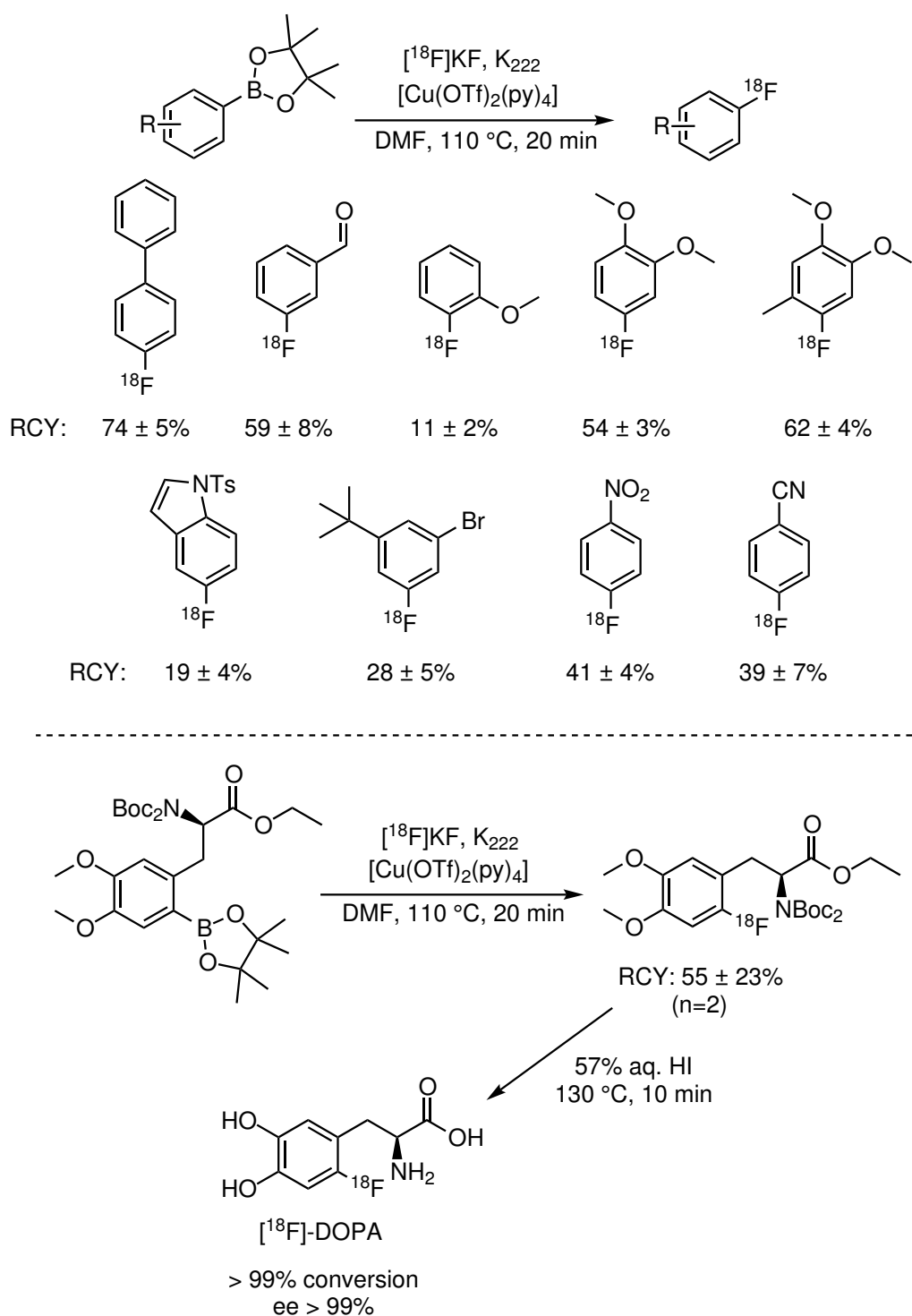


Scheme 2.20: Top: labelling of aryls using Pd(IV) complex, which acts as a source of electrophilic $[^{18}\text{F}]$ fluorine, developed by Lee and co-workers⁶⁹. Bottom: Radiosynthesis of $[^{18}\text{F}]$ paroxetine using the Pd(IV) complex, performed by Kamlet and co-workers⁷⁰.

The aforementioned Pd(IV)-mediated approach was employed by Kamlet *et al.* in the radiosynthesis of [^{18}F]paroxetine, an existing antidepressant medication⁷⁰. The molecule served as a proof-of-concept for the applicability of this strategy to radiolabelling of electron-rich aromatics. The authors did not provide RCYs or RCCs, instead, success of the reaction was measured in units of radioactivity (Ci, in this case) and specific activity (Ci/ μmol) (Scheme 2.20, bottom). Radio-HPLC was used for quality control. Suitable purity was obtained for further biological evaluation in baboons.

Copper-Mediated ^{18}F -Chemistry

Copper-promoted radiolabelling has been studied by numerous researchers worldwide. The Gouverneur group in Oxford has been particularly interested in strategies employing this versatile transition metal. Relying on the previously reported copper(II)-mediated formation of carbon-heteroatom bonds (Chan-Lam reaction) and fluorination of aryl stannanes and trifluoroborates via a copper(II) complex, Tredwell *et al.* proposed a strategy combining the best of both worlds^{71 72 73}. Using approximately 10 mol% loading of a copper pyridine complex, $[\text{Cu}(\text{OTf})_2(\text{py})_4]$, a broad scope of electronically-diverse aromatics was labelled (Scheme 2.21). 4- ^{18}F Fluoro-1,1-biphenyl was formed in an excellent RCY of $74 \pm 5\%$. ^{18}F Fluorination *meta* to a formyl group proceeded in $59 \pm 8\%$ RCY. Lower yields were obtained for substrates with activating substituents *para* to the leaving group ($39 \pm 7\%$ for CN and $41 \pm 4\%$ for NO_2). *N*-tosyl-protected indoles reacted with ^{18}F fluoride in $19 \pm 4\%$ RCY, while placement of a bulky and electron-rich *tert*-butyl and bromide *meta* to the boronic ester afforded the corresponding ^{18}F fluoroaryl in $28 \pm 5\%$ RCY. Substrates with electron-donating groups, such as anisoles, reacted efficiently with $^{18}\text{F}\text{F}^-$. With *ortho*-methoxy substitution, $11 \pm 2\%$ RCY was reached. 3,4-Dianisole reacted with ^{18}F fluoride in $54 \pm 3\%$ RCY. Addition of a methyl substituent *ortho* to the leaving group resulted in an enhanced RCY of $62 \pm 4\%$.

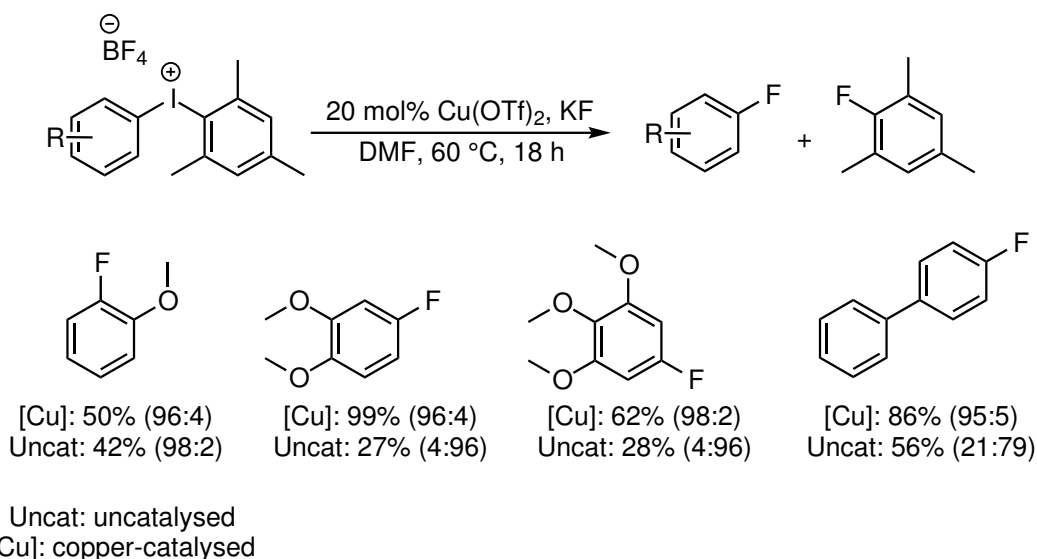


Scheme 2.21: Top: copper-mediated ¹⁸F-labelling of boronic esters. Most of the presented substrates are deactivated and non-activated arenes. RCYs are decay-corrected. Bottom: radiosynthesis of ¹⁸F-L-DOPA, performed by Tredwell and co-workers⁷³.

Tredwell *et al.* applied their strategy to prepare ^{18}F -DOPA, a well-established PET tracer for the imaging of various neurological pathologies, *e.g.* Parkinson's disease, and oncological targets, such as neuroendocrine tumours⁷⁴. Protection of the hydroxyl and amine moieties by methyl ethers and *N,N*-diBoc, respectively, was required. The protected intermediate was labelled enantioselectively in $55 \pm 23\%$ RCY. Subsequent deprotection in aqueous HI afforded ^{18}F -L-DOPA quantitatively. The loading of $[\text{Cu}(\text{OTf})_2(\text{py})_4]$ was increased, however, to 25 mol%. The route is presented in Scheme 2.21 (bottom).

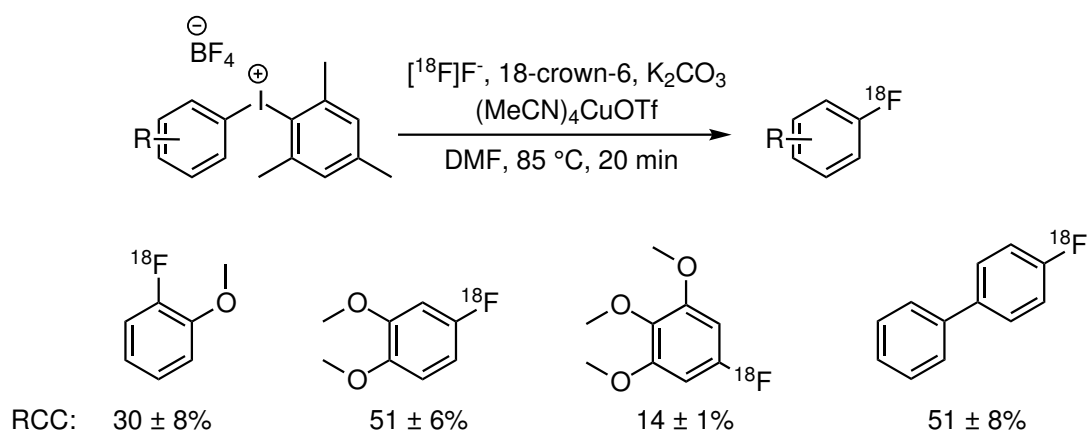
Copper-Assisted Diaryliodonium Salt ^{18}F -Labelling

Inspired by advances in the development of practical diaryliodonium salt chemistry for fluorine incorporation, Ichiishi *et al.* tested the potential impact of copper catalysis on the efficiency of C-F bond formation⁷⁵. Endeavours to facilitate fluorination of aromatic molecules are driven not only by the increasing proportion of fluorine-containing therapeutics, but also the growing demand for elegant solutions for fluorine-18 chemistry. Ichiishi and co-workers employed catalytic copper(II) triflate, in conjunction with KF, to effectuate fluorination of asymmetric diaryliodonium salts. The scope embraced aryls decorated with electron-withdrawing and electron-rich substituents, the latter being of particular interest. Fluorination of mono- to tri-methoxy-substituted phenyls proceeded more efficiently in the presence of copper. Surprisingly, for activated aryls possessing nitrile, carbonyl or methylsulfonyl moieties, fluorination was hampered when assisted by $\text{Cu}(\text{OTf})_2$. The authors complemented their investigation with *in silico* methods to uncover the reaction mechanism. Early findings pointed towards a catalytic cycle, in which Cu(II) is oxidised to Cu(III) by the iodonium salt. Subsequent reductive elimination of the fluorinated aryl was thought to occur via a low-lying transition state. Copper-catalysed transformations investigated by Ichiishi *et al.* are shown in Scheme 2.22.



Scheme 2.22: Copper-catalysed fluorination of diaryliodonium precursors, developed by Ichiishi and co-workers⁷⁵. Representative electron-rich substrates are shown, together with yields with and without Cu-mediation. Ratio of desired product to side-product (2-fluoro-1,3,5-trimethylbenzene) is shown in parentheses.

In the following publication, Ichiishi and co-workers utilised their newly-developed copper-mediated approach to incorporate [¹⁸F]fluoride into aromatic systems⁷⁶. (MeCN)₄CuOTf was found to mediate radiofluorination of anisoles more efficiently. A scope encompassing non-activated and deactivated substrates was incorporated into (mesityl)aryliodonium salts. Radiolabelling conditions and examples of successfully labelled scaffolds are shown in Scheme 2.23.

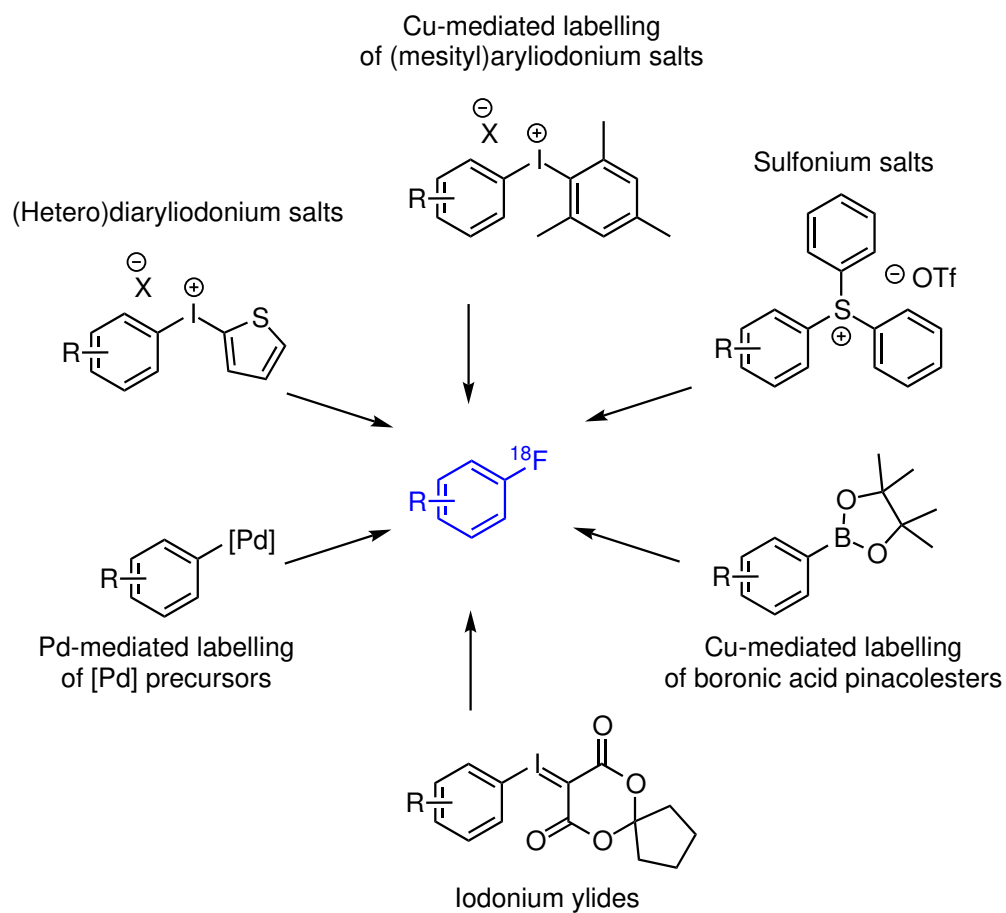


Scheme 2.23: Copper-catalysed [¹⁸F]fluorination of diaryliodonium precursors, performed by Ichiishi and co-workers⁷⁶. Representative electron-rich substrates are shown with RCCs.

2.4 Summary Review of ^{18}F -Labelling Strategies for Aryls

This chapter summarised the most important strategies for ^{18}F -incorporation into drug-like molecules for PET imaging. For aromatic molecules decorated with leaving groups, such as NO_2 or NMe_3^+ , $\text{S}_{\text{N}}2$ substitution usually affords radiolabelled products in good RCYs. Biomolecules, such as proteins and peptides, require intricate handling, hence ^{18}F -based prosthetic groups are used instead of $[^{18}\text{F}]\text{fluoride}$. Conveniently, installation proceeds under mild conditions without affecting sensitive entities. Performing organofluorine chemistry on aromatic scaffolds with $[^{18}\text{F}]\text{F}^-$ is particularly challenging and only scaffolds decorated with strong electron-withdrawing groups in the *ortho*- or *para*-positions react efficiently. Good leaving groups are required. Labelling of electron-rich and electron-neutral scaffolds has, for that reason, remained inaccessible. This, in turn, has hampered clinical manufacture of promising radiopharmaceuticals. A multitude of novel $[^{18}\text{F}]\text{fluorination}$ strategies have emerged in the last decade. Reviews by Preshlock and van den Born provide an extensive outlook on the state-of-the-art radiolabelling technologies, up until mid-2017^{6,32}. The routes presented in Scheme 2.24 were chosen based on their applications to radiolabelling of electron-rich and electron-neutral aromatics. They represent some of the most attractive and practical approaches to date.

One of the main challenges that researchers face is the lack of consistency in reporting experimental findings. This is particularly evident in the field of PET chemistry and radiochemistry. In addition, despite there being a plethora of extensive reviews, a critical perspective is often lacking. Essential information about the way RCYs are established is frequently omitted. Some authors do not discuss limitations of their approach or provide information about potential for GMP production. As a result, it is often difficult to make a fair comparison of the available technologies.



Scheme 2.24: Various strategies for late-stage aromatic [^{18}F]fluorination of electron-neutral and electron-poor scaffolds with [^{18}F]fluoride. Only the most recent or innovative routes are presented. Adapted from van der Born and co-workers³².

The potential of new [^{18}F]fluorination strategies is measured by: 1) RCY and ease of synthesis and purification, 2) precursor stability and 3) specific activity, among others. The method should be broadly applicable, automatable and adaptable to GMP environments⁷⁷.

Metal-based [^{18}F]fluorination is generally disfavoured and metallic residue-directed quality control must be performed to ensure that regulatory limits have been met. Although the emergence of palladium-mediated radiolabelling represents a major advancement in the field, preparation of precursors is challenging and expensive. Palladium complexes are air and moisture sensitive and must be synthesised fresh before each labelling experiment. Moderate RCYs are obtained for electron-rich and electron-neutral precursors.

Copper-mediated [^{18}F]fluorination using boronic esters is perhaps the most attractive strategy among the metal-based routes, however there are severe limitations associated with its use. Firstly, the presence of copper residues must be quantified for every tracer production, which is not only cumbersome and time-consuming, but could also suffer from reproducibility issues. This can be particularly problematic for large scale syntheses. In addition, high precursor loadings are employed (0.02-0.06 mmol \approx 14-40 mg), requiring robust and high yielding preparations⁷⁸. Moderate RCYs were obtained for electron-rich and electron-poor substrates.

Iodine(III)-based radiochemistry employs diaryliodonium salts or iodonium ylides to label scaffolds decorated with electron-donating substituents. Moderate RCYs were obtained with (hetero)aryliodonium salts. Precursors are prone to decomposition and have limited shelf-stability, requiring frequent resynthesis. Harsh reaction conditions ($> 150\text{ }^\circ\text{C}$) are required for their preparation, which poses severe restrictions on the type of scaffolds which can be labelled, particularly with regards to functional and protecting groups. Iodonium salts suffer from regioselectivity issues and the outcome of radiolabelling is often difficult to predict. Purification of undesired radioactive products is often challenging.

On the other hand, iodonium ylides offer a mild route to labelling non-activated aromatics. They address photostability issues of diaryliodonium salts and exhibit enhanced selectivity for [^{18}F]fluorination. Moderate RCYs were generally reported, favouring electron-deficient substrates. Applicability of the strategy to highly-functionalised drug-like molecules was exemplified using [^{18}F]FPEB. Precursors have long shelf-stability, however their preparation is restricted to non-oxidisable functional groups, which might limit practicality of the method in favour of simpler transformations.

Sulfonium salts have also been used as leaving groups in ^{18}F -labelling. The substrate scope investigated by Mu *et al.* was, however, confined to simple deactivated and non-activated [^{18}F]fluoroarenes³²⁶⁸. One of the major limitations lies in poor synthetic access to precursors.

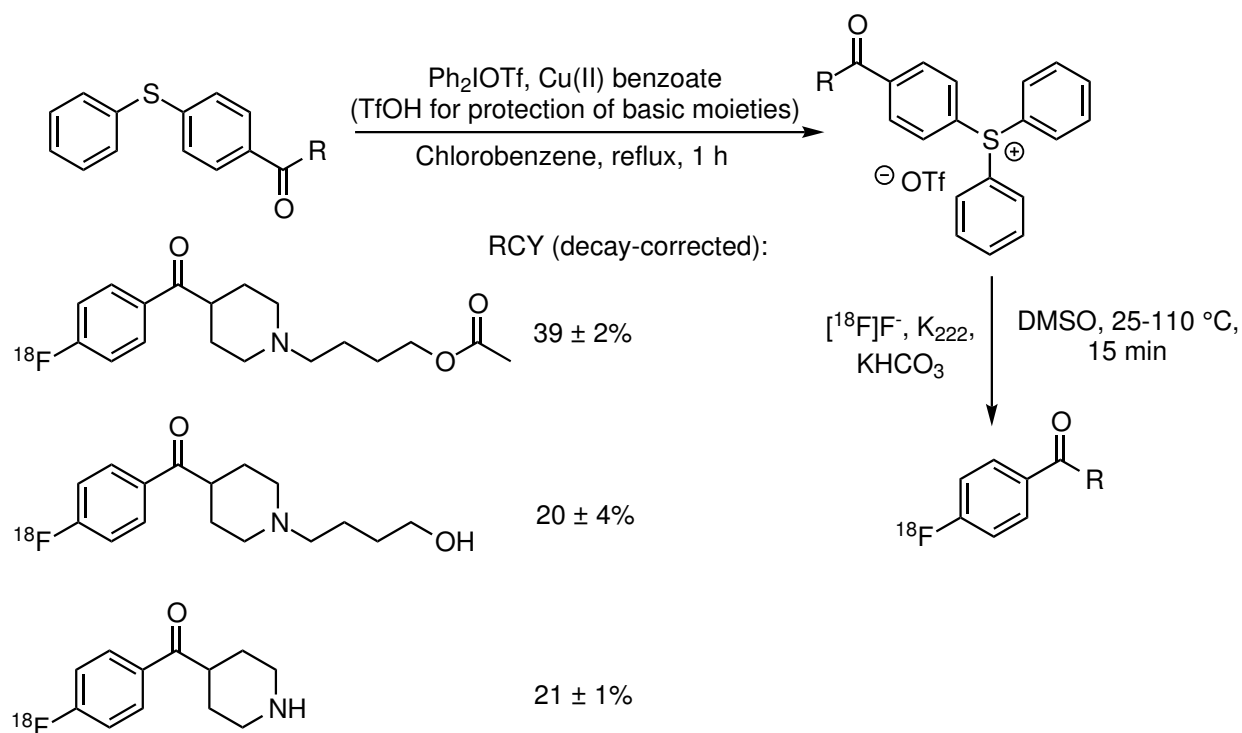
Despite remarkable developments in the field, there is little information about scalability of these methods to GMP environments. Applicability to clinical radiopharmaceutical production is the end goal of PET chemistry research. Novel alternative strategies are very much in demand, however most of the currently adopted protocols still rely on conventional methods, such as the GMP radiosynthesis of ^{18}F -DOPA (Section 2.2.2, Scheme 2.7, page 29). A more flexible platform is needed to access clinically attractive targets and sadly, the scope of robust, automatable and adaptable technologies remains insufficient.

3 | Sulfonium Salts as ^{18}F -Labelling Precursors

3.1 Triarylsulfonium Salts

Building on the pioneering work by Mu *et al.* (Chapter 2, Section 2.3.1, page 39), the Årstad group realised the potential of sulfonium salt chemistry for radiofluorination. Efforts were directed towards exploring the capacity of triarylsulfonium salts to act as leaving groups in radiolabelling, with the focus on non-activated and deactivated aromatic molecules. Mu and co-workers demonstrated that good RCYs can be obtained for [^{18}F]fluorobenzene and simple aromatics decorated with *para*-amide or *para*-halide substituents⁶⁸. The strategy proved inadequate for electron-rich methoxy and methyl groups. Scope elaboration to more sophisticated scaffolds was also required.

Sander *et al.* adopted and optimised the protocol for sulfonium salt synthesis, established by Crivello and Lam, to afford a *para*-ketone functionalised triarylsulfonium salt⁴⁷⁹. The precursors were prepared by coupling of diaryliodonium triflate with appropriate thioethers using copper(II) benzoate catalysis. Ketones substituted with aliphatic amine entities, such as piperidine, were protonated with TfOH prior to addition of the copper salt. Generic sulfonium salt formation reaction and the substrate scope, developed by Sander and co-workers, are shown in Scheme 3.1. Moderate to excellent yields of precursors were obtained in DMSO. Pleasingly, radio-labelling proceeded with satisfactory RCYs at 110 °C, in the presence of unprotected hydroxyl and amine moieties, representing a major breakthrough in nucleophilic [^{18}F]fluorination.



Scheme 3.1: First attempts at the synthesis and labelling of highly-functionalised triarylsulfonium salts, performed by Sander and co-workers⁴.

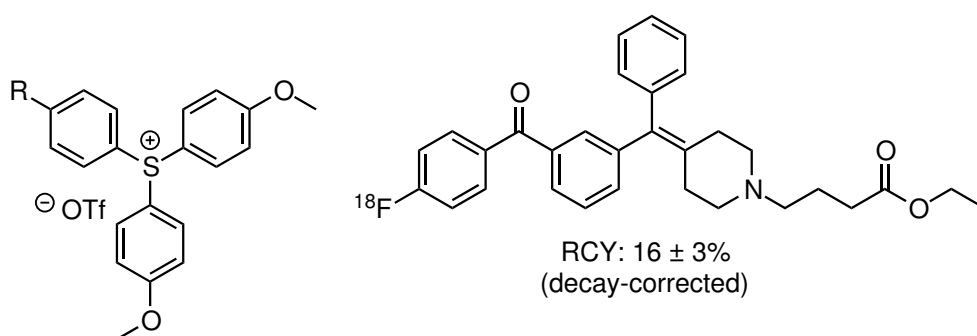


Figure 3.1: Left: optimised triarylsulfonium salt structure with methoxy groups in the *para*-position to the sulfur atom. Right: electron-neutral aromatic system successfully labelled using the optimised scaffold.

Installation of methoxy groups *para* to the sulfur atom of the sulfonium salt scaffold improved radiolabelling of an electron-neutral piperidin-4-ylidene-based scaffold (from 10 ± 1% to 16 ± 3% decay-corrected isolated RCY) by directing [¹⁸F]fluoride to the less electron-dense ring (Figure 3.1). Labelling of other *N*-heterocyclic sulfonium salts using this method is described further in later chapters. [¹⁸F]Fluorination of the pyridine moiety at the 2-position proceeded with excellent RCYs in the range of 68-84% (Chapter 7). An imidazole-decorated substrate underwent ¹⁸F-labelling in

a moderate decay-corrected isolated RCY of $20 \pm 2\%$ (Chapter 8).

Efforts of the Årstad group have opened opportunities for the synthesis of PET radiopharmaceuticals, previously unrealisable by conventional labelling methods. Despite improvements, the synthetic route to triarylsulfonium salts has its limitations. Substrates must be able to withstand high temperatures (up to $125\text{ }^{\circ}\text{C}$), which increases the risk of decomposition and side reactions, *e.g.* polymerisations. Whilst a versatile strategy has been established for electron-deficient systems, nucleophilic [^{18}F]fluorination at electron-rich aromatics still remains a challenge. Consequently, to expand the scope of PET radiotracers, it was essential to develop a new generation sulfonium salt which would complement the existing strategy.

3.2 New Generation Dibenzothiophene Sulfonium Salts

Preparation of challenging radiotracers can be facilitated by a different class of sulfonium salts designed and developed by Dr Thibault Gendron (UCL Radiochemistry, unpublished work). Dibenzothiophene sulfonium salts could address those labelling issues which cannot be solved by the acyclic counterpart (Section 3.1, Figure 3.1). It was speculated that with these structural modifications, it would be possible to expand the scope of ^{18}F -labelled aromatics. A dibenzothiophene sulfonium salt is a tricyclic scaffold, where the central sulfur atom is substituted by the molecular structure of the desired PET radiotracer (Figure 3.2, right). Once the labelling target is incorporated into the generic diaryl thioether scaffold, ring closure results in the formation of the desired sulfonium salt. A small library of diaryl thioether scaffolds was synthesised to elucidate the most appropriate leaving group for ^{18}F -labelling. The lead candidate offered the most favourable combination of: 1) regioselective radiolabelling of a model aromatic system (^{18}F fluorobenzene) and 2) yield of dibenzothiophene formation.

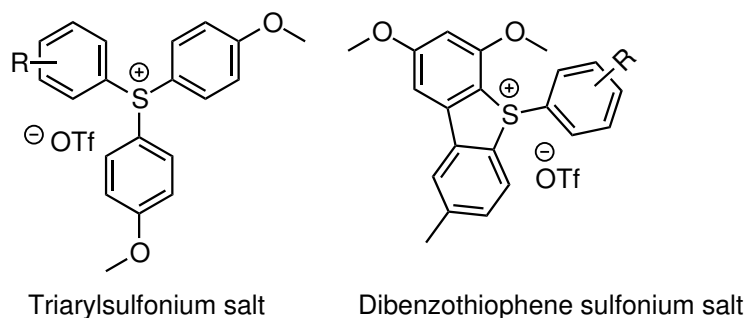
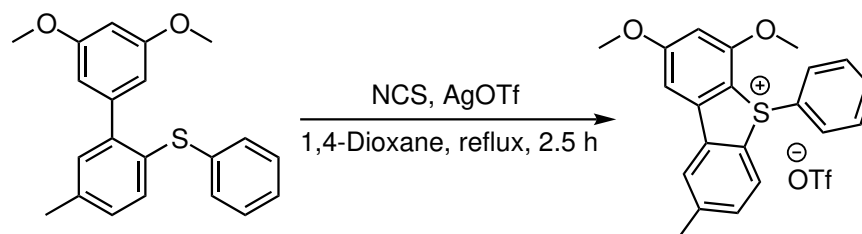


Figure 3.2: Left: triarylsulfonium salts optimised by Sander and co-workers⁴. Right: new generation dibenzothiophene sulfonium salt, developed by Dr Thibault Gendron (unpublished work). Both structures have been designed in the Årstad group (UCL Radiochemistry).

Dibenzothiophene sulfonium salts are accessed from the corresponding diaryl thioethers. Formation of the latter is achieved through a 2-step sequence of Pd-mediated transformations. Protection of the sensitive thiol moiety using an aliphatic thiol surrogate, 2-ethylhexyl 3-mercaptopropionate (Scheme 3.2), is required to avoid palladium catalyst poisoning. The protecting group was designed by Itoh and Mase in an effort to circumvent issues arising from palladium reactivity with standard carbonyl protecting groups, for example in Suzuki-Miyaura couplings⁸⁰. Conveniently, it is commercially available and affordable. The first step of the diaryl thioether synthesis involves installation of the aforementioned alkyl chain into 2-bromo-1-iodo-4-methylbenzene in a Pd-mediated coupling. Using conditions established by Itoh and Mase, the desired thioether can be accessed in quantitative yields using $\text{Pd}_2(\text{dba})_3$ and xantphos (ligand). The next step involves addition of the dimethoxybenzene moiety via Suzuki coupling, employing 3,5-dimethoxyphenylboronic acid and $\text{Pd}(\text{PPh}_3)_4$. The protected diaryl thioether, ready for further functionalisations, can be obtained in 84% yield. The entire synthetic route (Scheme 3.2) is practical and robust on a multigram scale and the protected diaryl entity has potential as a commercial product.

using *N*-chlorosuccinimide (NCS)⁸⁴. Similar intermediates can also be observed in the chlorination of unsymmetrical dialkyl sulfides with NCS, sulfuryl chloride or Cl₂, to afford α -chloro sulfides⁸⁵. Building on the described work, Gendron investigated analogous ring-closing reactions of diaryl thioethers, mediated by an electrophilic chlorine source.

NCS was chosen as the most convenient electrophilic reagent for the cyclisation. It is affordable and easy to handle, as opposed to molecular chlorine or SO₂Cl₂. AgOTf was employed to drive the reaction forward by forming AgCl precipitate, as well as to provide the triflate counterion. Encouragingly, an excellent yield of 79% was obtained with a non-activated model compound in refluxing 1,4-dioxane (Scheme 3.3). Interestingly, both NCS and AgOTf were required for the cyclisation to occur. Dibenzothiophene sulfonium salts can be purified by silica gel flash column chromatography using a DCM/MeOH eluent system. The protocol is straightforward, owing to the large difference in R_f values between the product and the starting material.



Scheme 3.3: Successful cyclisation of a model diaryl thioether mediated by AgOTf and NCS in refluxing 1,4-dioxane. The desired sulfonium salt was accessed in 79% yield.

These observations served as a proof-of-concept and foundations for further investigation. To demonstrate practical applications, the novel strategy required substantial substrate scope elaboration, with the focus on highly-functionalised non-activated and deactivated aromatics.

4 | Project Description: Aims and Objectives

This thesis builds on the knowledge gained in the investigation of sulfonium salts as leaving groups for ^{18}F -labelling, performed by Sander and Gendron of the Årstad group (UCL Radiochemistry).

The aim of this work was to explore the potential of dibenzothiophene sulfonium salts as a technically-simple, robust and versatile method for $[^{18}\text{F}]$ fluorination of highly-functionalised small drug-like molecules. It was evaluated through extension of the substrate scope, encompassing non-activated and deactivated aromatic systems with *N*-heterocyclic moieties. The strategy was exploited to: 1) simplify radiosyntheses of established and existing tracers and improve their radiochemical properties, 2) develop novel and more sophisticated PET tracers.

The potential of dibenzothiophene sulfonium salts as versatile precursors for ^{18}F -labelling was first exemplified using $[^{18}\text{F}]$ FPEB in Chapter 5, in a proof-of-concept radiolabelling, preceded by an optimisation process of sulfonium salt formation. Insights into the cyclisation mechanism are provided in Chapter 6, which describes the quest for a mild and robust reaction system using a simplified phenyl model compound. In Chapter 7 the scope is expanded to simple structures decorated with *N*-heterocycles (indole and pyridines), motifs commonly found in drug molecules and PET tracers. Efforts towards finding a compatible dibenzothiophene formation strategy are described.

Building on these results, Chapters 8 and 9 focus on the practical aspect of dibenzothiophene sulfonium chemistry work and present applications of this method to the synthesis of novel PET tracers for the imaging of aldosterone-producing adenomas

(APAs), one of the main causes of hyperaldosteronism. The scaffold described in Chapter 8 is a phenylimidazole-based small molecule inhibitor of aldosterone synthase. Synthetic challenges associated with formation of the corresponding sulfonium salts are described. Several approaches are also presented in an effort to obtain the desired product, followed by insights into ^{18}F -labelling. Chapter 9 presents an alternative pyridine-based tracer structure for the imaging of APAs. Successful cyclisation to the sulfonium salt, subsequent high-yielding radiolabelling and preliminary biological evaluation are described.

5 | Synthesis of Dibenzothiophene Sulfonium Salt Precursor to [^{18}F]FPEB: Proof-of-Concept

This chapter presents early stages of the research, based on the findings by Sander *et al.*, with insights into new generation dibenzothiophene sulfonium salts provided by Dr Thibault Gendron (UCL Radiochemistry). Successful formation of a cyclic sulfonium salt decorated with a phenyl moiety and subsequent labelling of [^{18}F]fluorobenzene inspired further investigation into their potential as versatile precursors for ^{18}F -labelling of highly-functionalised drug-like molecules. To demonstrate applicability of the method to structurally-sophisticated scaffolds, 3-[^{18}F]fluoro-5-(2-pyridinylolethynyl)benzotrile ([^{18}F]FPEB) was selected as a proof-of-concept molecule. This chapter summarises efforts towards the synthesis of a dibenzothiophene sulfonium salt precursor to [^{18}F]FPEB. Insights into reactivity of the sulfur centre are provided. Subsequent [^{18}F]fluorination allowed for the assessment of practicality and robustness of this strategy to access highly-functionalised deactivated molecules, such as [^{18}F]FPEB.

5.1 [^{18}F]FPEB: PET Tracer for Imaging of mGluR5 Receptor

[^{18}F]FPEB is a promising tracer candidate for the imaging of the metabotropic glutamate receptor 5 (mGluR5), implicated in various neurological pathologies (Figure 5.1). Its clinical applications have been impeded by the lack of efficient ^{18}F -incorporation strategies.

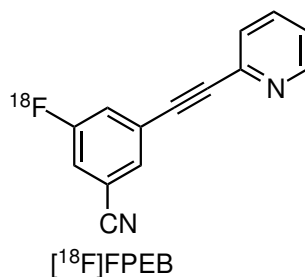


Figure 5.1: [¹⁸F]FPEB is a PET tracer candidate for the imaging of the mGlu5 receptor.

The mGluR5 receptor is a subtype of G-protein coupled mGluR receptors, responsible for signal transmission by glutamate, the key excitatory neurotransmitter in mammals^{86,87}. mGluR5 belongs to class I metabotropic glutamate receptors, which are known to activate phospholipase C - an enzyme responsible for lipid hydrolysis⁸⁸. mGluR5 receptors orchestrate various physiological processes in the brain, *e.g.* signal transduction, neuronal development and growth⁸⁷, dysregulation of which have been implicated in various pathologies, including Parkinson's disease⁸⁹, epilepsy⁹⁰ and amyotrophic lateral sclerosis (ALS)⁹¹. Expressed in various human cancer types, mGluR5 has also been involved in tumour development, *i.e.* glutamate has been shown to promote tumour cell growth⁹².

Design of specific mGluR5 receptor agonists and antagonists proved challenging due to high homology of the glutamate binding site across the mGluR receptor family. It was the development of high-affinity diaryl alkyne mGluR5 ligands (Figure 5.2) that opened up opportunities for PET imaging of the mGluR5 receptor⁹³. Hamill and co-workers radiolabelled promising mGluR5 antagonists and performed *in vitro* and *in vivo* analysis in rhesus monkeys.

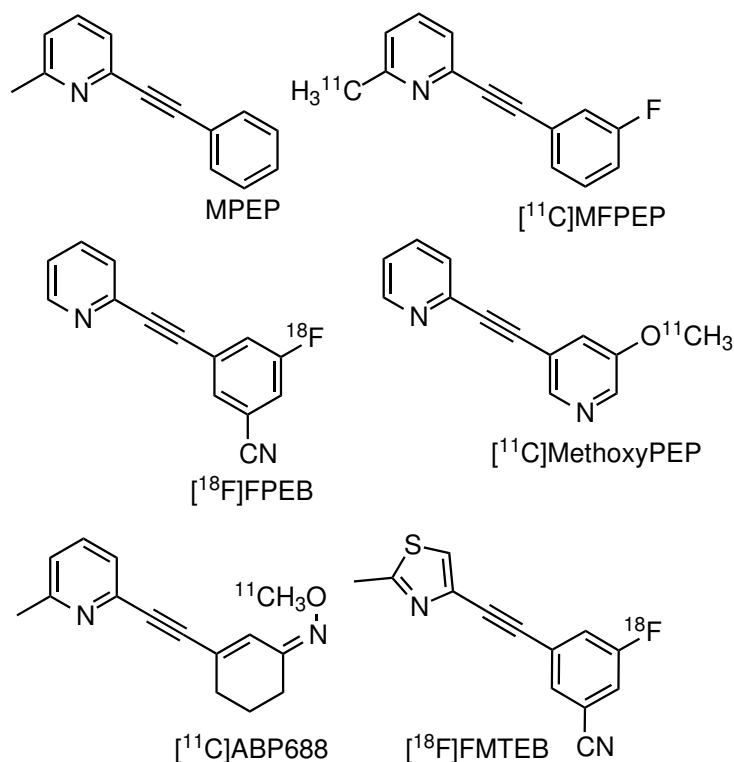
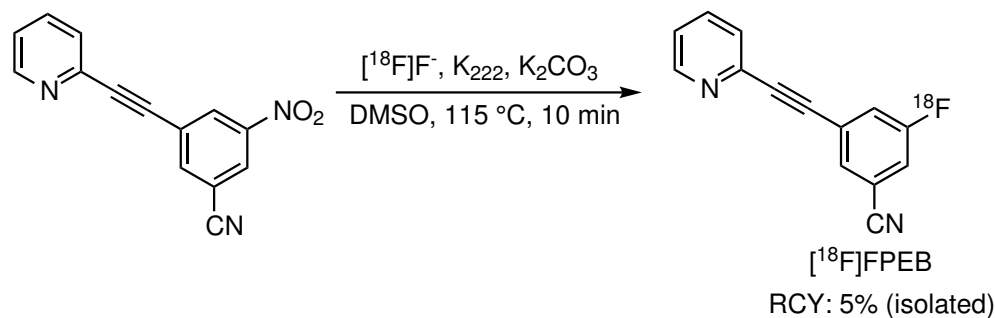


Figure 5.2: Existing mGluR5 ligands labelled with carbon-11 and fluorine-18 for PET studies⁹³.

Conveniently substituted with fluorine, [¹⁸F]FPEB displayed high potency for human mGluR5 ($IC_{50}=0.66$ nM), measured using calcium ion flux assays with glutamate, as well as suitable lipophilicity ($\log P=2.8$)⁹³. PET images in monkeys showed efficient brain-blood-barrier entry and specific signal, with significant uptake in the striatum, where mGluR5 is expressed. In 2013 Wong *et al.* reported the first PET study, in which [¹⁸F]FPEB was administered to healthy human subjects in an effort to establish the whole-body pharmacokinetics. The tracer accumulated in mGluR5-rich locations and was judged safe and tolerable for human use⁹⁴. Pleasingly, lower radiation doses were recorded than for similar scans with [¹⁸F]FDG.

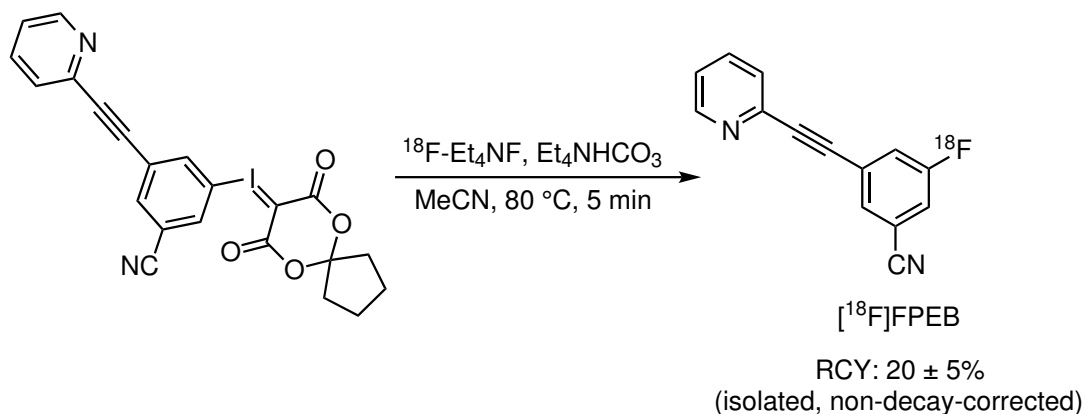
Recently, Felts *et al.* reported a blocking study using [¹⁸F]FPEB in their clinical evaluation of a novel mGluR5 allosteric modulator. Their observations provided further evidence towards potential suitability of the tracer for the imaging of mGluR5, and implications there-of in neurodegenerative diseases and cancer⁹⁵. Unfortunately, routine clinical use of [¹⁸F]FPEB has been impeded by the lack of efficient radiosynthetic routes.

The first ^{18}F -labelling was performed by Wang *et al.* A one-step nucleophilic aromatic substitution using a nitro-precursor (Scheme 5.1) afforded $[^{18}\text{F}]\text{FPEB}$ in a low RCY of 5%⁹⁶. The lack of efficient radiochemical routes has hampered clinical use of $[^{18}\text{F}]\text{FPEB}$.



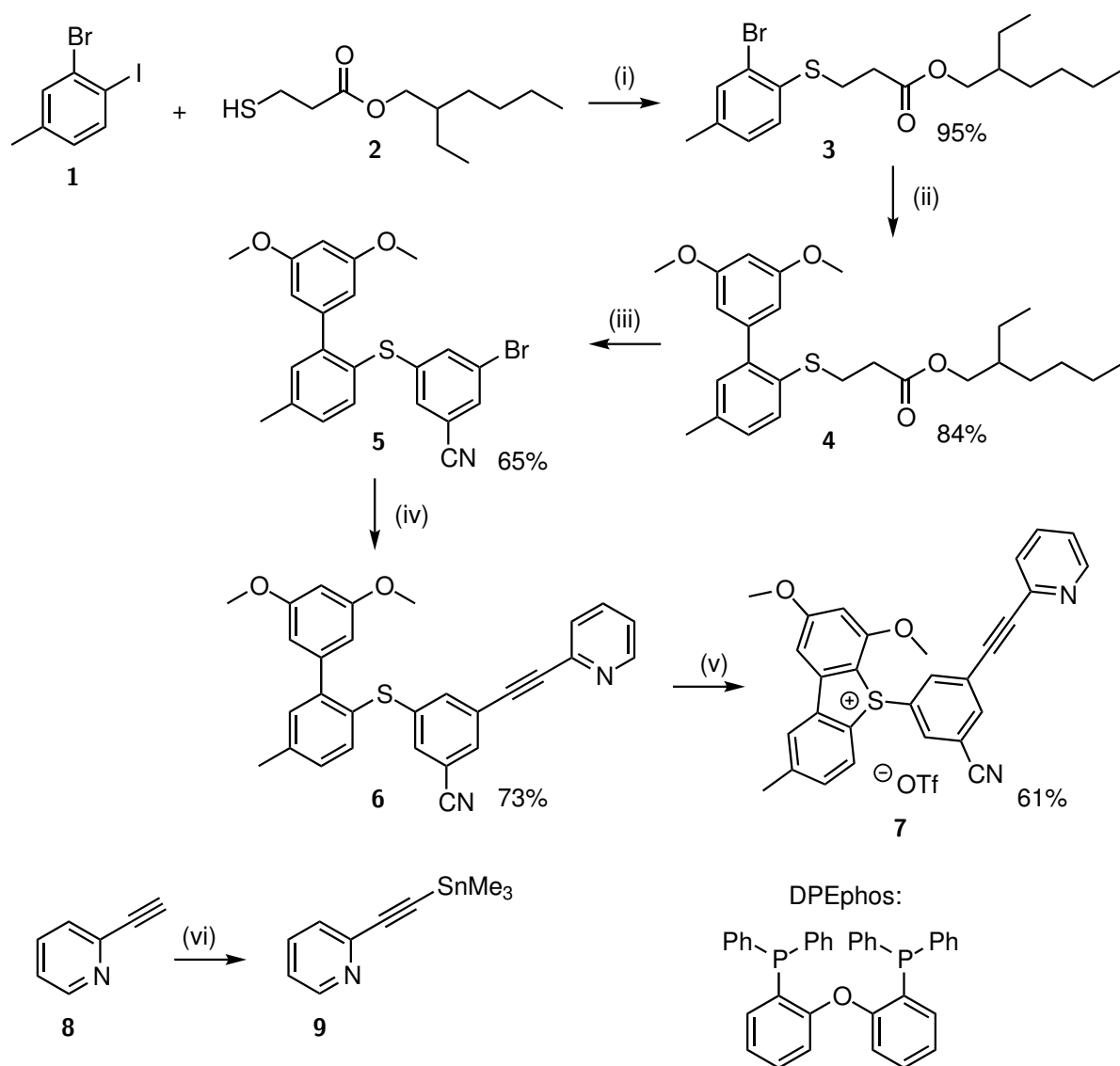
Scheme 5.1: Radiolabelling strategy for $[^{18}\text{F}]\text{FPEB}$, starting from a nitro-substituted precursor, performed by Wang and co-workers⁹⁶. The isolated RCY was 5%.

Radiosynthesis was significantly improved with the emergence of iodonium ylides (Chapter 1, Section 2.3.1, page 38) as precursors for ^{18}F -labelling (Scheme 5.2), developed by Stephenson *et al.*⁶⁵.



Scheme 5.2: Radiolabelling strategy for $[^{18}\text{F}]\text{FPEB}$, starting from an iodonium ylide precursor, developed by Stephenson and co-workers⁶⁵. The isolated non-decay-corrected RCY is 20 ± 5%.

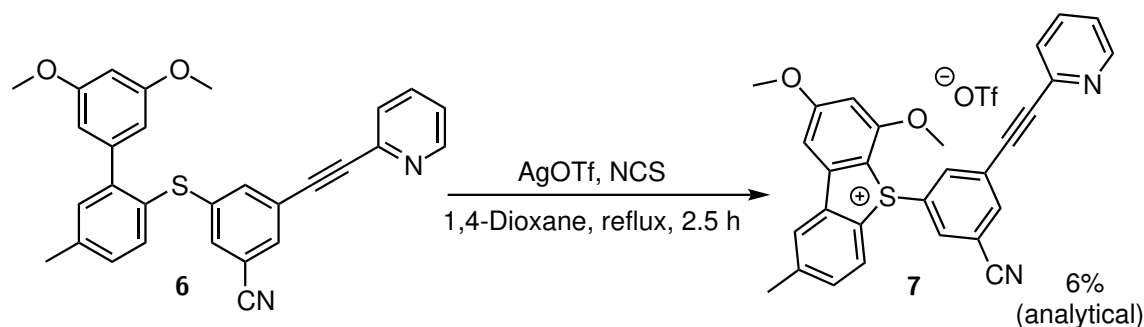
5.1.1 Synthesis of Sulfonium Salt Precursor to [¹⁸F]FPEB



Scheme 5.3: Synthesis of sulfonium salt **7**.

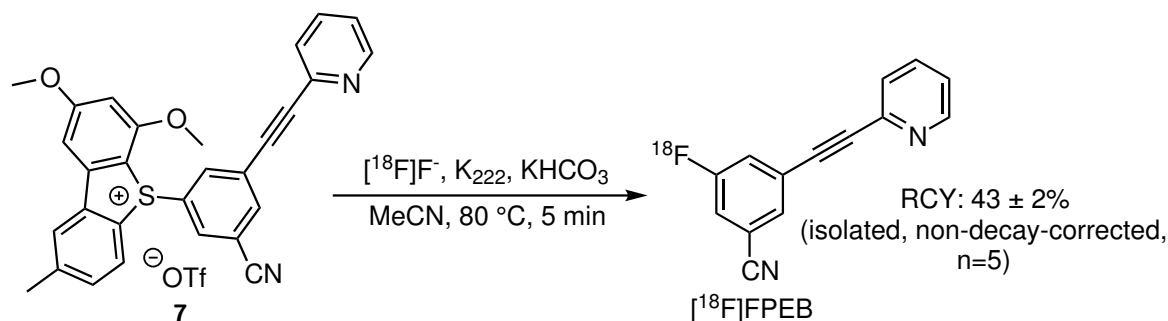
Reagents and conditions: (i) Pd₂(dba)₃, xantphos, Et₃N, toluene, reflux, 4.5 h; (ii) 3,5-Dimethoxyphenylboronic acid, Pd(PPh₃)₄, K₂CO₃, toluene/water, reflux, 5 h; (iii) 3,5-Dibromobenzonitrile, Pd₂(dba)₃, DPEphos, KO^tBu, toluene, reflux, 15 min; (iv) Pyridine **9**, Pd(PPh₃)₄, toluene, reflux, 2 h; (v) Optimisation of cyclisation conditions; (vi) *n*BuLi, Me₃SnCl, -78 °C → rt, 1 h.

Dibenzothiophene sulfonium salt precursor to [^{18}F]FPEB **7** was synthesised from diaryl thioether **4** (Chapter 3, Section 3.2, page 55), which was coupled to 3,5-dibromobenzonitrile in a Pd-mediated transformation with DPEphos as a ligand (Scheme 5.3)⁹⁷. Subsequent Stille coupling to 3-((trimethylstannyl)ethynyl)pyridine afforded thioether precursor **6** in 73% yield. Subsequent treatment with AgOTf and NCS in refluxing 1,4-dioxane (analogously to Scheme 3.3) afforded dibenzothiophene sulfonium salt precursor **7** in only 6% analytical yield (HPLC).



Scheme 5.4: Conditions established by Dr Thibault Gendron were initially used to effectuate formation of product **7**. It was obtained in poor yield.

[^{18}F]Fluorination of precursor **7** (performed by Dr Thibault Gendron) proceeded with an excellent non-corrected isolated RCY of $43 \pm 2\%$ (Scheme 5.5). This was the first experimental application of dibenzothiophene sulfonium salts to the synthesis of a PET tracer. In addition, to the best of my knowledge, this is the highest yielding radiolabelling of [^{18}F]FPEB to date, offering radiosynthetic advantages over the route proposed by Stephenson *et al.* (Scheme 2.17): (i) higher RCY and (ii) lower precursor load ($1.6 \mu\text{mol}$ vs $8 \mu\text{mol}$).



Scheme 5.5: Optimised ^{18}F -labelling of sulfonium salt **7**, carried out by Dr Thibault Gendron. The isolated non-decay-corrected yield ($n=5$) was $43 \pm 2\%$.

With this successful labelling in hand, it was imperative to develop an efficient

cyclisation strategy to increase the potential of dibenzothiophene sulfonium salts as precursors for ^{18}F -labelling. Low cyclisation efficiency renders the synthesis of sulfonium salt **7** impractical.

It was speculated that by increasing sulfur nucleophilicity, formation of the chlorosulfonium intermediate would proceed more readily. The role of Lewis acid in the cyclisation was considered. As demonstrated by Gendron on a simplified phenyl scaffold, both NCS and AgOTf were required for dibenzothiophene formation (Chapter 1, Section 3.2). Non-toxic and inexpensive Lewis acids, commonly employed in synthetic organic transformations, were selected for further investigation. A series of cyclisation experiments was designed, the results of which are presented in Table 5.1.

Table 5.1: Screening of Lewis acids and reaction conditions of the cyclisation reaction to form [^{18}F]FPEB sulfonium salt precursor **7**.

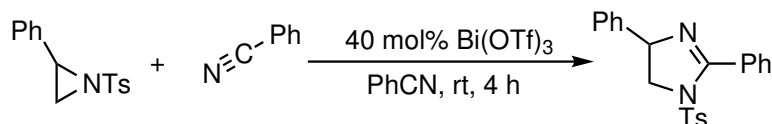
Entry	Lewis Acid	Solvent	Temperature [°C]	Time [h]	Reaction Conditions	Analytical Yield [%]
1	AgOTf	1,4-dioxane	Reflux	2.5	Anhydrous	6%
2	Ag(phen)OTf	1,4-dioxane	Reflux	2.5	Anhydrous	0%
3	La(OTf) ₃	1,4-dioxane	Reflux	2.5	Anhydrous	7%
4	TiCl ₄	1,4-dioxane	Reflux	2.5	Anhydrous	Side product ^a
5	Bi(OTf) ₃	1,4-dioxane	Reflux	2.5	Anhydrous	48%
6	Bi(OTf) ₃	DMF	120	2.5	Anhydrous	7%
7	Bi(OTf) ₃	DCE	Reflux	2.5	Anhydrous	Mixture of products ^b
8	Bi(OTf) ₃	MeCN	Reflux	2.5	Anhydrous	79%
9	Bi(OTf) ₃	MeCN	Reflux	0.5	Anhydrous	76%
10	10 mol% Bi(OTf) ₃	MeCN	Reflux	2.5	Anhydrous	2%
11	Bi(OTf) ₃	MeCN	rt	10 min	Anhydrous	53%
12	Bi(OTf) ₃	MeCN	rt	1	Anhydrous	62%
13	50 mol% Bi(OTf) ₃	MeCN	rt	10 min	Anhydrous	13%
14	Bi(OTf) ₃	MeCN	rt	10 min	Ambient ^c	65%
15 ^d	Bi(OTf) ₃	MeCN	rt	0.5	Ambient	0%
16 ^e	-	MeCN	rt	0.5	Ambient	0%

^a Mixture of products, co-elution on HPLC complicated identification of reaction components. ^b Mono- and dichlorinated sulfonium salts, later confirmed by LC-MS analysis. ^c Ambient refers to non-anhydrous conditions and no air exclusion. ^d Control experiment: no NCS.

^e Control experiment: no Bi(OTf)₃.

Ag(phen)OTf, a phenantroline-based silver complex, has shown superior catalytic properties to AgOTf in various intramolecular transformations⁹⁸. Sadly, no sulfonium salt formation was observed (Table 5.1, Entry 2). La(OTf)₃ performed only slightly better, and sulfonium salt **7** was obtained in 7% yield (Entry 3). Titanium tetrachloride reacted aggressively with thioether **6**, giving rise to a mixture of products. The hygroscopic nature of this reagent makes its handling cumbersome (Entry 4).

The high catalytic potential of bismuth salts in organic synthesis has been highlighted by many researchers in the field. Convenient transformations mediated by bismuth(III) complexes were reported for cyclisation-type reactions, for example Diels-Alder. In many instances, bismuth compounds outperformed the usually high-yielding scandium- or titanium-based catalysts^{99 100}. The recent review by Ondet *et al.* classifies Bi(OTf)₃-mediated cyclisations based on their mode of activation¹⁰¹. Of particular interest is its mode of heteroatom activation. The [3+2]-type cycloaddition of *N*-tosylaziridine and benzonitrile is thought to proceed via activation of aziridine nitrogen by the bismuth centre, resulting in enhancement of electrophilicity (Scheme 5.6). Bi(OTf)₃-mediated carbon-sulfur bond formations, such as sulfonylation of aromatics, were discussed by Leonard and co-workers¹⁰².



Scheme 5.6: Bi(OTf)₃-mediated catalytic imidazoline formation from aziridine and nitrile proceeded quantitatively. Adapted from Ondet and co-workers¹⁰¹.

When stoichiometric Bi(OTf)₃ was employed in the cyclisation reaction of thioether **6**, a significantly enhanced yield of 48% was reported (Table 5.1, Entry 5). To further explore the cyclisation potential of bismuth triflate, a range of high-boiling polar aprotic solvents was screened. Based on the assumption that a solvent with a higher dielectric constant would stabilise the charged transition state better, dichloroethane (DCE), DMF and MeCN were selected (Entries 6, 7 and 8). Although a promising HPLC trace was obtained with DCE, additional LC-MS and NMR analysis revealed the presence of mono- and dichlorinated side products (Figure 5.3). MeCN proved to be the most suitable solvent. Formation of desired sulfonium salt **7** (as the sole

product) proceeded with an excellent analytical yield of 79%. Nearly full consumption of starting material **6** was observed.

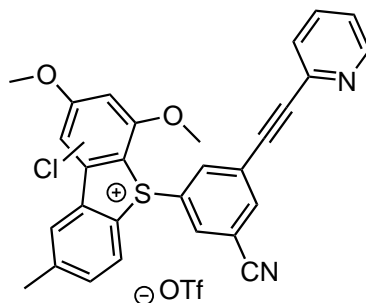


Figure 5.3: Mono and dichlorinated side products identified in the cyclisation reaction in refluxing DCE.

With these excellent results at hand, a kinetic study was performed to investigate (qualitatively) the reaction rate of $\text{Bi}(\text{OTf})_3$ -mediated cyclisations. Aliquots of the reaction mixture in refluxing MeCN were collected at 10, 20, 60, 90, 120 and 150 min and analysed by HPLC. Plotting HPLC conversion versus time revealed that a plateau had been reached between 10 and 30 min (Figure 5.4). An excellent analytical yield of 76% was obtained from a 30 min reaction in MeCN at 90 °C and the product was isolated by flash column chromatography in 68% yield (Table 5.1, Entry 9).

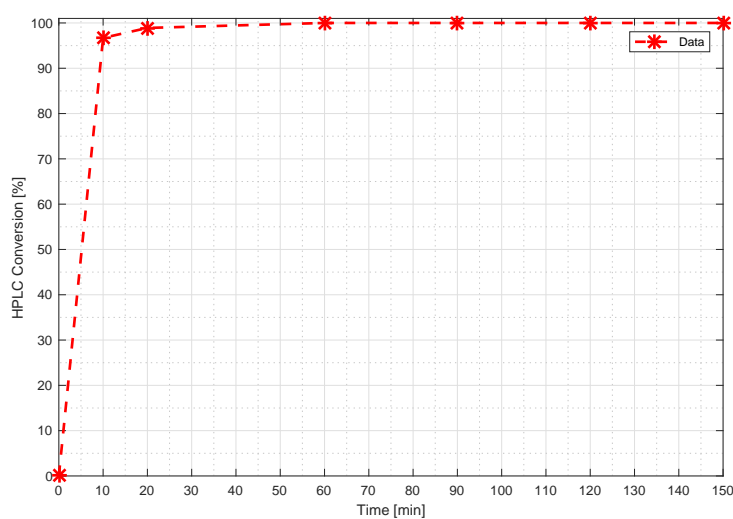


Figure 5.4: Plot of HPLC conversion to product **7** versus time with NCS and $\text{Bi}(\text{OTf})_3$ in refluxing MeCN.

In the next step, the effect of reaction temperature was investigated. An attempt to carry out the transformation at room temperature was met with success. A satisfactory analytical yield of 53% was obtained after 10 min. After 1 h, this increased to 62% (Table 5.1, Entries 11 and 12). Minimum losses occurred during purification of the reaction mixture by flash column chromatography. Precursor **7** was obtained in 61% yield.

In an endeavour to make dibenzothiophene sulfonium salts a competitive ^{18}F -labelling strategy, it was important to consider stoichiometry of $\text{Bi}(\text{OTf})_3$ in the cyclisation. Although bismuth triflate is not considered toxic, attempts were made to reduce its loading, with potential translation to GMP environments in mind. Disappointingly, the reaction proved less efficient when 10 and 50 mol% loadings were used (Table 5.1, Entries 10 and 13). It was therefore elucidated that cyclisation required stoichiometric quantities of the Lewis acid. Conveniently, the reaction also proved insensitive to air and moisture, yielding 65% of sulfonium salt **7** when performed in non-anhydrous MeCN at room temperature (Entry 14). Control experiments confirmed that both NCS and the Lewis acid are required for the reaction to take place (Entries 15 and 16).

5.2 Conclusion

Building on the pioneering work in the Årstad group, the dibenzothiophene sulfonium salt precursor to ^{18}F FPEB was prepared as a proof-of-concept for ^{18}F fluorination of highly-functionalised drug-like molecules.

In the first instance, emphasis was placed on establishing a robust, practical and efficient cyclisation route to ^{18}F FPEB. Several Lewis acids and solvents were screened in an endeavour to obtain sulfonium salt precursor **7**. Best results were obtained with stoichiometric $\text{Bi}(\text{OTf})_3$ and NCS in refluxing MeCN (68% isolated yield). Gratifyingly, the yield was closely reproduced when the reaction was carried out for 1 h at room temperature (61% isolated yield). A practical and robust protocol for the synthesis of sulfonium salt precursors has been developed, which allows to access highly-functionalised drug-like molecules in a rapid one-pot transformation

at room temperature, without the need for air or moisture exclusion. Conveniently, purification of precursor **7** can be performed by silica gel column chromatography, which allows for the isolation of the desired compound as a stable, non-hygroscopic, crystalline solid.

[¹⁸F]Fluorination of sulfonium salt **7** proceeded with an excellent isolated RCY of 43 ±2% (n=5, n.d.c.), representing an improvement on the state-of-art radiosyntheses employing nitro- or iodonium ylide-based leaving groups.

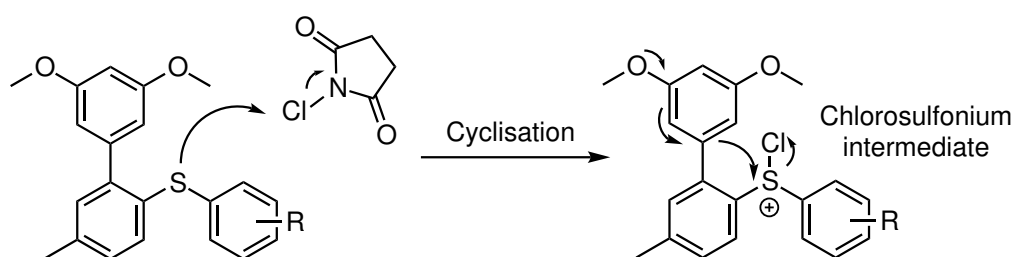
Dibenzothiophene sulfonium salts have the potential to become a practical route for clinical manufacture of [¹⁸F]FPEB. A scope study employing drug-abundant motifs is imperative to further ascertain the practical aspect and robustness of the presented strategy.

6 | Insights into Mechanism of Sulfonium Salt Formation

Building on the innovative work on dibenzothiophene sulfonium salts, this chapter summarises further investigation into the putative reaction mechanism. It was imperative to gain a more in-depth understanding of the factors orchestrating the cyclisation in order to expand the scope of substrates for ^{18}F -labelling. The sulfonium salt precursor to $[^{18}\text{F}]\text{FPEB}$ was initially used as substrate for NMR studies, later to be complemented by a simplified model compound.

6.1 Putative Mechanism of Sulfonium Salt Formation

In the early design stages, Gendron formulated a working hypothesis about the mechanism of dibenzothiophene sulfonium salt formation (Chapter 3, Section 3.2). It was proposed that activation of the nucleophilic sulfur atom by *N*-chlorosuccinimide resulted in the formation of a chlorosulfonium intermediate^{84,85}. It was also thought to be the rate-determining step. Breaking of the S-Cl bond triggered intramolecular cyclisation. This is simplistically illustrated in Scheme 6.1.



Scheme 6.1: Sulfur acts as a nucleophile towards NCS, resulting in the formation of a chlorosulfonium intermediate, which then collapses to generate a dibenzothiophene sulfonium salt.

6.2 Early Mechanistic Study with NMR Spectroscopy

In an effort to probe reaction intermediates, a preliminary mechanistic study was performed using thioether **6** (Figure 6.1), NCS and Bi(OTf)₃ in deuterated MeCN (Figure 6.1).

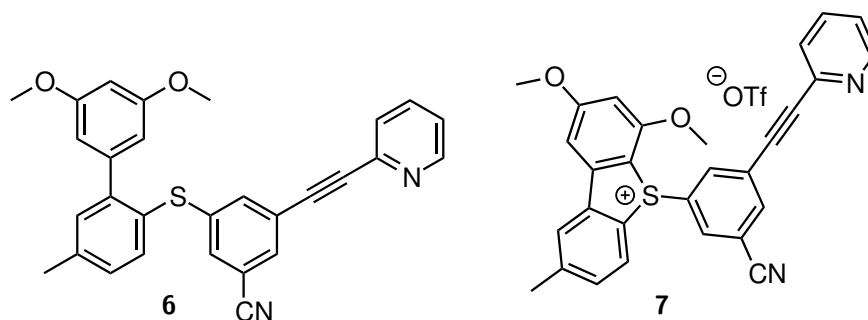


Figure 6.1: Thioether **6** and sulfonium salt precursor to [¹⁸F]FPEB.

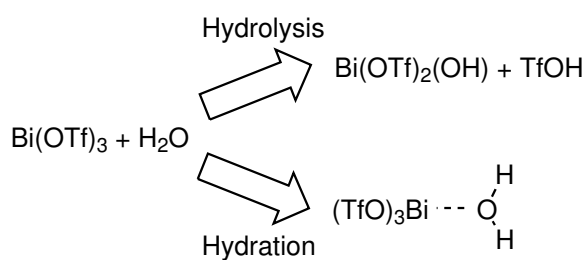
¹H NMR spectra were acquired of the following premixed combinations at room temperature: 1) thioether **6** and Bi(OTf)₃, 2) thioether **6** and NCS and 3) NCS and Bi(OTf)₃. Remarkably, no intermediates were observed in the spectrum of premixed Bi(OTf)₃ and NCS. Similarly, peak shifting/disappearance did not occur for the mixtures of thioether **6** and NCS or Bi(OTf)₃. A prominent triflic acid peak was, however, present in the latter. Various small multiplets were also observed in all Bi(OTf)₃ mixtures. This can be explained by the well-known interaction of TfOH and acetonitrile, resulting in the formation of various aliphatic derivatives¹⁰³. These NMR experiments provide further evidence that both the Lewis acid and the electrophile are required for cyclisation to occur.

The prominent presence of TfOH in the NMR spectra of Bi(OTf)₃ mixtures raised questions about its role in the cyclisation reaction. A small-scale control experiment was set up, in which triflic acid was added to a stirring solution of NCS and thioether **6** in MeCN. Three equivalents of acid were used: 1 equivalent is used to protonate the pyridyl moiety and an excess is available for the transformation. Gratifyingly, complete conversion to sulfonium salt **7** was achieved in merely 5 minutes at room temperature, as judged by TLC analysis. Identity of the product was then confirmed using HPLC. NMR experiments were set up at room temperature and -50 °C, in order to probe intermediate species, however the rate of cyclisation was significantly

faster than the NMR timescale and instantaneous full conversion to product **7** was observed.

6.2.1 NCS/TfOH System for Cyclisation: Formation of Superelectrophilic Species

Thioether **6** did not make a suitable substrate for mechanistic studies using NMR spectroscopy. Cyclisation occurred too rapidly to allow for observation of intermediates. Furthermore, these preliminary NMR studies uncovered that a Lewis acid might not be necessary to effect cyclisation - similar results can be achieved with a Brønsted acid at significantly lower temperatures. In an ongoing debate about the role of the Bi^{III} centre and triflic acid in organic synthesis, the following scenarios were previously outlined by Ondet *et al.* (Scheme 6.2).

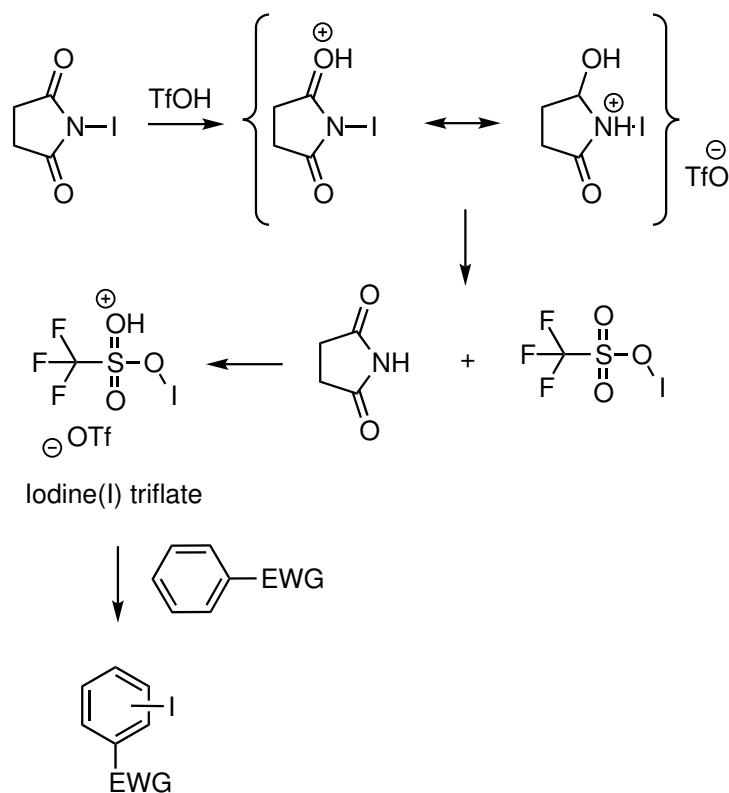


Scheme 6.2: Hydrolysis and hydration of bismuth triflate were identified as possible modes of its interaction with water. Adapted from Ondet and co-workers¹⁰¹.

For reactions catalysed by Bi(OTf)₃, the true catalytic species could be, according to the hydrolysis scenario, triflic acid. This process requires energy. Conversely, hydration is exothermic and the resulting complexation of water to the bismuth centre increases acidity of water protons. Versatility of Bi(OTf)₃ as a catalyst can be ascribed to its oxo- and carbophilic character. Lambert *et al.* carried out Bi(OTf)₃- and TfOH-mediated epoxide rearrangements to elucidate their role in the transformation. Remarkably, filtration and consequent removal of suspended Bi(OTf)₃ solids from the reaction mixtures hindered reaction progress. The authors suggested that TfOH, the true catalytic species in the reaction, was released following association of reagents with bismuth triflate salts. The metal centre was thought to facilitate this transformation, owing to its high Lewis acidity. For bismuth, it is the availability of σ* and d-orbitals, in addition to complexation by electron-withdrawing triflate

residues, which are considered to increase its Lewis acidic character.

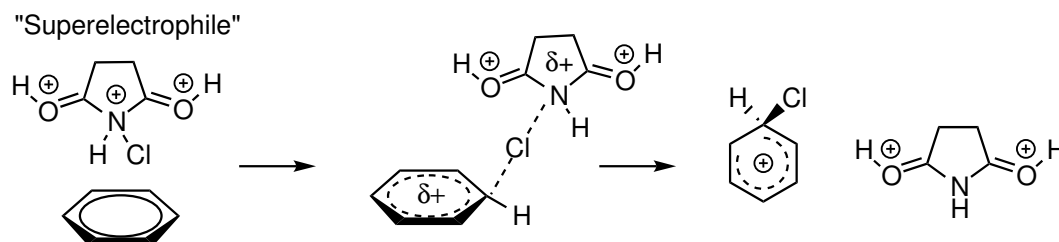
Olah and co-workers investigated the role of triflic acid in iodination reactions of electron-deficient aromatics with *N*-iodosuccinimide¹⁰⁴. Using ¹³C NMR studies of NIS in triflic acid at -20 °C, they speculated that iodine(I) triflate, formed *in situ*, could be the effective superelectrophilic species (Scheme 6.3).



Scheme 6.3: Interaction of NIS with TfOH was proposed to lead to the formation of a powerful superelectrophilic species, iodine(I) triflate, capable of iodinating deactivated aromatics. Scheme adapted from Olah and co-workers¹⁰⁴.

This protosolvated iodinating agent is particularly useful for severely deactivated aromatics, giving significantly higher yields than those reported with NIS and AgOTf at elevated temperatures¹⁰⁵. In their extensive *in silico* investigation, Prakash *et al.* generalised that all *N*-halosuccinimides (Cl, Br, I) are activated in the presence of triflic acid to form multiprotonated superelectrophiles, capable of halogenating aromatic systems decorated with electron-withdrawing substituents¹⁰⁶. The degree of protonation of NCS is directly related to its destabilisation. The release of chlorine(I) species is thought to reduce Coulombic repulsion, originating from the multiplicity of positive charges. This effect is likely to act as a driving force in electrophilic aromatic

chlorination, as depicted in Scheme 6.4. The authors speculated that at high acidities, multiprotonation produces enough Coulombic repulsion to force ring opening and formation of the corresponding acylium ion. Acid pK_a values are considered to be a good measure of reactivity of the superelectrophilic species in aromatic halogenations. Interestingly, Prakash *et al.* observed that deactivated aromatic systems failed to react in the presence of trifluoroacetic acid.



Scheme 6.4: Chlorination of aromatic systems mediated by protonated NCS species, resulting from the interaction of NCS with TfOH. The driving force of the reaction is thought to be extreme charge repulsion, which causes destabilisation and release of "Cl⁺". The true nature of the "superelectrophile" has not been confirmed¹⁰⁶.

The NCS/TfOH reagent pair is extremely efficient at cyclising thioether **6** to the corresponding sulfonium salt **7** (Figure 6.1), however, undesired ring chlorination could also be expected. In fact, the chlorinated counterpart (Figure 6.2) constituted less than 10% of the isolated sample, as elucidated using NMR spectroscopy, HPLC and LC-MS. Furthermore, it was noted that when an NMR tube containing thioether **6**, NCS and TfOH was left overnight, the spectrum obtained thereafter revealed a 50:50 ratio of sulfonium salt **7** to its chlorinated analogue **10**. This was later confirmed by LC-MS and HPLC. Surprisingly, a chlorinated analogue of thioether **6** has never been observed. These findings raised fundamental questions:

1. Could weaker acids promote the cyclisation step?
2. Is acid-free sulfonium salt formation possible?
3. Which factors influence the final product distribution?
4. Can ring chlorination be retarded or eliminated?

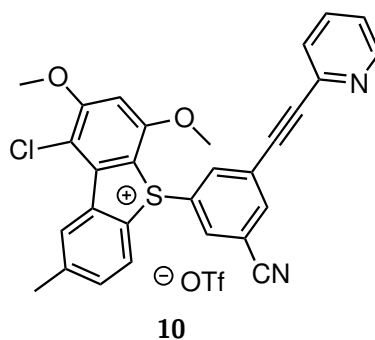
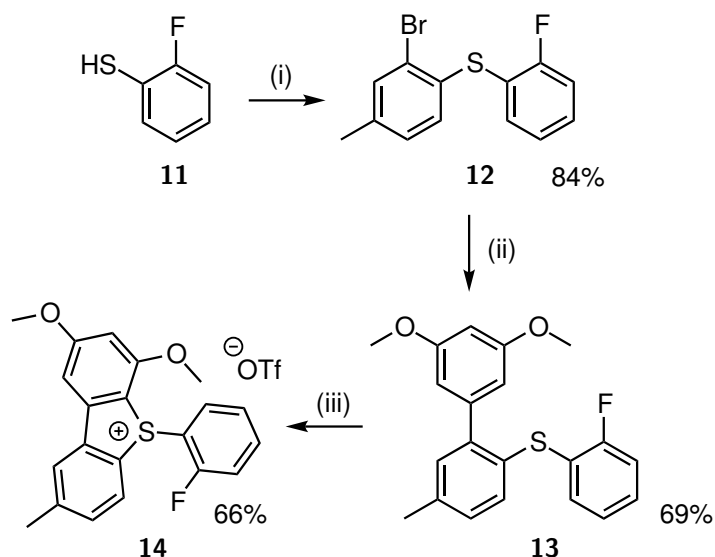


Figure 6.2: The structure of chlorinated sulfonium salt **10**, identified as a minor product in the reactions of **6** with NCS and TfOH/Bi(OTf)₃, was elucidated using proton NMR spectroscopy.

6.3 Design of Model Compound to Investigate Cyclisation Mechanism

To address multiple questions raised during the investigation, a simplified model compound was designed. Although thioether **6** was an interesting substrate for such studies, conversion to sulfonium salt **7** occurred almost instantly, rendering it unsuitable for mechanistic studies using NMR spectroscopy. No intermediates were observed, even at lower NMR operating temperatures (Section 6.2).

It was proposed that the model substrate should possess a fluorine atom, that would allow for additional analysis using ¹⁹F NMR spectroscopy. The advantage of having a fluorine tag is associated with its large spectral window, which eliminates issues of ambiguous peak identities, frequently observed in proton NMR. In addition, protons in close proximity to the fluorine atom display large J_{HF} coupling values and complex splitting patterns. This could perhaps be helpful in identifying intermediates formed in the cyclisation reaction. The position of the fluorine tag was selected based its proximity to the sulfur atom. Fluorine in the *ortho*-position is expected to experience pronounced changes in response to the formation of the chlorosulfonium intermediate. Thioether **13**, shown in Scheme 6.5, is the new substrate in the cyclisation mechanism investigation. It was obtained in 69% yield over two palladium-catalysed steps.



Scheme 6.5: Synthesis of sulfonium salt **14**.

Reagents and conditions: (i) 2-Bromo-1-iodo-4-methylbenzene, $\text{Pd}_2(\text{dba})_3$, DPEphos, $\text{KO}t\text{Bu}$, toluene, reflux, 2 h; (ii) 3,5-Dimethoxyphenylboronic acid, $\text{Pd}(\text{PPh}_3)_4$, K_2CO_3 , toluene/water, reflux, 5 h; (iii) Optimisation of cyclisation conditions.

6.3.1 Expansion of Scope of Cyclisation Reagents: Acids

The presence of strong acid in the cyclisation reaction raised potential incompatibility issues, particularly for dibenzothiophene sulfonium salts decorated with acid-sensitive protecting groups or *N*-heterocycles. The next step involved assessment of weaker Brønsted acids as NCS activators to form the superelectrophilic species advocated by Prakash *et al.* Common laboratory acids were selected based on their $\text{p}K_a$ values. The aim of the investigation was to provide rapid semi-quantitative analysis. Experiments were performed on a small scale (10-50 mg of thioether **13**) and reaction progress was monitored using HPLC and/or LC-MS. Precise analytical yields were of less importance than qualitative conclusions. The results are presented in Table 6.1. A graphical illustration is shown in Figure 6.3.

Table 6.1: The results of a Brønsted acid screen, performed in an effort to increase the practicality of dibenzothiophene sulfonium salt formation. All reactions were carried out with NCS in ambient MeCN, in the presence of NaOTf to provide the triflate counterion. Analytical yields were established using HPLC.

Entry	Acid	pK_a (MeCN) ¹⁰⁷	Product [%]	Starting Material [%]	Side Products [%]
1	Bi(OTf) ₃ ^a	2.6	90	10	0
2	TfOH	2.6	88	8	4 ^b
3	<i>p</i> -TSA	8.0	33	66	1 ^c
4	TFA	12.7	4	96	0
5	Benzoic acid	21.5	0	100	0

^a Source of TfOH. ^b Chlorinated sulfonium salt: 1%. Unknown impurity: 3%.

^c Chlorinated sulfonium salt.

Cyclisation of thioether **13** was attempted using NCS and Bi(OTf)₃ and afforded 90% conversion to sulfonium salt **14** within 10 minutes (Table 6.1, Entry 1). This result was closely reproduced with NCS and TfOH, however, negligible presence of the corresponding chlorinated sulfonium salt was observed (Entry 2). Subsequent flash column chromatography purification afforded sulfonium salt **14** in 66% yield. Both reactions proceeded too rapidly to allow for intermediates to be observed by NMR spectroscopy. In the next attempt, cyclisation was performed with *p*-toluenesulfonic acid (*p*-TSA). *p*-TSA is a solid and more convenient to handle than fuming TfOH. Sadly, only 33% of product **14** was obtained (Entry 3). Both TFA and benzoic acid gave unsatisfactory results (Entries 4 and 5). It can be inferred that efficiency of dibenzothiophene sulfonium salt formation is closely related to the strength of the Brønsted acid. It has been demonstrated that dibenzothiophene sulfonium salt formation can be achieved without the bismuth cation. The use of triflic acid, although less practical, eliminates concerns about trace metal residues in the precursor, paramount for potential GMP compliance of the strategy to the manufacture of, for instance [¹⁸F]FPEB. The optimised route to dibenzothiophene sulfonium salt **14** is shown in Scheme 6.6.

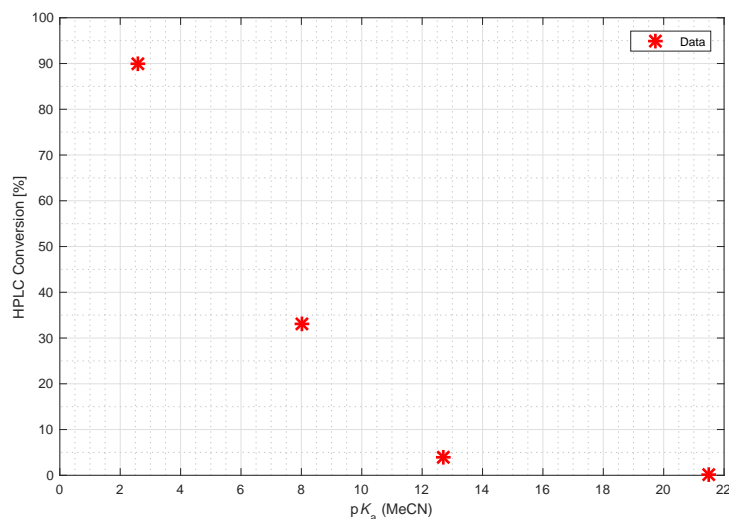
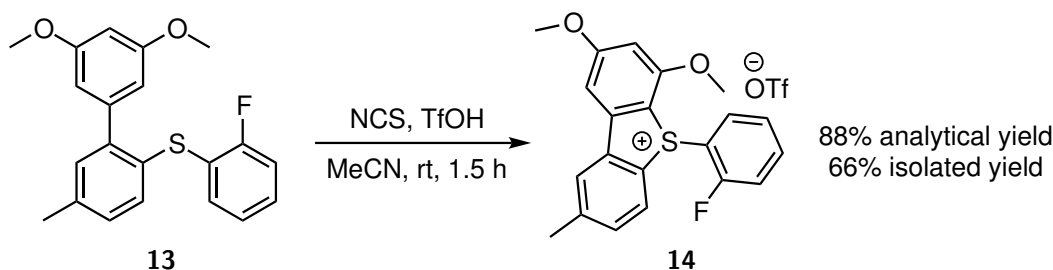


Figure 6.3: Plot of HPLC conversion to sulfonium salt **14** versus pK_a .



Scheme 6.6: Formation of sulfonium salt **14** with TfOH represents a breakthrough step in the optimisation process. The isolated yield was 66%.

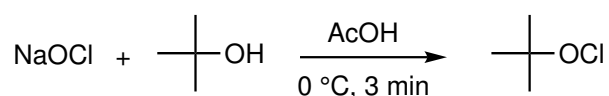
6.3.2 Expansion of Scope of Cyclisation Reagents: Hypochlorites

In a parallel study, the use of alternative reagents to achieve sulfonium salt formation was explored. To implement dibenzothiophene precursors for practical widespread applications, it was imperative to investigate milder chlorinating agents that could overcome the use of strongly acidic TfOH.

It was speculated that hypochlorites could be employed as electrophiles to effectuate ring closure. The range of commercially available hypochlorite reagents is limited. Organic hypochlorites are explosive and hazardous to handle, while most inorganic hypochlorites exist as solutions in water, *e.g.* sodium hypochlorite (bleach). Small-scale reactions of thioether **13** with hypochlorites, as the sole electrophilic reagent,

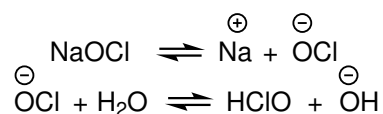
were analysed by HPLC and/or LC-MS.

The first candidate, *t*BuOCl, is a highly reactive organic hypochlorite, commonly employed in chlorination reactions of nitrogenous compounds, *e.g.* benzylamines and *N*-chloramines¹⁰⁸. Interestingly, and perhaps pertinent to the current investigation, *t*BuOCl does not chlorinate anisoles at low temperatures, unless assisted by an acid catalyst¹⁰⁹. It is synthesised using commercial grade bleach, acetic acid and *tert*-butanol (Scheme 6.7). Due to its inherent instability, it was immediately employed in cyclisation reactions. Fresh batches of *t*BuOCl were prepared on every occasion.



Scheme 6.7: Synthesis of *t*BuOCl.

Sodium hypochlorite exists as a mixture of species in water (Scheme 6.8). Bleach can be used to chlorinate phenols under basic conditions¹¹⁰.



Scheme 6.8: Active species in an aqueous solution of sodium hypochlorite.

Calcium hypochlorite is another member of the hypochlorite family, used in organic synthesis as an oxidant and chlorinating agent. Successful aromatic chlorinations mediated by $\text{Ca}(\text{OCl})_2$ were reported for electron-rich substrates at 0 °C in aqueous acetone or AcOH¹¹¹. The results of the hypochlorite investigation with thioether **13** are shown in Table 6.2.

Table 6.2: Hypochlorite-based reagents were screened in an effort to overcome the use of TfOH. All reactions were carried out in non-anhydrous MeCN, in the presence of NaOTf to provide the triflate counterion. Analytical yields were established using HPLC.

Entry	Hypochlorite Reagent	Product [%]	Starting Material [%]	Side Products [%]
1	<i>t</i> BuOCl	48	14	38 ^a
2	NaOCl (< 5%) ^b	76	24	0
3	NaOCl (10-15%) ^c	11	0	89 ^d
4	NaOCl (10-15%) ^e	51	47	2 ^f
5	Ca(OCl) ₂	34	63	3 ^g

^a Chlorinated sulfonium salt: 31%, chlorinated sulfoxides: 7%. ^b Commercial bleach.

^c Reagent grade bleach, used in approximately 25-37 equivalents.

^d Chlorinated sulfonium salt: 76%, chlorinated sulfoxides: 13%.

^e Reagent grade bleach, used in approximately 5-7 equivalents.

^f Chlorinated sulfonium salt: 1%. ^g Unknown impurities.

When thioether **13** was treated with 1 equivalent of *t*BuOCl, 48% conversion to sulfonium salt **14** was observed after 10 minutes. The chlorinated counterpart constituted 31% of the reaction mixture (Table 6.2, Entry 1). A small amount of the starting material was still present in the reaction mixture. In addition, an extra peak appeared on the trace, later to be identified using LC-MS as a mixture of various chlorinated sulfoxide species. Hypochlorites are strong oxidising agents, hence formation of various oxidation forms, such as sulfoxides, is not surprising. In addition, HCl, the by-product of sulfonium salt formation, can react with a hypochlorite ion to generate chlorine gas, thus increasing the chance of competing ring chlorination. It was assumed that by introducing an antioxidant into the reaction mixture, this process could be inhibited. Addition of ascorbic acid did not alter the HPLC profile. Another idea involved addition of *tert*-butanol. It was speculated that the alcohol could act as a trap for chloride ions to prevent their re-oxidation. Unfortunately, no changes in reaction composition were observed. With limited control over *t*BuOCl, the cyclisation was not robust and did not offer any practical advantages over the NCS/TfOH reagent pair.

Commercial bleach (> 5% active chlorine) was employed in a trial cyclisation reaction of thioether **13**. Encouragingly, after 10 min at room temperature, HPLC

analysis revealed 76% analytical yield of sulfonium salt **14**, with no chlorinated side products (Table 6.2, Entry 2). Furthermore, it was observed that the reaction was tolerant of substantial (50%) water content. The investigation was repeated with more concentrated reagent-grade bleach (10-15% available chlorine), which was used in approximately 25-37 fold excess. Sulfonium salt **14** constituted 11% of the reaction mixture, whereas the chlorinated counterpart accounted for nearly 76% (Entry 3). Starting material was consumed after 10 min. Reduction in the amount of NaOCl (5-7 fold excess) had an impact on the rate of chlorination. Conversion to sulfonium salt **14** was reduced to 51% (Entry 4). Disappointingly, attempts to reproduce these results in subsequent experiments were futile. Low reproducibility of aqueous hypochlorite reagents precluded their use in the cyclisation reaction. Despite the shortcomings, it has been demonstrated that dibenzothiophene sulfonium salt formation does not require the use of Brønsted acid. This was a turning point in the investigation, which inspired further efforts to optimise the cyclisation, in the hope to make it a versatile and robust strategy for the synthesis of radiolabelling precursors.

Encouraged by these results, NaOCl was replaced by $\text{Ca}(\text{OCl})_2$. The reagent is sold as a technical-grade solid, with a higher percentage of available chlorine (65%). Similarly to other calcium salts, it is insoluble in organic solvents, with very limited water solubility. Cyclisation of thioether **13** was first attempted with 1 equivalent of $\text{Ca}(\text{OCl})_2$. Gratifyingly, sulfonium salt **14** was obtained, as the sole product, in 34% analytical yield after 10 minutes (Table 6.2, Entry 5). Consequently, attempts were made to optimise this reaction in the hope of enhancing the yield. The results are presented in Table 6.3.

An analogous cyclisation to that of Entry 5 in Table 6.2 was set up. A 30 min reaction of thioether **13** with 1 equivalent of $\text{Ca}(\text{OCl})_2$ at room temperature afforded the desired sulfonium salt in 30% analytical yield. The reaction was shown to reach a plateau after 1 h (Table 6.3, Entries 1 and 2). It was proposed that better conversions could perhaps be obtained on increasing $\text{Ca}(\text{OCl})_2$ solubility. According to Le Châtelier's principle - if more hypochlorite reacts with the thioether, more will dissolve in MeCN. The impact of methanol as a solvent was tested, but only

a poor conversion of 8% was observed (Entry 3). The reaction proceeded slowly in 10% water/acetonitrile. Slow eluting impurities were observed in all described experiments. It was proposed that addition of water increases solubility of $\text{Ca}(\text{OCl})_2$ and in turn, hydrolysis to $\text{Ca}(\text{OH})_2$. Hydroxide could act as a nucleophile and cause ring opening of the newly-formed sulfonium salt (Entry 4). Increasing the number of equivalents of $\text{Ca}(\text{OCl})_2$ or sonication had little effect on the rate of cyclisation (Entries 5, 6 and 7).

Table 6.3: Further optimisation of cyclisation conditions using CaOCl_2 . All reactions were carried out in MeCN (unless stated otherwise) in the presence of NaOTf to provide the triflate counterion. Analytical yields were established using HPLC.

Entry	Time [min]	Product [%]	Starting Material [%]	Side Products [%]	Comments
1	30	20	78	2	New reaction ^a
2	60	19	78	3	Reaction mixture from Entry 1
3	10	8	82	10	In MeOH
4	10	1	89	10	In 9:1 MeCN:H ₂ O ^b
5	10	4	91	5	2 eq of $\text{Ca}(\text{OCl})_2$ with sonication ^c
6	60	10	87	3	Reaction mixture from Entry 5
7	10	19	78	3	10 eq of $\text{Ca}(\text{OCl})_2$ with sonication ^c

^a Analogous to Table 6.2, Entry 5, but stirred for 30 min. ^b Cloudy reaction mixture.

^c The reaction vessel was placed in an ultrasound bath.

$\text{Ca}(\text{OCl})_2$ offers certain advantages over other hypochlorite reagents: 1) ease of handling and 2) reduction of chlorinated sulfonium salt formation. Nevertheless, the use of $\text{Ca}(\text{OCl})_2$ significantly reduced reactivity of thioether **13**, and the desired product was obtained in low analytical yields. Increasing the solubility of $\text{Ca}(\text{OCl})_2$ in MeCN could address this issue. Further optimisation could include the use of an appropriate buffer for maintaining neutral pH in order to limit base-mediated ring opening of the dibenzothiophene ring. Although hypochlorite-mediated cyclisations showed limited practicality, the results constituted an advancement in sulfonium salt chemistry for the Årstad group. With further refinement, $\text{Ca}(\text{OCl})_2$ -mediated cyclisations could be rendered broadly applicable to a wider scope of substrates,

particularly for those with acid-sensitive moieties.

6.3.3 Expansion of Scope of Cyclisation Reagents: Alternative Chlorine Sources

Cyclisation of thioether **13** was also attempted with alternative reagents: 1) tungsten hexachloride and 2) sulfuryl chloride. WCl_6 was found to promote ring expansion-chlorination reactions of 1,3-dithiolanes and 1,3-dithanes¹¹². When employed in the cyclisation reaction with thioether **13** in non-anhydrous MeCN, in the presence of triethylamine and sodium triflate, a low analytical yield of 16% was obtained after 10 min. Sulfuryl chloride is another source of electrophilic chlorine and easier to handle than Cl_2 . Remarkably, nearly quantitative conversion to sulfonium salt **14** was observed after 10 min. Unfortunately, the ratio of sulfonium salt **14** to its chlorinated analogue could not be elucidated, owing to co-elution on the HPLC. Despite promoting fast product formation, reactivity of sulfuryl chloride is difficult to control. Significant side product formation, hygroscopicity and instability preclude its use as a practical reagent in dibenzothiophene sulfonium salt formation.

6.4 Conclusion

In this investigation insights into the cyclisation mechanism were presented. Synthetic route towards the sulfonium salt precursor to [^{18}F]FPEB and the simplified model compound was explored with alternative chlorinating reagents.

TfOH activation of NCS has been shown to promote dibenzothiophene sulfonium formation in an efficient and robust manner. The highly acidic nature of the reaction has inherent limitations. Compatibility issues can be expected for acid-labile protecting groups or other acid-sensitive moieties, *e.g.* *N*-heterocycles. Functionalities protonated during the cyclisation must be deprotonated before ^{18}F -labelling to avoid [^{18}F]fluoride deactivation. The NCS/ $Bi(OTf)_3$ reagent pair works in an analogous manner to NCS/TfOH. $Bi(OTf)_3$ acts as a source of Brønsted acid (in the presence of moisture), believed to promote formation of a superelectrophile with NCS. The strength of the acid affects reactivity of the multiprotonated NCS species. Conversion to the desired sulfonium salt increases as pK_a decreases. Disappointingly, the range

of useful pK_a values is narrow and cyclisation is significantly less efficient with weaker acids, such as *p*-TSA or TFA.

Hypochlorite reagents, *t*BuOCl, NaOCl and Ca(OCl)₂, all promote dibenzothiophene sulfonium salt formation at room temperature. They have limited shelf-stability and reproducibility issues were faced throughout. Calcium hypochlorite is a promising cyclisation reagent, however it was thought that low solubility in MeCN hampered its reactivity towards the *S*-centre.

Chlorination of the electron-rich methoxy-substituted ring could become problematic on scope expansion. Understanding and appreciation of the factors which orchestrate side product formation is essential.

7 | Expansion of Structural Scope of Sulfonium Salts for ^{18}F -Labelling

The main challenge of sulfonium salt chemistry for ^{18}F -labelling lies in the inherent reactivity conflict of the sulfur centre towards: 1) electrophilic chlorine, during the cyclisation reaction and 2) nucleophilic [^{18}F]fluoride, during radiolabelling.

The study into the cyclisation mechanism and cyclisation reagents, presented in the previous chapter, deepened our understanding of the factors that influence sulfonium salt formation. The best reagent pair, NCS in conjunction with $\text{Bi}(\text{OTf})_3$ or TfOH , proved extremely effective at mediating dibenzothiophene sulfonium salt formation. In comparison to triflic acid, bismuth triflate presents a more controlled and practical source of Brønsted acid. The presence of strongly acidic reaction environment is perhaps most concerning when it comes to assessing the applicability and limitations of the system with respect to acid-sensitive entities, for instance *N*-heterocycles.

This chapter describes efforts towards evaluation of *N*-heterocycles as substrates for ^{18}F -labelling with dibenzothiophene sulfonium salt precursors. Sulfonium salts bearing indole and *ortho*- and *meta*-pyridyl moieties were prepared. The choice was dictated by their: 1) complex reactivities towards electrophiles and nucleophiles and 2) increasing presence in PET tracers and drug-like molecules.

7.1 ^{18}F -AMT: PET Tracer for Imaging Tryptophan Metabolism

Indoles are commonly found in biologically active molecules and therapeutics¹¹³. They can participate in both nucleophilic and electrophilic transformations, however, it is the former that have been more thoroughly investigated¹¹⁴. The indole motif is found in tryptophan (Trp), one of the 22 essential amino acids. In addition to

being a building block in the synthesis of proteins, tryptophan serves as a substrate for two metabolic pathways: 1) serotonin and 2) kynurenine (Figure 7.2, page 88). Palego *et al.*, along with other researchers, reported that impairment of tryptophan homeostasis has been linked to pathologies of the immune and central nervous systems¹¹⁵. A carbon-11 analogue of tryptophan, α -methyl-L-tryptophan (AMT), has been used as a PET tracer for the imaging of both metabolic pathways (Figure 7.1). Conveniently, AMT cannot be incorporated into proteins.

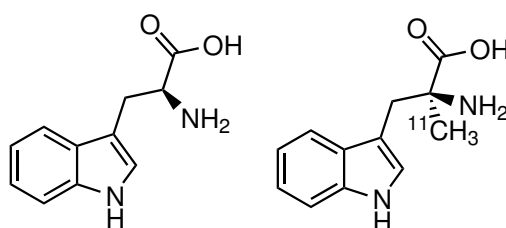


Figure 7.1: The structures of tryptophan and AMT.

The metabolic fate of tryptophan is depicted in Figure 7.2. The serotonin pathway, implicated in neurotransmission and insulin secretion, begins with hydroxylation of the Trp benzene ring by tryptophan hydroxylase (TPH), followed by decarboxylation^{116 117 118}. Studies in the 1990s, performed by Diksic, utilised AMT to measure brain serotonin production in rats and dogs^{119 120}. AMT metabolism follows that of Trp, with the end product being α -methylserotonin (α -M5HT) which, unlike serotonin, is not a substrate for monoamine oxidase (MAO), so it is accumulated in serotonergic cell bodies, making it a suitable tool for PET¹¹⁷. Encouraged by autoradiography results that allowed calculation of the rates of α -methylserotonin synthesis in rat brains, Diksic extended their investigation to dogs with elevated plasma Trp levels. PET was utilised to measure brain serotonin levels. Consistent with expectations, an increase in serotonin synthesis was observed. Diksic *et al.* advocated applicability of the method for PET imaging of the human brain. Of particular interest is the implication of serotonin in epilepsy - the link between the two has been highlighted by several researchers^{121 122 123}. Interestingly, further exploration of AMT in PET revealed increased uptake of AMT in epileptogenic tubers in patients with tuberous sclerosis, a genetic condition which frequently leads to the development of epilepsy. It develops through formation of benign hamartomas, for example in the brain^{118 121}. Kumar *et al.* further ascertained the imaging properties of AMT with regards to

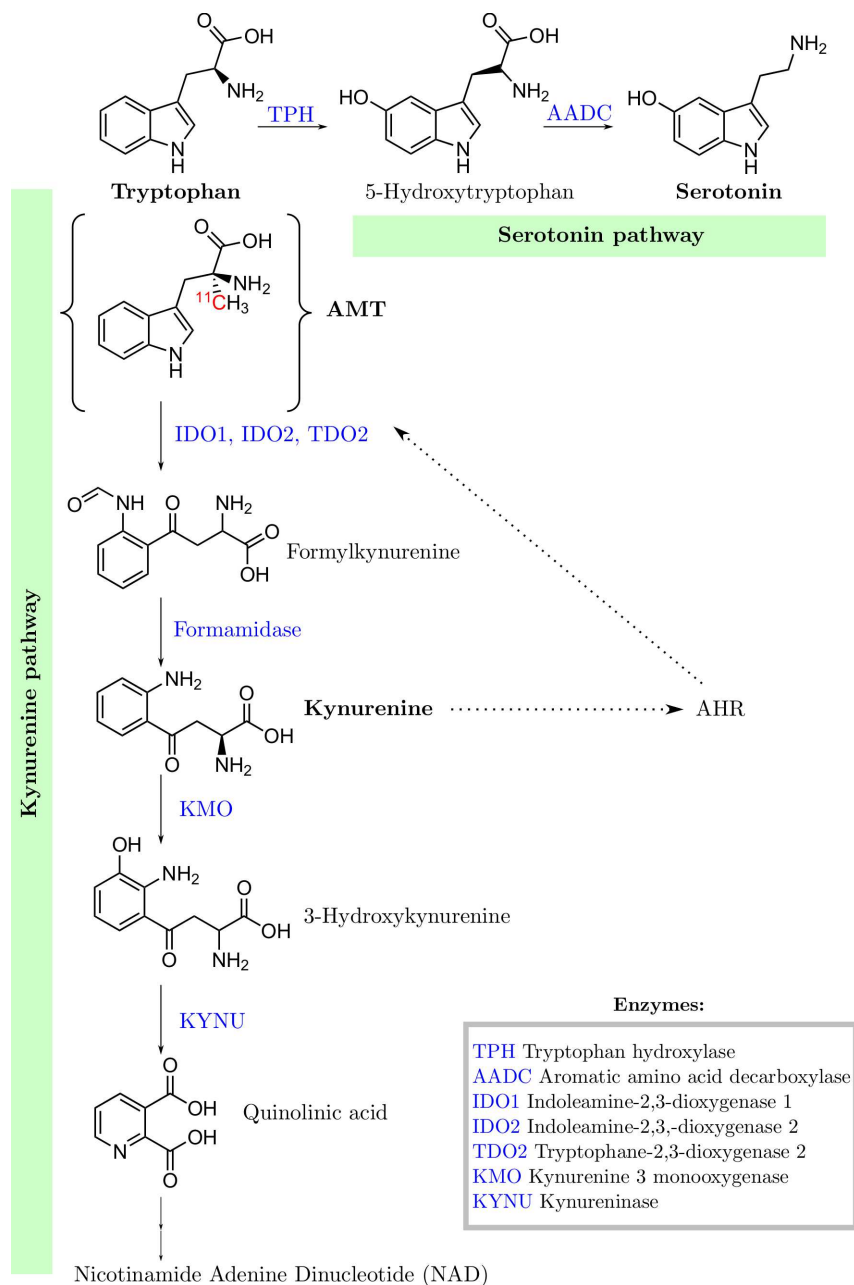


Figure 7.2: Tryptophan: the simplified kynurenine and serotonin pathways, with structures of metabolites. AMT is metabolised in the same way as Trp. Enzymes are marked in blue. Adapted from Guastella *et al.* and Chugani^{116 117}.

epileptogenic brain by comparing it against a PET gold standard, [^{18}F]FDG, and MRI imaging. Both provide useful information about: hypometabolism (PET) or anatomical detail of tubers (MRI), however only AMT allows epileptogenic and nonepileptogenic tubers to be distinguished¹²⁴.

The alternative metabolic pathway of tryptophan is orchestrated by indoleamine 2,3-dioxygenase (IDO), and is referred to as the kynurenine pathway (Figure 7.2). According to Peters, it accounts for over 95% of Trp metabolism¹²⁵. Tryptophan is a substrate for IDO1, IDO2 and TDO2 (all are dioxygenase enzymes), which catalyse formation of *N*-formylkynurenine, followed by kynurenine and other toxic downstream metabolites. Many publications have been devoted to implications of kynurenine imbalance in various pathologies, *e.g.* Alzheimer's disease, epilepsy and inflammation. Efforts have been directed towards investigating IDO1 expression and its links to the aforementioned disease states. IDO1 is expressed in many organs, including the brain, where it is produced by various cell types (dendritic cells, monocytes, macrophages, *etc.*), as well as tumours. Dounay *et al.* expressed interest in utilising IDO1 as a therapeutic for cancer and immunosuppressive disorders, calling it a "gatekeeper" enzyme¹²⁶. IDO1 is involved in the defence mechanism against pathogen infections through mopping up tryptophan and subsequently handicapping protein synthesis channels, yet simultaneously impeding the host's immune system. Two mechanisms of action have been proposed: 1) tryptophan concentration is reduced by IDO1, affecting proliferation in cells and promoting apoptosis and 2) increased IDO1 activity triggers enhanced downstream synthesis of toxic kynurenines. T-lymphocytes have been shown to respond to increased IDO1 levels. Fox *et al.* studied the response of T-cells to influenza virus, which acts by upregulating IDO levels in the host, leading to tryptophan depletion and loss of immunity¹²⁷. Kynurenine, 3-hydroxykynurenine, 3-hydroxyanthranilic and quinolinic acid are neurotoxic and changes in the concentration of these intermediates have been implicated in various immune system disorders¹²⁷. They have been shown to disrupt T-cell functioning and promote apoptosis¹²⁸.

Disruption of the kynurenine pathway has been implicated in various pathologies.

Recent publications describe involvement of dysregulated T-cell response in various cancer forms, *e.g.* melanoma and glioma^{116 129}. It has been hypothesised that IDO expression in cancer cells leads to a local depletion of tryptophan and consequent impediment of T-lymphocytes and increased concentration of toxic kynurenines¹³⁰. Although evidence is currently insufficient, it is thought that excessive presence of kynurenine metabolites in the brain, particularly 3-hydroxykynurenine and quinolinic acid, leads to neuronal degeneration¹³¹. AMT has also been employed to image the kynurenine pathway via monitoring of IDO activity to provide insights into cancer immunotherapy response.

The main limitation of ¹¹C-labelled AMT is the short half-life of carbon-11, limiting its clinical availability. Recent publications highlight the growing potential of [¹⁸F]fluorinated AMT analogues in tryptophan imaging (Figure 7.3).

Xin and Cai optimised radiolabelling of two enantiomers of [¹⁸F]FETrp (Figure 7.3, (a), left) and demonstrated potential use of the L-form as a PET tracer. Favourable uptake was seen in breast cancer cells, while significant reduction occurred in the presence of NLG919 (Figure 7.3, (a), right), an IDO inhibitor¹³². *Ex vivo* findings were consistent with PET imaging results. Michelhaugh *et al.* assessed [¹⁸F]FETrp using patient-derived brain tumour xenografts in mice with regards to tumour uptake against the ¹¹C-analogue¹³³. Higher standardised uptake value was obtained for the investigated cancer types, glioblastoma and metastasised brain tumours (lung and breast cancer), for the [¹⁸F]fluorinated counterpart, further ascertaining its potential for the imaging of tryptophan metabolism in cancer.

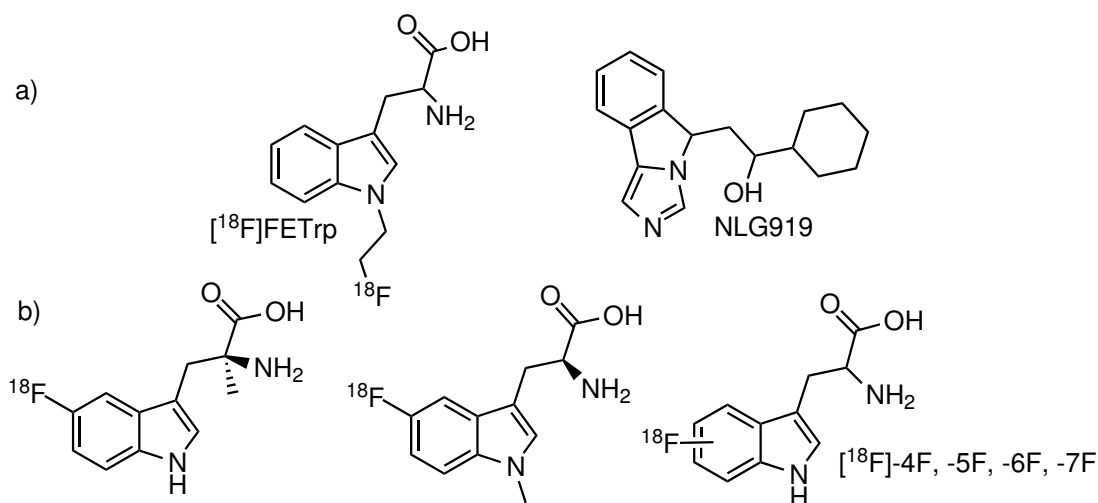
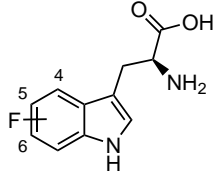


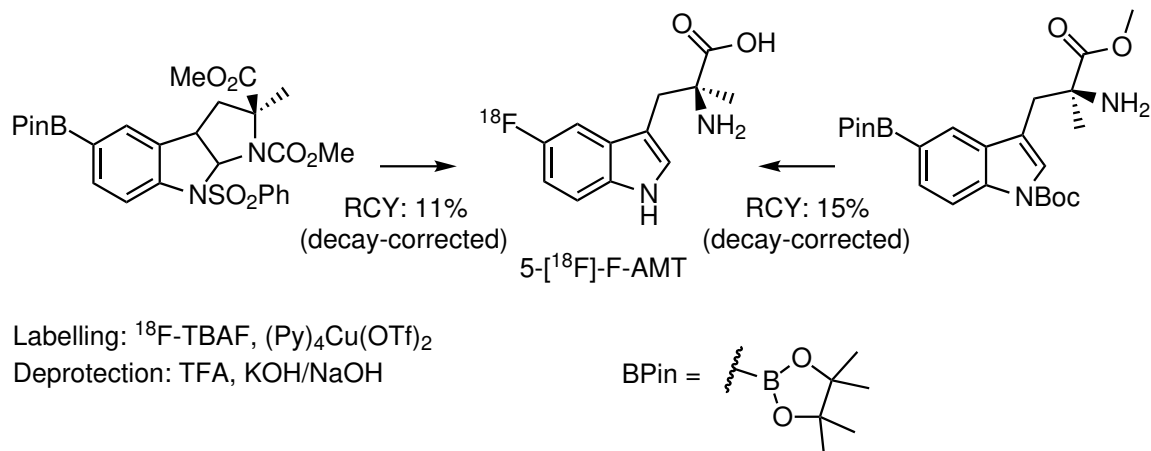
Figure 7.3: (a) Left: 1-¹⁸F-fluoroethyl-tryptophan ([¹⁸F]FETrp); right: NLG919, IDO inhibitor. (b) Other [¹⁸F]fluorinated tryptophan analogues with ¹⁸F-substitution at the aromatic moiety, investigated by Giglio *et al*¹³⁴.

Conveniently, structure-activity relationship analysis identified potential analogues of AMT as substrates for IDO. Derivatives substituted with fluorine in the 4-, 5- and 6-position on L-tryptophan (Figure 7.3, (b), right) exhibited high affinity binding (as judged by V_{\max} and K_m values) for IDO, rendering them attractive for ¹⁸F-labelling¹³⁵. V_{\max} is the maximum rate of catalysis when an enzyme is saturated with its substrate. K_m represents the required substrate concentration for the enzyme to reach its V_{\max} . K_m values of all tryptophan analogues are similar to unsubstituted Trp, however a slightly higher concentration of the 6-fluorinated form is required for IDO. The aforementioned regiomers has the highest V_{\max}/K_m ratio among substituted tryptophans (including methyl, methoxy and hydroxy substituents in the 5- or 6-position), rendering it the best substrate for IDO. The values are presented in Table 7.1.

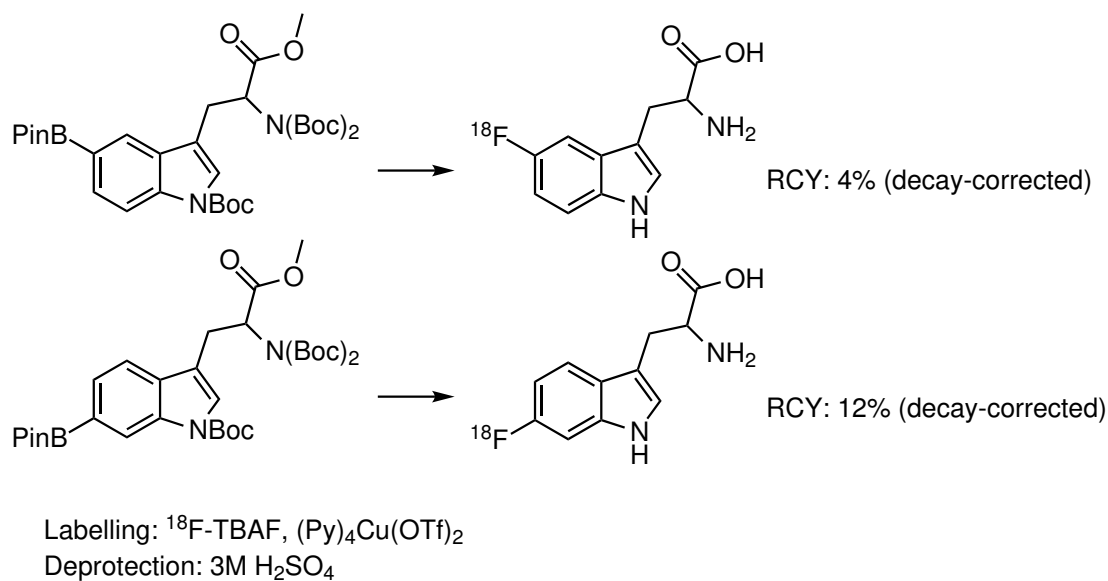
Table 7.1: V_{\max} , K_m , and V_{\max}/K_m values (pH=7.0) for ring-fluorinated L-tryptophan analogues as substrates for IDO, adapted from Sono *et al.*¹³⁵.

	L-Trp	4-F	5-F	6-F
K_m [μM]	13	13.2	13.2	15.3
V_{\max} [nmol/min/nmol IDO]	122	18	48	68
V_{\max}/K_m [$(\mu\text{Mmin})^{-1}$]	9.38	1.36	3.46	4.44

The recent study by Giglio *et al.* presents the synthesis and labelling of aromatically substituted [^{18}F]fluorinated variants of L-Trp¹³⁴. Their preliminary small animal PET experiments uncovered that 5- ^{18}F -AMT (Figure 7.3, (b), middle) exhibited significant uptake in B16F10, a murine melanoma cell line. Labelling at the 5-position of AMT is shown in Scheme 7.1, and [^{18}F]fluorination at the 6-position of tryptophan in Scheme 7.2.



Scheme 7.1: Radiosynthesis of 5- ^{18}F -AMT using different precursors, from Giglio and co-workers¹³⁴.



Scheme 7.2: Radiosynthesis of 5- and 6- ^{18}F -Trp, from Giglio and co-workers¹³⁴.

Based on the above literature review, ^{18}F fluorinated AMT variants make suitable PET tracer candidates for the imaging of tryptophan metabolism, both through the serotonin and kynurenine pathways. As pointed out by Giglio and co-workers, there are several structural modification sites at a tryptophan residue which could be probed to obtain a suitable PET tracer candidate (Figure 7.4).

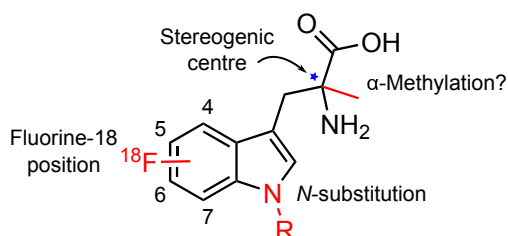
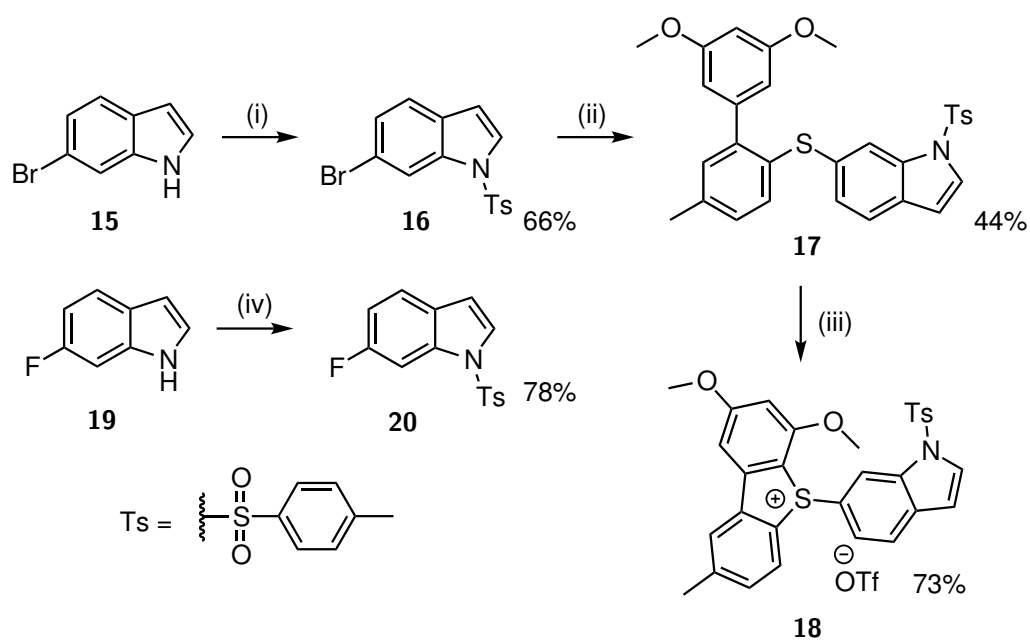


Figure 7.4: Structural modifications of tryptophan analogues that should be investigated to design a promising ^{18}F -labelled PET tracer candidate.

7.2 Synthesis of Sulfonium Salt with Indole Moiety

A simple indole-based model compound was selected to test its compatibility to undergo cyclisation to the dibenzothiophene sulfonium salt with the current reaction system: NCS and $\text{Bi}(\text{OTf})_3/\text{TfOH}$. The synthetic route towards the compound is shown in Scheme 7.3.

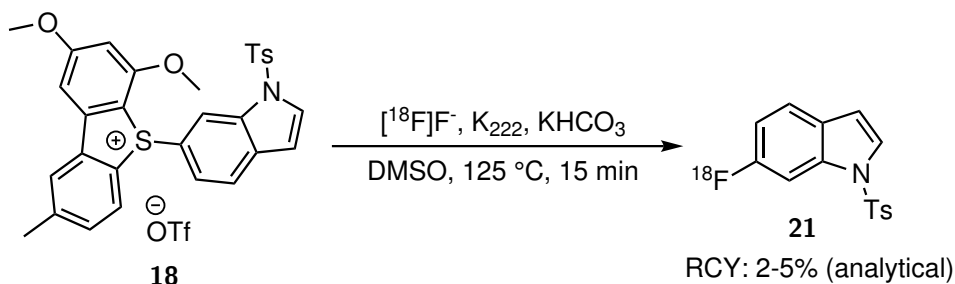


Scheme 7.3: Syntheses of sulfonium salt **18** and fluorinated reference **20**.

Reagents and conditions: (i) KOH, *p*-TsCl, Aliquat[®] 336, toluene/water, rt, 1 h; (ii) Thioether **4**, Pd₂(dba)₃, DPEphos, KO^{*t*}Bu, toluene, reflux, 1 h; (iii) NCS, Bi(OTf)₃, MeCN, rt, 20 min; (iv) KOH, *p*-TsCl, Aliquat[®] 336, DCM, rt, 1 h.

N-tosyl protected bromoindole **16** was coupled to diaryl thioether **4** (Chapter 5, Scheme 5.3) in a palladium-catalysed reaction to afford thioether **17** in 44% yield. It was then employed in a cyclisation reaction with Bi(OTf)₃ and NCS, which reached full conversion within 20 min. The corresponding sulfonium salt **18** was isolated in 73% yield. Fluorinated reference compound **20**, for HPLC co-injection after radiolabelling, was obtained in 36% yield.

Preliminary ¹⁸F-labelling of sulfonium salt **18**, performed by Dr Thibault Gendron, proceeded with a low analytical RCY of 2-5% (Scheme 7.4). Nucleophilic substitution on indoles is challenging due to their electron-rich nature. This issue could perhaps be resolved with further optimisation of the dibenzothiophene substitution pattern to enhance its leaving group ability and consequently, improve radiolabelling efficiency.



Scheme 7.4: Radiosynthesis of 6- $[^{18}\text{F}]$ fluoroindole using sulfonium salt **18** (performed by Dr Thibault Gendron).

7.3 Radiotracers with Pyridyl Moiety

The pyridine moiety can be found in over 100 drugs on the market¹³⁶. It is a bioavailable motif - nicotinic acid (niacin) and nicotinamide (niacinamide) are part of the vitamin B₃ complex. Pyridine itself is notorious for its toxicity, however an increase in the proportion of pyridine-containing drugs can be rationalised by its metabolic stability^{137,138}. Vast functionalisations of the pyridine moiety in drug-like molecules have seen a reflection in the number of PET tracer candidates containing this heterocycle¹³⁹. A prominent representative of this category is $[^{18}\text{F}]$ FPEB, discussed in Chapter 5. Examples of other pyridine-based PET tracers are shown in Figure 7.5.

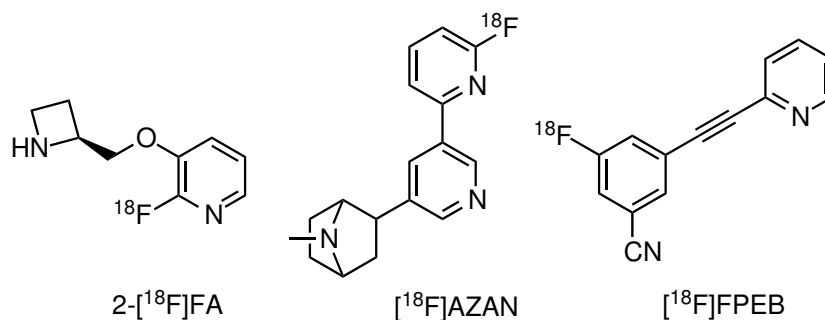
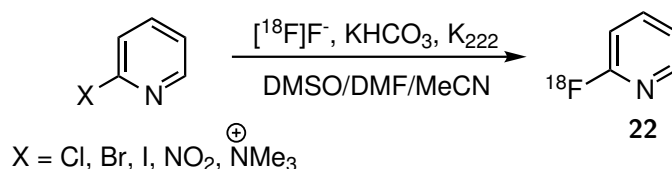


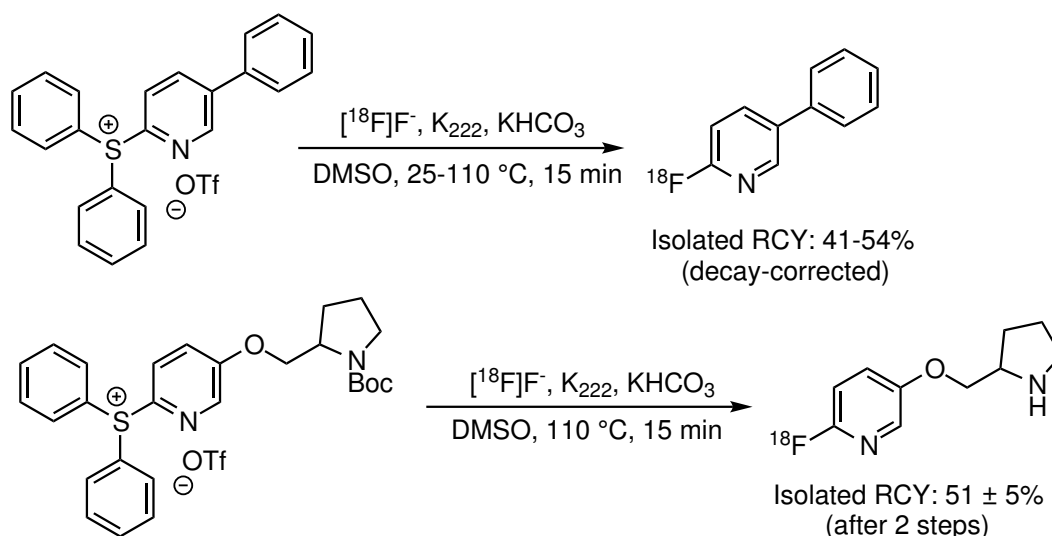
Figure 7.5: Existing pyridine-based PET tracers.

Direct $[^{18}\text{F}]$ fluorination of the pyridyl moiety using traditional leaving groups, such as NMe_3^+ and NO_2 , proceeds efficiently at the *ortho* position (Scheme 7.5). RCYs in the range of 82-91% can be obtained after 20 min at 120 °C with trimethylammonium and nitropyridines. Halopyridines require temperatures up to 180 °C to achieve efficient radiolabelling (19-87%)¹⁴⁰.



Scheme 7.5: Generic radiolabelling of activated *ortho*-pyridines with [¹⁸F]fluoride⁶.

Sander *et al.* attempted radiolabelling of pyridines in the *ortho*-position using triarylsulfonium salts (Chapter 3, Section 3.1), which proceeded in good isolated decay-corrected RCYs (Scheme 7.6).



Scheme 7.6: Radiosynthesis of functionalised 2-[¹⁸F]fluoropyridines using first generation triarylsulfonium salts, developed by Sander and co-workers⁴.

One of the most recent examples of promising 2-[¹⁸F]fluoropyridine-based structures is [¹⁸F]DCFPyL (Figure 7.6), a PET tracer candidate for the imaging of metastatic prostate cancer¹⁴¹. It is a low-molecular weight inhibitor designed to bind to the prostate-specific membrane antigen (PSMA), which is overexpressed in prostate cancer epithelial cells even up to 80 times higher than in healthy prostate^{142,143}. Elucidation of this structure represents a great achievement in the field. Chen *et al.* argued that issues associated with development of high quality tracers for prostate cancer imaging are caused by: 1) slow growth and metabolism of cancer cells, hence limited suitability for [¹⁸F]FDG studies, 2) close location of prostate and urinary bladder, requiring rapid scanning and 3) lack of markers for differentiation of slow from fast developing cancer.

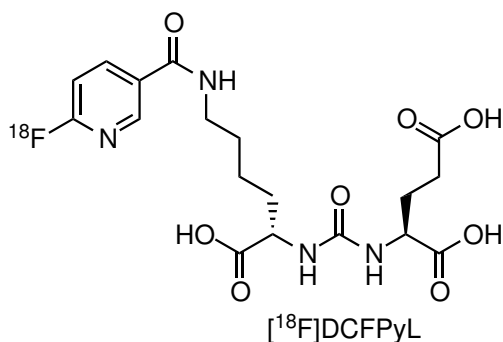
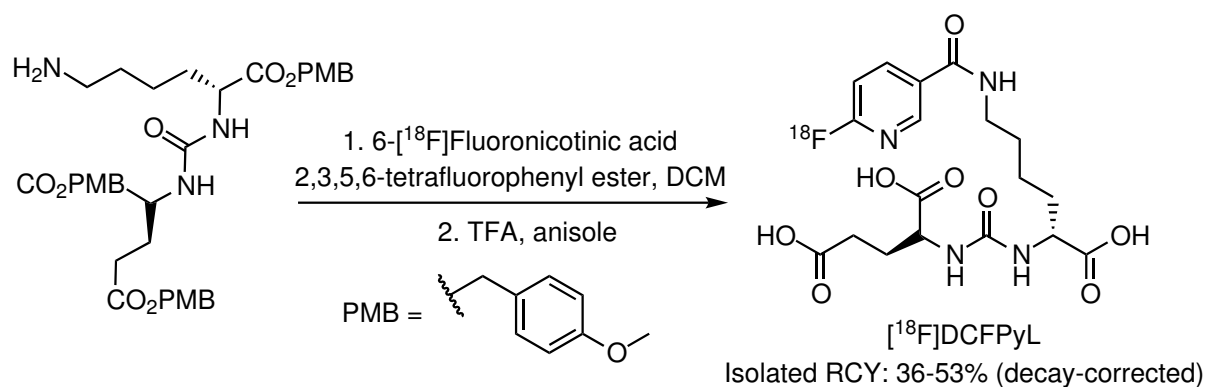
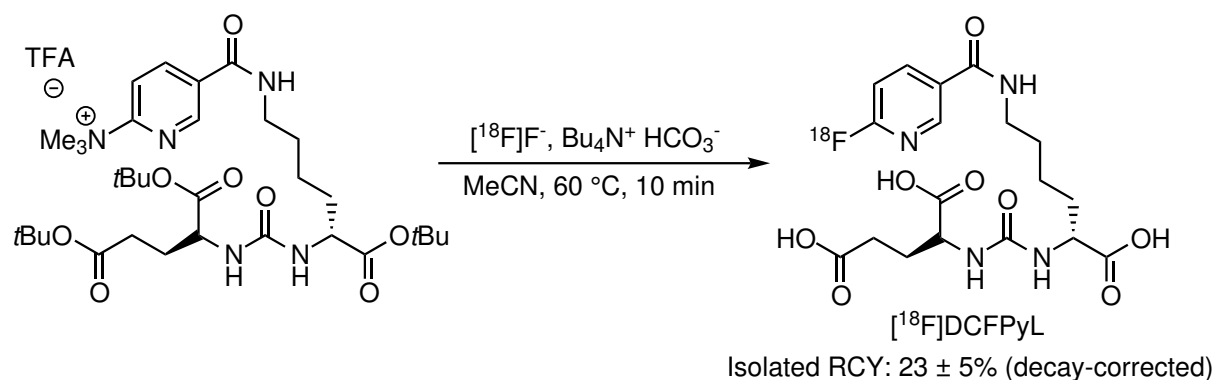


Figure 7.6: PET tracer candidate for the imaging of prostate cancer, $[^{18}\text{F}]\text{DCFPyL}$ ¹⁴¹.

Bouvet *et al.* published an optimised automated synthesis of $[^{18}\text{F}]\text{DCFPyL}$, which proceeded in $23 \pm 5\%$ isolated decay-corrected RCY¹⁴⁴. The RCY had to be compromised, in comparison to the original synthesis by Chen *et al.* (36-53%, decay corrected, Scheme 7.7), to avoid the use of prosthetic groups.

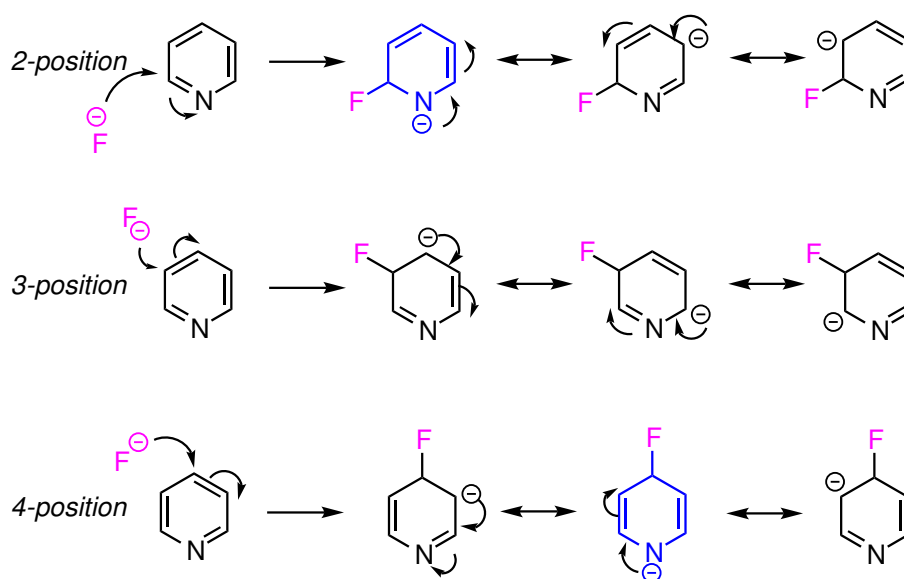


Scheme 7.7: Radiosynthesis of $[^{18}\text{F}]\text{DCFPyL}$ by Chen and co-workers¹⁴¹.



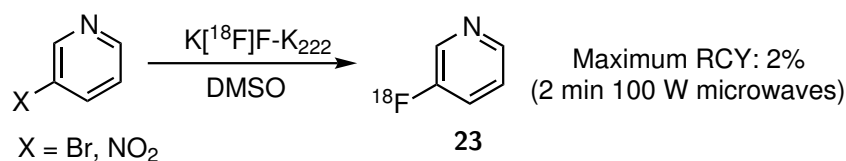
Scheme 7.8: Automated radiosynthesis of $[^{18}\text{F}]\text{DCFPyL}$ by Bouvet and co-workers¹⁴⁴.

The relative ease of [^{18}F]fluorination at the *ortho*-position of the pyridine is reflected in the growing number of PET tracer structures thereof, in comparison to 3- ^{18}F fluoropyridine. Nucleophilic substitution at the 3-position of the pyridine ring is challenging, owing to its electron-withdrawing character. During nucleophilic attack, both the 2- and 4-positions are targeted preferentially, due to greater stability of the resulting Meisenheimer complexes, in which the negative charge is placed on the nitrogen atom. This effect is strengthened in the presence of electron-deficient substituents, *e.g.* NO_2 , NMe_3^+ .



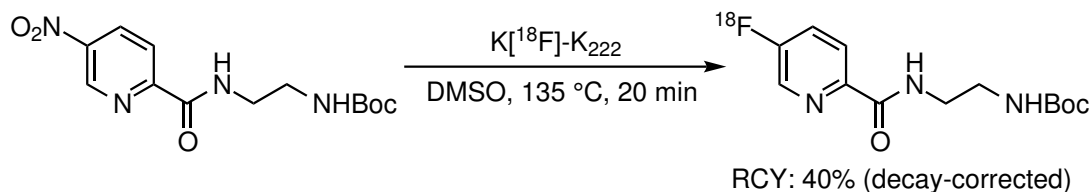
Scheme 7.9: Nucleophilic attack at the pyridine. Resonance forms are shown for the *ortho*-, *meta*- and *para*-positions. Most favourable resonance forms (structures in blue) result in the negative charge on the nitrogen. Fluoride incorporation is therefore favoured at the 2- and 4-positions.

Unsuccessful attempts at ^{18}F -labelling at the *meta*-position by nucleophilic aromatic substitution of bromo- and nitro-precursors were described by Karramkam *et al.* (Scheme 7.10)¹⁴⁵.



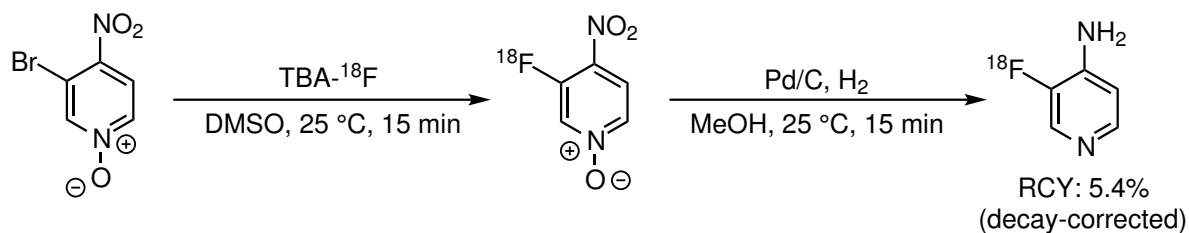
Scheme 7.10: Failed attempts to incorporate fluorine-18 at the *meta* to the pyridyl nitrogen. Adapted from Karramkam and Preshlock⁶¹⁴⁵.

There is the only example of direct labelling of a PET tracer scaffold at the 3-position (Figure 7.11), dating back to the 1990s. Beer *et al.* labelled a promising radiotracer for the imaging of monoamine oxidase-B (MAO-B) in 40% decay-corrected RCY¹⁴⁶. Activation of the 3-position towards the nucleophile was achieved by placing an electron-withdrawing amide *para* to the nitro leaving group.



Scheme 7.11: The only documented case of successful ¹⁸F-incorporation at the *meta*-pyridine entity of a PET tracer candidate, by Beer and co-workers¹⁴⁶.

Recently Brugarolas *et al.* described direct [¹⁸F]fluorination at the 3-position of pyridine *N*-oxides as a way of accessing *meta*-[¹⁸F]fluoropyridines¹⁴⁷. The main limitation lies in the post-labelling reduction step using Pd/C (Scheme 7.12). The decay-corrected RCY before reduction was established at $10.4 \pm 1.8\%$ (n=8), however, interestingly, co-injection of the crude reaction mixture with the non-radioactive reference compound resulted in a significant RCY increase to $25 \pm 4\%$. This phenomenon was hypothesised to occur via exchange of fluorine-19 of the cold reference with unreacted [¹⁸F]fluoride. The total synthesis time was under 2 hours, however the final RCY was reduced to 5.4% after decay-correction. Despite efforts from Brugarolas and co-workers, the method does not alleviate the challenging task of labelling at the *meta*-position. Activation by a nitro substituent *ortho* to the leaving group is still required to promote labelling. Masking of the pyridyl moiety using *N*-oxide adds an extra synthetic step during radiolabelling, severely affecting the practical aspects of the method.



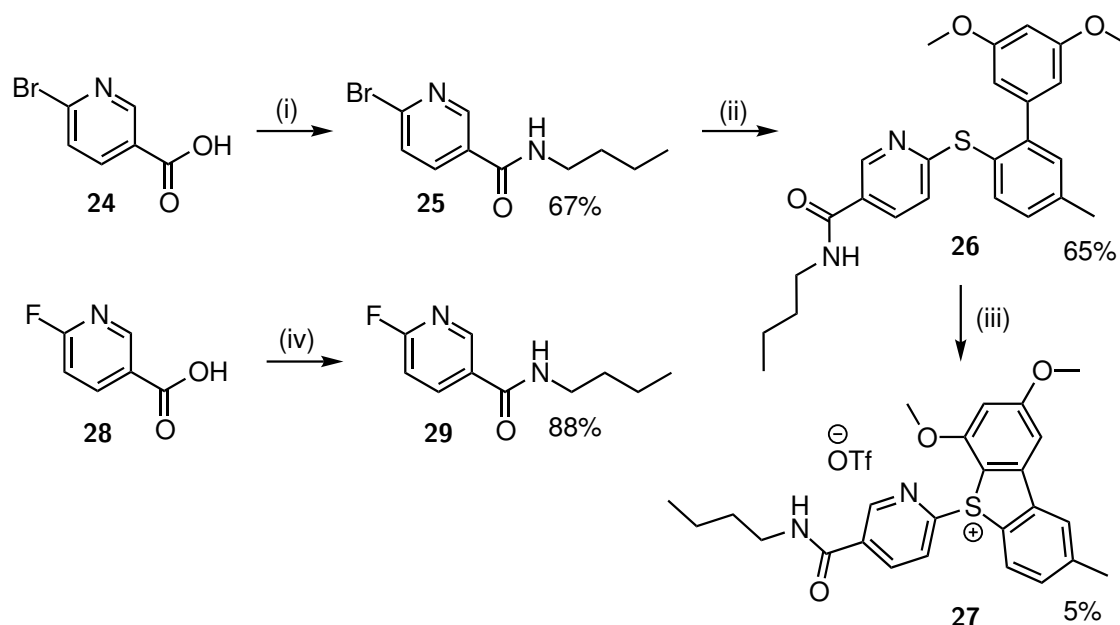
Scheme 7.12: Direct ^{18}F -incorporation at the *meta*-position of *N*-oxide pyridines by Brugarolas and co-workers¹⁴⁷. Subsequent palladium-mediated hydrogenation allows for simultaneous reduction of the *N*-oxide back to pyridine and nitro group to amine (for further functionalisations).

Perhaps the most elegant solution, to date, is offered by Rotstein *et al.*⁶². Radiolabelling using an iodonium ylide precursor afforded 3- ^{18}F fluoropyridine in an analytical RCY of 65%, without the need for an activating group (Chapter 2, Section 2.3.1, page 36). No information about isolated RCY or ease of purification was, however, given by the authors, making it difficult to assess the practicality of the method. To the best of my knowledge, a PET tracer scaffold has not yet been accessed using this method.

7.4 Synthesis of Sulfonium Salts with 2-Pyridyl Moiety

Labelling of the *ortho*-pyridine position using triarylsulfonium salts by Sander and co-workers (Section 7.3, Figure 7.6) proceeded efficiently. Implementation of the novel dibenzothiophene sulfonium salt strategy to direct labelling of pyridines remains yet to be undertaken. The PSMA selective radiotracer, ^{18}F DCFPyL (Section 7.3, Figure 7.6), was published in 2011 and remains an attractive candidate for the imaging of prostate cancer using PET, despite challenges with the original radiosynthesis, requiring prosthetic groups (Scheme 7.7). A simplified analogue of ^{18}F DCFPyL makes an ideal case study for ^{18}F -labelling using dibenzothiophene sulfonium salts. Model compound (Scheme 7.13, structure **29**) was designed to provide an adequate mimic of the target tracer. The scaffold was simplified to include basic 2-pyridine and amide functionalities, expected to provide further insights into the potential of cyclic sulfonium salt precursors for radiolabelling of aromatic scaffolds decorated with such entities. The terminal amine moiety of urea on the ^{18}F DCFPyL scaffold is predicted to undergo a straightforward coupling to a 2-nicotinic acid in later stages.

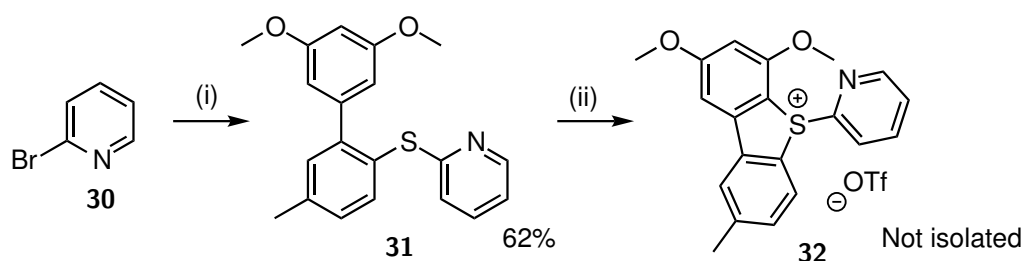
The synthetic route is presented in Scheme 7.13.



Scheme 7.13: Syntheses of sulfonium salt **27** and fluorinated reference **29**.

Reagents and conditions: (i) But-1-ylamine, HATU, HOBT, DIPEA, DCM, rt, 1 h; (ii) Thioether **4**, Pd₂(dba)₃, DPEphos, KO^tBu, toluene, reflux, 2.5 h; (iii) NCS, TfOH, MeCN, rt, 3 h; (iv) But-1-ylamine, HATU, HOBT, DIPEA, DCM, rt, 2 h.

Amide **25** was synthesised using standard peptide coupling procedure with HATU, HOBT and DIPEA in DMF in 67% yield. It was then employed in the Pd-catalysed thioetherification with thioether **4** (Scheme 5.3) and the desired sulfonium salt precursor **26** was obtained in 65% yield. Cyclisation mediated by NCS and TfOH delivered sulfonium salt **27** in a poor yield of 5%, with no signs of side chlorination. A simple *ortho*-pyridine thioether scaffold failed to undergo cyclisation with NCS and TfOH (Scheme 7.14).



Scheme 7.14: Syntheses of sulfonium salt **32**.

Reagents and conditions: (i) Thioether **4**, Pd₂(dba)₃, DPEphos, KO^tBu, toluene, reflux, 24 h; (ii) NCS, TfOH, rt, 2 h.

Challenging cyclisation to *ortho*-pyridine scaffolds **27** and **32** can be explained by the electron-withdrawing effect of the nitrogen atom, leading to a decrease in the nucleophilicity of sulfur and consequently, low reactivity towards the electrophilic reagent pair. Pyridine is protonated during the cyclisation reaction, giving rise to a positive charge *ortho* to the thioether, which further deactivates the substrates towards the electrophile. As discussed on page 86, an electron-deficient *S*-centre is expected to react readily with nucleophilic [¹⁸F]fluoride but electrophilic transformations proceed sluggishly.

Inherent problems arising from highly acidic reaction conditions were highlighted in Chapter 6. Although it has been demonstrated that a simple phenyl-based sulfonium salt can be cyclised under basic conditions with hypochlorite reagents, the method lacks robustness and suffers from decomposition issues due to the release of hydroxide ions. The search for mild and neutral cyclisation reagents arrived at *N*-chlorosulfonamides as chlorinating agents (described fully in Section 7.5, Scheme 7.17 and Figure 7.8). Reactions of thioether **31** with *N*-chlorosulfonamides did not yield sulfonium salt **32**. Interestingly, NMR analysis of crude reaction mixtures revealed the presence of 2 side-products - chlorinated and dichlorinated analogues of thioether **31** (Figure 7.7). Perhaps it can be inferred that for electron-deficient substrates, such as *ortho*-pyridines, the rate of diaryl thioether chlorination surpasses the rate of chlorosulfonium intermediate formation, leading to the observed product distribution.

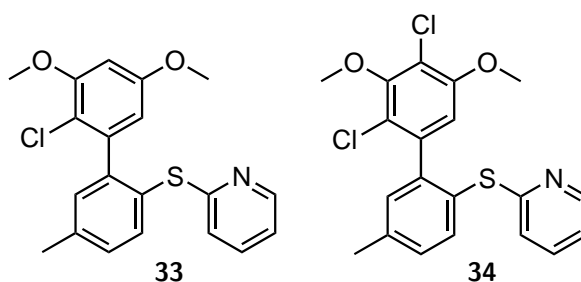
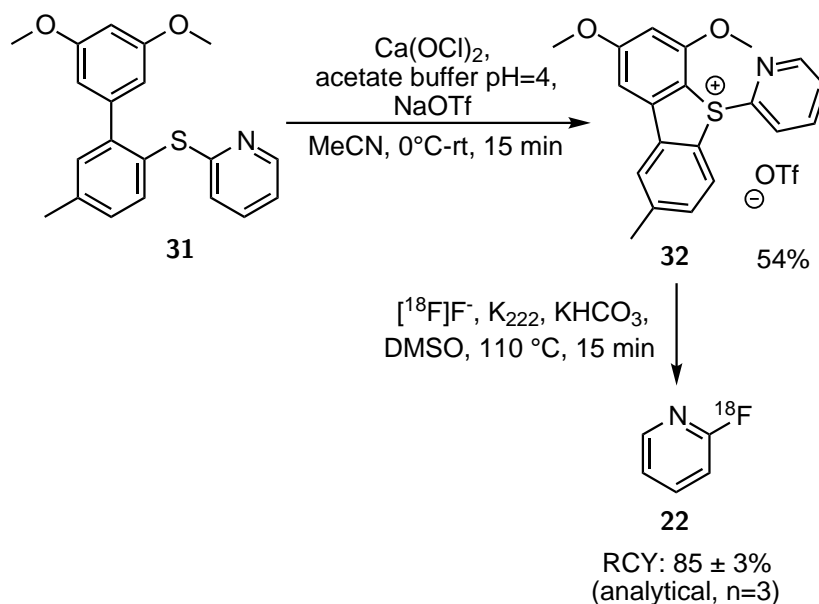


Figure 7.7: Chlorinated and dichlorinated analogues of thioether **31**.

At the time of writing this thesis, Dr Thibault Gendron optimised reaction conditions for the cyclisation of acid-sensitive substrates. Building on the foundations of hypochlorite-mediated reagents for sulfonium salt formation (Chapter 6, Section 6.3.2,

Table 6.3), he established that efficient and robust cyclisation of thioether **31** could be achieved with $\text{Ca}(\text{OCl})_2$, which became soluble in MeCN, when used in conjunction with acetate buffer (pH=4). The latter ensured mopping up of hydroxide anions to prevent base-mediated decomposition. The method elegantly avoided the use of TfOH or $\text{Bi}(\text{OTf})_3$, hence offering a mild, inexpensive and complementary solution for substrates which do not tolerate the acidic environment. Using this method, Gendron accessed sulfonium salt **32** in a gratifying yield of 54%. Radiolabelling proceeded with an analytical RCY of $85 \pm 3\%$ (n=3). Both reactions are shown in Scheme 7.15. In comparison, with the same precursor load (2 mg), Rotstein *et al.* labelled the *ortho*-pyridine position using an iodonium ylide precursor with $65 \pm 11\%$ RCY (n=3).

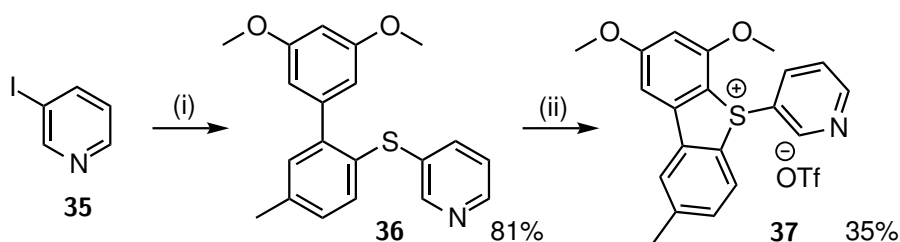


Scheme 7.15: Formation of sulfonium salt **32** proceeded efficiently in the presence of $\text{Ca}(\text{OCl})_2$ and acetate buffer, a newly proposed hypochlorite-based cyclisation system for acid-sensitive substrates. Radiolabelling afforded 2- $[\text{}^{18}\text{F}]$ fluoropyridine in an excellent analytical RCY of $85 \pm 3\%$. Both reactions were performed by Dr Thibault Gendron at the time of writing this thesis.

7.5 Synthesis of Sulfonium Salt with 3-Pyridyl Moiety

Synthesis of a *meta*-pyridine dibenzothiophene sulfonium salt was expected to proceed more readily than for the *ortho*-regioisomer **32**, owing to the electron-withdrawing nature of the nitrogen atom in the 3-position. The synthetic route to 3-pyridine

thioether **36** is shown in Scheme 7.16.



Scheme 7.16: Synthesis of sulfonium salt **37**.

Reagents and conditions: (i) Thioether **4**, Pd₂(dba)₃, DPEphos, KO^tBu, toluene, reflux, 2 h; (ii) Optimisation of cyclisation conditions.

Thioether **36** was obtained through a palladium-mediated coupling of 3-iodopyridine to thioether **4** (Scheme 5.3) in 81% yield. Efforts were then directed to finding suitable cyclisation conditions. These results are summarised in Table 7.2.

Table 7.2: Optimisation of cyclisation with thioether **36**. All reactions were performed in MeCN at room temperature. Chlorinated sulfonium salt (structure **41**) is shown in Scheme 7.19.

Entry	Acid	Chlorinating Agent	Time	Result
1	TfOH	NCS	overnight	52% yield ^a
2	TfOH	NCS	30 min	14% yield ^b
3	BiOTf ₃ ^c	NCS	overnight	No reaction
4	-	Sulfonamide 40	3 h	No reaction
5	-	Sulfonamide 38	2 h	Trace product ^d
6	TfOH	Sulfonamide 38	1.5 h	29% yield ^e
7	Bi(OTf) ₃	Sulfonamide 38	2.5 h	35% yield ^f
8	-	Palau'Chlor [®]	overnight	No reaction
9	- ^g	NCS	10 min	Decomposition
10	- ^h	NCS	overnight	No reaction

^a Yield calculation based on NMR data. Isolated sample: **3:1** Sulfonium salt: chlorinated sulfonium salt. ^b **15.7:1** Sulfonium salt: chlorinated sulfonium salt. Also isolated from the reaction mixture was a mixture of starting material derivatives. ^c Source of TfOH.

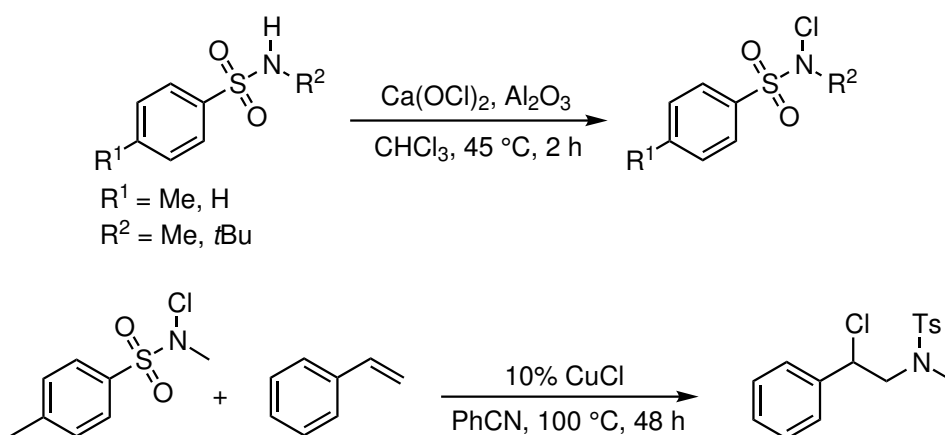
^d LC-MS revealed a mixture of sulfonium salt and its chlorinated counterpart.

^e Yield calculation based on NMR data. **3.5:1** Sulfonium salt: chlorinated sulfonium salt. Incomplete conversion. ^f Yield calculation based on NMR data. **4.6:1** Sulfonium salt: chlorinated sulfonium salt. ^g 10 mol% 2,4,6-Trimethylaniline.

^h 10 mol% Triphenylphosphine sulfide.

With NCS and TfOH, sulfonium salt formation was observed early on, however a significant amount of starting material remained even after prolonged stirring. (Table 7.2, Entry 1). Sulfonium salt **37** was afforded in 52% analytical yield, however separation from its chlorinated analogue was not achieved. Both products have similar R_f values, which makes flash column chromatography separation arduous. An analogous attempt, with a significantly shorter reaction time, afforded the desired sulfonium salt with a reproducible yield and pleasingly, with a more favourable ratio of the sulfonium salt to its chlorinated derivative (Entry 2). Interestingly, NMR analysis of the recovered starting material revealed the presence of both the mono- and dichlorinated thioether derivatives. No product was formed when the cyclisation was mediated by $\text{Bi}(\text{OTf})_3$ and NCS (Entry 3).

At the time of the investigation, Heuger and Göttlich published an elegant strategy of electrophilic addition to unsaturated compounds, mediated by copper(I)¹⁴⁸. *N*-chlorosulfonamides were described as a mild yet reactive source of chlorine without the need for acid activation. Inspired by these findings, it was speculated that *N*-chlorosulfonamides could act as electrophiles for sulfonium salt formation, perhaps offering better regioselectivity over ring chlorination due to increased steric bulk on the sulfonamide moiety. Their formation and a representative reaction are shown in Scheme 7.17. A selection of *N*-chlorosulfonamides was prepared according to the method by Heuger and Göttlich is presented in Figure 7.8.



Scheme 7.17: Preparation of *N*-chlorosulfonamides and their representative high-yielding addition to styrene, both from Heuger and Göttlich¹⁴⁸.

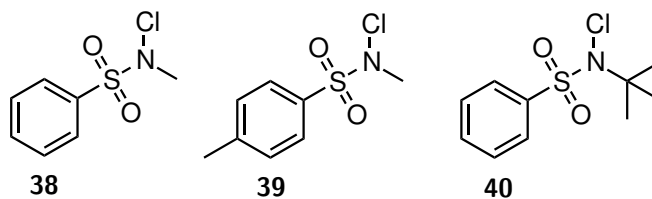


Figure 7.8: Scope of *N*-chlorosulfonamides prepared for further optimisation of the cyclisation protocol, synthesised using the method from Heuger and Göttlich (Scheme 7.17).

N-chlorosulfonamides **38** and **40**, used as the sole reagent, were unable to effectuate dibenzothiophene sulfonium salt formation (Table 7.2, Entries 4 and 5). Gratifyingly, when employed in conjunction with TfOH or Bi(OTf)₃, sulfonium salt **37** was obtained in 29% yield or 35% yield (based on NMR), respectively, nevertheless its chlorinated analogue constituted approximately 20% of the sample (Entries 6 and 7).

Several chlorination technologies were recently introduced as practical alternatives to highly reactive reagents such as chlorine gas or sulfuryl chloride, yet exhibiting greater potential than conventional NCS. Rodriguez *et al.* have commercialised a guanidine-based chlorinating reagent, CBMG, also known as Palau'chlor[®] (Figure 7.9, (a))¹⁴⁹. It has shown superior properties for direct electrophilic chlorinations of various heteroaromatic systems, in comparison with NCS or *t*BuOCl. A wide scope of aromatic heterocycles was screened, including benzimidazoles, indoles and pyrroles. Examples of substrates which underwent elegant chlorination with Palau'chlor[®] are shown in Figure 7.9.

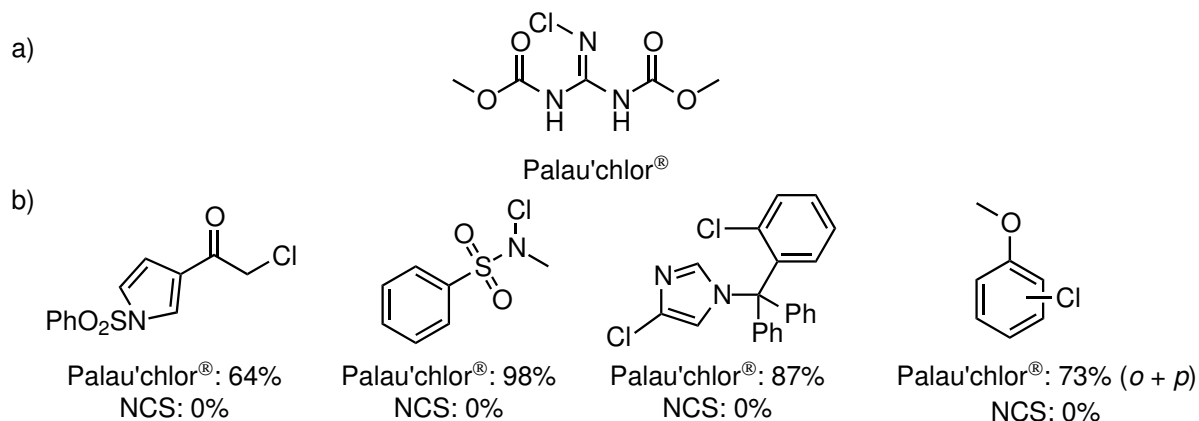
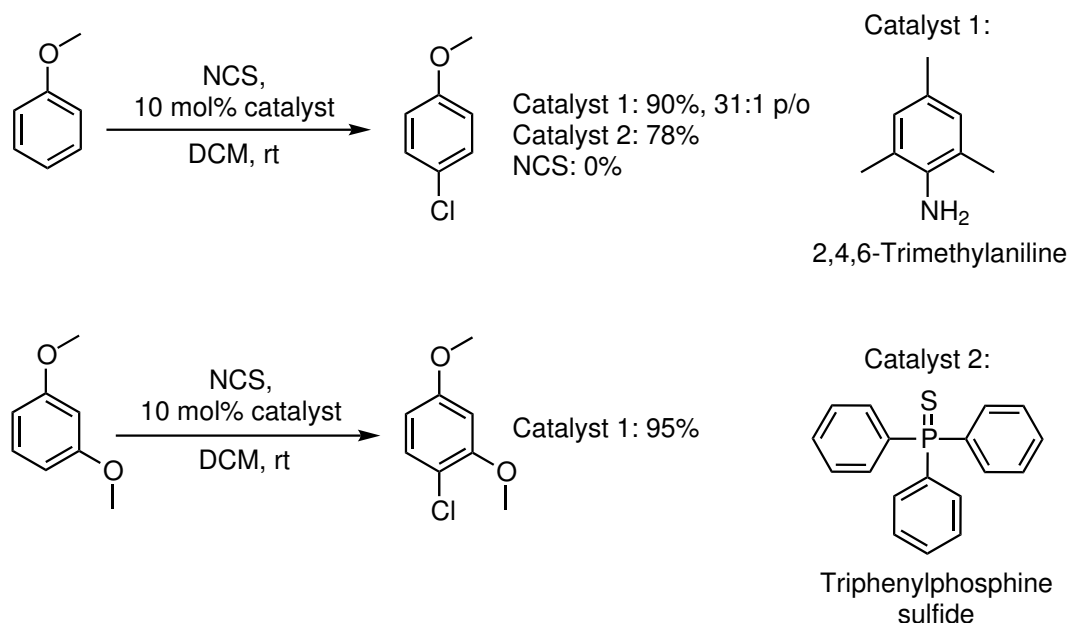


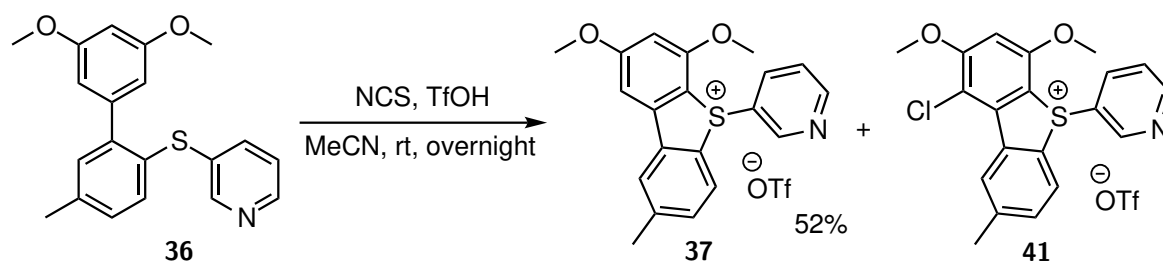
Figure 7.9: (a) Palau'chlor[®]. (b) Representative compounds chlorinated using Palau'chlor[®], with yields compared against NCS.

Shortly after Rodriguez *et al.* published their Palau'chlor[®] chlorination strategy, Samanta and Yamamoto proposed the use of aniline catalysis to achieve selective electrophilic halogenations¹⁵⁰. 2,4,6-Trimethylaniline was employed in conjunction with NCS in electrophilic chlorination of various aromatic systems, including anisoles, which were of immediate interest to this study. The proposed mechanism assumes formation of an *N*-haloaniline adduct, which then acts as a halogen donor to the structure of interest. The optimum catalyst loading was established to be between 5 and 10 mol%. The route is particularly attractive due to the absence of Brønsted acid. Maddox *et al.* also performed a mild and efficient chlorination of aromatic systems using the concept of Lewis base catalytic activation of *N*-halosuccinimides, in lieu of conventional Lewis or Brønsted acid activation¹⁵¹. They demonstrated that catalytic triphenylphosphine sulfide was capable of activating NCS, hence boosting its reactivity towards arenes. Both technologies are presented in Scheme 7.18.



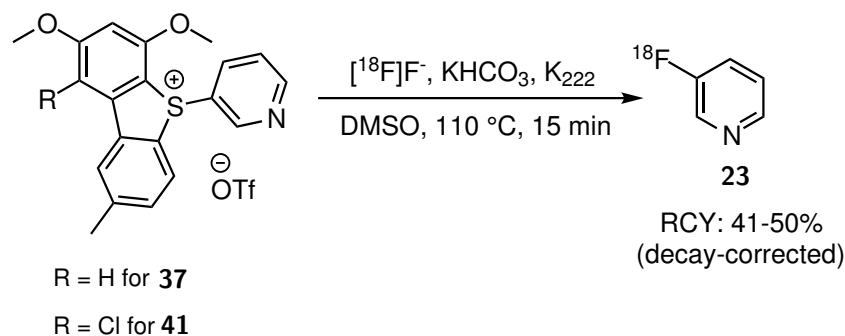
Scheme 7.18: Novel strategies for electrophilic chlorination: 1) using NCS and an aniline-based catalyst, proposed by Samanta and Yamamoto and 2) triphenylphosphine sulfide, proposed by Maddox and co-workers^{150 151}. Excellent yields were obtained for anisole substrates.

Disappointingly, none of the presented alternative approaches afforded sulfonium salt **37** (Table 7.2, Entries 8, 9 and 10). Scheme 7.19 presents the most successful cyclisation of thioether **36** to sulfonium salt **37** using NCS and TfOH.



Scheme 7.19: Most successful cyclisation of thioether **36** with NCS and TfOH in MeCN overnight. NMR yield of sulfonium salt **37** was 52%, however it could not be isolated from its chlorinated analogue **41**.

The mixture of sulfonium salts **37** and **41** (Scheme 7.19) was subjected to ¹⁸F-labelling. The chlorinated analogue was still expected to undergo labelling, although the leaving group ability of dibenzothiophene could perhaps be affected. Radiolabelling was carried out in DMSO at 110 °C for 15 min (Scheme 7.20). The isolated decay-corrected RCY was 41-50% (n=2).



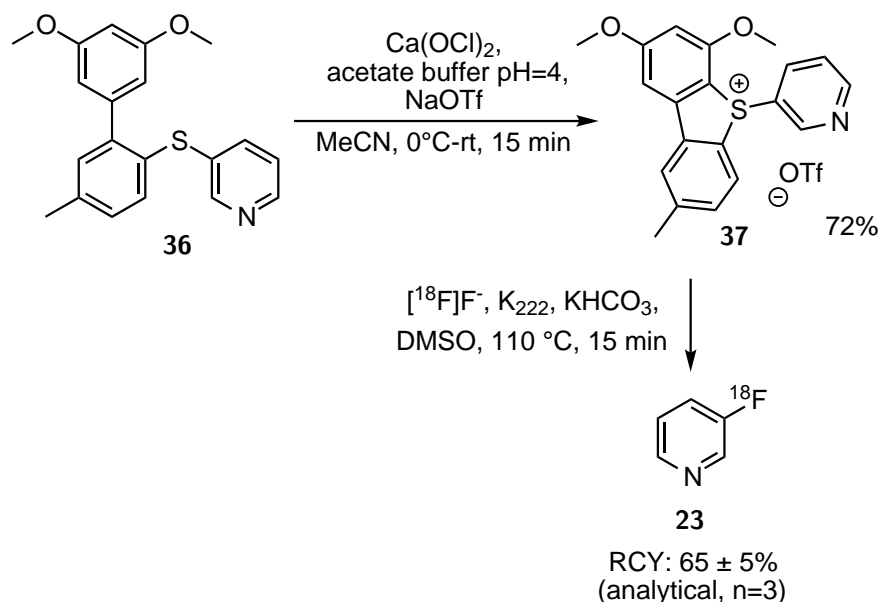
Scheme 7.20: Successful direct ^{18}F -incorporation into the pyridyl *meta*-position with a mixture of sulfonium salts **37** and **41**.

This is an elegant example of direct one-step incorporation of fluorine-18 into the *meta*-position of pyridine, offering advantages over the recently published findings by Brugarolas *et al.*¹⁴⁷. The pyridine nitrogen does not have to be activated by *N*-oxide transformation or possess strongly-electron withdrawing groups *ortho* or *para* to the leaving group. Brugarolas *et al.* obtained 3- ^{18}F fluoro-4-nitropyridine *N*-oxide in $10.4 \pm 1.8\%$ RCY, compared to 41-50% RCY of unsubstituted 3- ^{18}F fluoropyridine presented in this work. Rotstein *et al.* obtained compound **23** using an iodonium ylide precursor in an analytical RCY of 65% (Chapter 2, Section 2.3.1, Scheme 2.16).

As described in Section 7.4 (Scheme 7.15), the *ortho*-pyridine-based thioether was successfully cyclised using $\text{Ca}(\text{OCl})_2$ and acetate buffer (pH=4) in MeCN at 0 °C (Dr Thibault Gendron). At the time of writing this thesis, cyclisation was also attempted with *meta*-pyridine isomer **36**. Gratifyingly, sulfonium salt **37** was obtained as the sole product in 72% yield. Subsequent labelling afforded 3- ^{18}F fluoropyridine in $65 \pm 5\%$ analytical RCY. Both reactions are shown in Scheme 7.21. Interestingly, both dibenzothiophene sulfonium salts (developed in the Årstad group) and iodonium ylides delivered the radiolabelled product with the same analytical RCY. As no information on the ease of isolation is available, both strategies constitute practical, and to the best of my knowledge, competitive solutions to direct radiolabelling of the 3-pyridyl moiety, to date.

The aforementioned radiolabelling of sulfonium salt **37** uncovered an important finding, which provides further evidence towards the robust nature of dibenzothio-

phene sulfonium salts as precursors for ^{18}F -labelling. The presence of the chlorinated sulfonium salt does not affect the RCY. Provided successful isolation and similar end of synthesis time, the isolated RCY expected from radiolabelling of **37** by Gendron oscillates in the same range as that obtained from radiolabelling of the mixture of sulfonium salts **37** and **41**.



Scheme 7.21: Successful cyclisation to sulfonium salt **37** as the sole product. Subsequent radiolabelling proceeded very efficiently, reaching a high analytical RCY. Both reactions were performed by Dr Thibault Gendron.

7.6 Conclusion

Synthesis of dibenzothiophene sulfonium salts bearing *N*-heterocyclic aromatic moieties allowed for further verification of their use as versatile and robust precursors for ^{18}F -labelling. Indole and pyridine-decorated sulfonium salts were constructed as model compounds of highly-functionalised drug-like molecules.

Indole, due to its electron-rich nature, is a better substrate for the cyclisation with NCS and $\text{Bi}(\text{OTf})_3/\text{TfOH}$ than 2- or 3-pyridines. The lower cyclisation yield of pyridine thioethers results from protonation of the nitrogen atom in the presence of triflic acid, leading to a reduction of electron density on the sulfur centre. This effect is more pronounced for the 2-pyridyl moiety. NMR spectra of crude reaction mixtures revealed significant progress of side chlorination (and dichlorination) of

the electron-rich dibenzothiophene. This is not surprising, as ring chlorination is a competing reaction which depletes the available electrophile (Chapter 6). It is believed that by taking certain measures, such as: 1) reducing reaction time and temperature or 2) changing the order of addition, ring chlorination could perhaps be controlled, to an extent. The rate of side chlorination is a function of electrophile strength and sulfur nucleophilicity. Generally, the rate of sulfonium salt formation is expected to outpace ring chlorination for electron-rich scaffolds. This is illustrated in Figure 7.10.

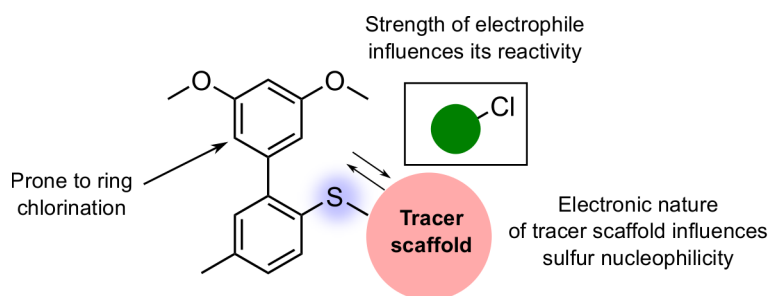
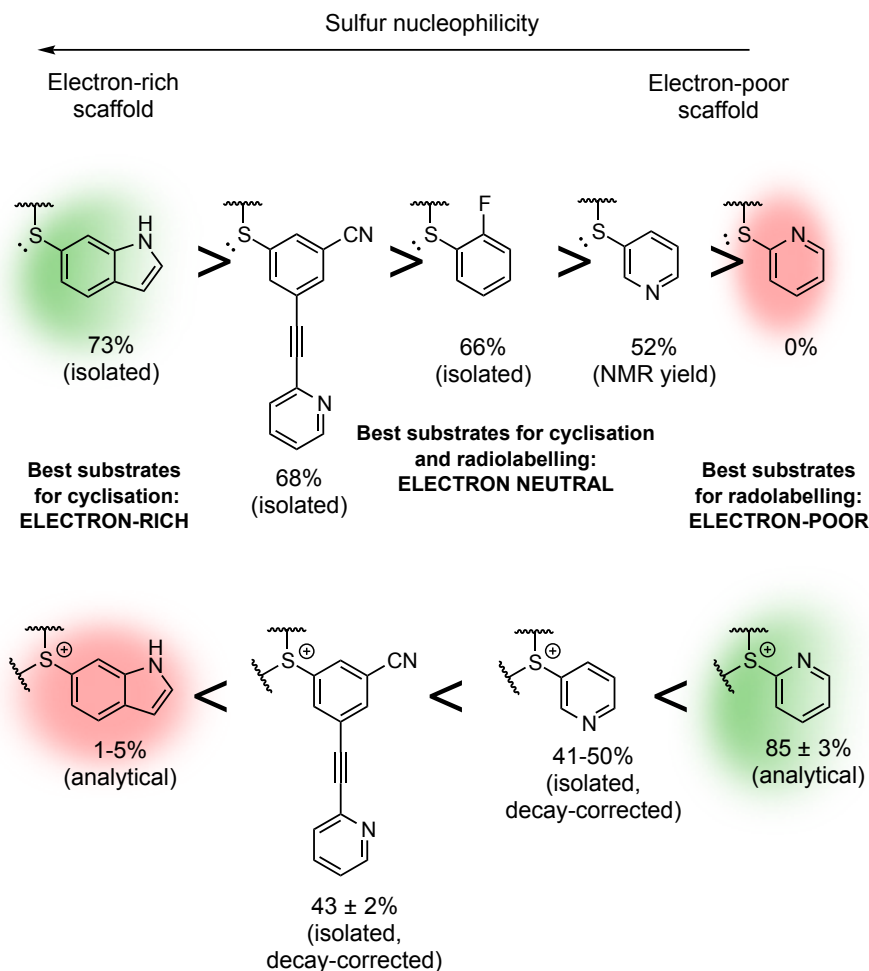


Figure 7.10: Illustration of factors orchestrating reactivity of the sulfur centre in the cyclisation step.

Reactivity trend for the *S*-centre can be elucidated using the cyclisation yields obtained for all substrates afforded using NCS and TfOH or Bi(OTf)₃. This is a qualitative illustration, as direct comparison of substituent effects or yields cannot be made without a deeper investigation and at least 3 repetitions for statistical significance. Electron-poor scaffolds are expected to react slowly towards electrophilic chlorine sources and highest cyclisation yields were obtained for scaffolds with electron-rich indole or phenyl entities. Cyclisation of the 2-pyridine-decorated thioether was eventually possible with Ca(OCl)₂, as shown in Section 7.4. In the presence of triflic acid, the proximal pyridine nitrogen is protonated, which leads to a significant decrease in thioether nucleophilicity. The 3-pyridyl dibenzothiophene sulfonium salt was also synthesised using the newly-established non-acidic reaction conditions but a higher yield was observed (72% vs 54%).

Reactivity of S-centre towards NCS and TfOH/Bi(OTf)₃ electrophilic system
(based on highest yield of corresponding sulfonium salt)



Reactivity of sulfonium salt towards [¹⁸F]F⁻ (based on RCY)

Figure 7.11: Experimentally established reactivity pattern of investigated thioethers towards the NCS and TfOH/Bi(OTf)₃ electrophilic system. Reactivity of synthesised sulfonium salts towards [¹⁸F]F⁻ is inversely proportional to the ease of cyclisation. The highest isolated (where possible) cyclisation yields are shown. Whenever possible, isolated decay-corrected RCY as shown.

As described on page 86, the inherent challenge of dibenzothiophene sulfonium salts lies in an attempt to make the sulfur centre reactive towards an electrophile in the cyclisation, and a nucleophile in the radiolabelling. Synthesis of sulfonium salts of electron-rich substrates proceed readily, however labelling is challenging, and vice versa. On balance, sulfonium salts as a strategy for [¹⁸F]fluorination is most practical and robust for electron-neutral and mildly-activated substrates. Compromises in cyclisation and radiochemical yields might be necessary for certain strongly electron-

rich or electron-poor systems. This is illustrated in Figure 7.11.

8 | Applications of Dibenzothiophene Sulfonium Salts: PET Tracer 1

This chapter presents efforts towards the synthesis of an imidazole-based PET tracer for the imaging of aldosterone-producing adenomas (APAs), using dibenzothiophene sulfonium salts as precursors for ^{18}F -labelling.

8.1 Towards Novel Tracer for Imaging of Aldosterone-Producing Adenomas

8.1.1 Aldosterone-Producing Adenomas

Aldosterone, a steroid hormone, is the third pillar of the renin-angiotensin-aldosterone system (RAAS), a controlling hormonal cascade for arterial blood pressure (Figure 8.3, bottom)¹⁵².

An overproduction of aldosterone under low renin conditions, for instance through APAs, has a major impact on the blood pressure regulatory system. Although hypertension has been associated with excessive aldosterone secretion, clinical and experimental evidence demonstrated that even in cases of balanced aldosterone activity, a hypertensive condition might occur¹⁵³. Among several APA-related pathologies is primary hyperaldosteronism (PA), a type of drug-resistant hypertension. According to Mattson and Young, PA affects 10% of the US population¹⁵⁴. In their recent study Monticone *et al.* described that patients diagnosed with PA exhibited cardiovascular related issues and organ damage, in comparison to other hypertensive patients¹⁵⁵.

APAs can be recognised and differentiated non-invasively using PET tracers that have been structurally optimised to interact with an enzyme involved in the overexpression of aldosterone. CYP11B2, also known as aldosterone synthase or steroid

18-hydroxylase (Figure 8.1), is a mitochondrial protein of the cytochrome P450 family expressed in the zona glomerulosa in the adrenal cortex. It acts as a catalyst for the conversion of 11-deoxycorticosterone to aldosterone¹⁵⁶. The intermediates and enzymes involved in this transformation are presented in Figure 8.3.

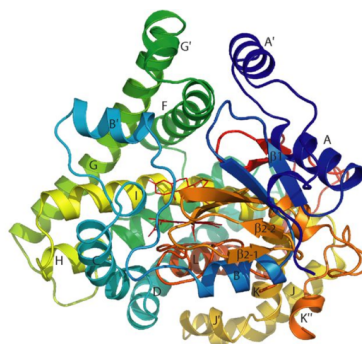


Figure 8.1: Co-crystal structure of CYP11B2 with a steroid substrate (11-deoxycorticosterone) at its active site. Image courtesy of Strushkevich and co-workers¹⁵⁷.

Aldosterone synthase shares 93% homology with steroid 11- β -hydroxylase (CYP11B1), an enzyme which participates in cortisol biosynthesis. The corresponding genes for the proteins, *CYP11B2* and *CYP11B1*, are both present on the human chromosome 8, located approximately 40 kilobase pairs apart from each other, very likely due to an evolutionary gene duplication (Figure 8.2)^{157 158}.

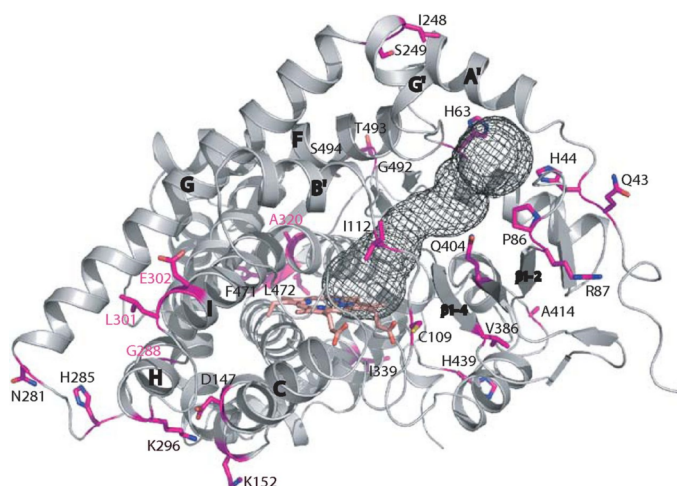


Figure 8.2: Visualisation of structural homology of CYP11B2 and CYP11B1. Differing residues are labelled. Access channels, through which the enzyme active site can be reached, are shown in mesh. Image courtesy of Strushkevich and co-workers¹⁵⁷.

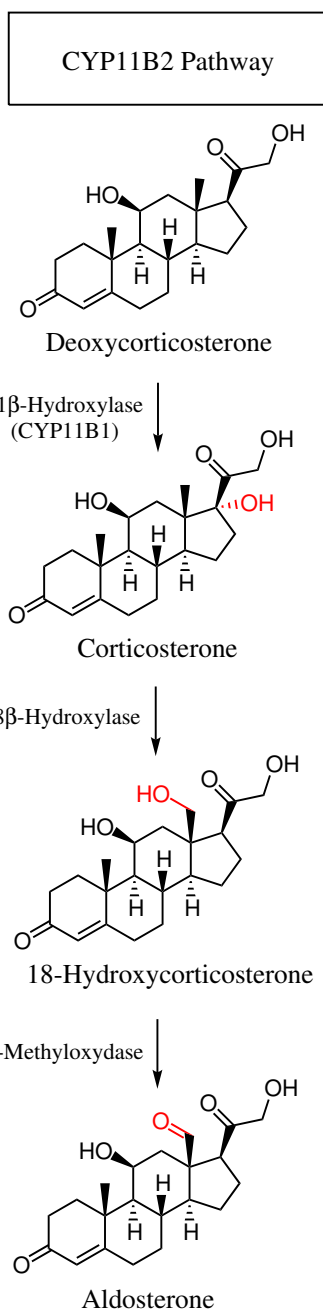


Figure 8.3: Enzymatic pathway of CYP11B2 (including CYP11B1), showing intermediate product structures. Chemical transformations are marked in red. Adapted from Shojaati and co-workers¹⁵⁹.

8.1.2 PET Imaging of Aldosterone-Producing Adenomas

A small difference of 29 residues between mature CYP11B2 and CYP11B1 handicaps design of potent CYP11B2 inhibitors for PET imaging of APAs. Table 8.1 summarises CYP11B2 inhibitors that have been extensively studied in the last two decades, owing to their potential therapeutic usage in the treatment of aldosterone-

related pathologies. [^{18}F]Fluorinated candidates for PET imaging of APAs are also presented. The key properties that define potential value of these compounds for preliminary clinical applications are: 1) IC_{50} CYP11B2, 2) IC_{50} CYP11B1 and 3) CYP11B2/CYP11B1 selectivity.

Table 8.1: PET tracer structures based on clinically attractive CYP11B2 inhibitors, with inhibition potencies. Compound **42** was a potential therapeutic.

Inhibitor	$[^{11}\text{C}]\text{MTO}^{160}$	$[^{18}\text{F}]\text{FETO}^{160}$	$[^{18}\text{F}]\text{LCI699}^{161}$	42 ¹⁶²	43 (this work)
	Properties				
CYP11B2					
IC_{50} [nM]	16.7	20.2	0.7	1.7	-
CYP11B1					
IC_{50} [nM]	4.6	2.9	2.5	28	-
Selectivity (B1/B2)	0.28	0.15	3.57	16.5	-

An imidazole-based CYP11B2 and CYP11B1 inhibitor, metomidate (MTO, Figure 8.4), previously serving as a veterinary anaesthetic, gained significant attention in 1998, when its ^{11}C -labelled analogue was first used as a PET tracer for the imaging of tumours of adrenocortical origin in primates¹⁶³.

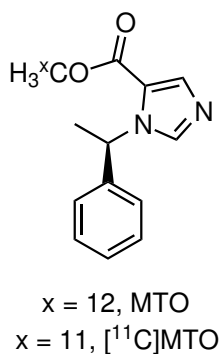


Figure 8.4: Metomidate its carbon-11 analogue, [^{11}C]MTO.

It exhibits high and selective uptake in the adrenal cortex, while having low affinity towards noncortical masses (the standardised uptake value (SUV) of 30.7 versus 18.4, respectively). PET imaging with [^{11}C]MTO offered a non-invasive route for diagnosis of primary hyperaldosteronism. It was not only a more cost-effective but also less practically-demanding alternative to the current state-of-art invasive diagnosis via adrenal vein sampling (AVS). AVS, a clinical procedure for the assessment of unilaterality or bilaterality of hormonal production, is not straightforward. Issues have been reported, particularly with the small-sized right adrenal vein, which suffers from a surprisingly low success rate for cannulation (50-80%) even in the most experienced institutions^{163 164}. Complications following AVS include blood vessel rupture and haemorrhage, which could have a disruptive effect on laparoscopic surgery. In addition to its non-invasive nature, the applicability of PET in diagnostic tumour imaging extends to distinguishing not only its origin, cortical (such as adrenal adenomas) or noncortical (such as cyst or lipomas), but also malignancy¹⁶⁵. Although implementation of ^{11}C -metomidate for the imaging of APAs represented a major advancement in PHA diagnosis, its widespread clinical use is inherently handicapped by its far from perfect selectivity towards aldosterone synthase in comparison with 11β -hydroxylase (B1/B2, Table 8.1). The study by Bergström *et al.* unveiled that high uptake of [^{11}C]MTO was also observed in adenomas that were not hormone-secreting, hence limiting its use as an APA tracer¹⁶⁵. Evaluation of the imaging powers of [^{11}C]MTO and [^{18}F]FDG for adrenal incidentalomas, performed by Minn *et al.*, confirmed the superior properties of the former in characterising tumour origin and malignancy. [^{11}C]MTO displayed lower uptake in noncortical tumours in contrast to [^{18}F]FDG¹⁶⁶. The short half-life of carbon-11 (20 min) and challenging radiosynthesis played a major role in the assessment of its practicality for widespread use. The use of carbon-11 is limited to institutions with an on-site cyclotron. The cost adds up quickly as only one patient can be scanned per tracer batch. Researchers have expressed moderate excitement for the future of [^{11}C]MTO as a diagnostic tool for incidentalomas. Efforts have been directed towards the synthesis of its [^{18}F]fluorinated analogue.

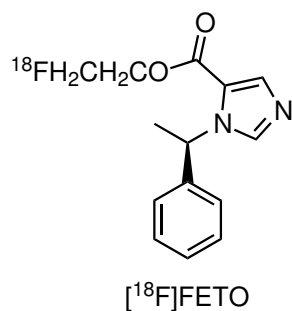


Figure 8.5: [¹⁸F]FETO.

Wadsak and Mitterhauser designed [¹⁸F]FETO as an alternative to [¹¹C]MTO, based on the higher affinity of the ethyl ester for CYP11B1, compared to the methyl analogue (metomidate versus etomidate). In addition, ¹⁸F-incorporation via aliphatic nucleophilic substitution is more facile than radiosynthesis of [¹¹C]MTO¹⁶⁷. Despite advantages associated with the half-life of fluorine-18 (110 min), such as wider availability, [¹⁸F]FETO exhibits a similar binding profile to CYP11B2 to [¹¹C]MTO (Table 8.1), as well as equally fast metabolism¹⁶⁸. An investigation of biological properties of [¹⁸F]FETO analogues was performed by Erlandsson *et al.*, who introduced halogen substituents at the *para*-position and/or increased the ester chain size to 3 carbons¹⁶⁹. They concluded that better tracer uptake in the adrenals was observed for the *para*-substituted analogues than for [¹¹C]MTO, with decreased uptake in other organs (kidneys, liver, pancreas and lungs). The 4-chloro derivative was considered the most suitable candidate for further studies, based on: 1) favourable uptake ratio between the adrenals and liver, 2) smaller degree of defluorination and 3) highest specific binding in the series, despite relatively faster metabolism.

The search for potent CYP11B2 inhibitors arrived at fadrozole (Figure 8.6), a cyanated derivative of metomidate, originally a CYP19 (aromatase) inhibitor. Interestingly, chiral separation led to the differentiation into enantiomers of nearly opposing inhibition with respect to CYP11B2 and CYP11B1.

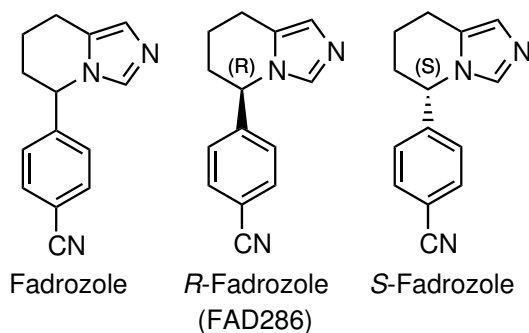


Figure 8.6: Fadrozole, CYP11B2 inhibitor, and its enantiomers.

R-Fadrozole, FAD286, was shown to exhibit superior aldosterone synthase inhibition in male Chinese hamster cell lines, in comparison to 11 β -hydroxylase (B1/B2 selectivity of 19.8). *S*-Fadrozole is less selective for B2 than B1 (B1/B2=0.23), similarly to [^{11}C]MTO, however with significantly less potency for both enzymes¹⁷⁰. Simultaneously, structure-activity relationship studies of FAD286, carried out by Meredith *et al.* at Novartis, aimed to investigate its biological potential and evaluate its use as an inhibitor of aldosterone synthase¹⁶¹. Inspired by the intriguing reversal of B2/B1 selectivity on inversion of configuration, efforts were made to explore the substitution pattern at the chiral carbon, as well as at the *ortho*-position on the phenyl ring. Decreasing the size of the cyclohexane by one carbon and introduction of an *ortho*-fluorine atom gave rise to LCI699 (Figure 8.7), with a significantly higher recombinant human CYP11B2 inhibition potency than FAD286 (1.8 nM vs 0.7 nM). Good inhibition was also obtained for CYP11B1. LCI699 is favoured over MTO and FETO based on: 1) higher potency against CYP11B2 and 2) better selectivity for B2.

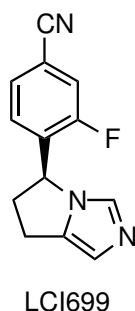


Figure 8.7: LCI699, a derivative of FAD286.

In 2013 Schumacher *et al.* described their findings on the behaviour of LCI699

in vivo, following phase II clinical trials for patients with 4 types of hypertension: essential, controlled, resistant and secondary¹⁷¹. Particularly relevant to the subject of this research were results of the proof-of-concept study with patients diagnosed with primary hyperaldosteronism. The impact of LCI699 on the activity of CYP11B2 was investigated. The levels of 11-deoxycorticosterone (a substrate for aldosterone synthase, Figure 8.3) were significantly elevated, more than it was observed with fadrozole. Plasma aldosterone levels were depleted, ascertaining the inhibitory action of LCI699 on aldosterone biosynthesis. The compound also exhibited good metabolic stability and it was well tolerated at the employed doses (0.25-2 mg). Despite promising results, the route to LCI699 becoming a therapeutic agent is impeded by its insufficient selectivity for aldosterone synthase versus 11 β -hydroxylase. This manifests itself in elevated levels of 11-deoxycortisol (a substrate for CYP11B1), which triggers a hypothalamic-pituitary-adrenal feedback axis in response to the shortage of cortisol. Novartis expressed concerns about the suitability of LCI699 as a selective CYP11B2 inhibitor. Despite clear limitations of LCI699 as a therapeutic strategy, the presence of a fluorine atom offers an opportunity for quantification of aldosterone-secreting adenomas using PET imaging with fluorine-18. Tracers for PET studies are employed in subpharmacological doses (*cf.* nanomolar for PET to mmol for therapeutic doses) with the intention to image biochemical changes without homeostatic disruption. An [¹⁸F]fluorinated analogue of LCI699 makes a suitable tracer candidate for the imaging of APAs.

Encouragingly, an analogue of LCI699 has already been prepared by the Årstad group (Figure 8.8). The findings published were by Sander *et al.* in the proof-of-concept investigation of functionalised triarylsulfonium salts as precursors for ¹⁸F-labelling (Chapter 3)⁴. An imidazole-based scaffold (Scheme 8.1) was prepared in 52% yield over 5 steps. The sulfonium salt was labelled in 20 \pm 2% decay-corrected isolated RCY. This example represented a major advancement in the field of fluorine-18 chemistry. A mildly-activated aromatic system was successfully labelled directly, in the presence of a basic moiety.

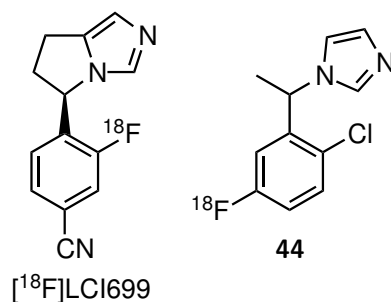
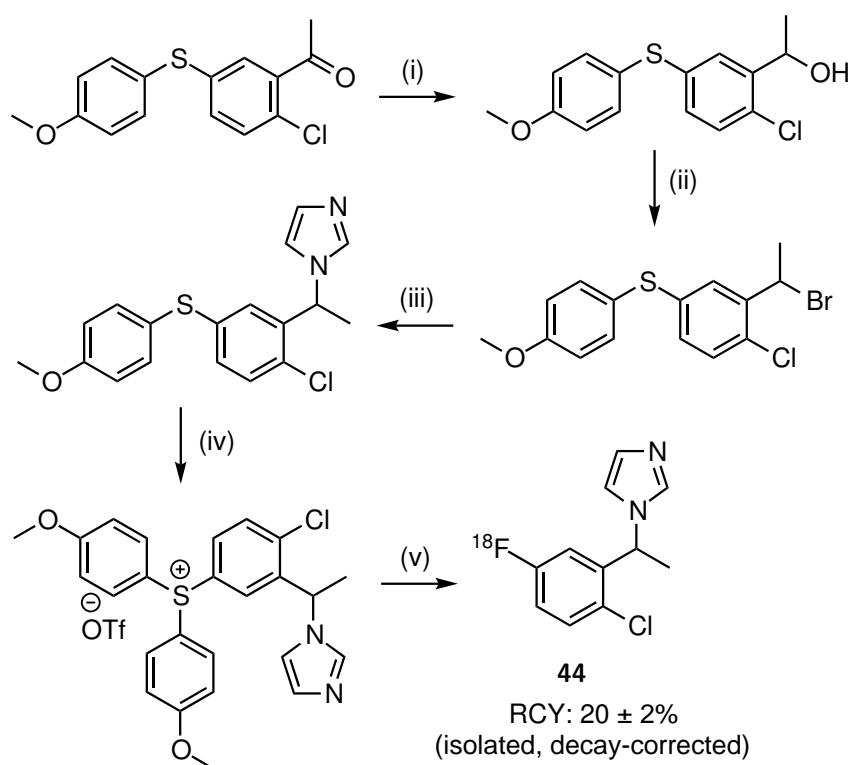


Figure 8.8: $[^{18}\text{F}]\text{LCI699}$ (left) and its imidazole-based structural derivative (right), investigated by Sander and co-workers⁴.



Scheme 8.1: Synthesis and radiolabelling of the imidazole scaffold performed by Sander and co-workers.

Reagents and conditions: (i) NaBH_4 , MeOH, $0\text{ }^\circ\text{C}$ - rt, 2 h; (ii) PBr_3 , DMC, $0\text{ }^\circ\text{C}$ - rt, 6 h; (iii) NaH , imidazole, DMF, rt, 16 h; (iv) Bis(4-methoxyphenyl)iodonium, Cu(II) benzoate, TfOH, chlorobenzene, reflux, 12 h; (v) $[^{18}\text{F}]\text{F}^-$, K_{222} , KHCO_3 DMSO, $110\text{ }^\circ\text{C}$, 15 min.

LCI699, among many others, is a product of extensive structural modifications of *R*-fadrozole. They were carried out in the hope of arriving at a more potent CYP11B2 inhibitor for the study and treatment of aldosterone-dependant pathologies, including primary hyperaldosteronism. These alterations involved basic heterocycles, such as

imidazoles, pyridines or isoquinolines, owing to their affinity for the central Fe^{2+} ion of hemoproteins, *e.g.* CYP11B1 and CYP11B2. Roumen *et al.* employed molecular docking to investigate the structure-activity relationship of fadrozole analogues¹⁶². The list of possibilities was condensed to 1-benzyl-1*H*-imidazoles, devoid of chiral centres or bicyclics, based on the interaction of 18-hydroxycorticosterone, a CYP11B2 substrate, with the active site of the enzyme. The results of *in silico* research were complemented by *in vitro* screening in hamster cells modified to express human cortisol and aldosterone synthases. Substitution pattern at the phenyl ring was explored through F, Br, Cl, CN, methoxy, amine and hydroxy substituents in the *meta*- and *para*-positions, as well as the 5-position on the imidazole. Structure **42** proposed by Roumen and co-workers possesses a nitrile group in the 4-position and a phenylimidazole moiety (Figure 8.9).

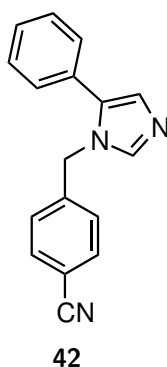


Figure 8.9: Compound **42**, investigated by Roumen and co-workers, is a structural derivative of fadrozole.

Imidazole **42** was found to exhibit high potency for CYP11B2 and the highest selectivity for B2 versus B1 (Table 8.1, page 117). The *para*-CN substituent and its interaction with arginine Arg123 was found to be essential for achieving desired selectivity for aldosterone synthase. The bulky 5-phenyl substituent introduces steric hindrance and reduces conformational freedom experienced by the 1-benzyl-1*H*-imidazole skeleton of fadrozole.

8.1.3 Synthesis of Imidazole-Based Dibenzothiophene Sulfonium Salt Precursor to Novel PET Tracer Candidate

First Attempt at Cyclisation and ^{18}F -Labelling

Having explored numerous avenues in the search for promising PET tracers, high hopes were placed on candidate **43** as a potential CYP11B2 inhibitor for the imaging of aldosterone-producing adenomas.

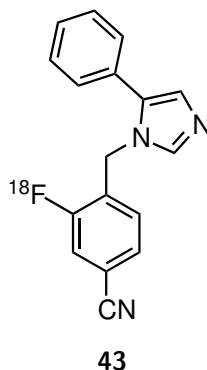
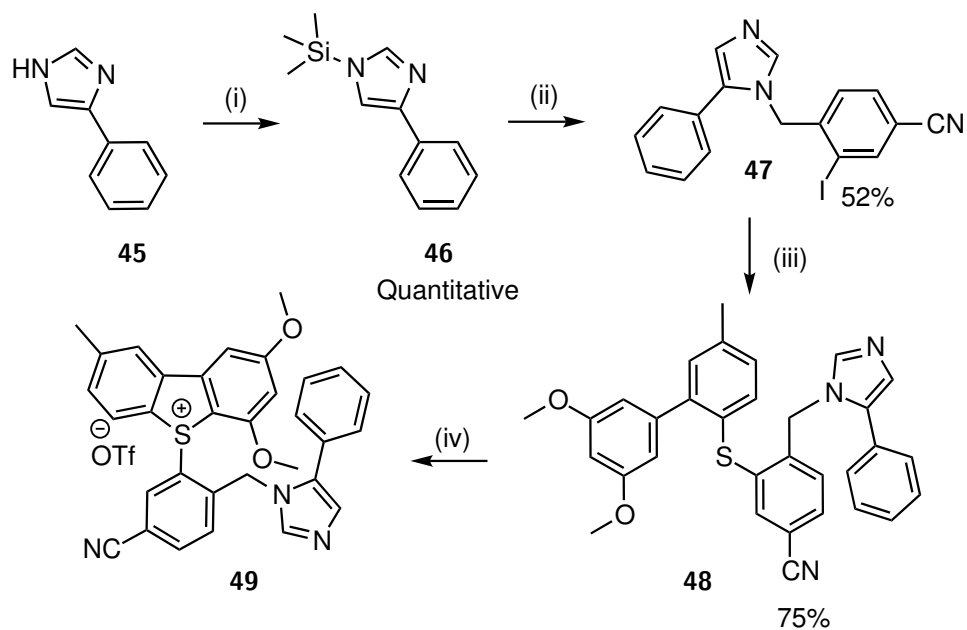


Figure 8.10: Compound **43**, with a fluorine-18 tag at the 2-position of the phenyl ring, was proposed as the new lead structure for the imaging of APAs.

Encouraged by the successful labelling of metomidate derivative **44** by Sander *et al.* (Scheme 8.1), a synthetic route towards compound **43** was designed (Figure 8.10). It was speculated that radiolabelling efficiency could be improved, given the more electron-withdrawing power of the nitrile group *meta* to the ^{18}F substituent (Hammett constant for CN, $\sigma_{\text{meta}} = 0.56$) in comparison with chlorine in the 4-position ($\sigma_{\text{para}} = 0.23$)¹⁷². The synthetic route to sulfonium salt precursor **49** is shown in Scheme 8.2.



Scheme 8.2: Synthesis of sulfonium salt **49**.

Reagents and conditions: (i) HMDs, reflux, 20 h; (ii) 4-(Bromomethyl)-3-iodobenzonitrile, K_2CO_3 , DMF, 100 °C, 3 h; (iii) Thioether **4**, $Pd_2(dba)_3$, DPEphos, $KOtBu$, toluene, reflux, 3.5 h; (iv) Optimisation process of cyclisation conditions.

Initial stages of the investigation were performed by Dr Vincent Gray (formerly UCL Radiochemistry), who synthesised the non-radioactive fluorinated counterpart to compound **43** and established the synthetic route to thioether **48**. Phenylimidazole was first protected with a trimethylsilyl group in an overnight reaction with hexamethyldisilazene (HMDs) at 100 °C. The resulting compound was used without purification in the next step, where it underwent an S_N2 reaction with 4-(bromomethyl)-3-iodobenzonitrile to form imidazole **47**. Coupling to thioether **4** (Scheme 5.3), mediated by $Pd_2(dba)_3$, afforded thioether **48** in 75% yield. It was then employed in the cyclisation reaction to form sulfonium salt **49**, a precursor for ^{18}F -labelling.

Cyclisation was first attempted with NCS and $Bi(OTf)_3$ in MeCN at room temperature for 2 h. Disappointingly, only a negligible yield of the desired product was obtained. NMR analysis revealed the presence of a chlorinated sulfonium salt analogue (Figure 8.11), resulting from the competitive side chlorination, as observed for sulfonium salt **37** (Chapter 7, Section 7.5, Table 7.2). HPLC analysis revealed

that the chlorinated product constituted as much as 83% of the sample. Its mass was confirmed by LC-MS analysis. Similar results were obtained when NCS and TfOH were used in the cyclisation. In addition, it was observed that any efforts towards deprotonation of the imidazole moiety failed or resulted in decomposition. In the presence of strong bases such as NaH or NaOH decomposition occurred, while milder bases, such as potassium carbonate, failed to accomplish deprotonation. In contrast, the imidazole-decorated triarylsulfonium salt (Scheme 8.1) was washed with 3 M NaOH, before column chromatography purification, without decomposition. When subjected to $[^{18}\text{F}]\text{F}^-$, the mixture of sulfonium salt **49** and its chlorinated analogue **50**, failed to deliver the radiolabelled product. Although both are expected to undergo radiolabelling in a similar manner, $[^{18}\text{F}]\text{F}^-$ is deactivated by the extra proton as a result of hydrogen bonding. Precursors for labelling are used in large excess, hence no radiolabelling is expected to occur. This is illustrated in Figure 8.11.

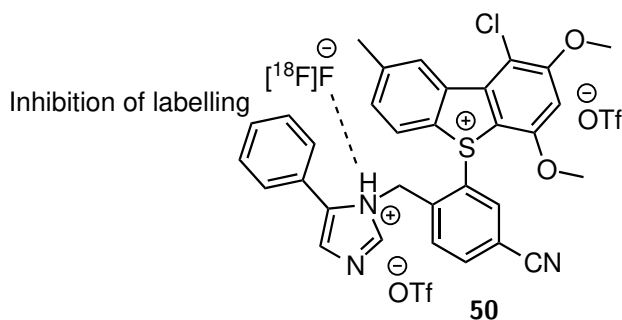


Figure 8.11: The major product of the cyclisation reaction of thioether **48** with NCS/ $\text{Bi}(\text{OTf})_3$ and NCS/TfOH is chlorinated sulfonium salt **50**.

Taking over the investigation from Dr Vincent Gray, an initial explanation for his results was formulated. It was based on a hydrogen-bond interaction of the proton with a neighbouring methoxy group on the dibenzothiophene scaffold. This could result in stabilisation of the protonated form and unsuccessful deprotonation attempts (Figure 8.12). To test this hypothesis, a radiolabelling experiment was set up, in which the sulfonium salt precursor to $[^{18}\text{F}]\text{FPEB}$ (Chapter 5) was labelled in the presence of sulfonium salt **49** and **50**. Remarkably, the reaction failed and no $[^{18}\text{F}]\text{FPEB}$ formation was observed, leading to the conclusion that $[^{18}\text{F}]\text{fluorination}$ of the corresponding sulfonium salt **6** was blocked. Protonation of the imidazole

moiety of sulfonium salts **49** and **50** could be a potential explanation for the findings.

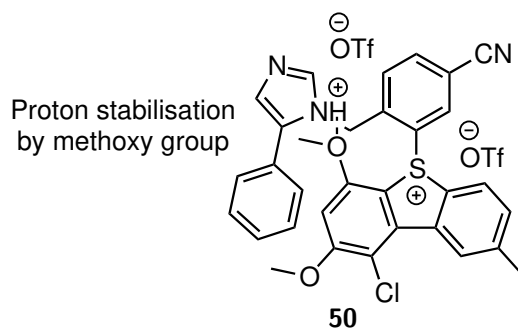


Figure 8.12: Hypothetical "proton sponge". Interaction of the OMe substituent with the protonated imidazole leads to the formation of a stabilised structure.

It was proposed that the problem could be approached from two angles by: 1) by performing the cyclisation with hypochlorite-based reagents to avoid protonation (Chapter 6) or 2) removing the problematic methoxy group to help deprotonation.

In the first instance, hypochlorite reagents were employed to effect ring closure. Both NaOCl and Ca(OCl)₂ dissociate in water to form HOCl and strong bases, NaOH or Ca(OH)₂, respectively. For a sulfonium salt to be formed from the corresponding thioether, a proton needs to be eliminated to restore aromaticity. In basic conditions, undesired imidazole protonation would not occur. Small-scale cyclisations of thioether **48** were set up with NaOCl (10-15%, reagent grade) and Ca(OCl)₂.

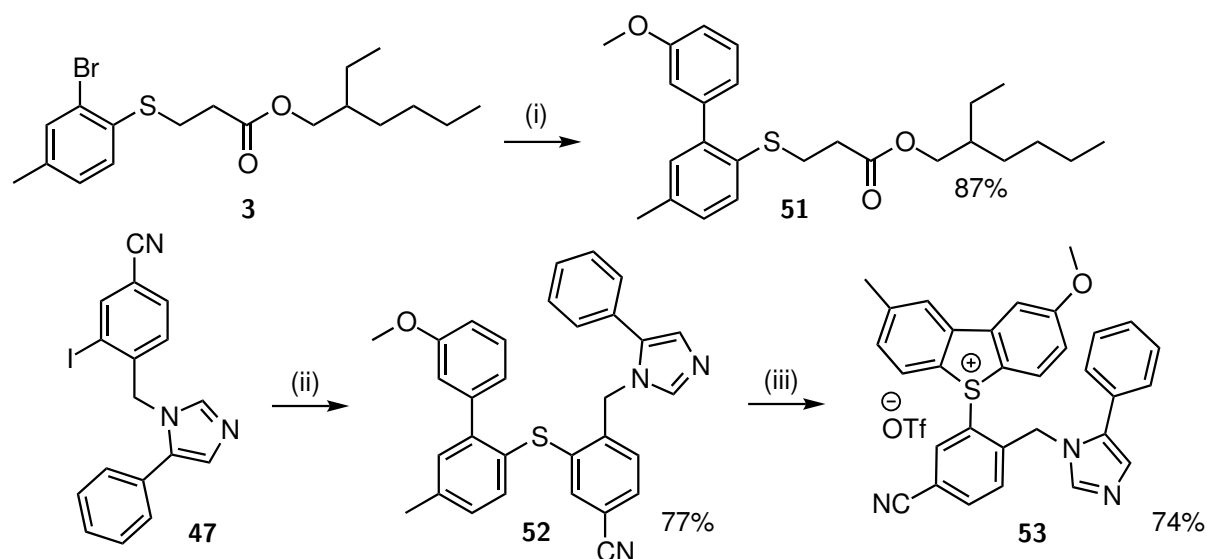
HPLC analysis of a 10 min reaction of thioether **48** with NaOCl at room temperature revealed the presence of sulfonium salt **49** with a relatively small proportion of the chlorinated side product. A significant proportion of the starting material was still observed in the reaction profile, with prominent lipophilic impurities. It was difficult to quantify conversion due to peak tailing and the presence of shoulders. When the reaction was repeated, the profile could not be reproduced and only decomposition was observed. This scenario was already seen in the optimisation process with thioether **14** (Chapter 6, Section 6.3.2). Cyclisation with Ca(OCl)₂ did not afford any product at room temperature, yet prominent decomposition peaks appeared after 10 min. Despite the underlying potential of hypochlorite-mediated dibenzothiophene sulfonium salt formation, the method suffers from reproducibility and robustness

issues and an alternative approach was required.

Modifications of Dibenzothiophene Sulfonium Salt Scaffold

In order to prove the existence of the "proton sponge" effect (Figure 8.11), the proximal *ortho*-methoxy group was removed from the dibenzothiophene scaffold. There were two potential benefits associated with this modification: 1) interruption of the hypothetical stabilisation effect caused by H-bonding between the protonated imidazole and the *ortho*-methoxy group, 2) reduction of electron density on the diaryl thioether scaffold, thus lowering probability of side chlorination.

The modified thioether **52** was accessed in an analogous synthetic route to thioether **48** (Scheme 8.2). Suzuki coupling of thioether **3** with 3-methoxyphenylboronic acid afforded thioether **51** in an excellent yield of 87%. Thioether **52** was obtained in 77% yield. The entire synthetic strategy is presented in Scheme 8.3.



Scheme 8.3: Synthesis of sulfonium salt **53**.

Reagents and conditions: (i) 3-Methoxyphenylboronic acid, Pd(PPh₃)₄, K₂CO₃, toluene/water, reflux, 16 h; (ii) Thioether **51**, Pd₂(dba)₃, DPEphos, KO^tBu, toluene, reflux, 3.5 h; (iii) NCS, TfOH, MeCN, rt, 2 h.

The first cyclisation was performed with NCS and Bi(OTf)₃ in MeCN. After 10 min at room temperature, a sample of the reaction mixture was analysed by HPLC, however only starting material was observed. Another aliquot was collected after 2 h but no changes occurred. With 1 equivalent of NCS and 3 equivalents of TfOH,

the cyclisation reached full conversion after 2 h. Only 20% analytical yield was obtained from a 10 min reaction but no other side products were identified. It can thus be inferred that the rate of chlorination was significantly impeded. Flash column chromatography was performed with an addition of ammonia in the eluent. As judged from a 2D TLC plate, no decomposition occurred. Sulfonium salt **53** was isolated in 74% yield. Conveniently, only one regioisomer was formed in the cyclisation, as elucidated from the splitting pattern of the aromatic protons on the dibenzothiophene scaffold, depicted in Figure 8.13.

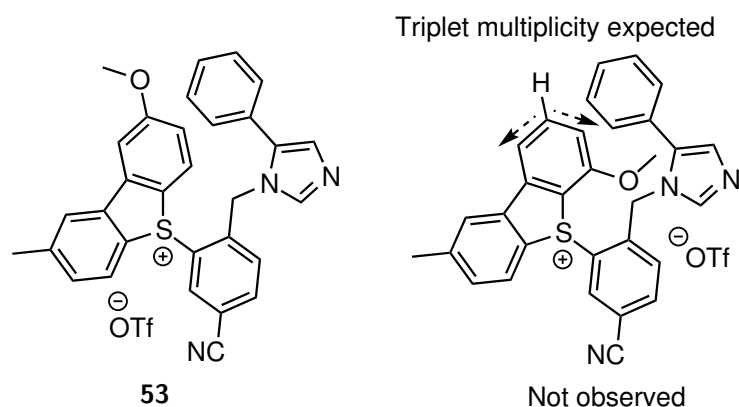


Figure 8.13: Two possible regioisomers of sulfonium salt **53**, expected from the cyclisation reaction of thioether **52**. Only the left-hand side structure was observed by proton NMR.

NMR analysis of the purified product showed a noticeable chemical shift difference of the methylene bridging moiety, compared to the parent thioether spectrum. A shift of 1.1 ppm is too large to result from temperature or pH fluctuations. The likely explanation is the persistent presence of the protonated imidazole form. The change in the methylene peak multiplicity (from singlet to doublet) results from chirality at the sulfur core, which induces In thioether **52**, CH₂ exists as singlet, in the case of sulfonium salt **53**, two well resolved doublets are observed due to chirality at the *S*-centre. Interestingly, no nitrogen-bonded protons were observed by NMR spectroscopy. This is shown in Figure 8.14. A similar picture was also observed by Dr Vincent Gray, with thioether **48** and sulfonium salt **49** (Scheme 8.2). The protonated sulfonium salt form was also identified in the ESI mass spectrum. Sulfonium salt **53**, similarly to sulfonium salt **49**, failed to undergo [¹⁸F]fluorination.

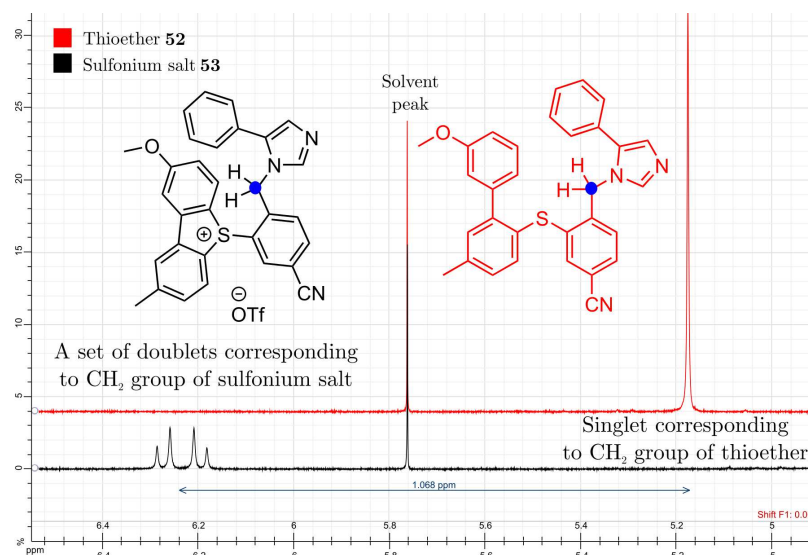


Figure 8.14: Superimposition of proton NMR spectra of thioether **52** (red) and sulfonium salt **53** (black) in d_6 -DMSO. The difference in chemical shift for the methylene protons between the compounds is approximately 1.1 ppm.

Further Modifications to Dibenzothiophene Sulfonium Salt Scaffold

Removing the *ortho*-methoxy group allowed for the following observations. Firstly, electron density on the dibenzothiophene scaffold influences the rate of sulfonium salt formation as well as the rate of chlorination. Secondly, there are other factors implicated in the unusual stability of the protonated form of sulfonium salt **53**, which cannot be ascribed solely to the hydrogen bonding interaction between the *ortho*-methoxy substituent. It was proposed that by replacing the dibenzothiophene methyl group with a methoxy, electron density of the system would increase, resulting in a more efficient cyclisation. It was speculated that sulfonium salt formation could perhaps be achieved in the presence of hypochlorite reagents, such as $\text{Ca}(\text{OCl})_2$. Consequently, the problem of imidazole protonation would be eliminated. The described scenario is illustrated in Figure 8.15. Another benefit of this approach could include deconvolution of NMR spectra analysis of sulfonium salt, as a result of formation of a symmetrical dibenzothiophene scaffold. The proposed synthetic route to sulfonium salt **58** is presented in Scheme 8.4.

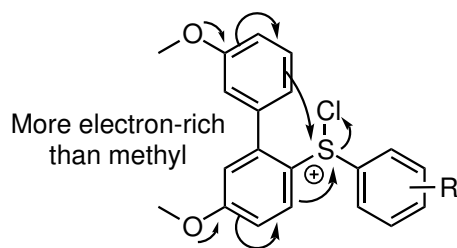
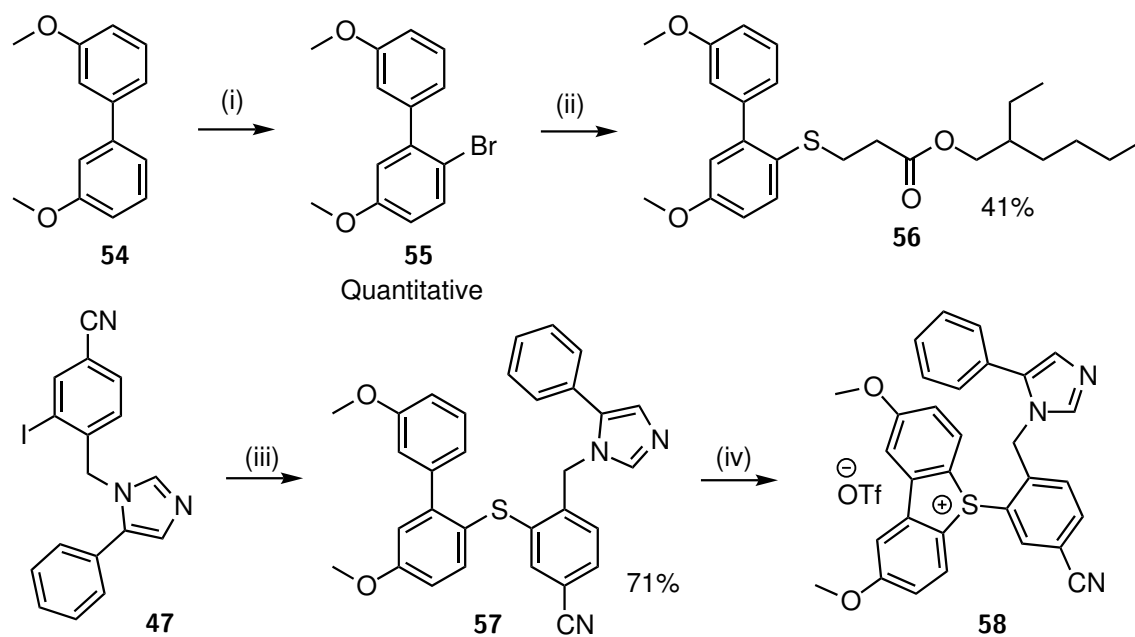


Figure 8.15: Replacing the methyl group with a methoxy is expected to increase electron density on the dibenzothiophene scaffold and facilitate cyclisation, even with milder reagents.



Scheme 8.4: Synthesis of sulfonium salt **58**.

Reagents and conditions: (i) NBS, DMF, $-5\text{ }^{\circ}\text{C}$, 1 h; (ii) $\text{Pd}_2(\text{dba})_3$, xantphos, Et_3N , toluene, reflux, 18 h; (iii) Thioether **56**, $\text{Pd}_2(\text{dba})_3$, DPEphos, $\text{KO}t\text{Bu}$, toluene, reflux, 18 h; (iv) Optimisation process of cyclisation conditions.

Aromatic bromination of 3,3'-dimethoxy-1,1'-biphenyl at the *para*-position afforded the desired bromoarene **55** quantitatively. Installation of the alkyl protecting group was completed after refluxing overnight, however flash chromatography purification proved more challenging due to the formation of impurities, which co-eluted with product **56**. As a result, two consecutive chromatography purifications were required. A 0-10% DCM/toluene elution allowed for a seemingly successful separation, however as the presence of impurities was revealed by NMR spectroscopy, a 10-30% ether/petroleum ether gradient was required to obtain a high-purity sample of thioether **56**. Eventually, it was isolated in 41% yield. Subsequent coupling with imidazole **47** afforded thioether **57** in 71% yield.

Cyclisation of thioether **57** was attempted with $\text{Ca}(\text{OCl})_2$ in MeCN at room temperature, yet no sulfonium salt formation was observed. LC-MS analysis of the reaction mixture revealed the presence of starting material and its chlorinated analogue. Perhaps the substantial increase in electron density, resulting from the replacement of the methyl entity by methoxy, favoured aromatic chlorination over S-Cl bond formation.

Further Insights into Dibenzothiophene Sulfonium Salt Formation

An alternative hypothesis was proposed to explain the unusual stability of the protonated imidazole towards deprotonation. It was based on its interaction with the soft triflate counterion. Replacement with hydroxide caused decomposition of the sulfonium salt scaffold. This is illustrated in Figure 8.16. One piece of evidence towards this assumption was provided by Dr Vincent Gray, who at the beginning of the investigation, attempted deprotonation of sulfonium salt **49** with NaOH. Decomposition was observed as an almost instantaneous darkening of the reaction mixture during liquid-liquid extraction.

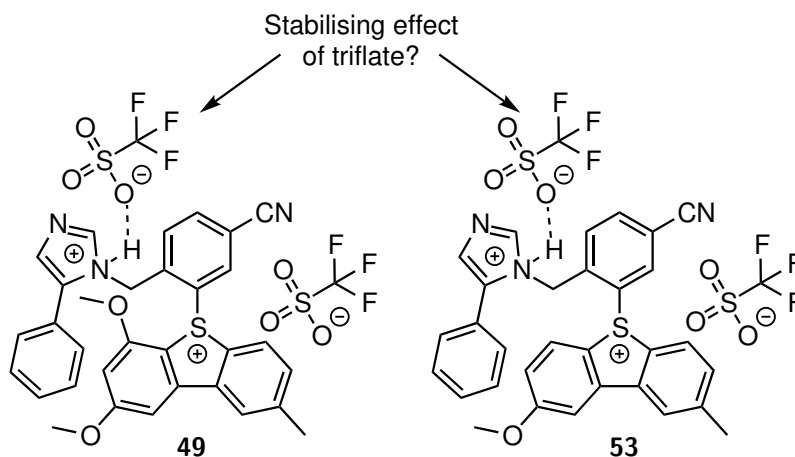


Figure 8.16: Hypothetical stabilising effect of the triflate ion, illustrated on sulfonium salts **49** and **53**.

To test this concept, imidazole **47** (Scheme 8.4) was protonated with 1 equivalent of TfOH and subsequently washed with 2 M NaOH. Proton NMR spectrum of the resulting organic extracts showed no signs of decomposition or peak shifting (Figure 8.17).

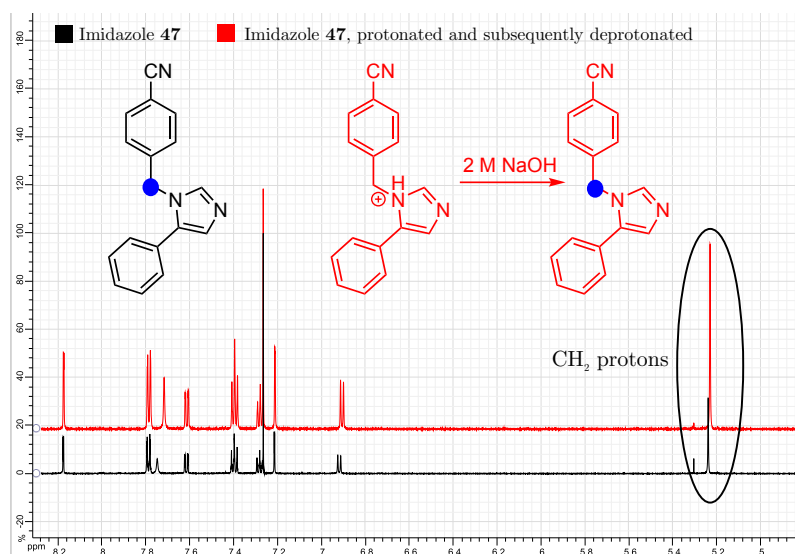


Figure 8.17: Superimposition of imidazole **47** proton NMR onto that of the protonated and subsequently deprotonated equivalent. No decomposition or peak shifting could be observed.

This issue could perhaps be resolved with replacement of the triflate counterion during sulfonium salt formation. Crivello *et al.* successfully synthesised triarylsulfonium salts with fluoride-based counterions: BF_4^- , AsF_6^- , SbF_6^- and PF_6^- .⁷⁹ The

aforementioned anions are soft and non-nucleophilic, thus very good at stabilising the positive charge on the sulfur. Limitations of this method lie in the potential significant decrease of specific activity of $[^{18}\text{F}]\text{F}^-$ due to isotopic exchange by the counterion. Small nucleophilic anions, such as Cl^- or Br^- are not suitable for this application. Swain and Kaiser reported decomposition of trialkyl- and triarylsulfonium halides¹⁷³.

Modifications of PET Tracer Structure

Findings described in previous sections inspired further investigation into 1-phenyl-1*H*-imidazoles as inhibitors of aldosterone synthase. Migration of the phenylimidazole moiety from the *ortho*-position, with respect to the nitrile, to the *meta*, gave rise to a novel PET tracer candidate for the imaging of APAs (Figure 8.18). Substituent shift is expected to: 1) change electronics of the system, 2) affect the rate of sulfonium salt formation and 3) reactivity towards $[^{18}\text{F}]\text{F}^-$. This investigation also served as a practical approach for further validation of the counterion effect hypothesis (Figure 8.16).

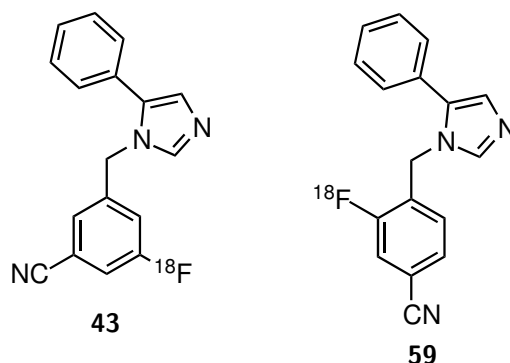
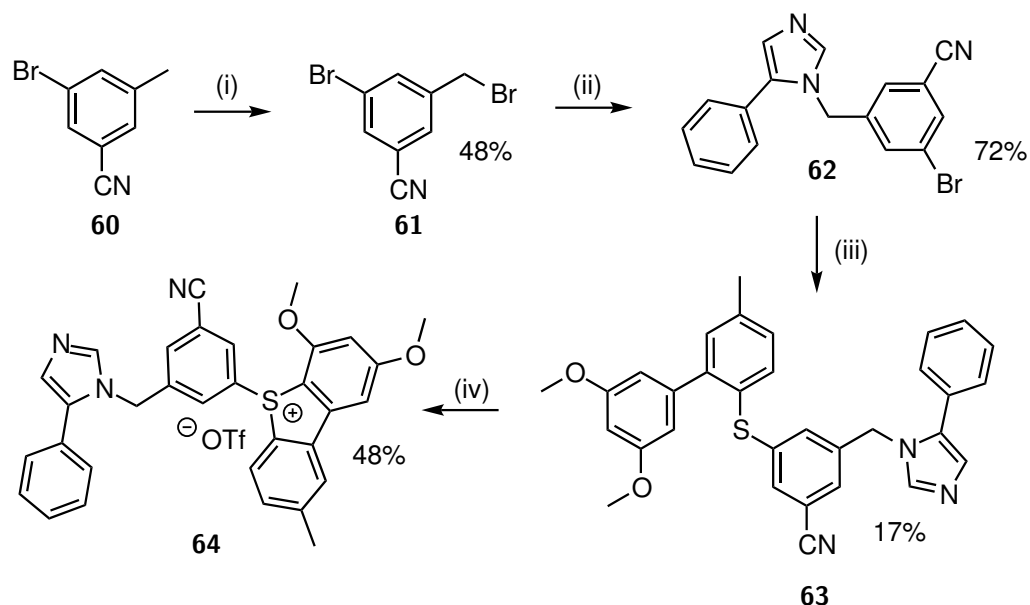


Figure 8.18: Target tracer **43** has not been obtained. Regioisomer **59** could address the limitations of its *ortho*-analogue during radiolabelling.

Although *in vitro* binding affinities of CYP11B2 and CYP11B1 were established for various structurally related 1-phenyl-1*H*-imidazoles, for most of these compounds, the imidazole moiety is situated *para* to the phenyl substituent¹⁶². Although no potencies were available for compound **59** at the time of this investigation, the structure made an interesting case study from the chemistry and radiochemistry point of view. It was thought to complement the scope of highly-functionalised drug-like molecules in the ongoing evaluation of dibenzothiophene sulfonium salts as

precursors for ^{18}F -labelling. The synthetic route to sulfonium salt **64** is presented in Scheme 8.5.



Scheme 8.5: Synthesis of sulfonium salt **64**.

Reagents and conditions: (i) AIBN, NBS, chlorobenzene, reflux, 4 h; (ii) Phenylimidazole **46**, K_2CO_3 , DMF, $100\text{ }^\circ\text{C}$, 1 h; (iii) Thioether **4**, $\text{Pd}_2(\text{dba})_3$, DPEphos, $\text{KO}t\text{Bu}$, toluene, reflux, 2 h; (iv) NCS, TfOH, MeCN, rt, 2 h.

Benzyl bromide **61** was accessed in 48% yield from a Wohl-Ziegler bromination of arene **60** with NBS and a radical initiator AIBN¹⁷⁴. It was then employed in a regioselective *N*-alkylation with the TMS-protected imidazole **46** (Scheme 8.2). Imidazole **62** was synthesised in 72% yield. Palladium-mediated thioetherification with thioether **4** (Scheme 5.3) afforded compound **63** in a surprisingly low yield of 17%. Pleasingly, sulfonium salt **64** was formed in 48% yield.

Analysis of proton NMR shifts of the bridging CH_2 protons of thioether **63** and sulfonium salt **64**, revealed a difference of approximately 0.4 ppm (Figure 8.19), much smaller than observed for thioether **52** and sulfonium salt **53** (Figure 8.14). For the latter, unsuccessful ^{18}F -labelling attempts, together with NMR data, served as evidence towards protonation of the imidazole moiety and formation of a highly-stable complex.

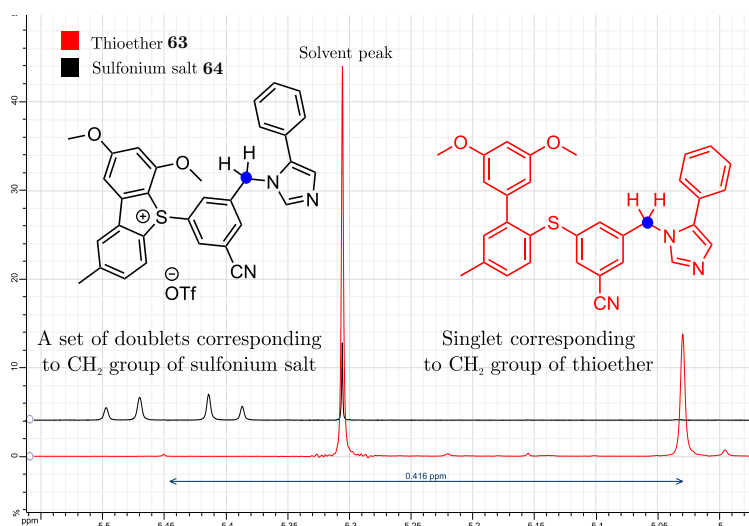
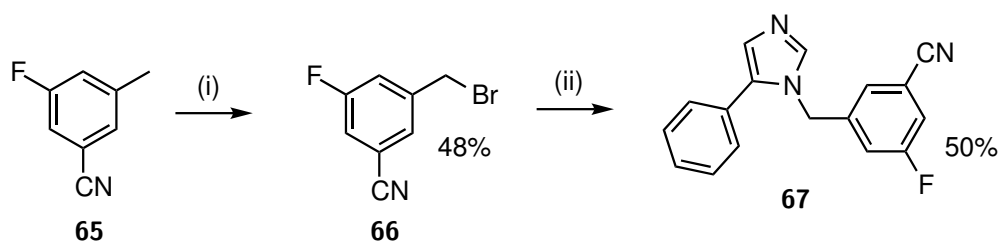


Figure 8.19: Superimposition of proton NMR spectra of thioether **63** (red) and sulfonium salt **64** (black) in CDCl_3 . The difference in chemical shift is calculated as approximately 0.4 ppm.

The cold reference compound for co-injections, imidazole **67**, was accessed in a 2-step route, starting from 3-fluoro-5-methylbenzonitrile. The brominated intermediate **66** was obtained in 48% yield. Finally, coupling to imidazole **46** yielded reference compound **67** in 50% yield (Scheme 13.11).



Scheme 8.6: Synthesis of reference compound **67**.

Reagents and conditions: (i) AIBN, NBS, chlorobenzene, reflux, 4 h; (ii) Phenylimidazole **46**, K_2CO_3 , DMF, 100 °C, 2 h.

Radiolabelling of Novel Imidazole-Based Dibenzothiophene Precursor

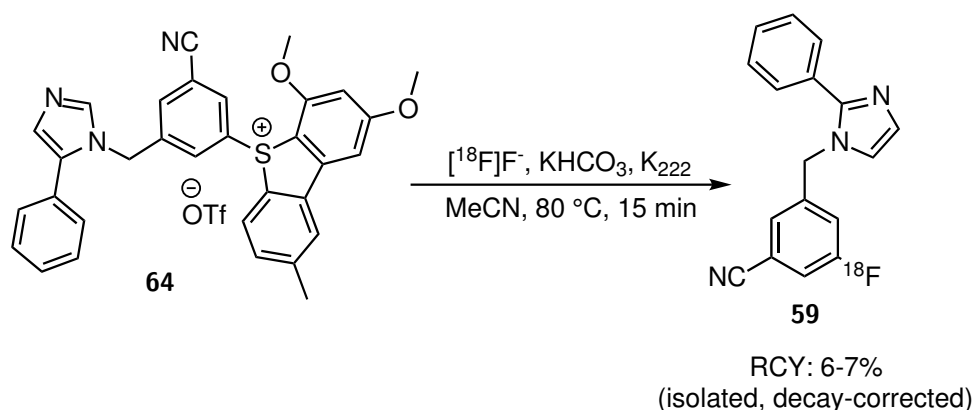
Sulfonium salt **64** was employed in a series of ^{18}F -labelling experiments, however poor RCYs were obtained, as shown in Table 8.2. When $[^{18}\text{F}]$ fluorination was performed in DMSO, radio-HPLC purification of the entire reaction mixture was not possible due to precipitation after quenching with water. As a result, only an approximate analytical RCY of 7-12% was obtained. In MeCN, tracer **59** was isolated in 6-7%

RCY (Scheme 8.7).

Table 8.2: Radiolabelling experiments with sulfonium salt **64**. All isolated yields are decay-corrected and represent the end of synthesis HPLC yields. Whenever the radiolabelled product was not isolated, analytical radio-HPLC yields are provided.

Entry	Precursor Load [mg]	Solvent	Temperature [°C]	Time [min]	Radio-HPLC Yield [%]
1	2	DMSO	110	15	7 ^a
2	5	DMSO	110	15	12 ^a
3	5	MeCN	80	15	7 ^b
4	5	MeCN	80	15	6

^a Analytical radio-HPLC yield. Only half of the crude reaction mixture analysed due to precipitation. ^b Only half of the crude reaction mixture was analysed.



Scheme 8.7: Most successful labelling of sulfonium salt **64** with $[^{18}\text{F}]\text{F}^-$. Isolated decay-corrected RCY was 6-7%.

Despite low radiochemical efficiency, the results of the labelling experiment represent a significant advancement in the study of imidazole-based dibenzothiophene sulfonium salts. Following a long investigation, it was possible to achieve $[^{18}\text{F}]\text{F}^-$ fluorination of sulfonium salt **64**. It served as a learning curve experiment, through which better understanding of sulfonium salt chemistry was gained. Firstly, the dibenzothiophene scaffold can be modified to modulate the rate of chlorination at the methoxy-decorated ring. Secondly, the sulfur centre is highly sensitive to changes in the electronic structure of the PET scaffold, and both cyclisation and $[^{18}\text{F}]\text{F}^-$ fluorination efficiencies will be affected.

The striking difference in the ease of deprotonation for sulfonium salt **64** versus sulfonium salt **53** remains unaccounted for. The counterion stability hypothesis (Figure 8.16) cannot be backed up by this observation. It can be speculated that sulfonium salt **49** (Figure 8.20) adopts a stable conformation, in which the protonated imidazole is stabilised by the methoxy-substituent and/or the dibenzothiophene as a result of π - π stacking. This could perhaps be the consequence of rotational freedom around the methylene bridge. This interaction might not be possible when the imidazole substituent is moved to the *meta*-position. Structural evidence, for example, crystallography data or *in silico* methods, are required to gain more insights into the factors orchestrating reactivity of these sulfonium salts towards $[^{18}\text{F}]\text{F}^-$. A crystal structure of the allegedly protonated forms could help confirm protonation of the imidazole moiety. Given unsuccessful labelling experiments of sulfonium salts **49** and **53**, even in the presence of $[^{18}\text{F}]\text{FPEB}$ (labelled in good RCYs, Chapter 5), the unusual proton stability and consequences thereof are the most likely explanation for the above findings. All imidazole-based sulfonium salts described in this chapter are shown in Figure 8.20.

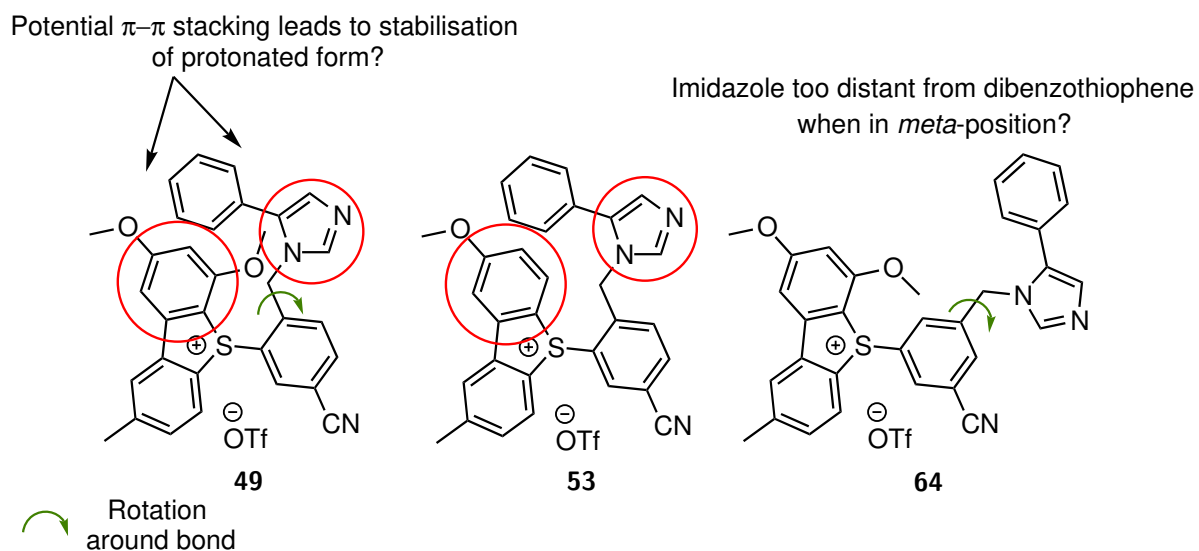


Figure 8.20: All imidazole-based sulfonium salt precursors to the novel PET tracer candidate for the imaging of APAs. The difference in the position of the imidazole substituent could affect the ease of deprotonation, decomposition under basic conditions and radiolabelling efficiency.

8.2 Conclusion

The investigation presented in this chapter has deepened knowledge into the factors orchestrating formation, stability and reactivity of imidazole-based dibenzothiophene sulfonium salts.

Removal of the *ortho*-methoxy group (Figure 8.20) caused significant retardation of the rate of competitive aromatic chlorination. The corresponding sulfonium salt was afforded as the sole product, however, it was obtained in its protonated form due to the acidic nature of the cyclisation with NCS and TfOH. Efforts to deprotonate the product by addition of ammonia to the eluent during flash chromatography proved futile. Disappointingly, alternative reagents did not mediate sulfonium salt formation.

Attempts to explain the unusual stability of the protonated sulfonium salt form were unsuccessful. The triflate counterion was initially thought to stabilise the imidazolium moiety as deprotonation with strong bases resulted in decomposition. This effect was not observed when the imidazole precursor (Figure 8.17) was protonated with triflic acid and subsequently successfully deprotonated with sodium hydroxide. Unsurprisingly, sulfonium salt **53** did not undergo ^{18}F -labelling.

The *meta*-isomer **64** (Figure 8.20) was successfully deprotonated with sodium hydroxide before being subjected to ^{18}F -labelling. A surprisingly low isolated RCY of 6-7% was obtained. It had initially been speculated that radiolabelling of sulfonium salt **64** could proceed with similar RCY to that of sulfonium salt **7**, the precursor to [^{18}F]FPEB (Chapter 5, Section 5.1.1, Scheme 5.5). At this moment, it is difficult to rationalise the difference in reactivity towards [^{18}F]F $^-$ of these structurally-similar substrates.

In addition to the limited practicality of the radiolabelling, there currently is no biological data, specifically binding affinities for CYP11B2 and CYP11B1, to back up further development of precursor **64**.

9 | Applications of Dibenzothiophene Sulfonium Salts: PET Tracer 2

This chapter presents efforts towards the synthesis of a *meta*-pyridine-based PET tracers for the imaging of aldosterone-producing adenomas (APAs), using dibenzothiophene sulfonium salts as precursors for ^{18}F -labelling. It builds on the foundations of Chapter 7, which provides insights into the synthesis and radiolabelling of a simplified *meta*-pyridine sulfonium salt scaffold.

9.1 Synthesis of Dibenzothiophene Sulfonium Salt Based on Aldosterone Synthase Inhibitor

9.1.1 Selection of Novel PET Tracer Candidate for Imaging of APAs

A selection of small molecule CYP11B2 inhibitors were described in Chapter 8. LCI699 was shown to lower aldosterone levels and blood pressure in the clinic, thereby validating this mechanism as a treatment for hypertension. In cell-based *in vitro* assays, LCI699 inhibited CYP11B2 with a modest 4-fold selectivity versus CYP11B1. It also produced an undesired, dose-limiting impairment of cortisol response, presumably as a result of CYP11B1 inhibition. Clinical candidates with higher B2/B1 selectivity are required in antihypertensive therapies¹⁷⁵.

In 2015 Merck published their discovery of benzimidazole-based CYP11B2 inhibitors, which demonstrated good pharmacokinetic properties in rat and rhesus monkeys¹⁷⁵. This extensive optimisation involved screening the Merck compound library to search for a candidate with a high CYP11B2 inhibition potency and selectivity versus CYP11B1. A selection of Merck's benzimidazole series is shown in Figure 9.1.

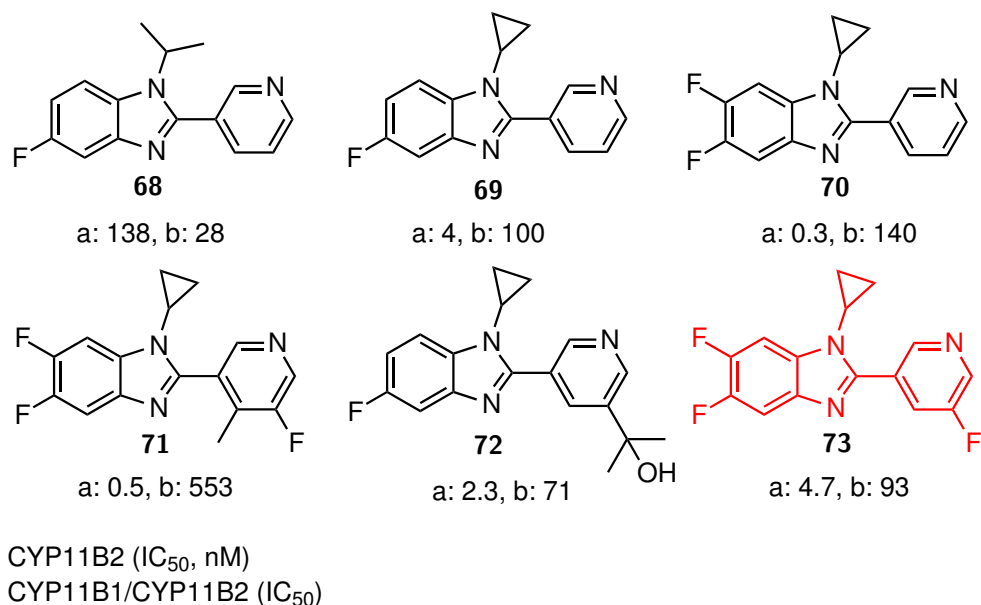


Figure 9.1: Selected benzimidazole inhibitors of CYP11B2 investigated by Merck, with reported IC₅₀ values for CYP11B2 (a) and B1/B2 selectivity (b).

Initially *N*-substitution pattern on the benzimidazole moiety was studied. A correlation was found between potency deterioration and increasing the size of the aliphatic substituent. Interestingly, *N*-cyclopropyl-substituted benzimidazole **69** outperformed its isopropyl counterpart **68** in terms of CYP11B2 inhibition. Subsequent optimisation of benzimidazole phenyl ring substitution identified 5,6-disubstituted analogues, such as compound **70**, with favourable IC₅₀ values for CYP11B2 and good B1/B2 inhibition ratios. Investigation of pyridine substitution lead to the refinement of CYP11B2 potencies, particularly with electron-donating groups, such as methyl or alkoxy. Structure **71**, exhibited excellent inhibition of CYP11B2, however its B1/B2 selectivity was compromised. Inhibitor **72** was identified as the benchmark compound, which owing to a good inhibition and convenient pharmacokinetics, was evaluated in rhesus monkeys. Structure **73** displayed decent CYP11B2 potency (IC₅₀ of 4.7 nM), with favourable selectivity over B1. A comparison of its inhibition profile with LCI699 is shown in Table 9.1. Despite a lower CYP11B2 inhibition value, LCI699 is significantly less selective for B2 than benzimidazole **73**.

Table 9.1: Inhibition profiles of benzimidazole **73** (Merck) and LCI699 (Novartis).

Inhibitor	LCI699 ¹⁶¹	Benzimidazole 73 ¹⁷⁵
CYP11B2 IC₅₀ [nM]	0.7	4.7
CYP11B1 IC₅₀ [nM]	2.5	435
Selectivity (B1/B2)	3.57	93

With a good *in vivo* PK profile, plasma clearance and half-life, the molecule represents a suitable radioligand candidate for PET imaging of aldosterone-producing adenomas. Substitution of the *meta*-fluoro substituent on the pyridine with fluorine-18 was chosen as a proof-of-concept case study for dibenzothiophene sulfonium salts as leaving groups in [¹⁸F]fluorination. Encouraged by the successful labelling of a simplified *meta*-pyridyl moiety (Chapter 7, Section 7.5), the strategy was then implemented to access more structurally demanding drug-like scaffolds. Target PET tracer candidate **74** is shown in Figure 9.2.

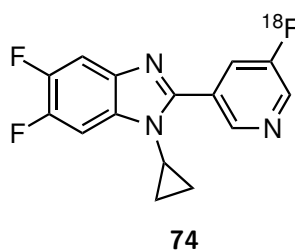
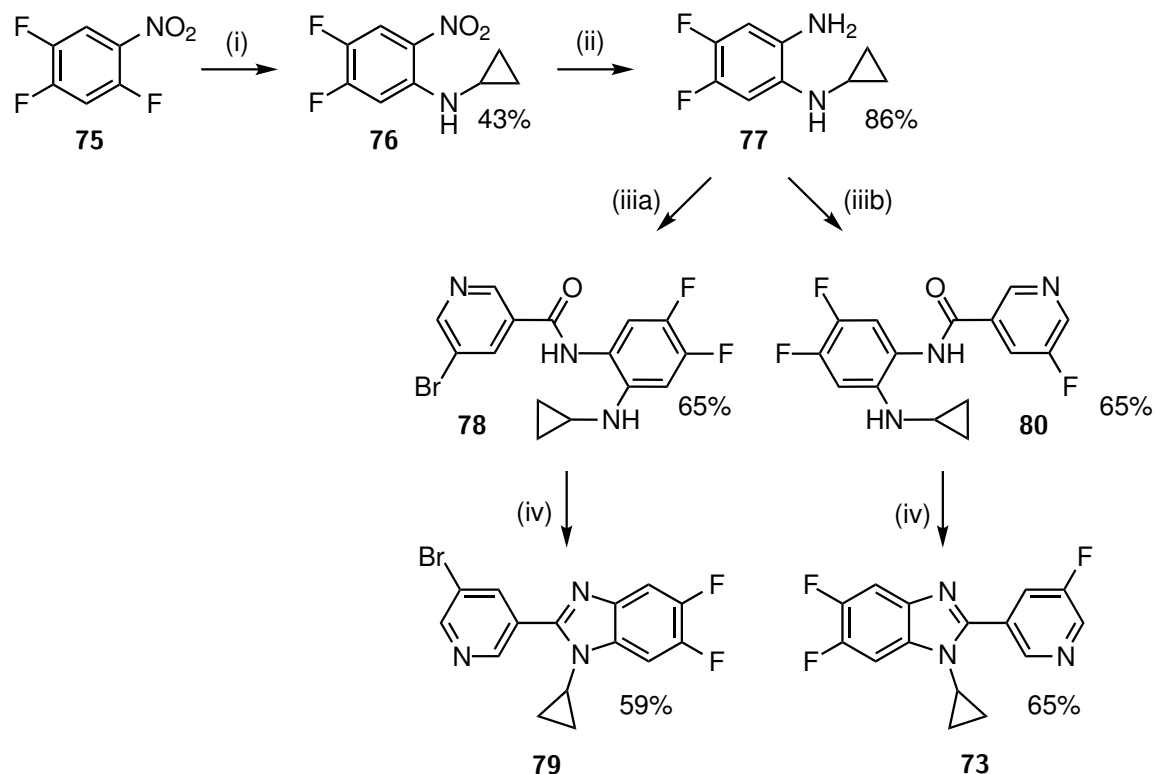


Figure 9.2: Benzimidazole **74** was selected as the novel tracer candidate for PET imaging of APAs.

9.1.2 Synthesis of 3-Pyridyl-Based Dibenzothiophene Sulfonium Salt Precursor to Novel PET Tracer

Syntheses of the sulfonium salt precursor to tracer **74** proved less facile than initially anticipated. It was based on patent procedures published by Merck, often lacking

full method descriptions and characterisation¹⁷⁵. The early efforts are presented in Scheme 9.1.



Scheme 9.1: First attempt at the synthesis of benzimidazole **79** and cold reference compound for co-injections **73**, based on the patent by Merck¹⁷⁵.

Reagents and conditions: (i) Cyclopropylamine, KF, K₂CO₃, MeCN, reflux, 1 h; (ii) Pd/C, H₂, MeOH, rt, 20 h; (iiiia) 5-Bromonicotinic acid, HATU, HOBT, DIPEA, DCM, rt, 2 h; (iiiib) 5-Fluoronicotinic acid, HATU, HOBT, DIPEA, DCM, rt, 17 h; (iv) AcOH, 100 °C, 1 h.

Formation of amine **76** was perhaps the most challenging transformation. Hoyt *et al.* accessed this compound via a nucleophilic aromatic substitution using microwaves. Due to equipment restrictions, a thermal reaction was attempted instead. S_NAr reactions favour polar aprotic solvents, so acetonitrile was chosen, based on its convenient boiling point. The reaction was expected to give 2 regioisomers (Figure 9.3) as the nitro group is both an *ortho*- and *para*-activator.

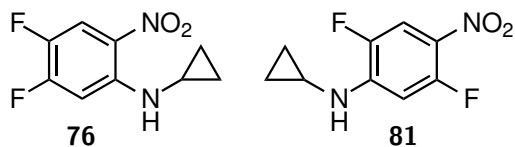


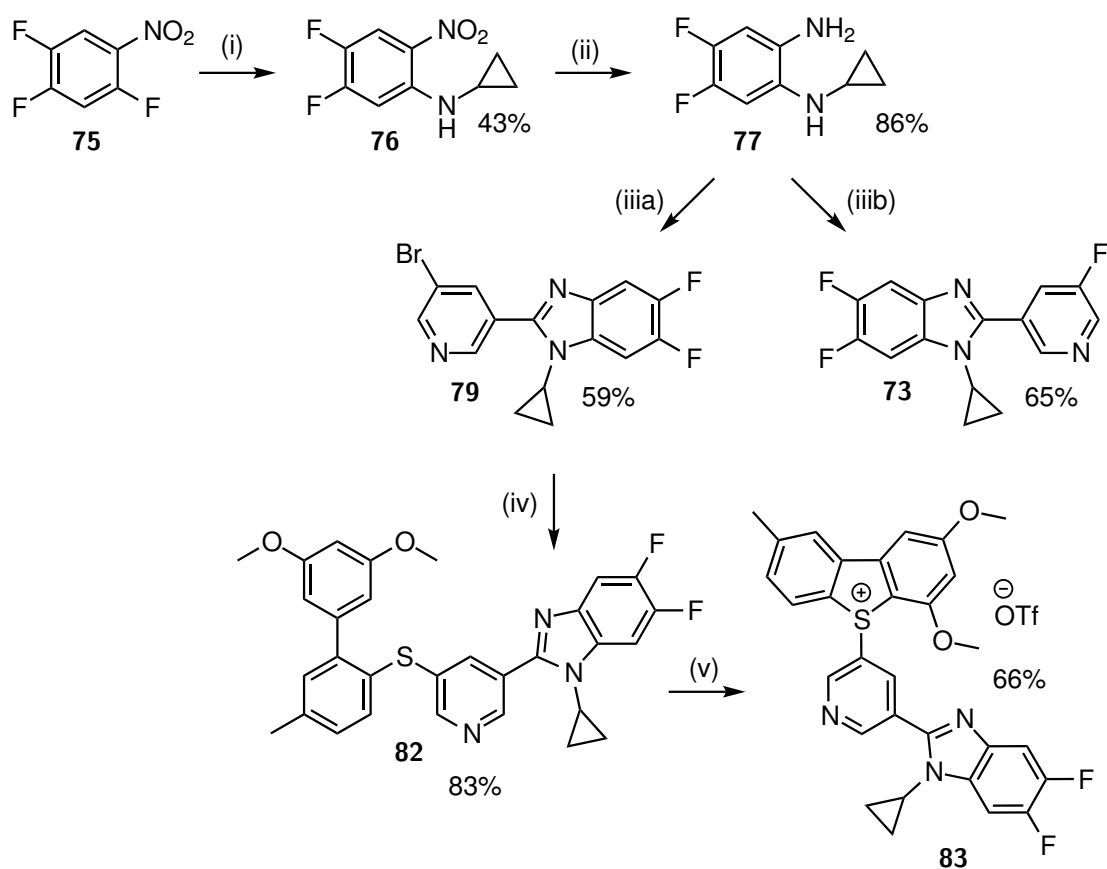
Figure 9.3: Two products were obtained in the substitution reaction of 1,2,4-trifluoro-5-nitrobenzene with cyclopropylamine. Compound **76** is required for further transformations.

The following variables were investigated: 1) order of addition, 2) stoichiometry with respect to KF and 3) temperature. The reaction proved challenging to optimise and it suffered from reproducibility issues. Yields between 4 and 43% were obtained, with undesired regiomer **81** as the major product. To achieve the maximum potential of this reaction, it was essential to use at least 1.5 equivalents of KF, while feeding cyclopropylamine dropwise into the refluxing reaction mixture. For best results, uniform heat distribution was ensured through the use of a sand bath. In addition, frequent monitoring of reaction progress was essential. Product **76** (orange solid) was easily separated from its regiomer (yellow solid) by flash column chromatography, as the fast eluting fraction. Full consumption of starting material is critical as it has a similar R_f value to amine **75**.

The nitro group of amine **76** was reduced to form diamine **77** in 86% yield, in an overnight reaction with Pd/C and hydrogen gas. Subsequent coupling to 5-fluoronicotinic acid using HATU, HOBt and DIPEA afforded the corresponding amide **80** in 65% yield. Formation of non-radioactive reference compound **73** was achieved by heating the former in refluxing acetic acid, which proceeded quantitatively. Analogously, 5-bromonicotinic acid was coupled to diamine **77** in 65% yield and subsequent dehydration afforded the corresponding benzimidazole **79** in 74% yield.

Benzimidazoles **79** and **73** can also be obtained directly from diamine **77** in a one-step convenient Oxone[®]-mediated condensation with the corresponding aldehydes. 5-Fluoro- and 5-bromonicotinaldehyde were coupled to diamine **77** in 65% and 59% yield, respectively. Although the yields are slightly lower than those obtained in Scheme 9.1, the new route is quicker and more practical. Subsequent

palladium-catalysed coupling of thioether **4** (Scheme 5.3) and benzimidazole **79** afforded thioether **82** in 88% yield. Reference compound **73** (for co-injections) was isolated in 65% yield. Sulfonium salt **83** was accessed in 66% yield. A short optimisation process with alternative milder reagents, such as hypochlorites, did not produce satisfactory results. Reproducible yields were obtained when the appropriate amount of NCS was added from stock solution of NCS to thioether **82**, followed by neat TfOH. The synthesis is summarised in Scheme 9.2.



Scheme 9.2: Syntheses of sulfonium salt **83** and cold reference compound **73**.

Reagents and conditions: (i) Cyclopropylamine, KF, K₂CO₃, MeCN, reflux, 1 h; (ii) Pd/C, H₂, MeOH, rt, 20 h; (iii) 5-Bromonicotinaldehyde, Oxone[®], DMF/H₂O, rt, 1 h; (iiib) 5-Fluoronicotinaldehyde, Oxone[®], DMF/H₂O, rt, 1 h; (iv) Thioether **4**, Pd₂(dba)₃, DPEphos, KOtBu, toluene, reflux, 2 h; (v) NCS (stock solution), TfOH, MeCN, rt, 30 min.

9.2 Radiolabelling of Novel PET Tracer Candidate

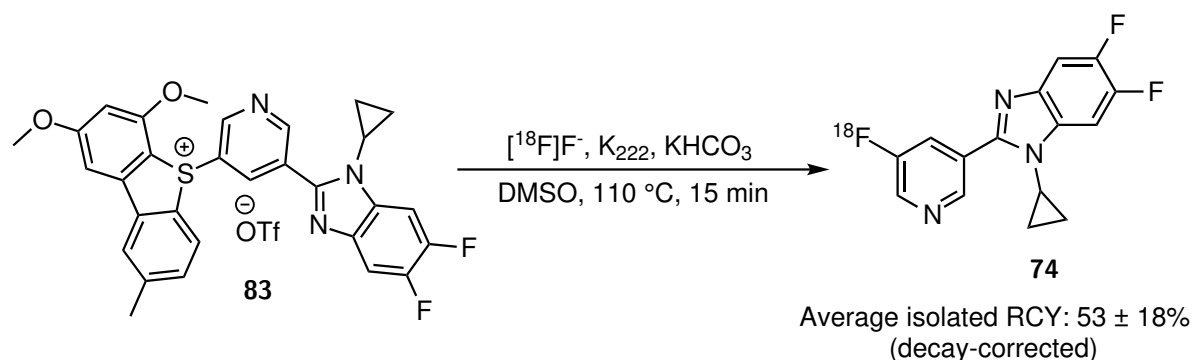
Substantial efforts were directed towards establishing optimum ^{18}F -labelling conditions for sulfonium salt **83**. The results are presented in Table 9.2.

Table 9.2: Radiolabelling experiments with sulfonium salt **83**. All reactions employed 2 mg of the precursor. All isolated yields are isolated (unless stated otherwise), decay-corrected and represent the end of synthesis HPLC yields.

Entry	Solvent	Temperature [°C]	Time [min]	Radio-HPLC Yield [%]
1	DMSO	110	15	18-87
2	DMSO	110	5	43
3	DMSO	50	15	- ^a
4	MeCN	80	15	24

^a Not isolated. Analytical radio-HPLC yield: 56%.

The first radiolabelling attempt, with K_{222} and KHCO_3 in DMSO at 110 °C, afforded a high analytical RCY of 72%. The tracer was isolated with 46% RCY. In subsequent experiments, RCYs in the range of 18 to 87% were obtained (Table 9.2, Entry 1). A decrease in reaction time to 5 min had little impact on the RCY - 43% of the labelled product was isolated (Entry 2). The reaction proceeded remarkably well at 50 °C for 15 min and an analytical RCY of 56% was obtained (Entry 3). Radiolabelling was also evaluated with MeCN, a preferred solvent under Good Manufacturing Practice synthesis of PET tracers, however a significantly lower isolated RCY were obtained (Entry 4). Benchmark labelling conditions were established as: DMSO at 110 ° for 15 min (Scheme 9.3). The average decay-corrected isolated RCY obtained for this reaction system was $53 \pm 18\%$ (n=12). The average specific activity was established at $14.7 \pm 9.6 \text{ GBq}/\mu\text{mol}$. Considerable amount of spread in the data can be expected for manual labelling experiments. It is speculated that large temperature fluctuations in the radiochemistry lab had a major impact on radio-HPLC retention times, often causing co-elution of the tracer with impurities, resulting in lower RCYs. Some discrepancies can also be expected as two different sulfonium salt batches were used for radiolabelling. At this stage of the investigation, no efforts were made to control these variables. To the best of my knowledge, this is currently the most efficient direct ^{18}F -labelling of a highly-functionalised tracer scaffold at the *meta*-pyridine moiety without the use of activating groups.



Scheme 9.3: Optimised ^{18}F -labelling conditions for sulfonium salt **83**. Average isolated RCY was established at $53 \pm 18\%$ (decay-corrected, $n=12$).

9.3 Preliminary Biological Evaluation of Novel PET Tracer Candidate

With radiolabelling of precursor **83** proceeding in high isolated RCYs, preliminary biological evaluation was initiated without further delay. All animal experiments were performed by Dr Kerstin Sander (UCL Radiochemistry). Tracer **74** was evaluated in healthy wildtype mice. Radioactivity distribution was assessed at 5 different time intervals (from 0 to 60 min) after injection of 5-8 MBq of the tracer. In 2-5 minutes post-injection, the tracer was shown to accumulate in the liver and in the next 10 minutes, excretion process began. After 15 min, the tracer began accumulating in the joints and skull, potentially due to defluorination. Reassuringly, no uptake was detected in the adrenal region, hence no background signal in that region is expected for subjects overexpressing aldosterone synthase.

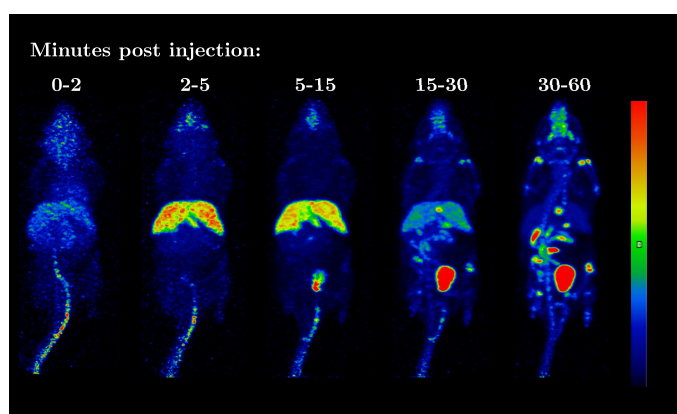


Figure 9.4: Preliminary biological evaluation of tracer **74** in healthy wildtype mice. PET experiments were performed by Dr Kerstin Sander. Pharmacokinetic profile was established using 5-8 MBq of tracer candidate after intravenous injection.

Additional scans, together with biodistribution and metabolite analysis, are required to confirm these preliminary results. Further evaluation includes autoradiography using adenoma-affected adrenal masses. This investigation has now been taken over by fellow members of the Årstad group at UCL Radiochemistry.

9.4 Conclusion

In the presented investigation, a dibenzothiophene sulfonium salt precursor to a novel PET tracer candidate was synthesised. Its structure is based on a potent aldosterone synthase inhibitor structure, developed by Merck. The tracer is a potential candidate for the imaging of aldosterone-producing adenomas, one of the causes of drug-resistant hypertension.

Dibenzothiophene sulfonium salt **83** was of particular interest to the Årstad group for the following reasons. Firstly, it is a precursor to a potent CYP11B2 inhibitor, displaying good selectivity versus CYP11B1. Secondly, it is a highly-functionalised drug-like molecule, based on basic *N*-heterocycles - benzimidazole and pyridine. Thirdly, it represents a deactivated aromatic system, with a pyridyl moiety situated *meta* to the sulfur atom. In this investigation, an attempt was made to label a more complex scaffold without the use of directing groups.

Building on the work of Chapter 7, sulfonium salt precursor **83** was obtained in an gratifying yield of 66% from a cyclisation reaction mediated by NCS and TfOH. Conveniently, no chlorinated sulfonium salt was observed. Successful ¹⁸F-labelling allowed for isolation of tracer **74** in an average decay-corrected RCY of 53 ± 18%.

The presented work constitutes a ground-breaking advancement in radiolabelling of deactivated aromatic scaffolds. It is, to the best of my knowledge, the first example of direct one-step incorporation of fluorine-18 at the *meta*-pyridyl position of a biologically active drug-like molecule, without the use of activating groups. The use of dibenzothiophene sulfonium salt precursors opens up an opportunity to access various 3-[¹⁸F]fluorinated scaffolds.

10 | Conclusion

Despite remarkable advances in fluorine-18 incorporation into aromatic scaffolds for PET imaging, the lack of broadly applicable methods renders labelling of biologically active compounds challenging. As a result, the selection of established tracers for clinical imaging is limited. Frequently, their radiosyntheses are not operationally simple, RCYs and specific activities are low and cannot be adapted to clinical manufacture. Sadly, despite impressive technological advances, the potential of PET to revolutionise experimental medicine is not fully realised.

A novel strategy employing dibenzothiophene sulfonium salts as leaving groups for [^{18}F]fluorinations of highly-functionalised molecules has been developed. Building on the ground-breaking work by Sander *et al.* and Dr Thibault Gendron (UCL Radiochemistry), an efficient and robust system to access dibenzothiophene precursors for labelling was established. The compounds can be accessed in rapid one-pot transformation, their purification is straightforward and can be achieved by flash column chromatography. The resulting products exhibit remarkable stability, yet are very reactive towards [^{18}F]fluoride, and radiolabelling occurs with high regioselectivity. [^{18}F]fluorinations were performed on non-activated and electron-deficient aromatic systems, in the presence of *N*-heterocycles, such as pyridines, indoles and imidazoles.

Dibenzothiophene sulfonium salts were accessed from the corresponding diaryl thioethers in a novel ring-closing reaction mediated by NCS (electrophile) and TfOH (activator of NCS) in acetonitrile at room temperature. Electron-rich aromatics reacted most readily with the resulting superprotonated NCS species ("superelectrophile") as they increase nucleophilicity of the *S*-centre. Good cyclisation yields were obtained for *N*-protected indole and mildly-deactivated scaffolds, such as the

precursor to [^{18}F]FPEB. Sulfonium salts were also formed in the presence of basic pyridine and imidazole moieties. One of the main challenges of this chemistry was protonation of these entities by TfOH. Firstly, formation of positive charge on the 2-pyridyl moiety resulted in loss of reactivity of the sulfur centre. Secondly, unusual stabilisation of the protonated imidazole resulted in radiolabelling inhibition. Efforts to find milder, non-acidic cyclisation reagents were moderately successful. Although sulfonium salt formation is possible with standard hypochlorite-based reagents, the method was not robust enough to allow broad implementation. At the time of writing this thesis, the cyclisation system was further optimised by Dr Thibault Gendron. Refining of the $\text{Ca}(\text{OCl})_2$ -mediated dibenzothiophene sulfonium salt formation protocol resulted in a remarkably mild and robust strategy.

[^{18}F]Fluorinations of dibenzothiophene sulfonium salts proceeded most efficiently for deactivated scaffolds, such as 2-pyridine moieties, however excellent RCYs were also obtained for non-activated aromatics. A prominent example of this is radiolabelling of [^{18}F]FPEB, which offers certain advantages over existing technologies. Preparation of the corresponding sulfonium salt precursor is high yielding, technically simple and delivers a highly pure product.

The major achievement of this work is the successful synthesis and radiolabelling of a dibenzothiophene sulfonium salt precursor to a novel PET tracer candidate. The structure is based on a potent aldosterone inhibitor investigated by Merck. Cyclisation proceeded in a good yield and subsequent labelling at the 3-pyridyl position afforded the tracer in high RCY. This work constitutes, to the best of my knowledge, the first direct incorporation of fluorine-18 at the *meta*-pyridyl position of a highly-functionalised drug-like scaffold without the need for activating groups. The candidate is currently undergoing biological evaluation in mice.

These results illustrate the enormous potential of dibenzothiophene sulfonium salts as precursors for [^{18}F]fluorination of aromatic molecules. Precursor synthesis does not involve the use of toxic metals, harsh reaction conditions or intricate equipment. Radiolabelling can also be tailored to GMP environment. As a result, the

method exhibits great potential for broad applications in clinical radiopharmaceutical manufacture for PET imaging.

11 | General Procedures

11.1 General Procedures: Synthetic Chemistry

Solvents and Reagents: Anhydrous solvents were purchased from Sigma Aldrich. Reagents were purchased from Sigma Aldrich, Fluorochem, Acros Organics and Alfa Aesar and were used without additional purification. **Flash Column Chromatography:** Purification was performed using Merck Geduran Silica Gel 60 40-63 μm . TLC was performed on aluminium-backed plates pre-coated with silica (0.2 mm, 60 F₂₅₄). The plates were developed using the following visualising agents: UV fluorescence (254 nm), KMnO_4 , *p*-anisaldehyde and Dragendorff, as appropriate. **¹H NMR Spectra:** These were recorded at 300, 400, 500 or 600 MHz on respective Bruker Avance machines. All samples were prepared as solutions in 0.7 mL CDCl_3 , d_3 -MeCN or d_6 -DMSO. Chemical shifts (δ_{H}) are quoted in ppm, referenced to an appropriate residual solvent peak and rounded up to the nearest 0.01 ppm. Coupling constants (J) are rounded up to the nearest 0.1 Hz. **¹³C NMR Spectra:** These were recorded at 150 MHz on a Bruker AV-600 instrument. Chemical shifts (δ_{C}) are reported in ppm, referenced to an appropriate residual solvent peak and rounded up to the nearest 0.1 ppm. **¹⁹F NMR Spectra:** These were recorded at 282 MHz on a Bruker AV-300 instrument. Chemical shifts (δ_{F}) are reported in ppm, referenced to an appropriate residual peak and rounded up to the nearest 0.1 ppm. **Infrared Spectra:** These were recorded as thin films on a Bruker Alpha FTIR spectrometer. Only selected absorbances (ν_{max}) are reported to the nearest cm^{-1} . **Mass Spectra:** These were performed by the Mass Spectrometry Facility of the Chemistry Department of University College London. **Melting Points:** These were measured on a Gallenkamp melting point apparatus to the nearest 0.1°C.

11.2 General Procedures: Radiochemistry

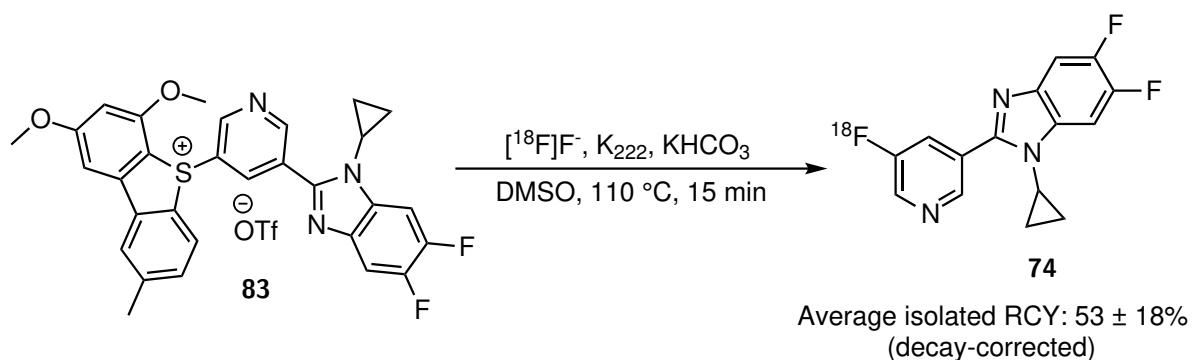
All radiolabelling experiments were performed manually using [^{18}F]fluoride in [^{18}O]H₂O. Radio-HPLC was performed with an Agilent 1200 HPLC system equipped with a 1200 Series Diode Array Detector and a GABI Star NaI(Tl) scintillation detector (energy window 400-700 keV). The system was used for purification as well as characterisation of radiotracers. Column specifications are provided.

Radiolabelling:

A solution of [^{18}F]fluoride (50 MBq-1.5 GBq) in [^{18}O]H₂O was trapped on a Sep-Pak[®] QMA cartridge, released with a solution of KHCO₃ (30 mM) and Kryptofix 222 (30 mM) in 15% MeCN/H₂O solution (0.5 mL). The solvent was removed by azeotropic distillation at 90 °C under a stream of nitrogen. Anhydrous MeCN was added and distillation was continued. This was repeated once more until a dry residue was observed and the reaction vial was capped. The appropriate sulfonium salt precursor (2-5 mg) was dissolved in anhydrous MeCN or DMSO (0.5 mL) and added to the reaction vial. The resulting mixture was stirred at an appropriate temperature for the specified duration. After cooling, the reaction was quenched by addition of water (1.0-1.5 mL) and purified by semi-preparative radio-HPLC using either a Luna[®] 5 μm C18(2) (10 \times 250 mm, Phenomenex) or a Chromolith[®] Performance RP18-e column. The analytical yield was determined by integrating the area under the curve in the radio-HPLC chromatogram. The decay-corrected isolated RCY was calculated by measuring the amount of radioactivity of the purified radiotracers with respect to the initial amount of [^{18}F]fluoride in [^{18}O]H₂O, accounting for the total synthesis time (from [^{18}F]fluoride in water to the end of purification or formulation). The analytical RCY was determined by integrating the area under the curve in the semi-preparative radio-HPLC chromatogram. The identity of the ^{18}F -labelled product was confirmed by co-injection with its non-radioactive analogue. Quality control was performed using either a Zorbax[®] C18 (4.5 \times 250 mm) or a Zorbax[®] Eclipse Plus 5 μm C18 column. Together with the eluent, they were checked for residual radioactivity to ensure all of the ^{18}F -compounds/products were eluted.

12 | Radiolabelling

12.1 Preparation of Tracer 74



Radiolabelling was performed with 2 mg of precursor **83** in anhydrous DMSO at 110 °C for 15 min. After cooling, the reaction mixture was quenched with H₂O (1.5 mL) and the resulting solution was purified on a Luna[®] 5 μm C18(2) column (10 × 250 mm, Phenomenex) at room temperature using H₂O and MeOH (each containing 0.5% TFA). Isocratic elution was performed at 41% MeOH content and with a flow rate of 5 mL/min. Retention time was ≈ 22 min. Quality control was performed on a Zorbax[®] Eclipse Plus 5 μm C18 column (4.6 × 150 mm) at room temperature and at a flow rate of 1.5 mL/min using H₂O and MeOH. Gradient elution started with 50% MeOH content that was increased to 75% in 10 min and further to 90% in 2 min. Retention time was ≈ 6.3 min. The decay-corrected isolated RCY at the end of HPLC purification was $53 \pm 18\%$ (n=12). The specific activity was 14.7 ± 9.6 GBq/μmol. The total synthesis time, from [¹⁸F]fluoride in [¹⁸O]H₂O to the end of HPLC purification, was < 90 min. The column and eluent were checked for residual radioactivity to ensure all of the ¹⁸F-compounds/products were eluted.

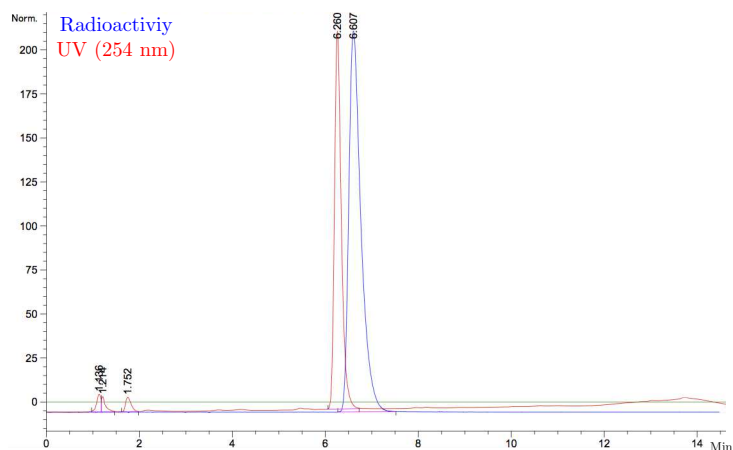


Figure 12.1: HPLC chromatogram of isolated tracer **74**, co-injected with non-radioactive reference compound **73**. UV detection at 254 nm.

Preclinical studies:

1.0 GBq of [^{18}F]fluoride in [^{18}O]H $_2$ O was used. Purification was performed using the previously described conditions. The tracer solution was diluted with H $_2$ O to a final solution of 20 mL, passed through a Sep-Pak[®] Alumina N cartridge and then trapped on a Sep-Pak[®] SPE C-18 light cartridge, from which the labelled product was released with EtOH (0.5 mL). Having reduced the volume to < 0.1 mL under a stream of nitrogen, the solution was diluted with saline (1.0 mL), to give the final ethanol concentration of < 5%, and sterilised by filtration. Quality control was performed using the previously described conditions. Specific activity was 30.6 GBq/ μmol . The identity of the tracer was confirmed by co-injection with the non-radioactive analogue **73** (Figure 12.1). The total production time, from [^{18}F]fluoride in [^{18}O]H $_2$ O to the end of the tracer preparation for injection, was 80 min. The column and eluent were checked for residual radioactivity to ensure all of the ^{18}F -compounds/products were eluted.

12.1.1 Calculation of Specific Activity of Tracer 74

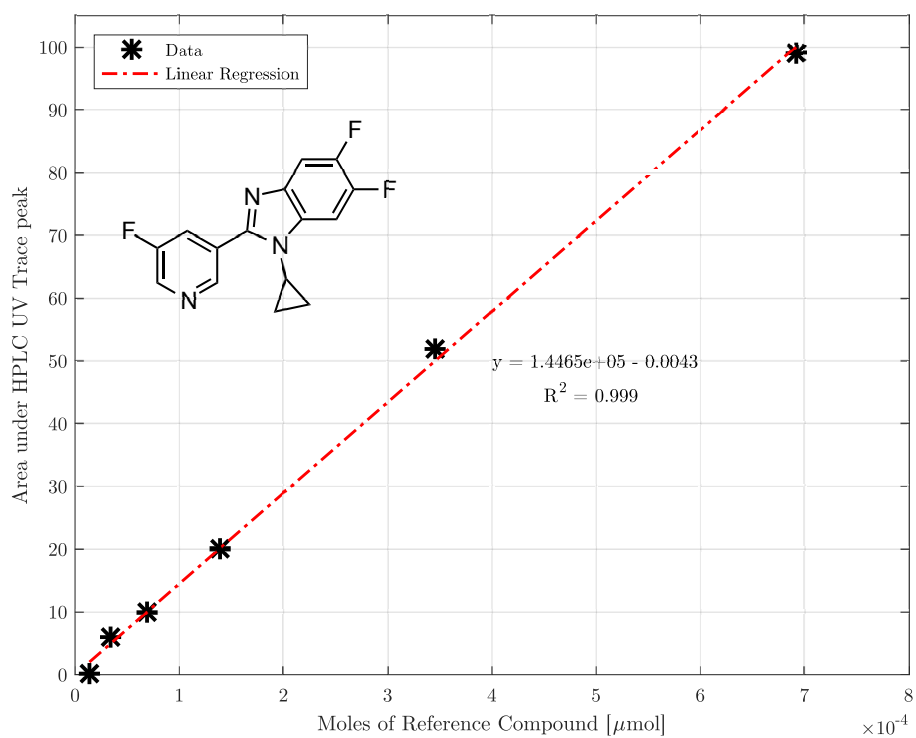
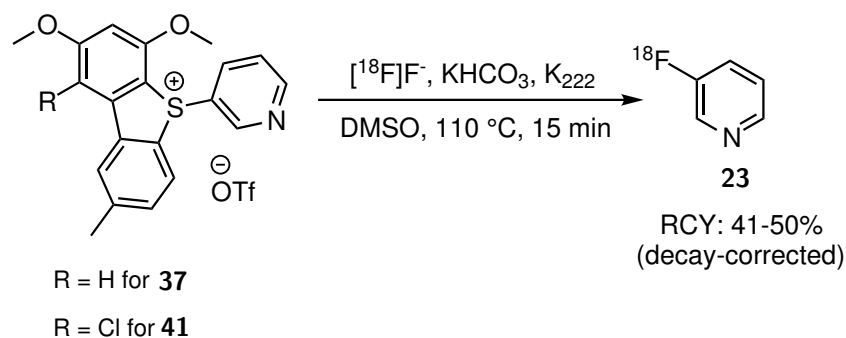


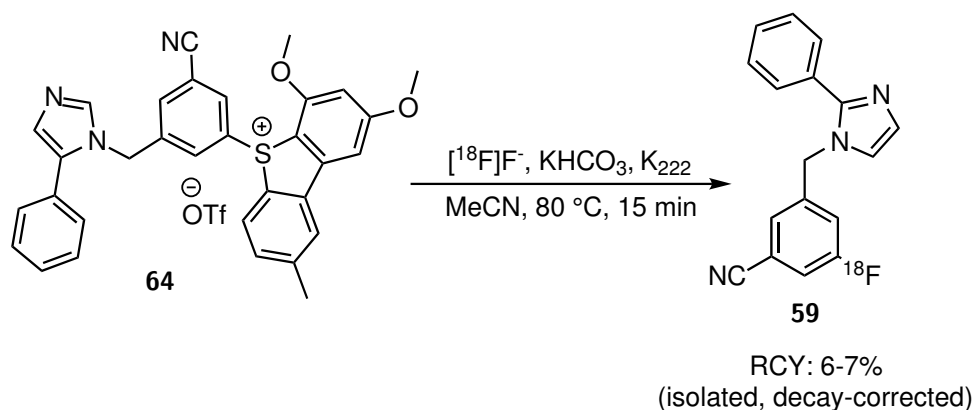
Figure 12.2: Calibration curve of reference compound **73** for specific activity calculation of tracer **74**.

12.2 Preparation of 3-¹⁸F]fluoropyridine



Radiolabelling was performed with 2 mg of mixture of compounds **37** and **41** in anhydrous DMSO at 110 °C for 15 min. After cooling, the reaction mixture was quenched with H₂O (1.0 mL) and the resulting solution was purified using a Luna[®] 5 μm C18(2) column (10 × 250 mm, Phenomenex) at room temperature using H₂O and MeOH (each containing 0.5% TFA) and with a flow rate of 5 mL/min. Gradient elution started with 5% MeOH content that was increased to 95% in 10 min. Retention time was ≈ 9.1 min. The decay-corrected isolated RCY at the end of HPLC purification was 41-50%. Quality control was performed on a Zorbax[®] C18 column (4.5 × 250 mm) at room temperature and at a flow rate of 3.0 mL/min using H₂O and MeOH (each containing 0.5% TFA). Gradient elution started with 3% MeOH content that kept constant for 7 min, increased to 95% in 7 min and kept at that for 6 min. Retention time was ≈ 7.1 min. The total production time, from [¹⁸F]fluoride in [¹⁸O]H₂O to the end of HPLC purification, < 60 min. The column and eluent were checked for residual radioactivity to ensure all of the ¹⁸F-compounds/products were eluted.

12.3 Preparation of Tracer 59



The most successful radiolabelling was performed with 5 mg of precursor **64** in anhydrous MeCN at 80 °C for 15 min. After cooling, the reaction mixture was quenched with 20% EtOH/H₂O (1.0 mL) and the resulting solution was purified on a Chromolith[®] Performance RP18-e column (100 × 10 mm) at room temperature using H₂O and MeOH (each containing 0.5% TFA) and a flow rate of 1.5 mL/min. Gradient elution started with 20% MeOH content kept constant for 5 min. It was increased to 50% in 10 min and then further to 90% in 5 min. Retention time was ≈ 12.8 min. Quality control was performed on a Zorbax[®] Eclipse Plus 5 μm C18 column (4.6 × 150 mm) at room temperature and at a flow rate of 1.5 mL/min using H₂O and MeOH (each containing 0.5% TFA). Gradient elution started with 30% MeOH that was increased to 90% in 13 min. Retention time was ≈ 6.7 min. The identity of the tracer was confirmed by co-injection with the non-radioactive analogue **67** (Figure 12.4). The decay-corrected isolated RCY at the end of HPLC purification was 6%. The total synthesis time, from [¹⁸F]fluoride in [¹⁸O]H₂O to the end of HPLC purification, was 60 min. The column and eluent were checked for residual radioactivity to ensure all of the ¹⁸F-compounds/products were eluted.

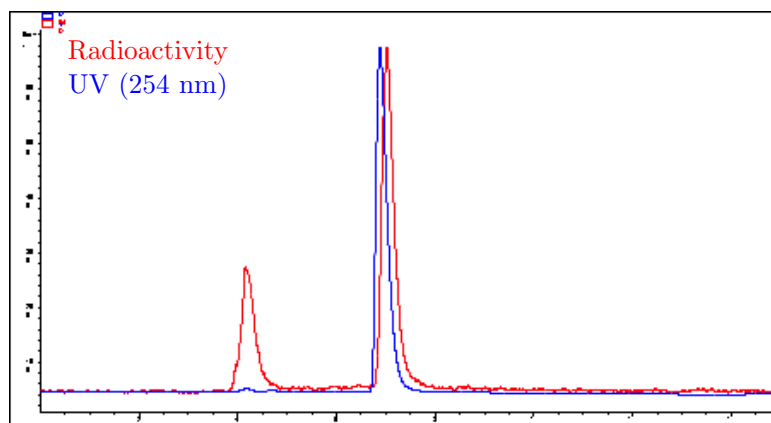


Figure 12.3: HPLC chromatogram of crude 3-[^{18}F]fluoropyridine, co-injected with 3-fluoropyridine. UV detection at 254 nm.

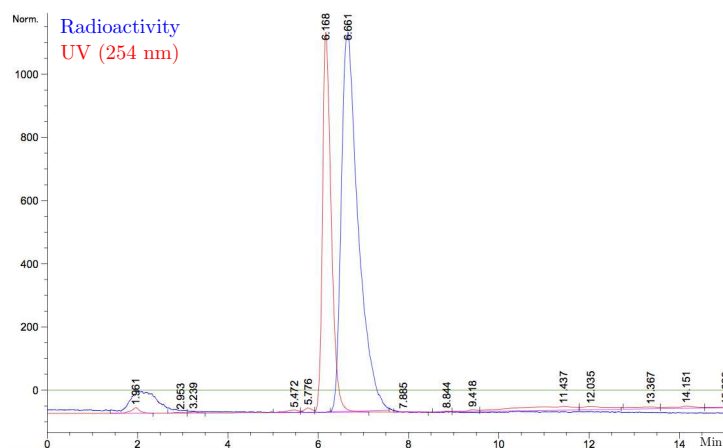
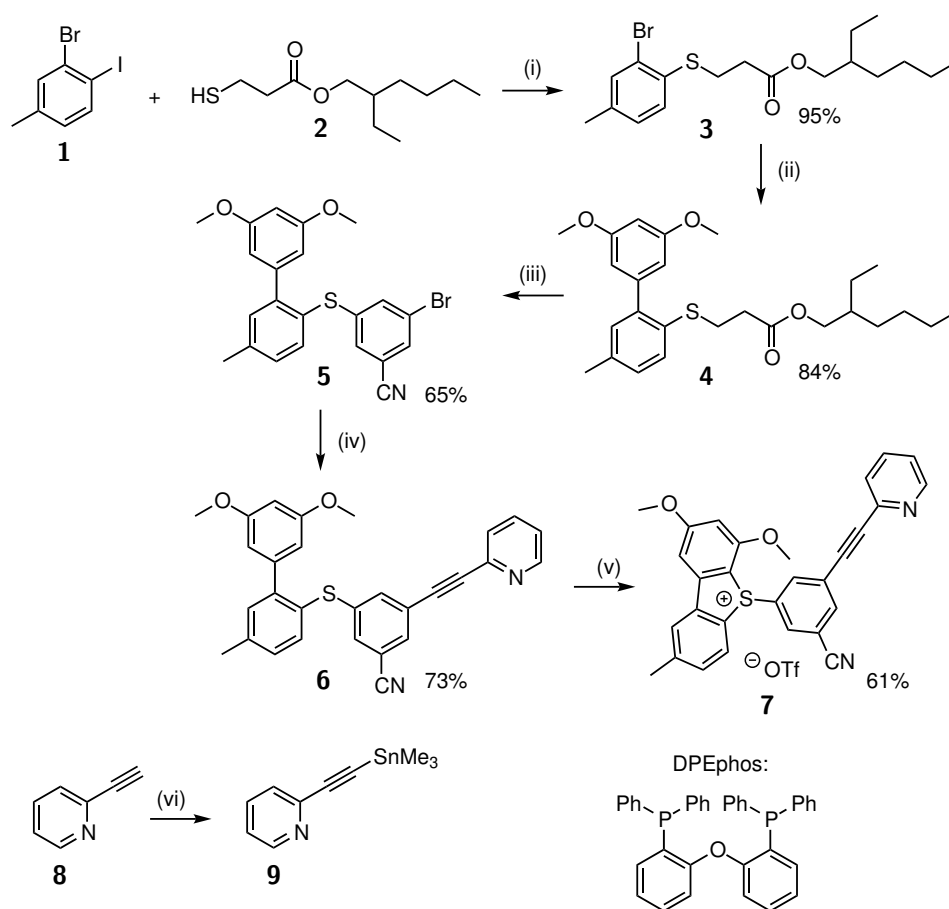


Figure 12.4: HPLC chromatogram of isolated tracer **59**, co-injected with non-radioactive reference compound **67**. UV detection at 254 nm.

13 | Characterisation of Synthesised Compounds

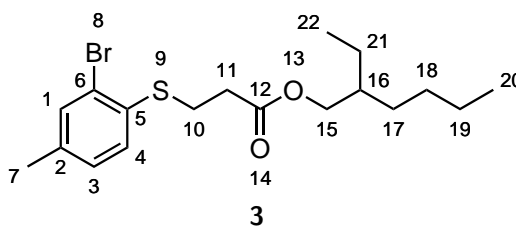
13.1 Synthetic Route Towards Sulfonium Salt 7 (Chapter 5)



Scheme 13.1: Synthesis of sulfonium salt **7**.

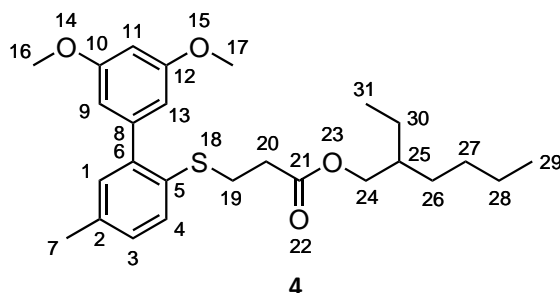
Reagents and conditions: (i) $\text{Pd}_2(\text{dba})_3$, xantphos, Et_3N , toluene, reflux, 4.5 h; (ii) 3,5-Dimethoxyphenylboronic acid, $\text{Pd}(\text{PPh}_3)_4$, K_2CO_3 , toluene/water, reflux, 5 h; (iii) 3,5-Dibromobenzonitrile, $\text{Pd}_2(\text{dba})_3$, DPEphos, $\text{KO}t\text{Bu}$, toluene, reflux, 15 min; (ivb) Pyridine **9**, $\text{Pd}(\text{PPh}_3)_4$, toluene, reflux, 2 h; (v) NCS, $\text{Bi}(\text{OTf})_3$, MeCN, rt, 1 h; (vi) $n\text{BuLi}$ Me_3SnCl , $-78^\circ\text{C} \rightarrow \text{rt}$, 1 h.

Octan-3-yl-3-((2-bromo-4-methylphenyl)thio)propanoate **3**



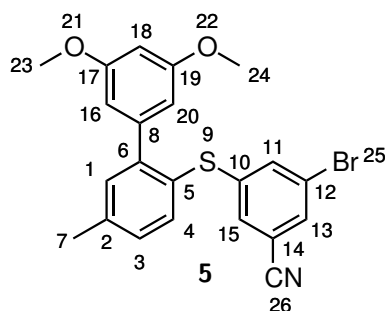
To a flame-dried three-neck round-bottom flask equipped with an argon inlet and condenser were added toluene (88.0 mL), 2-bromo-1-iodo-4-methylbenzene (2.88 g, 9.70 mmol, 1.0 equiv.) and Et_3N (1.27 g, 12.6 mmol, 1.3 equiv.). The reaction vessel was degassed by argon purging before $\text{Pd}_2(\text{dba})_3$ (266 mg, 0.291 mmol, 0.03 equiv.) was added, followed by xantphos (337 mg, 0.582 mmol, 0.06 equiv.) and 2-ethylhexyl 3-mercaptopropanoate (2.12 g, 9.70 mmol, 1.0 equiv.). The resulting mixture was purged with argon before being plunged into a preheated block maintained at 125 °C. The reaction mixture was refluxed for 4.5 h. After cooling to room temperature, it was filtered through a pad of Celite and concentrated *in vacuo*. Flash column chromatography purification (10 → 50% DCM/PE) of the resulting yellow oil afforded the title compound as a colourless oil (3.57 g, 95%). $\nu_{\text{max}}/\text{cm}^{-1}$ 2924, 1730, 1461, 1238. ^1H NMR (600 MHz, CDCl_3) δ_{H} 7.42 (1H, d, J 2.1, H1), 7.24 (1H, d, J 7.9, H4), 7.08 (1H, dd, J 7.9, 2.1, H3), 4.01 (2H, 2 × m, H15), 3.17 (2H, t, J 7.5, H10), 2.64 (2H, t, J 7.5, H11), 2.31 (3H, s, H7), 1.60-1.54 (1H, m, H16), 1.38-1.26 (8H, m, H17, H18, H19 and H21), 0.90-0.88 (6H, m, H20 and H22). ^{13}C NMR (150 MHz, CDCl_3) δ_{C} 171.9 (C), 138.2 (C), 133.9 (CH), 132.8 (C), 130.4 (CH), 128.9 (CH), 125.4 (C), 67.4 (CH_2), 38.8 (CH), 34.1 (CH_2), 30.1 (CH_2), 29.0 (CH_2), 28.8 (CH_2), 23.9 (CH_2), 23.1 (CH_2), 20.7 (CH_3), 14.2 (CH_3), 11.1 (CH_3). HRMS (EI) Calculated for $\text{C}_{18}\text{H}_{27}\text{O}_2\text{BrS}$ $[\text{M}]^+$: 386.0910; found: 386.0909.

Octan-3-yl 3-((3',5'-dimethoxy-5-methyl-[1,1'-biphenyl]-2-yl)thio)propanoate **4**



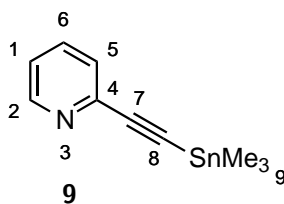
To a flame-dried three-neck round-bottom flask equipped with an argon inlet and condenser were added toluene (22.0 mL) and thioether **3** (4.09 g, 10.6 mmol, 1.0 equiv.), followed by a solution of K₂CO₃ (5.86 g, 42.4 mmol, 4.0 equiv.) in H₂O (22 mL) and 3,5-dimethoxyphenylboronic acid (2.41 g, 13.3 mmol, 1.25 equiv.). The reaction vessel was degassed by argon purging with vigorous stirring to ensure efficient removal of O₂ trapped in the aqueous layer. Pd(PPh₃)₄ (612 mg, 0.530 mmol, 0.05 equiv.) was added and after additional degassing, the resulting mixture was plunged into a preheated block maintained at 125 °C. The reaction mixture was refluxed for 5 h. After cooling to room temperature, it was washed with a saturated aqueous solution of K₂CO₃. The combined organic layers were dried over MgSO₄ and concentrated *in vacuo*. Flash column chromatography purification (3 → 7% EtOAc/PE) of the resulting yellow oil afforded the title compound as a colourless oil (4.08 g, 84%). $\nu_{\max}/\text{cm}^{-1}$ 2923, 1730, 1461. ¹H NMR (600 MHz, CDCl₃) δ_{H} 7.32 (1H, d, *J* 8.0, H4), 7.13 (1H, dd, *J* 8.0, 2.3, H3), 7.10 (1H, d, *J* 2.3, H1), 6.54 (2H, d, *J* 2.3, H9 and H13), 6.47 (1H, t, *J* 2.3, H11), 3.96 (2H, 2 × m, H24), 3.82 (6H, s, H16 and H17), 2.97 (2H, t, *J* 7.7, H19), 2.51 (2H, t, *J* 7.7, H20), 2.35 (3H, s, H7), 1.54 (1H, m, H25), 1.35-1.24 (8H, m, H26, H27, H28 and H30), 0.90-0.86 (6H, m, H29 and H31). ¹³C NMR (150 MHz, CDCl₃) δ_{C} 172.1 (C), 160.4 (C), 143.0 (C), 142.8 (C), 136.2 (C), 131.3 (CH), 130.3 (C), 129.6 (CH), 128.9 (CH), 107.6 (CH), 99.7 (CH), 67.2 (CH₂), 55.5 (CH₃), 38.8 (CH), 34.3 (CH₂), 30.5 (CH₂), 29.0 (CH₂), 28.8 (CH₂), 23.8 (CH₂), 23.1 (CH₂), 21.0 (CH₃), 14.2 (CH₃), 11.1 (CH₃). HRMS (EI) Calculated for C₂₆H₃₆O₄S [M]⁺: 444.2329; found: 444.2329.

**3-Bromo-5-((3',5'-dimethoxy-5-methyl-[1,1'-biphenyl]-2-yl)thio)
benzonitrile 5**



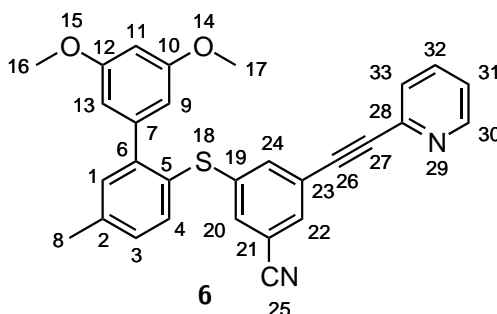
To a flame-dried three-neck round-bottom flask equipped with an argon inlet and condenser were added toluene (27.0 mL), 3,5-dibromobenzonitrile (1.92 g, 7.36 mmol, 1.4 equiv.) and *KOt*Bu (958 mg, 8.54 mmol, 1.6 equiv.). The reaction vessel was degassed by argon purging before $\text{Pd}_2(\text{dba})_3$ (49.0 mg, 53.4 μmol , 0.01 equiv.) was added, followed by DPEphos (58.0 mg, 0.107 mmol, 0.02 equiv.) and thioether **4** (2.37 g, 5.34 mmol, 1.0 equiv.). The resulting mixture was purged with argon before being plunged into a preheated block maintained at 125 °C. The reaction mixture was refluxed for 15 min. After cooling to room temperature, it was filtered through a pad of Celite and concentrated *in vacuo*. Flash column chromatography purification (5 \rightarrow 10% $\text{Et}_2\text{O}/\text{PE}$) of the resulting brown oil afforded the title compound as a yellow oil (1.51 g, 65%). $\nu_{\text{max}}/\text{cm}^{-1}$ 1728, 1589, 1546, 1201. ^1H NMR (600 MHz, CDCl_3) δ_{H} 7.45 (1H, d, J 7.9, H4), 7.44 (1H, dd, J 1.7, 1.4, H13) 7.34 (1H, t, J 1.7, H11), 7.25 (1H, d, J 1.9, H1), 7.22 (1H, dd, J 7.9, 1.9, H3), 7.12 (1H, dd, J 1.7, 1.4, H15), 6.42 (1H, t, J 2.3, H18), 6.36 (2H, d, J 2.3, H16 and H20), 3.75 (6H, s, H23 and H24), 2.48 (3H, s, H7). ^{13}C NMR (150 MHz, CDCl_3) δ_{C} 160.3 (C), 146.0 (C), 143.3 (C), 142.3 (C), 140.4 (C), 135.6 (CH), 134.9 (CH), 132.2 (CH), 131.2 (CH), 129.8 (CH), 129.8 (CH), 126.0 (C), 122.9 (C), 117.1 (C), 114.2 (C), 107.4 (CH), 99.7 (CH), 55.5 (CH_3), 21.4 (CH_3). HRMS (EI) Calculated for $\text{C}_{22}\text{H}_{18}\text{NO}_2\text{BrS}$ $[\text{M}]^{+}$: 439.0236; found: 439.0235.

2-((Trimethylstannyl)ethynyl)pyridine **9**



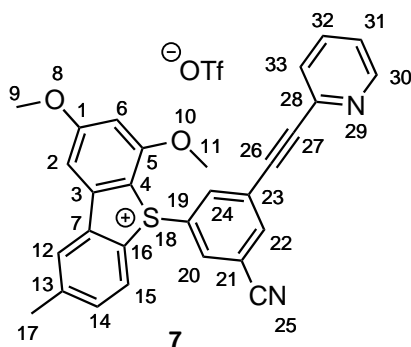
To a flame-dried round-bottom flask equipped with an argon inlet were added anhydrous THF (2.0 mL) and 2-ethynylpyridine (710 mg, 6.89 mmol, 1.0 equiv.). The mixture was cooled to -78 °C and a 1.6 M solution of *n*-butyllithium in hexane (4.31 mL, 6.89 mmol, 1.0 equiv.) was introduced dropwise. After stirring for 1 h at -78 °C, a 1 M solution of Me₃SnCl in THF (8.27 mL, 8.27 mmol, 1.2 equiv.) was added. The reaction mixture was allowed to warm up to room temperature and stirred for 1 h. It was then quenched with a saturated solution of NH₄Cl, extracted with EtOAc and concentrated *in vacuo* to afford the title compound as a black oil (2.00 g) of ≈ 70% purity as determined by ¹H NMR spectroscopy. The crude product was employed in the next step without further purification. ¹H NMR (600 MHz, CDCl₃) δ_H 8.56-8.55 (1H, m, H2), 7.62 (1H, m, H6), 7.44-7.30 (1H, m, H1), 7.21-7.19 (1H, m, H5), 0.38 (9H, s, H9).

3-((3',5'-Dimethoxy-5-methyl-[1,1'-biphenyl]-2-yl)thio)-5-(pyridin-2-ylethynyl)benzonitrile **6**



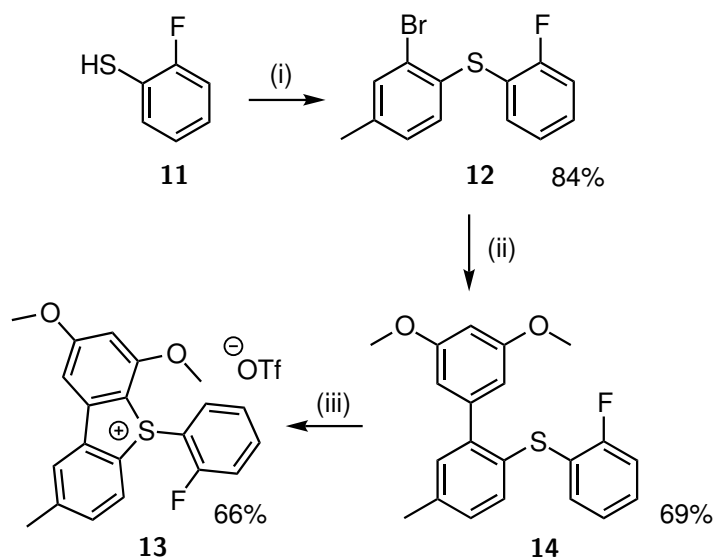
To a flame-dried three-neck round-bottom flask equipped with an argon inlet were added toluene (5.0 mL), thioether **5** (1.09 g, 2.48 mmol, 1.0 equiv.) and tin precursor **9** (70%, 1.32 g, 3.72 mmol, 1.5 equiv.). The reaction vessel was degassed by argon purging before Pd(PPh₃)₄ (143 mg, 0.124 mmol, 0.05 equiv.) was added. The resulting mixture was purged with argon before being plunged into a preheated block maintained at 125 °C. The reaction mixture was refluxed for 2 h. After cooling to room temperature, it was diluted with EtOAc, washed with an aqueous solution of KF, followed by brine. The organic layer was dried over MgSO₄ and concentrated *in vacuo*. Flash column chromatography purification (25 → 40% EtOAc/PE) of the resulting brown oil afforded the title compound as an orange oil (835 mg, 73%). $\nu_{\max}/\text{cm}^{-1}$ 1583, 1460, 1420, 1201. ¹H NMR (600 MHz, CDCl₃) δ_{H} 8.63 (1H, dd, *J* 5.0, 1.7, H30), 7.71 (1H, td, *J* 7.8, 1.7, H32), 7.53 (1H, t, *J* 1.7, H22), 7.51 (1H, d, *J* 7.8, H33), 7.45 (1H, d, *J* 7.9, H4), 7.43 (1H, t, *J* 1.7, H24), 7.29 (1H, dd, *J* 7.8, 5.0, H31), 7.25 (1H, d, *J* 2.3, H1), 7.21 (1H, dd, *J* 7.9, 2.3, H3), 7.20 (1H, t, *J* 1.7, H20), 6.42 (1H, t, *J* 2.3, H11), 6.38 (2H, d, *J* 2.3, H9 and H13), 3.74 (6H, s, H16 and H17), 2.44 (3H, s, H8). ¹³C NMR (150 MHz, CDCl₃) δ_{C} 160.3 (C), 150.4 (CH), 145.9 (C), 142.4 (C), 141.8 (C), 140.1 (C), 136.5 (CH), 135.5 (CH), 135.2 (CH), 132.2 (CH), 132.0 (CH), 131.3 (CH), 129.9 (CH), 127.6 (CH), 126.3 (C), 124.2 (C), 123.6 (CH), 117.7 (CN), 113.3 (C), 107.4 (CH), 99.8 (CH), 90.8 (C), 86.1 (C), 55.5 (CH₃), 21.4 (CH₃). HRMS (ESI) Calculated for C₂₉H₂₃N₂O₂S [M+H]⁺: 463.1480; found: 463.1462.

5-(3-Cyano-5-(pyridin-2-ylethynyl)phenyl)-2,4-dimethoxy-8-methyl-5*H*-dibenzo[*b,d*]thiophen-5-ium trifluoromethanesulfonate 7



To a round-bottom flask were added MeCN (2.0 mL), thioether **6** (116 mg, 0.250 mmol, 1.0 equiv.), NCS (34.0 mg, 0.250 mmol, 1.0 equiv.) and Bi(OTf)₃ (164 mg, 0.250 mmol, 1.0 equiv.). The reaction mixture was stirred at room temperature for 1 h. It was then concentrated *in vacuo* and the residue resuspended in DCM and washed with H₂O. The organic layer was dried over MgSO₄ and concentrated *in vacuo*. Flash column chromatography purification (5 → 10% 1 N NH₃ in MeOH/DCM) afforded the title compound as an off-white solid (98.0 mg, 61%), mp 252 °C (dec). $\nu_{\max}/\text{cm}^{-1}$ 1589, 1248. ¹H NMR (600 MHz, d₆-DMSO) δ_{H} 8.64 (1H, ddd, *J* 4.8, 1.8, 1.0, H30), 8.49 (1H, t, *J* 1.4, H22), 8.42 (1H, s, H2), 8.29 (1H, dd, *J* 1.8, 1.4, H20), 8.26 (1H, d, *J* 8.3, H15), 8.15 (1H, t, *J* 1.8, H24), 7.91 (1H, td, *J* 7.7, 1.8, H32), 7.74 (1H, d, *J* 2.2, H2), 7.69 (1H, dt, *J* 7.7, 1.0, H33), 7.60 (1H, d, *J* 8.3, H14), 7.49 (1H, ddd, *J* 7.7, 4.9, 1.0, H31), 6.94 (1H, d, *J* 2.1, H6), 4.01 (3H, s, H11), 3.95 (3H, s, H9), 2.55 (3H, s, H17). ¹³C NMR (150 MHz, d₆-DMSO) δ_{C} 167.2 (C), 158.0 (C), 150.5 (CH), 145.1 (C), 142.5 (C), 141.0 (C), 140.5 (CH), 139.7 (C), 137.1 (CH), 136.3 (CH), 133.6 (CH), 132.5 (CH), 130.6 (C), 129.5 (C), 128.2 (CH), 128.0 (CH), 125.8 (CH), 125.1 (C), 124.6 (CH), 116.1 (C), 114.8 (C), 107.3 (C), 102.5 (CH), 100.8 (CH), 92.8 (C), 84.2 (C), 57.5 (CH₃), 56.8 (CH₃), 21.3 (CH₃). ¹⁹F (282 MHz, d₆-DMSO) δ_{F} -78.2. HRMS (ESI) Calculated for C₂₉H₂₁N₂O₂S [M]⁺: 461.1324; found: 461.1320.

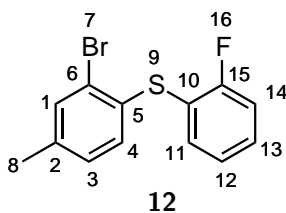
13.2 Synthetic Route Towards Sulfonium Salt 14 (Chapter 6)



Scheme 13.2: Synthesis of sulfonium salt 14.

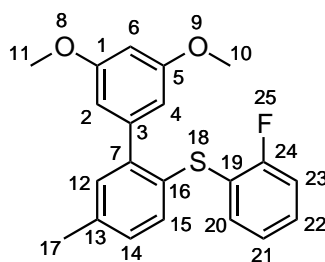
Reagents and conditions: (i) 2-Bromo-1-iodo-4-methylbenzene, $\text{Pd}_2(\text{dba})_3$, DPEphos, $\text{KO}t\text{Bu}$, toluene, reflux, 2 h; (ii) 3,5-Dimethoxyphenylboronic acid, $\text{Pd}(\text{PPh}_3)_4$, K_2CO_3 , toluene/water, reflux, 5 h; (iii) NCS, $\text{Bi}(\text{OTf})_3$, MeCN, rt, 1.5 h.

(2-Bromo-4-methylphenyl)(2-fluorophenyl)sulfane **12**



To a flame-dried three-neck round-bottom flask equipped with an argon inlet were added toluene (94.0 mL), 2-bromo-1-iodo-4-methylbenzene (3.47 g, 11.7 mmol, 1.0 equiv.) and *KOtBu* (1.54 g, 12.9 mmol, 1.1 equiv.). The reaction vessel was degassed by argon purging before $\text{Pd}_2(\text{dba})_3$ (107 mg, 0.117 mmol, 0.01 equiv.), DPEphos (135 mg, 0.234 mmol, 0.02 equiv.) and 2-fluorothiophenol (1.50 g, 11.7 mmol, 1.0 equiv.) were added. The resulting mixture was purged with argon before being plunged into a preheated block maintained at 125 °C. The reaction mixture was refluxed for 2 h. After cooling to room temperature, it was washed with a 2 M aqueous NaOH solution, filtered through a pad of Celite and concentrated *in vacuo*. Flash column chromatography purification (2 → 8% DCM/PE) of the resulting brown oil afforded the title compound as a colourless oil (2.92 g, 84%). $\nu_{\text{max}}/\text{cm}^{-1}$ 1591, 1253, 1169. ^1H NMR (600 MHz, CDCl_3) δ_{H} 7.45 (1H, d, *J* 1.9, H1), 7.35-7.31 (1H, m, H13), 7.29-7.27 (1H, m, H12), 7.16-7.11 (2H, m, H11 and H14), 7.01 (1H, dd, *J* 7.8, 1.9, H3), 6.97 (1H, d, *J* 7.8, H4), 2.31 (3H, s, H8). ^{13}C NMR (150 MHz, CDCl_3) δ_{C} 162.5 & 160.8 (d, *J* 249.0, C), 138.8 (C), 134.2 (CH), 133.9 (CH), 132.3 (C), 131.2 (CH), 130.2 & 130.1 (d, *J* 7.8, CH), 129.1 (CH), 125.1 & 125.0 (d, *J* 3.9, CH), 124.6 (C), 121.4 & 121.3 (d, *J* 17.9, C), 116.4 & 116.2 (d, *J* 21.9, CH), 20.8 (CH_3). ^{19}F NMR (282 MHz, CDCl_3) δ_{F} -108.1. HRMS (CI) Calculated for $\text{C}_{13}\text{H}_{10}\text{BrFS}$ $[\text{M}]^{+\cdot}$: 295.9665; found: 295.9964.

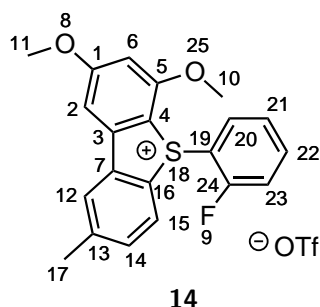
(3',5'-Dimethoxy-5-methyl-[1,1'-biphenyl]-2-yl)(2-fluorophenyl)sulfane **13**



13

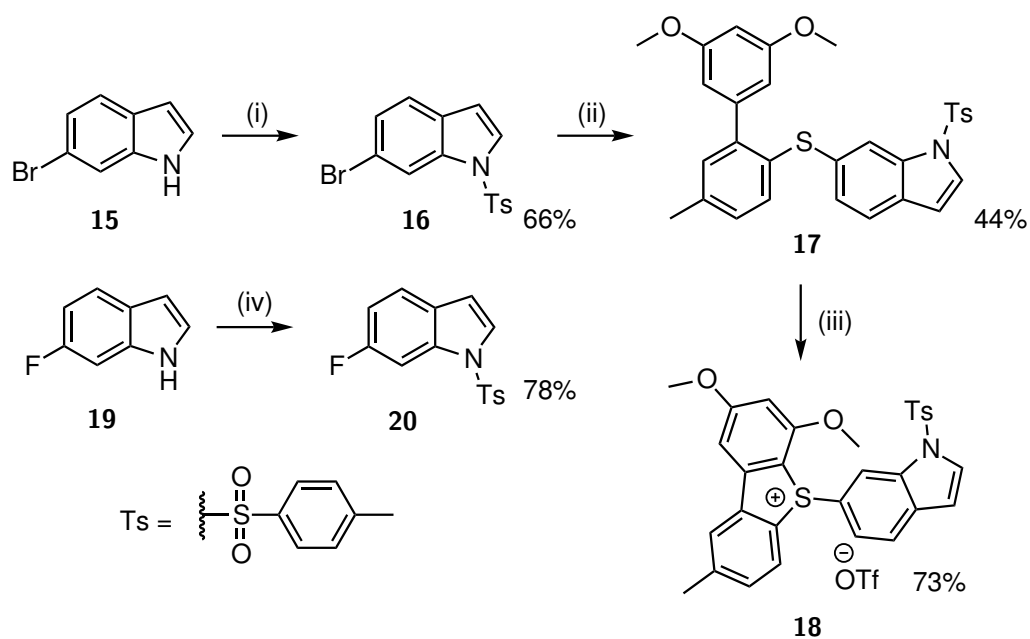
To a three-neck round-bottom flask equipped with an argon inlet and condenser were added toluene (12.0 mL) and thioether **12** (1.89 g, 6.36 mmol, 1.0 equiv.), followed by a solution of K_2CO_3 (3.52 g, 25.4 mmol, 4.0 equiv.) in H_2O (12.0 mL) and 3,5-dimethoxyphenylboronic acid (1.45 g, 7.95 mmol, 1.25 equiv.). The reaction vessel was degassed by argon purging with vigorous stirring to ensure efficient removal of O_2 trapped in the aqueous layer. $Pd(PPh_3)_4$ (367 mg, 0.318 mmol, 0.05 equiv.) was added and after additional degassing, the resulting mixture was plunged into a preheated block maintained at 125 °C. The reaction mixture was refluxed for 5 h. After cooling to room temperature, it was washed with a saturated aqueous solution of K_2CO_3 . The combined organic layers were dried over $MgSO_4$ and concentrated *in vacuo*. Flash column chromatography purification (3 → 12% EtOAc/PE) of the resulting yellow oil afforded the title compound as a colourless oil (1.54 g, 69%). ν_{max}/cm^{-1} 1611, 1583, 1467, 1334. 1H NMR (600 MHz, $CDCl_3$) δ_H 7.22-7.18 (2H, m, H12 and H22), 7.18 (1H, d, J 7.9, H15), 7.12 (1H, td, J 7.8, 1.6, H21), 7.09 (1H, dd, J 7.9, 1.2, H14), 7.04-7.01 (2H, m, H20 and H23), 6.52 (2H, d, J 2.3, H2 and H4), 6.45 (1H, t, J 2.3, H6), 3.76 (6H, s, H10 and H11), 2.37 (3H, s, H17). ^{13}C NMR (150 MHz, $CDCl_3$) δ_C 161.9 & 160.3 (d, J 246.5, C), 160.3 (C), 143.8 (C), 142.7 (C), 137.6 (C), 133.3 (CH), 132.3 (CH), 131.5 (CH), 129.2 (CH), 129.1 (C), 128.9 (d, J 7.8, CH), 124.7 & 124.6 (d, J 3.7, CH), 124.0 & 123.9 (d, J 17.5, C), 115.9 & 115.8 (d, J 22.1, CH), 107.4 (CH), 100.0 (CH), 55.4 (CH_3), 21.2 (CH_3). ^{19}F NMR (282 MHz, $CDCl_3$) δ_F -109.0. HRMS (ESI) Calculated for $C_{21}H_{20}O_2FS$ $[M+H]^+$: 355.1168; found: 355.1161.

5-(2-Fluorophenyl)-2,4-dimethoxy-8-methyl-5*H*-dibenzo[*b,d*]thiophen-5-ium trifluoromethanesulfonate



To a round-bottom flask were added MeCN (2.0 mL), thioether **13** (100 mg, 0.282 mmol, 1.0 equiv.), NCS (37.0 mg, 0.282 mmol, 1.0 equiv.) and Bi(OTf)₃ (185 mg, 0.282 mmol, 1.0 equiv.). The reaction mixture was stirred at room temperature for 1.5 h. It was then diluted with DCM and washed with H₂O. The organic layer was dried over MgSO₄ and concentrated *in vacuo*. Flash column chromatography purification (1 → 5% MeOH/DCM) afforded the title compound as a white solid (94.0 mg, 66%), mp 210-212 °C (dec). $\nu_{\max}/\text{cm}^{-1}$ 1590, 1252, 1219. ¹H NMR (600 MHz, d₆-DMSO) δ_{H} 8.43 (1H, d, *J*, 2.0, H12), 8.29 (1H, d, *J* 8.2, H15), 7.80-7.77 (1H, m, H22), 7.72 (1H, d, *J* 2.2, H2), 7.63-7.59 (2H, m, H14 and H23), 7.34-7.31 (1H, m, H20), 7.09 (1H, td, *J* 7.4, 1.6, H21), 6.9 (1H, d, *J* 2.2, H6), 3.98 (3H, s, H10 or H11), 3.92 (3H, s, H10 or H11), 2.56 (3H, s, H17). ¹³C NMR (150 MHz, d₆-DMSO) δ_{C} 166.8 (C), 162.3 & 160.6 (d, *J* 256.7, C), 157.6 (C), 145.1 (C), 141.6 (C), 140.4 (C), 137.3 & 137.2 (CH), 132.5 (CH), 130.0 (CH), 128.5 (CH), 128.3 (C), 127.3 (d, *J* 3.0, CH), 125.5 (CH), 119.6 (C), 118.1 & 117.9 (d, *J* 19.8, CH), 114.7 & 114.6 (d, *J* 14.3, C), 102.1 (CH), 100.7 (CH), 57.4 (CH₃), 56.8 (CH₃), 21.3 (CH₃). ¹⁹F NMR (282 MHz, d₆-DMSO) δ_{F} -77.8, -109.8. HRMS (CI) Calculated for C₂₁H₁₉O₂FS [M]⁺: 353.1084; found: 353.1083.

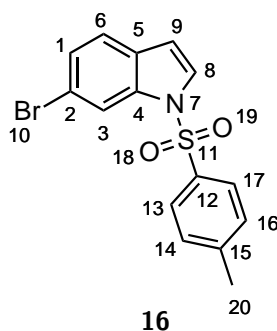
13.3 Synthetic Route Towards Sulfonium Salt **18** (Chapter 6)



Scheme 13.3: Syntheses of sulfonium salt **18** and fluorinated reference **20**.

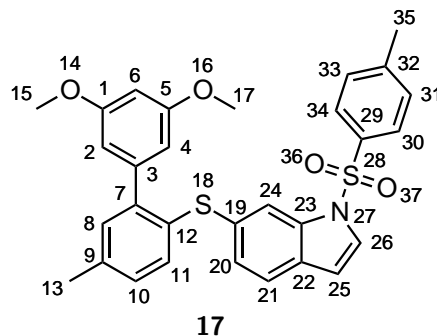
Reagents and conditions: (i) KOH, *p*TsCl, Aliquat[®] 336, toluene/water, rt, 1 h; (ii) Thioether **4**, Pd₂(dba)₃, DPEphos, KO*t*Bu, toluene, reflux, 1 h; (iii) NCS, Bi(OTf)₃, MeCN, rt, 20 min; (iv) KOH, *p*TsCl, Aliquat[®] 336, DCM, rt, 1 h.

6-Bromo-1-tosyl-1*H*-indole 16



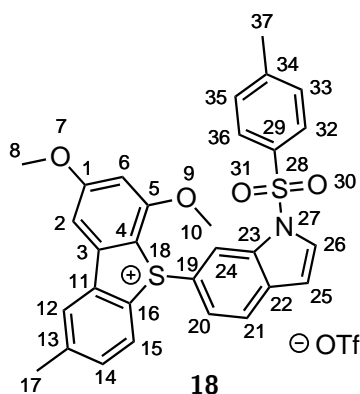
To a round-bottom flask were added toluene (20.0 mL) and 6-bromoindole (2.00 g, 10.2 mmol, 1.0 equiv.), followed by a solution of KOH (1.72 g, 30.6 mmol, 3.0 equiv.) in H₂O (10.0 mL), *p*-toluenesulfonyl chloride (2.33 g, 12.2 mmol, 1.2 equiv.) and a few droplets of Aliquat[®] 336. The resulting biphasic mixture was stirred at room temperature for 1 h. After dilution with H₂O, the organic layer was washed with more H₂O brine, dried over MgSO₄ and concentrated *in vacuo*. Flash column chromatography purification (5 → 15% Et₂O/PE) of the resulting brown solid afforded the title compound as a white solid (2.35 g, 66%), mp 134-135 °C. $\nu_{\text{max}}/\text{cm}^{-1}$ 3137, 3108, 2927, 1595, 1523, 1420, 1354. ¹H NMR (600 MHz, CDCl₃) δ_{H} 8.17 (1H, d, *J* 1.7, H3), 7.77 (2H, d, *J* 8.4, H13 and H17), 7.53 (1H, d, *J* 3.7, H8), 7.38 (1H, d, *J* 8.4, H6), 7.34 (1H, dd, *J* 8.4, 1.7, H1), 7.26-7.25 (2H, m, H14 and H16), 6.62 (1H, dd, *J* 3.7, 0.8, H9), 2.37 (3H, s, H20). ¹³C NMR (150 MHz, CDCl₃) δ_{C} 145.4 (C), 135.6 (C), 135.1 (C), 130.2 (CH), 129.9 (C), 126.9 (CH), 126.9 (CH), 126.8 (CH), 122.6 (CH), 118.4 (C), 116.7 (CH), 108.9 (CH), 21.8 (CH₃). HRMS (CI) Calculated for C₁₅H₁₂BrNO₂S [M+H]⁺: 348.9767; found: 348.9766.

6-((3',5'-Dimethoxy-5-methyl-[1,1'-biphenyl]-2-yl)thio)-1-tosyl-1*H*-indole 17



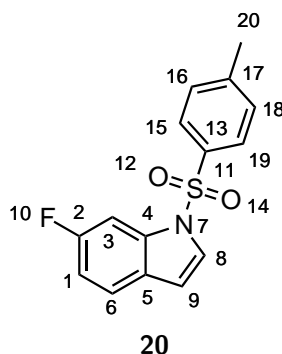
To a flame-dried three-neck round-bottom flask equipped with an argon inlet were added toluene (1.3 mL), bromoindole **16** (100 mg, 0.286 mmol, 1.0 equiv.) and *KOtBu* (42.0 mg, 0.372 mmol, 1.3 equiv.). The reaction vessel was degassed by argon purging before $\text{Pd}_2(\text{dba})_3$ (2.60 mg, 2.86 μmol , 0.01 equiv.), DPEphos (3.10 mg, 5.72 μmol , 0.02 equiv.) and thioether **4** (127 mg, 0.286 mmol, 1.0 equiv.) were added. The resulting mixture was purged with argon before being plunged into a preheated block maintained at 125 °C. The reaction mixture was refluxed for 1 h. After cooling to room temperature, it was filtered through a pad of Celite and concentrated *in vacuo*. Flash column chromatography purification (15 \rightarrow 20% EtOAc/PE) of the resulting brown oil afforded the title compound as a yellow oil (62.0 mg, 44%). $\nu_{\text{max}}/\text{cm}^{-1}$ 2932, 2837, 1590, 1517, 1493, 1452, 1419. ^1H NMR (600 MHz, CDCl_3) δ_{H} 7.83 (1H, d, J 0.8, H24), 7.61 (2H, d, J 8.4, H30 and 34), 7.52 (1H, d, J 3.7, H26), 7.38 (1H, d, J 8.2, H11), 7.21 (1H, d, J 2.0, H8), 7.16 (2H, d, J 8.4, H31 and H33), 7.12-7.10 (2H, m, H20 and H21), 7.08 (1H, dd, J 8.2, 2.0, H10), 6.59 (1H, d, J 3.7, H25), 6.48 (2H, d, J 2.3, H2 and H4), 6.44 (1H, t, J 2.3, H6), 3.68 (6H, s, H15 and H17), 2.41 (3H, s, H13), 2.34 (3H, s, H35). ^{13}C NMR (150 MHz, CDCl_3) δ_{C} 160.3 (C), 145.1 (C), 143.6 (C), 142.8 (C), 137.2 (C), 135.5 (C), 135.3 (C), 135.0 (C), 133.1 (C), 132.4 (CH), 131.3 (CH), 131.3 (C), 130.0 (CH), 129.7 (C), 129.1 (CH) 127.0 (CH), 126.7 (CH), 121.8 (CH), 116.3 (CH), 108.9 (CH), 108.8 (CH), 107.4 (CH), 107.3 (CH), 100.0 (CH), 55.4 (CH_3), 21.7 (CH_3), 21.2 (CH_3). HRMS (ESI) Calculated for $\text{C}_{30}\text{H}_{28}\text{NO}_4\text{S}_2$ $[\text{M}+\text{H}]^+$: 530.1460; found: 530.1434.

**2,4-Dimethoxy-8-methyl-5-(1-tosyl-1*H*-indol-6-yl)-5*H*-
dibenzo[*b,d*]thiophen-5-ium trifluoromethanesulfonate **18****



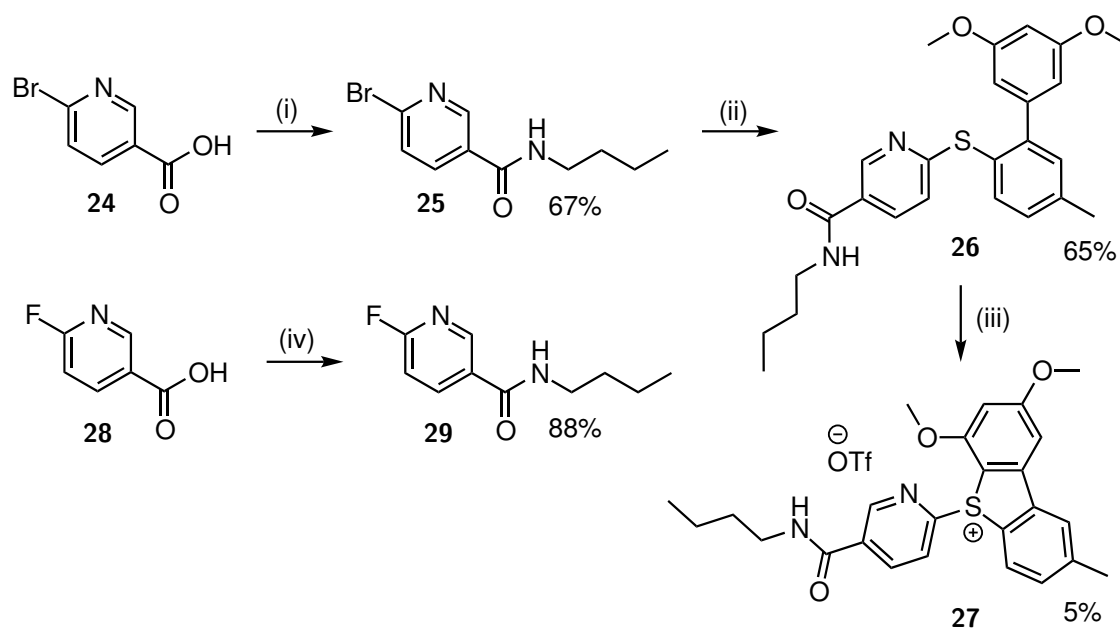
To a round-bottom flask were added MeCN (1.0 mL), thioether **17** (62.0 mg, 0.114 mmol, 1.0 equiv.), NCS (15.0 mg, 0.114 mmol, 1.0 equiv.) and Bi(OTf)₃ (75.0 mg, 0.114 mmol, 1.0 equiv.). The reaction mixture was stirred at room temperature for 20 min. After concentration the residue was resuspended in DCM and washed with H₂O. The organic layer was dried over MgSO₄ and concentrated *in vacuo*. Flash column chromatography purification (5 → 10% MeOH/DCM) afforded the title compound as an off-white solid (62.0 mg, 73%), mp 125-127 °C. $\nu_{\max}/\text{cm}^{-1}$ 1591, 1253. ¹H NMR (600 MHz, CDCl₃) δ_{H} 8.33 (1H, d, *J* 1.8, H24), 8.13 (1H, d, *J* 8.3, H15), 8.05 (1H, d, *J* 1.8, H12), 7.73-7.71 (3H, m, H26, H32 and H36), 7.63 (1H, d, *J* 8.6, H21), 7.47 (1H, dd, *J* 8.3, 1.8, H14), 7.36 (1H, d, *J* 2.1, H2), 7.31 (2H, d, *J* 8.3, H33 and H35), 7.22 (1H, dd, *J* 8.6, 1.9, H20), 6.70 (1H, d, *J* 3.7, H25), 6.60 (1H, d, *J* 2.1, H6), 4.07 (3H, s, H8), 3.89 (3H, s, H10), 2.60 (3H, s, H17), 2.40 (3H, s, H37). ¹³C NMR (150 MHz, CDCl₃) δ_{C} 167.8 (C), 158.6 (C), 146.4 (C), 145.7 (C), 142.2 (C), 138.9 (C), 135.4 (C), 134.4 (C), 134.2 (C), 132.8 (CH), 130.6 (CH), 130.5 (CH), 130.1 (C), 128.9 (CH), 127.2 (CH), 125.2 (CH), 124.4 (CH), 122.9 (CH), 122.1 (C), 120.0 (C), 116.5 (CH), 108.8 (CH), 101.4 (CH), 100.6 (CH), 57.1 (CH₃), 21.9 (CH₃), 21.8 (CH₃). ¹⁹F NMR (282 MHz, CDCl₃) δ_{F} -78.1. HRMS (ESI) Calculated for C₃₀H₂₆NO₄S₂ [M]⁺: 528.1303; found: 528.1287.

6-Fluoro-1-tosyl-1*H*-indole 20



To a flame-dried round-bottom flask equipped with an argon inlet were added DCM (3.0 mL) and 6-fluoroindole (100 mg, 0.740 mmol, 1.0 equiv.), followed by powdered NaOH (130 mg, 3.25 mmol, 4.4 equiv.), *p*-toluenesulfonyl chloride (169 mg, 0.890 mmol, 1.2 equiv.) and a droplet of Aliquat[®] 336. The resulting mixture was stirred at room temperature for 1 h. It was then diluted with DCM and washed with H₂O. The aqueous layer was extracted with DCM and the combined organic extracts were washed with brine, dried over MgSO₄ and concentrated *in vacuo*. Flash column chromatography purification (15 → 20% Et₂O/PE) afforded the title compound as a white solid (77.0 mg, 78%), mp 105-106 °C. $\nu_{\max}/\text{cm}^{-1}$ 3143, 3118, 2927, 1614, 1591, 1530, 1479, 1429. ¹H NMR (600 MHz, CDCl₃) δ_{H} 7.77 (2H, d, *J* 8.4, H15 and H19), 7.72 (1H, dd, *J* 9.6, 2.4, H3), 7.54 (1H, d, *J* 3.7, H8), 7.44 (1H, dd, *J* 8.9, 5.3, H6), 7.25 (2H, d, *J* 8.4, H16 and H18), 6.99 (1H, td, *J* 8.9, 2.4, H1), 6.62 (1H, dd, *J* 3.7, 0.8, H9), 2.36 (3H, s, H20). ¹³C NMR (150 MHz, CDCl₃) δ_{C} 161.7 & 160.1 (d, *J* 242.1, C), 145.3 (C), 135.1 (C), 135.0 (C), 130.1 (CH), 127.0 (CH), 126.7 (d, *J* 4.1, CH), 122.2 (d, *J* 9.9, CH), 112.0 & 111.8 (d, *J* 24.4, CH), 108.9 (CH), 101.1 & 101.0 (d, *J* 28.1, CH), 21.7 (CH₃). ¹⁹F NMR (282 MHz, CDCl₃) δ_{F} -116.5. HRMS (ESI) Calculated for C₁₅H₁₃FNO₂S [M+H]⁺: 290.0651; found: 290.0649.

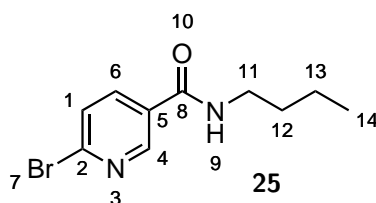
13.4 Synthetic Route Towards Sulfonium Salt **27** (Chapter 7)



Scheme 13.4: Syntheses of sulfonium salt **27** and fluorinated reference **29**.

Reagents and conditions: (i) But-1-ylamine, HATU, HOBt, DIPEA, DCM, rt, 1 h; (ii) Thioether **4**, Pd₂(dba)₃, DPEphos, KO^tBu, toluene, reflux, 2.5 h; (iii) NCS, TfOH, MeCN, rt, 3 h; (iv) But-1-ylamine, HATU, HOBt, DIPEA, DCM, rt, 2 h.

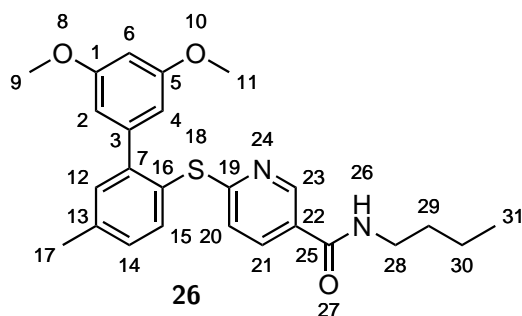
6-Bromo-*N*-butylnicotinamide 25



To a stirring solution of but-1-ylamine (808 μL , 8.18 mmol, 1.1 equiv.) in DCM (25.0 mL) were added 6-bromonicotinic acid (1.50 g, 7.43 mmol, 1.0 equiv.), HATU (3.12 g, 8.21 mmol, 1.1 equiv.), HOBt (1.10 g, 8.14 mmol, 1.1 equiv.) and DIPEA (5.18 mL, 29.7 mmol, 4.0 equiv.). The resulting yellow solution was stirred at room temperature for 1 h. The reaction mixture was then diluted with DCM, washed with H_2O and brine, dried over MgSO_4 and concentrated *in vacuo*. Flash column chromatography purification (0 \rightarrow 50% EtOAc/PE) afforded the title compound as a shiny white solid (1.28 g, 67%), mp 110-111 $^\circ\text{C}$. $\nu_{\text{max}}/\text{cm}^{-1}$ 3304, 3046, 2932, 2868, 1636, 1577, 1538, 1454. ^1H NMR (600 MHz, CDCl_3) δ_{H} 8.69 (1H, d, J 2.7, H4), 7.97 (1H, dd, J 8.2, 2.7, H6), 7.58 (1H, d, J 8.2, H1), 6.10 (1H, bs, H9), 3.47 (2H, td, J 7.1, 5.7, H11), 1.62 (2H, m, H12), 1.42 (2H, m, H13), 0.97 (3H, t, J 7.4, H14). ^{13}C NMR (150 MHz, CDCl_3) δ_{C} 164.7 (C), 148.2 (CH), 145.2 (C), 137.7 (CH), 129.8 (C), 128.4 (CH), 40.2 (CH_2), 31.7 (CH_2), 20.3 (CH_2), 13.9 (CH_3). HRMS (ESI) Calculated for $\text{C}_{10}\text{H}_{14}\text{BrN}_2\text{O}$ $[\text{M}+\text{H}]^+$: 257.0290; found: 257.0292.

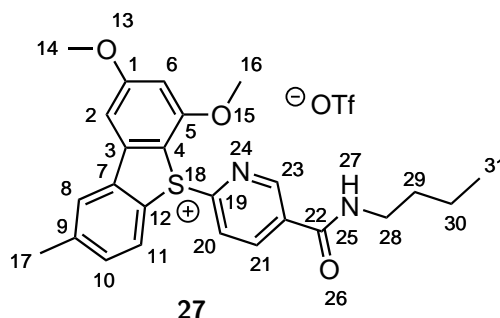
N-Butyl-6-((3',5'-dimethoxy-5-methyl-[1,1'-biphenyl]-2-yl)thio)nicotinamide

26



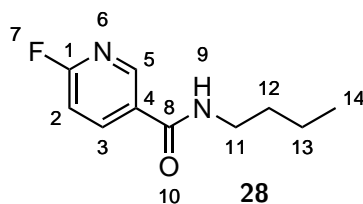
To a flame-dried three-neck round-bottom flask equipped with an argon inlet and condenser were added toluene (7.0 mL), Pd₂(dba)₃ (178 mg, 0.194 mmol, 0.1 equiv.) and DPEphos (209 mg, 0.388 mmol, 0.2 equiv.), followed by amide **25** (500 mg, 1.94 mmol, 1.0 equiv.), KO*t*Bu (239 mg, 2.13 mmol, 1.1 equiv.) and thioether **4** (949 mg, 2.13 mmol, 1.1 equiv.). The resulting mixture was purged with argon before being plunged into a preheated block maintained at 125 °C and refluxed for 2.5 h. After cooling to room temperature, it was filtered through a pad of Celite and concentrated *in vacuo*. Flash column chromatography purification (50 → 100% Et₂O/PE) afforded the title compound as a yellow oil (551 mg, 65%). $\nu_{\text{max}}/\text{cm}^{-1}$ 3306, 2956, 2932, 1588, 1494, 1452. ¹H NMR (600 MHz, CDCl₃) δ_{H} 8.65 (1H, d, *J* 2.5, H23), 7.82 (1H, dd, *J* 8.4, 2.5, H21), 7.56 (1H, d, *J* 7.8, H15), 7.3 (1H, d, *J* 2.2, H12), 7.24 (1H, dd, *J* 7.8, 2.2, H14), 6.87 (1H, dd, *J* 8.4, 0.6, H20), 6.44 (2H, d, *J* 2.3, H2 and H4), 6.39 (1H, t, *J* 2.3, H6), 6.01 (1H, t, *J* 5.7, H26), 3.68 (6H, s, H9 and H11), 3.43 (2H, td, *J* 7.2, 5.8, H28), 2.44 (3H, s, H17), 1.58 (2H, m, H29), 1.4 (2H, m, H3), 0.95 (3H, t, *J* 7.4, H31). ¹³C NMR (150 MHz, CDCl₃) δ_{C} 166.2 (C), 165.4 (C), 160.2 (C), 147.3 (CH), 146.9 (C), 142.7 (C), 140.5 (C), 137.2 (CH), 135.5 (CH), 132.1 (CH), 129.7 (CH), 126.2 (C), 124.7 (C), 120.6 (CH), 107.4 (CH), 99.8 (CH), 55.4 (CH₃), 40.0 (CH₂), 31.8 (CH₂), 21.5 (CH₃), 20.3 (CH₂), 13.9 (CH₃). HRMS (ESI) Calculated for C₂₅H₂₉N₂O₃S [M+H]⁺: 437.1899; found: 437.1895.

5-(5-(Butylcarbamoyl)pyridin-2-yl)-2,4-dimethoxy-8-methyl-5*H*-dibenzo[*b,d*]-thiophen-5-ium trifluoromethanesulfonate **27**



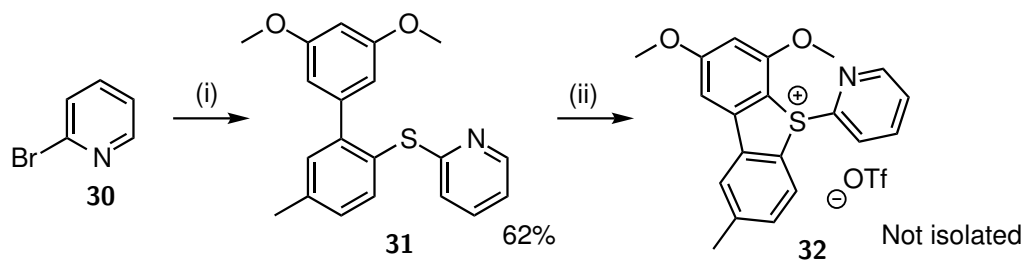
To a stirring solution of thioether **26** (71.0 mg, 0.163 mmol, 1.0 equiv.) in MeCN (1.5 mL) at -10 °C were added NCS (21.7 mg, 0.163 mmol, 1.0 equiv.) and TfOH (43 μ L, 0.489 mmol, 3.0 equiv.). The reaction mixture was stirred at -10 °C for 20 min but as no conversion was observed, it was allowed to warm to room temperature, at which it was stirred for 3 h. As the reaction did not progress, the mixture was concentrated *in vacuo*, the residue dissolved in DCM, washed with 2 M NaOH solution, dried over MgSO₄ and concentrated *in vacuo*. Flash column chromatography purification (0 \rightarrow 10% MeOH/DCM) afforded the title compound as a yellow residue (5.0 mg, 5%). The sample was not clean enough to allow for mass spectrometry so ¹H, ¹³C and ¹⁹F NMR spectroscopy were used to confirm identity of the title compound. ¹H NMR (600 MHz, CDCl₃) δ_{H} 9.03 (1H, dd, *J* 2.4, 0.6, H23), 8.58 (1H, dd, *J* 8.3, 2.4, H21), 8.02 (1H, d, *J* 8.2, H11), 7.89 (1H, d, *J* 1.8, H8), 7.78 (1H, dd, *J* 8.3, 0.6, H20), 7.49 (1H, dd, *J* 8.2, 1.8, H10), 7.23 (1H, d, *J* 2.0, H2), 6.68 (1H, d, *J* 2.0, H6), 4.05 (3H, s, H14), 4.00 (3H, s, H16), 3.39 (2H, dt, *J* 7.7, 6.1, H28), 2.58 (3H, s, H17), 1.59 (2H, m, H29), 1.36 (2H, m, H30), 0.91 (3H, t, *J* 7.4, H31). ¹³C NMR (150 MHz, CDCl₃) δ_{C} 168.3 (C), 163.9 (C), 159.4 (C), 152.8 (CH), 149.4 (C), 146.0 (C), 143.6 (C), 139.7 (CH), 139.4 (C), 135.4 (C), 133.1 (CH), 128.1 (CH), 127.4 (C), 125.1 (CH), 125.0 (CH), 103.2 (C), 101.9 (CH), 100.4 (CH), 57.3 (CH₃), 56.8 (CH₃), 40.3 (CH₂), 31.2 (CH₂), 22.1 (CH₃), 20.3 (CH₂), 13.8 (CH₃). ¹⁹F NMR (282 MHz, CDCl₃) δ_{F} -78.4.

N-Butyl-6-fluoronicotinamide **28**



To a stirring solution of but-1-ylamine (154 μ L, 1.56 mmol, 1.1 equiv.) in DCM (7.0 mL) were added 6-fluoronicotinic acid (200 mg, 1.42 mmol, 1.0 equiv.), HATU (597 mg, 1.57 mmol, 1.1 equiv.), HOBt (211 mg, 1.56 mmol, 1.1 equiv.) and DIPEA (989 μ L, 5.68 mmol, 4.0 equiv.). The resulting yellow solution was stirred at room temperature for 2 h. The reaction mixture was then diluted with DCM, washed with H₂O and brine, dried over MgSO₄ and concentrated *in vacuo*. Flash column chromatography purification (20 \rightarrow 60% EtOAc/PE) afforded the title compound as a white solid (246 mg, 88%), mp 112-115 $^{\circ}$ C. $\nu_{\text{max}}/\text{cm}^{-1}$ 3309, 2977, 2958, 2872, 1636, 1593, 1535, 1474, 1465. ¹H NMR (600 MHz, CDCl₃) δ_{H} 8.58 (1H, d, *J* 2.5, H5), 8.24 (1H, ddd, *J* 8.5, 7.5, 2.5, H3), 7.01 (1H, ddd, *J* 8.5, 2.5, 0.7, H2), 6.12 (1H, bs, H9), 3.48 (2H, td, *J* 7.4, 5.7, H11), 1.62 (2H, p, *J* 7.4, H12), 1.42 (2H, sex, *J* 7.4, H13), 0.97 (3H, t, *J* 7.4, H14). ¹³C NMR (150 MHz, CDCl₃) δ_{C} 165.9 & 164.2 (d, *J* 244.0, C), 164.6 (C), 146.5 & 146.4 (d, *J* 16.0, CH), 141.0 & 140.9 (d, *J* 8.8, CH), 129.0 & 128.9 (d, *J* 4.4, C), 110.0 & 109.8 (d, *J* 37.4, CH), 40.1 (CH₂), 31.8 (CH₂), 20.3 (CH₂), 13.9 (CH₃). ¹⁹F NMR (282 MHz, CDCl₃) δ_{F} -63.7. HRMS (ESI) Calculated for C₁₀H₁₄N₂OF [M+H]⁺: 197.1090; found: 197.1091.

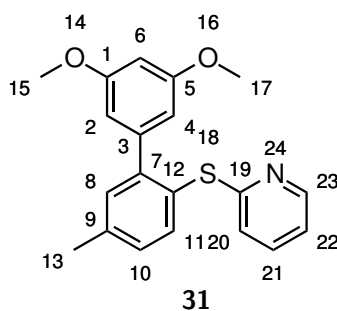
13.5 Synthetic Route Towards Sulfonium Salt **32** (Chapter 7)



Scheme 13.5: Synthesis of sulfonium salt **32**.

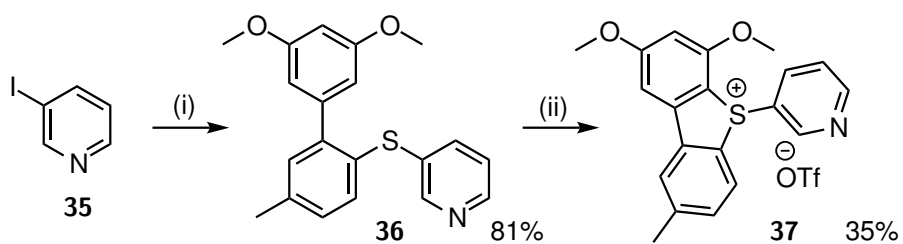
Reagents and conditions: (i) Thioether **4**, Pd₂(dba)₃, DPEphos, KO^tBu, toluene, reflux, 24 h; (ii) No reaction.

2-((3',5'-Dimethoxy-5-methyl-[1,1'-biphenyl]-2-yl)thio)pyridine **31**



To a flame-dried three-neck round-bottom flask equipped with an argon inlet and condenser were added toluene (5.0 mL), Pd₂(dba)₃ (124 mg, 0.135 mmol, 0.1 equiv.) and DPEphos (145 mg, 0.269 mmol, 0.2 equiv.), followed by 2-bromopyridine (278 mg, 1.76 mmol, 1.3 equiv.), KO^tBu (167 mg, 1.49 mmol, 1.1 equiv.) and thioether **4** (600 mg, 1.35 mmol, 1.0 equiv.). The resulting mixture was purged with argon before being plunged into a preheated block maintained at 125 °C and refluxed for 24 h. After cooling to room temperature, the mixture was filtered through a pad of Celite and concentrated *in vacuo*. Flash column chromatography purification (0 → 12% EtOAc/toluene) afforded the title compound as a white solid (283 mg, 62%), mp 85-88 °C. $\nu_{\text{max}}/\text{cm}^{-1}$ 2956, 2927, 2830, 1591, 1571, 1445, 1413. ¹H NMR (600 MHz, CDCl₃) δ_{H} 8.36 (1H, ddd, *J* 4.9, 2.0, 1.0, H23), 7.57 (1H, d, *J* 7.9, H11), 7.41 (1H, ddd, *J* 8.2, 7.5, 2.0, H21), 7.28 (1H, d, *J* 2.1, H8), 7.21 (1H, dd, *J* 7.9, 2.1, H10), 6.93 (1H, ddd, *J* 7.5, 4.9, 1.2, H22), 6.86 (1H, ddd, *J* 8.2, 1.2, 1.0, H20), 6.47 (2H, d, *J* 2.3, H2 and H4), 6.40 (1H, t, *J* 2.3, H6), 3.67 (6H, s, H15 and H17), 2.43 (3H, s, H13). ¹³C NMR (150 MHz, CDCl₃) δ_{C} 162.2 (C), 160.2 (C), 149.6 (CH), 146.6 (C), 143.0 (C), 139.7 (C), 137.0 (CH), 136.5 (CH), 131.8 (CH), 129.5 (CH), 125.9 (C), 121.5 (CH), 119.6 (CH), 107.4 (CH), 100.0 (CH), 55.4 (CH₃), 21.4 (CH₃). HRMS (ESI) Calculated for C₂₀H₂₀NO₂S [M+H]⁺: 338.1215; found: 338.1208.

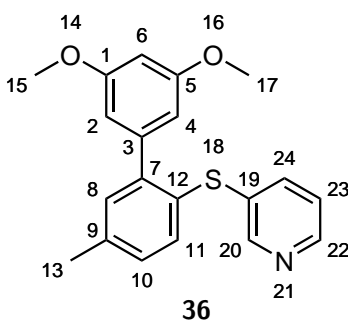
13.6 Synthetic Route Towards Sulfonium Salt **37** (Chapter 7)



Scheme 13.6: Synthesis of sulfonium salt **37**.

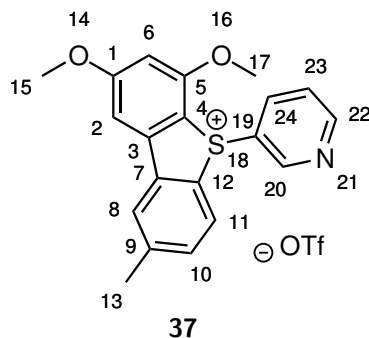
Reagents and conditions: (i) Thioether **4**, Pd₂(dba)₃, DPEphos, KO^tBu, toluene, reflux, 2 h; (ii) Bi(OTf)₃, Sulfonamide **38**, MeCN, 2.5 h, rt.

3-((3',5'-Dimethoxy-5-methyl-[1,1'-biphenyl]-2-yl)thio)pyridine **36**



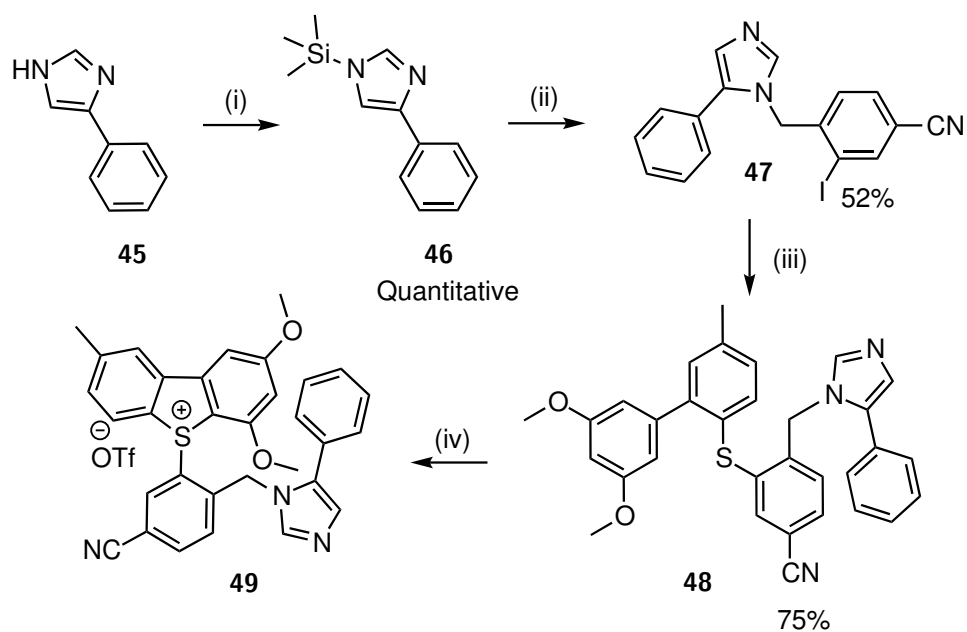
To a flame-dried three-neck round-bottom flask equipped with an argon inlet and condenser were added toluene (15.0 mL), Pd₂(dba)₃ (223 mg, 0.244 mmol, 0.1 equiv.) and DPEphos (263 mg, 0.488 mmol, 0.2 equiv.), followed by 3-iodopyridine (500 mg, 2.44 mmol, 1.0 equiv.), KO^tBu (301 mg, 2.68 mmol, 1.1 equiv.) and thioether **4** (1.19 g, 2.68 mmol, 1.1 equiv.). The resulting mixture was purged with argon before being plunged into a preheated block maintained at 125 °C and refluxed for 2 h. After cooling to room temperature, the mixture was filtered through a pad of Celite and concentrated *in vacuo*. Flash column chromatography purification (50 → 70% Et₂O/PE) afforded the title compound as an orange oil (663 mg, 81%). $\nu_{\max}/\text{cm}^{-1}$ 2998, 2936, 2835, 1589, 1453, 1421. ¹H NMR (600 MHz, CDCl₃) δ_{H} 8.38-8.37 (2H, m, H20 and H22), 7.43-7.41 (1H, m, H23), 7.28 (1H, d, *J* 7.8, H11), 7.19 (1H, d, *J* 2.3, H8), 7.14-7.11 (2H, m, H10 and H24), 6.45-6.44 (3H, m, H2, H4 and H6), 3.75 (6H, s, H15 and H17), 2.38 (3H, s, H13). ¹³C NMR (150 MHz, CDCl₃) δ_{C} 160.4 (C), 150.9 (CH), 147.4 (CH), 144.5 (C), 142.6 (C), 138.4 (C), 137.6 (CH), 134.7 (C), 133.4 (CH), 131.7 (CH), 129.4 (CH), 128.8 (C), 123.7 (CH), 107.5 (CH), 99.8 (CH), 55.5 (CH₃), 21.2 (CH₃). HRMS (ESI) Calculated for C₂₀H₂₀NO₂S [M+H]⁺: 338.1214; found: 338.1215.

2,4-Dimethoxy-8-methyl-5-(pyridin-3-yl)-5*H*-dibenzo[*b,d*]thiophen-5-ium tri-fluoromethanesulfonate **37**



To a stirring solution of $\text{Bi}(\text{OTf})_3$ (194 mg, 0.296 mmol, 1.0 equiv.) and *N*-chloro-*N*-methylbenzenesulfonamide **38** (61.0 mg, 0.296 mmol, 1.0 equiv.) in MeCN (0.5 mL) was added a solution of thioether **36** (100 mg, 0.296 mmol, 1.0 equiv.) in MeCN (0.5 mL). The resulting solution was stirred at room temperature for 2.5 h. The mixture was then concentrated *in vacuo*, diluted with DCM, washed with a solution of EDTA in saturated aqueous K_2CO_3 , followed by H_2O , dried over MgSO_4 and concentrated *in vacuo*. Flash column chromatography purification (0 \rightarrow 10% 1 N NH_3 in MeOH/DCM) to afford a mixture of the title compound and its chlorinated analogue (62 mg). A pure sample could not be obtained, owing to the challenging separation of sulfonium salt **37** and its chlorinated analogue **41**. ^1H , ^{13}C and ^{19}F NMR spectroscopy were used to confirm the molecular structure. NMR yield of the title compound corresponds to 35% (51 mg). ^1H NMR (600 MHz, d_6 -DMSO) δ_{H} 9.01 (1H, d, J 2.5, H20), 8.85 (1H, dd, J 4.7, 1.5, H24), 8.42 (1H, d, J 1.7, H8), 8.26 (1H, d, J 8.3, H11), 7.73 (1H, d, J 2.0, H2), 7.69 (1H, ddd, J 8.4, 2.5, 1.5, H22), 7.61 (1H, dd, J 8.3, 1.7, H10), 7.56 (1H, dd, J 8.4, 4.7, H23), 6.92 (1H, d, J 2.0, H6), 3.99 (3H, s, H15), 3.93 (3H, s, H17), 2.55 (3H, s, H13). ^{13}C NMR (150 MHz, d_6 -DMSO) δ_{C} 166.9 (C), 157.7 (C), 154.5 (CH), 150.6 (CH), 145.0 (C), 141.9 (C), 139.7 (C), 136.4 (CH), 132.5 (CH), 129.6 (C), 128.2 (CH), 126.4 (CH), 126.3 (C), 125.6 (CH), 108.5 (C), 102.2 (CH), 100.8 (CH), 57.4 (CH_3), 56.8 (CH_3), 21.3 (CH_3). ^{19}F NMR (282 MHz, d_6 -DMSO) δ_{F} -77.8.

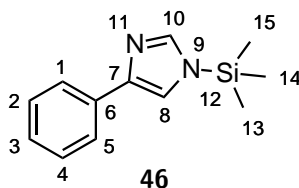
13.7 Synthetic Route Towards Sulfonium Salt 48 (Chapter 8)



Scheme 13.7: Synthesis of sulfonium salt 49.

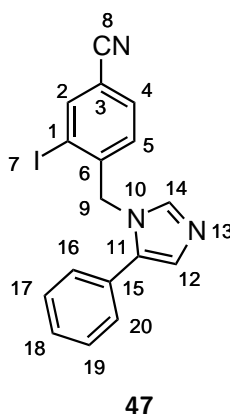
Reagents and conditions: (i) HMDS, reflux, 20 h; (ii) 4-(Bromomethyl)-3-iodobenzonitrile, K_2CO_3 , DMF, 100 °C, 3 h; (iii) Thioether 4, $Pd_2(dba)_3$, DPEphos, $KOtBu$, toluene, reflux, 3.5 h; (iv) TfOH/ $Bi(OTf)_3$, NCS, MeCN, 2.5 h, rt (isolated and analysed by Dr Vincent Gray).

4-Phenyl-1-(trimethylsilyl)-1*H*-imidazole **46**



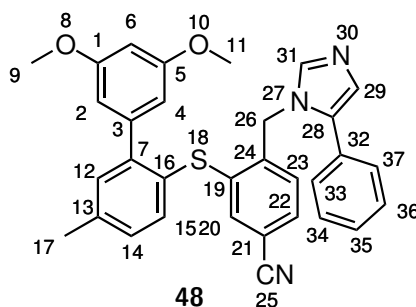
To a flame-dried three-neck round-bottom flask equipped with an argon inlet were added 4-phenyl-1*H*-imidazole (1.00 g, 6.94 mmol, 1.0 equiv.) and hexamethyldisilazane (7.30 mL, 34.8 mmol, 5.0 equiv.). The reaction vessel was degassed by argon purging before being plunged into a preheated block maintained at 130 °C. The reaction mixture was refluxed for 20 h. The reaction progress was monitored by ¹H NMR spectroscopy. The title compound was obtained in quantitative yield and was used immediately in the next step without further purification. ¹H NMR (600 MHz, CDCl₃) δ_H 7.81 (2H, dd, *J* 8.1, 1.6, H1 and H5), 7.60 (1H, d, *J* 1.4, H10), 7.37 (2H, t, *J* 7.7, H2 and H4), 7.24-7.22 (2H, m, H3 and H8), 0.49 (9H, s, H13, H14 and H15).

3-Iodo-4-((5-phenyl-1*H*-imidazol-1-yl)methyl)benzonitrile **47**



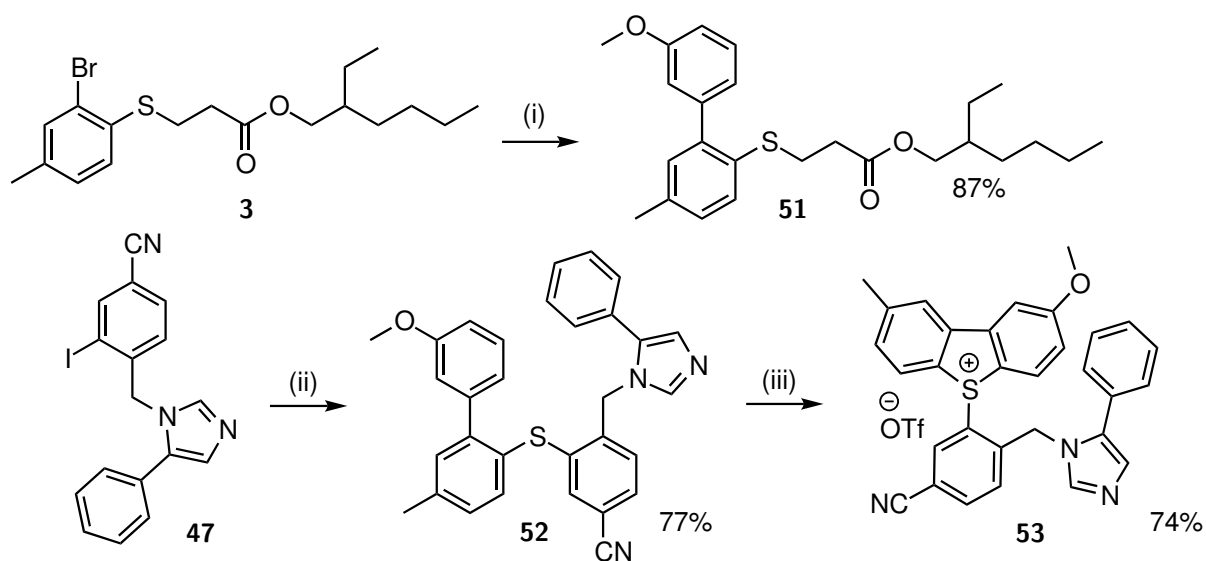
To a flame-dried three-neck round-bottom flask equipped with an argon inlet were added DMF (10.0 mL), phenylimidazole **46** (1.50 g, 6.94 mmol, 1.0 equiv.), followed by 4-(bromomethyl)-3-iodobenzonitrile (2.68 g, 8.33 mmol, 1.2 equiv.) and K_2CO_3 (1.05 g, 7.63 mmol, 1.1 equiv.). The reaction vessel was degassed by argon purging before being plunged into a preheated block maintained at 100 °C. The reaction mixture was heated for 3 h. After cooling to room temperature, it was diluted with DCM, washed with H_2O and a saturated aqueous solution of LiCl. The organic layer was dried over $MgSO_4$ and concentrated *in vacuo*. Flash column chromatography purification (0 → 20% EtOAc/DCM) of the resulting brown oil afforded the title compound as a yellow solid (1.39 g, 52%), mp 148-151 °C. ν_{max}/cm^{-1} 2225, 1605, 1553, 1487, 1439. 1H NMR (600 MHz, $CDCl_3$) δ_H 8.17 (1H, d, J 1.7, H2), 7.79 (2H, dd, J 7.8, 1.5, H16 and H20), 7.77 (1H, bs, H14), 7.61 (1H, dd, J 8.1, 1.7, H4), 7.40 (2H, t, J 7.8, H17 and H19), 7.28 (1H, t, J 7.8, H18), 7.21 (1H, d, J 1.4, H12), 6.93 (1H, d, J 8.1, H5), 5.24 (2H, s, H9). δ_C (150 MHz, $CDCl_3$) δ_C 144.0 (C), 143.1 (C), 142.7 (CH), 138.0 (CH), 133.2 (C), 132.6 (CH), 128.9 (CH), 128.4 (CH), 127.6 (CH), 125.0 (CH), 116.6 (C), 115.0 (C), 114.1 (CH), 97.3 (C), 55.7 (CH₂). HRMS (CI) Calculated for $C_{17}H_{13}IN_3$ $[M+H]^+$: 386.0154; found: 386.0136.

3-((3',5'-Dimethoxy-5-methyl-[1,1'-biphenyl]-2-yl)thio)-4-((5-phenyl-4,5-dihydro-1H-imidazol-1-yl)methyl)benzonitrile 48



To a flame-dried three-neck round-bottom flask equipped with an argon inlet were added toluene (7.0 mL), Pd₂(dba)₃ (30.0 mg, 32.5 μmol, 0.025 equiv.) and DPEphos (35.0 mg, 65.0 μmol, 0.05 equiv.). The reaction vessel was degassed by argon purging before thioether **4** (694 mg, 1.56 mmol, 1.2 equiv.) and KO^tBu (175 mg, 1.56 mmol, 1.2 equiv.) were added. The resulting suspension was stirred at room temperature for 10 min and imidazole **47** (500 mg, 1.30 mmol, 1.0 equiv.) was added. The reaction vessel was degassed by argon purging once more before being plunged into a preheated block maintained at 125 °C. It was refluxed for 3.5 h. After cooling to room temperature, it was diluted with DCM, washed with brine, dried over MgSO₄ and concentrated *in vacuo*. Flash column chromatography purification (0 → 12% Et₂O/DCM) afforded the title compound as a yellow oil (535 mg, 75%). ν_{max}/cm⁻¹ 2228, 1588, 1452, 1421. ¹H NMR (600 MHz, CDCl₃) δ_H 7.76 (2H, dd, *J* 8.2, 1.6, H33 and H37), 7.58 (1H, d, *J* 1.4, H31), 7.42-7.38 (3H, m, H15, H34 and H36), 7.34 (1H, dd, *J* 8.0, 1.6, H22), 7.28-7.25 (2H, m, H12 and H20), 7.23-7.22 (2H, m, H14 and H35), 7.06 (1H, d, *J* 1.4, H29) 6.77 (1H, d, *J* 8.0, H23), 6.43 (1H, t, *J* 2.4, H6), 6.32 (2H, d, *J* 2.4, H2 and H4), 5.03 (2H, s, H26), 3.72 (6H, s, H9 and H11), 2.44 (3H, s, H17). ¹³C NMR (150 MHz, CDCl₃) δ_C 160.4 (C), 145.4 (C), 142.8 (C), 142.5 (C), 140.6 (C), 140.2 (C), 138.4 (C), 138.0 (CH), 135.0 (CH), 134.1 (CH), 133.5 (C), 132.4 (CH), 130.1 (CH), 129.9 (CH), 128.8 (CH), 127.6 (CH), 127.4 (CH), 126.7 (C), 124.0 (CH), 118.1 (C), 115.2 (CH), 112.6 (C), 107.3 (CH), 107.3 (CH), 100.0 (CH), 55.5 (CH₃), 48.5 (CH₂), 21.4 (CH₃). HRMS (ESI) Calculated for C₃₂H₂₈N₃O₂S [M+H]⁺: 518.1897; found: 518.1893.

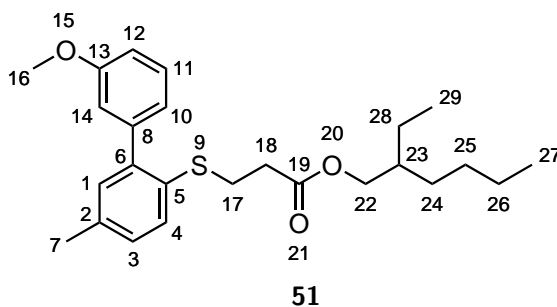
13.8 Synthetic Route Towards Sulfonium Salt **53** (Chapter 8)



Scheme 13.8: Synthesis of sulfonium salt **53**.

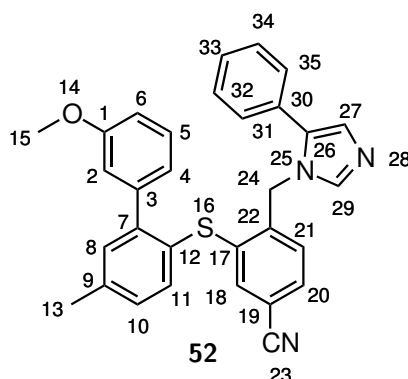
Reagents and conditions: (i) 3-Methoxyphenylboronic acid, Pd(PPh₃)₄, K₂CO₃, toluene/water, reflux, 16 h; (ii) Thioether **51**, Pd₂(dba)₃, DPEphos, KOtBu, toluene, reflux, 3.5 h; (iii) NCS, TfOH, MeCN, rt, 2 h.

Octan-3-yl 3-((3'-methoxy-5-methyl-[1,1'-biphenyl]-2-yl)thio)propanoate **51**



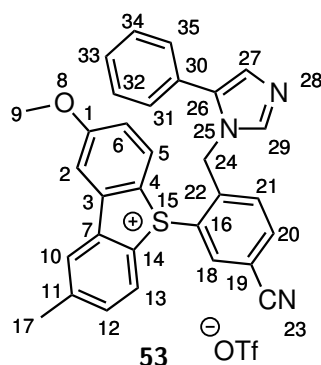
To a flame-dried three-neck round-bottom flask equipped with an argon inlet were added toluene (10.0 mL) and thioether **3** (2.00 g, 5.16 mmol, 1.0 equiv.), followed by a solution of K_2CO_3 (3.57 g, 25.8 mmol, 5.0 equiv.) in H_2O (10.0 mL) and 3-methoxyphenylboronic acid (980 mg, 6.45 mmol, 1.25 equiv.). The reaction vessel was degassed by argon purging with vigorous stirring to ensure efficient removal of O_2 trapped in the aqueous layer. $\text{Pd}(\text{PPh}_3)_4$ (373 mg, 0.323 mmol, 0.06 equiv.) was added and after additional degassing, the resulting mixture was plunged into a preheated block maintained at 125 °C. The reaction mixture was refluxed for 16 h. After cooling to room temperature, it was washed with a saturated aqueous solution of K_2CO_3 . The combined organic layers were dried over MgSO_4 and concentrated *in vacuo*. Flash column chromatography purification (0 → 10% $\text{Et}_2\text{O}/\text{PE}$) of the resulting brown oil afforded the title compound as a colourless oil (1.86 g, 87%). $\nu_{\text{max}}/\text{cm}^{-1}$ 2957, 2927, 1732, 1597, 1579, 1462. ^1H NMR (600 MHz, CDCl_3) δ_{H} 7.35 (1H, d, J 8.0, H4), 7.32 (1H, t, J 7.8, H11), 7.14 (1H, dd, J 8.0, 2.1, H3), 7.11 (1H, d, J 2.1, H1), 6.99-6.97 (1H, m, H10), 6.95 (1H, dd, J 2.6, 1.6, H14), 6.92-6.90 (1H, m, H12), 3.99-3.94 (2H, 2 × m, H22), 3.84 (3H, s, H16), 2.95 (2H, t, J 7.6, H17), 2.50 (2H, t, J 7.6, H18), 2.36 (3H, s, H7), 1.56-1.51 (1H, m, H23), 1.35-1.25 (8H, m, H24, H25, H26 and H28), 0.90-0.86 (6H, m, H27 and H29). ^{13}C NMR (150 MHz, CDCl_3) δ_{C} 172.1 (C), 159.2 (C), 143.1 (C), 142.3 (C), 136.4 (C), 131.4 (CH), 130.3 (C), 129.9 (CH), 129.1 (CH), 128.9 (CH), 121.9 (CH), 115.0 (CH), 113.1 (CH), 67.2 (CH₂), 55.4 (CH₃), 38.8 (CH), 34.3 (CH₂), 30.5 (CH₂), 29.0 (CH₂), 28.9 (CH₂), 23.9 (CH₂), 23.1 (CH₂), 21.0 (CH₃), 14.2 (CH₃), 11.1 (CH₃). HRMS (EI) Calculated for $\text{C}_{25}\text{H}_{34}\text{O}_3\text{S}$ $[\text{M}]^+$: 414.2223; found: 414.2222.

3-((3'-Methoxy-5-methyl-[1,1'-biphenyl]-2-yl)thio)-4-((5-phenyl-1*H*-imidazol-1-yl)methyl)benzonitrile **52**



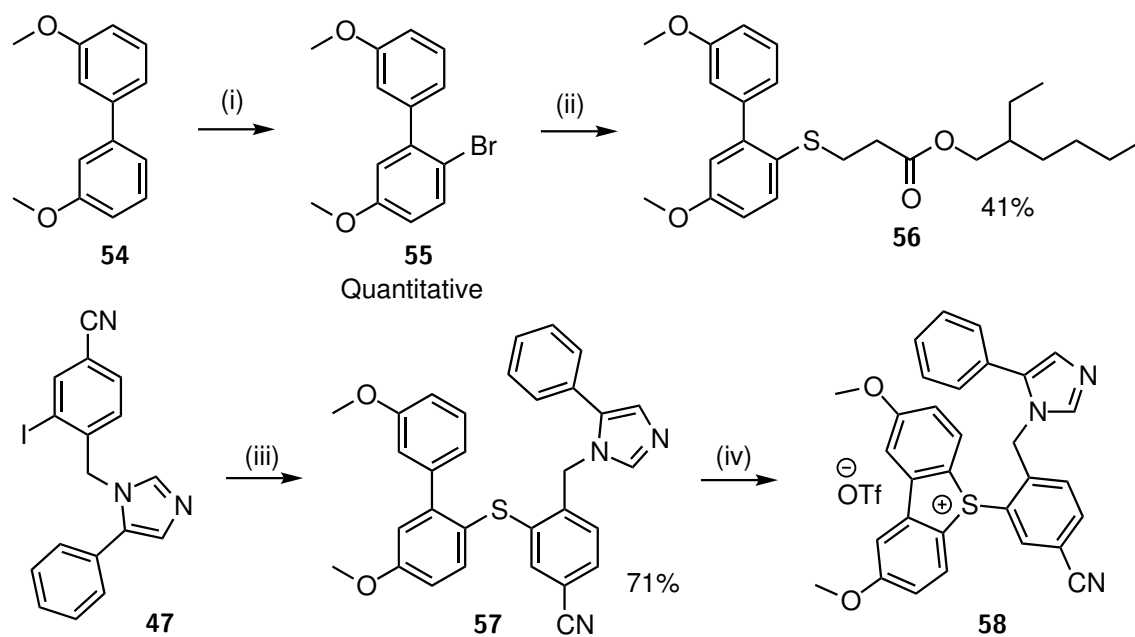
To a flame-dried three-neck round-bottom flask equipped with an argon inlet were added toluene (3.0 mL), Pd₂(dba)₃ (59.4 mg, 64.9 μmol, 0.01 equiv.) and DPEphos (69.9 mg, 0.130 mmol, 0.02 equiv.). The reaction vessel was degassed by argon purging before thioether **51** (377 mg, 0.909 mmol, 1.4 equiv.) and KO*t*Bu (102 mg, 0.909 mmol, 1.4 equiv.) were added. The resulting suspension was stirred at room temperature for 10 min and imidazole **47** (250 mg, 0.649 mmol, 1.0 equiv.) was added. The reaction vessel was degassed by argon purging once more before being plunged into a preheated block maintained at 125 °C. It was refluxed for 3.5 h. After cooling to room temperature, it was diluted with DCM, washed with brine, dried over MgSO₄ and concentrated *in vacuo*. Flash column chromatography purification (0 → 5% Et₂O/PE) of the resulting brown oil afforded the title compound as a yellow oil (243 mg, 77%). ν_{max}/cm⁻¹ 2228, 1595, 1578, 1445. ¹H NMR (600 MHz, d₆-DMSO) δ_H 7.71 (4H, m, H20, H27, H31 and H35), 7.44 (1H, d, *J* 1.4, H29), 7.39 (1H, d, *J* 1.7, H18), 7.35-7.30 (4H, m, H5, H11, H32 and H34), 7.27-7.26 (2H, m, H8 and H10), 7.19 (1H, t, *J* 7.4, H33), 7.04 (1H, d, *J* 8.0, H21), 6.93-6.91 (2H, m, H4 and H6), 6.84 (1H, dd, *J* 2.6, 1.5, H2), 5.18 (2H, s, H24), 3.71 (3H, s, H15), 2.37 (3H, s, H13). ¹³C NMR (150 MHz, d₆-DMSO) δ_C 158.8 (C), 144.0 (C), 142.4 (C), 141.4 (C), 141.1 (C), 138.9 (C), 138.4 (CH), 136.7 (C), 134.3 (C), 134.2 (CH), 133.5 (CH), 131.8 (CH), 131.2 (CH), 129.8 (CH), 129.2 (CH), 128.8 (CH), 128.5 (CH), 127.4 (C), 126.4 (CH), 124.2 (CH), 121.3 (CH), 118.0 (C), 115.9 (CH), 114.4 (CH), 113.3 (CH), 111.6 (C), 55.1 (CH₃), 47.6 (CH₂), 20.7 (CH₃). HRMS (ESI) Calculated for C₃₁H₂₆N₃OS [M+H]⁺: 488.1791; found: 488.1794.

5-(5-Cyano-2-((5-phenyl-1*H*-imidazol-1-yl)methyl)phenyl)-2-methoxy-8-methyl-5*H*-dibenzo[*b,d*]thiophen-5-ium trifluoromethanesulfonate **53**



To a round-bottom flask were added MeCN (1.0 mL), thioether **52** (49.0 mg, 0.100 mmol, 1.0 equiv.), NCS (13.0 mg, 0.100 mmol, 1.0 equiv.) and TfOH (26.5 μ L, 0.300 mmol, 3.0 equiv.). The reaction mixture was stirred at room temperature for 2 h. After concentration, the residue was dissolved in DCM and washed with H₂O. The organic layer was dried over MgSO₄ and concentrated *in vacuo*. Flash column chromatography purification (1 \rightarrow 10% 1 N NH₃ in MeOH/DCM) afforded the title compound as an off-white solid (47.0 mg, 74%), mp 150-152 $^{\circ}$ C (dec). $\nu_{\max}/\text{cm}^{-1}$ 1591, 1482. ¹H NMR (600 MHz, d₆-DMSO) δ_{H} 8.46 (1H, d, *J* 1.4, H10), 8.19 (1H, dd, *J* 8.1, 1.6, H20), 8.13 (1H, d, *J* 2.6, H2), 8.06 (1H, bs, H29) 7.91 (1H, d, *J* 8.9, H6), 7.85 (1H, bs, H27), 7.82 (2H, dd, *J* 8.1, 1.6, H31 and 35), 7.61 (1H, d, *J* 8.3, H13), 7.58 (1H, d, *J* 8.1, H21), 7.48 (1H, dd, *J* 8.3, 1.4, H12), 7.41-7.38 (2H, m, H32 and H34), 7.35 (1H, d, *J* 1.6, H18), 7.28-7.24 (2H, m, H6 and H33), 6.26 (1H, d, *J* 16.3, H24), 6.19 (1H, d, *J* 16.3, H24), 3.99 (3H, s, H9), 2.53 (3H, s, H17). ¹³C NMR (150 MHz, d₆-DMSO) δ_{C} 164.4 (C), 148.2 (C), 147.7 (C), 146.1 (C), 145.1 (C), 142.6 (C), 141.7 (C), 139.5 (C), 138.7 (CH), 138.5 (CH), 132.3 (CH), 132.2 (CH), 130.5 (C), 129.5 (CH), 128.7 (CH), 127.3 (CH), 126.9 (CH), 125.7 (CH), 124.5 (CH), 123.6 (CH), 121.5 (C), 118.0 (CH), 116.4 (C), 116.3 (CH), 114.2 (C), 109.9 (CH), 56.6 (CH₃), 47.6 (CH₂), 21.3 (CH₃). ¹⁹F NMR (282 MHz, d₆-DMSO) δ_{F} -77.8. HRMS (ESI) Calculated for C₃₁H₂₄N₃OS [M]⁺: 486.1637; found: 486.1740.

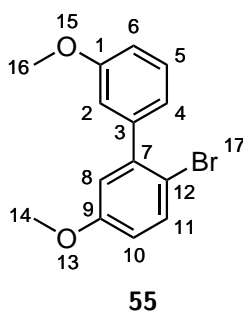
13.9 Synthetic Route Towards Sulfonium Salt **58** (Chapter 8)



Scheme 13.9: Synthesis of sulfonium salt **58**.

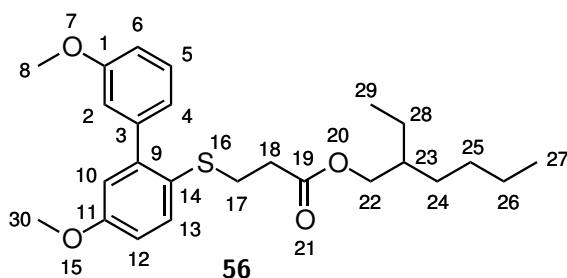
Reagents and conditions: (i) NBS, DMF, -5 °C, 1 h; (ii) Pd₂(dba)₃, xantphos, Et₃N, toluene, reflux, 18 h; (iii) Thioether **56**, Pd₂(dba)₃, DPEphos, KOtBu, toluene, reflux, 18 h; (iv) Not isolated.

2-Bromo-3',5-dimethoxy-1,1'-biphenyl **55**



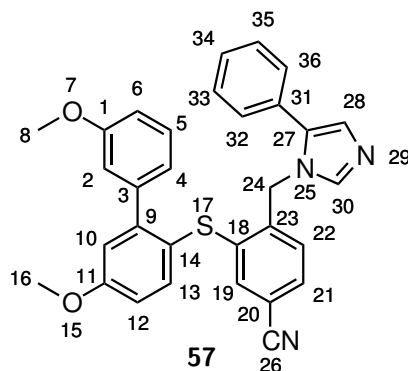
To a stirring solution of 3,3'-dimethoxy-1,1'-biphenyl (750 mg, 3.50 mmol, 1.0 equiv.) in DMF (10.0 mL) maintained -5 °C was added dropwise over 1 h a solution of NBS (685 mg, 3.85 mmol, 1.1 equiv.) in DMF (10.0 ml). The reaction mixture was diluted with water and extracted with Et₂O. The combined organic extracts were washed with an aqueous solution of 1 M Na₂S₂O₃, then a saturated solution of LiCl, dried over MgSO₄ and concentrated *in vacuo* to afford the title compound as an off-white solid in quantitative yield. It was employed used in the next step without further purification. ¹H NMR (600 MHz, CDCl₃) δ_H 7.54 (1H, d, *J* 8.8, H11), 7.36-7.33 (1H, m, H5), 7.00-6.98 (1H, m, H4), 6.96-6.93 (2H, m, H2 and H6), 6.88 (1H, d, *J* 3.0, H8), 6.78 (1H, dd, *J* 8.8, 3.0, H10), 3.85 (3H, s, H14 or H16), 3.81 (3H, s, H14 or H16).

Octan-3-yl 3-((3',5-dimethoxy-[1,1'-biphenyl]-2-yl)thio)propanoate **56**



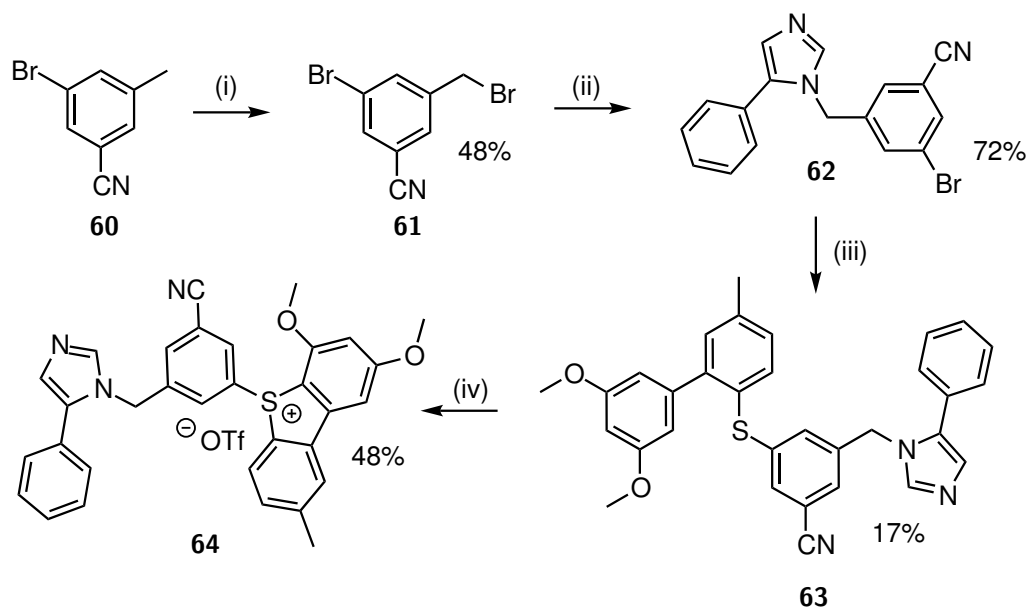
To a flame-dried three-neck round-bottom flask equipped with an argon inlet and condenser were added toluene (14.0 mL), anisole **55** (1.00 g, 3.41 mmol, 1.0 equiv.) and NEt_3 (0.950 mL, 6.82 mmol, 2.0 equiv.). The reaction vessel was degassed by argon purging before $\text{Pd}_2(\text{dba})_3$ (94.0 mg, 0.102 mmol, 0.03 equiv.) was added, followed by xanthphos (118 mg, 0.204 mmol, 0.06 equiv.) and thiol **2** (745 mg, 3.41 mmol, 1.0 equiv.). The resulting mixture was purged with argon before being plunged into a preheated block maintained at 125 °C. The reaction mixture was refluxed for 18 h. After cooling to room temperature, it was filtered through a pad of Celite and concentrated *in vacuo*. Flash column chromatography purification (10 → 30% $\text{Et}_2\text{O}/\text{PE}$) of the resulting yellow oil afforded the title compound as a colourless oil (600 mg, 41%). $\nu_{\text{max}}/\text{cm}^{-1}$ 2957, 2929, 1731, 1591, 1463. ^1H NMR (600 MHz, CDCl_3) δ_{H} 7.44 (1H, dd, J 8.1, 0.8, H12), 7.33 (1H, dd, J 8.2, 7.5, H5), 6.99-6.98 (1H, m, H4), 6.96 (1H, dd, J 2.5, 1.6, H2), 6.92 (1H, dd, J 8.2, 2.5, H6), 6.88-6.86 (2H, m, H10 and H13), 3.97-3.91 (2H, 2 × m, H22), 3.84 (3H, s, H8 or H30), 3.82 (3H, s, H8 or H30), 2.82 (2H, t, J 7.5, H17), 2.42 (2H, t, J 7.5, H18), 1.55-1.51 (1H, m, H23), 1.34-1.25 (8H, m, H24, H25, H26 and H28), 0.90-0.85 (6H, m, H27 and H29). ^{13}C NMR (150 MHz, CDCl_3) δ_{C} 172.1 (C), 158.9 (C), 158.8 (C), 145.8 (C), 142.3 (C), 133.9 (CH), 129.1 (CH), 124.0 (C), 121.9 (CH), 116.2 (CH), 115.1 (CH), 113.9 (CH), 113.2 (CH), 67.2 (CH), 55.6 (CH_3), 55.4 (CH_3), 38.8 (CH_2), 34.5 (CH_2), 30.5 (CH_2), 30.0 (CH_2), 29.0 (CH_2), 23.8 (CH_2), 23.1 (CH_2), 14.2 (CH_3), 11.1 (CH_3). HRMS (EI) Calculated for $\text{C}_{25}\text{H}_{34}\text{O}_4\text{S}$ $[\text{M}]^+$: 430.2172; found: 430.2171.

3-((3',5-Dimethoxy-[1,1'-biphenyl]-2-yl)thio)-4-((5-phenyl-4,5-dihydro-1*H*-imidazol-1-yl)methyl)benzonitrile **57**



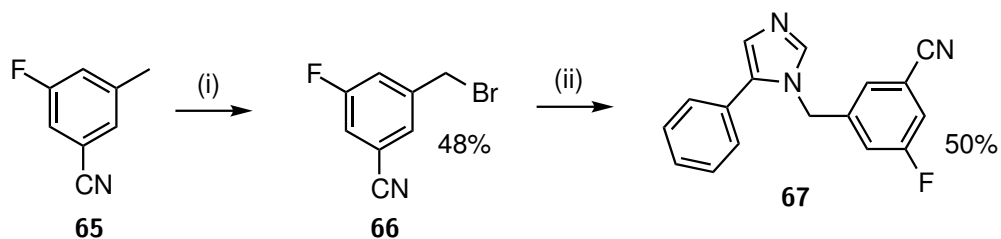
To a flame-dried three-neck round-bottom flask equipped with an argon inlet were added toluene (2.0 mL), Pd₂(dba)₃ (24.0 mg, 26.0 μmol, 0.02 equiv.) and DPEphos (28.0 mg, 52.0 μmol, 0.04 equiv.). The reaction vessel was degassed by argon purging before thioether **56** (268 mg, 0.623 mmol, 1.2 equiv.) and KO*t*Bu (70.0 mg, 0.623 mmol, 1.2 equiv.) were added. The resulting suspension was stirred at room temperature for 10 min and imidazole **47** (200 mg, 0.519 mmol, 1.0 equiv.) was added. The reaction vessel was degassed by argon purging once more before being plunged into a preheated block maintained at 125 °C. The reaction mixture was refluxed for 18 h. After cooling to room temperature, it was diluted with DCM, washed with brine, dried over MgSO₄ and concentrated *in vacuo*. Flash column chromatography purification (1 → 16% Et₂O/DCM) of the resulting brown oil afforded the title compound as an orange oil (243 mg, 71%). ν_{max}/cm⁻¹ 2228, 1589, 1561, 1463. ¹H NMR (600 MHz, d₆-DMSO) δ_H 7.71-7.70 (2H, m, H30, H32 and H36), 7.63 (1H, dd, *J* 8.0, 1.7, H21), 7.52 (1H, d, *J* 8.6, H13), 7.46 (1H, d, *J* 1.3, H28), 7.36-7.33 (2H, m, H33 and H35), 7.29 (1H, dd, *J* 8.4, 7.6, H5), 7.21-7.18 (2H, m, H19 and H34), 7.08 (1H, dd, *J* 8.6, 3.0, H12), 7.02 (1H, d, *J* 3.0, H10), 6.99 (1H, d, *J* 8.0, H22), 5.15 (2H, s, H24), 6.92-6.90 (2H, m, H4 and H6), 6.83 (1H, dd, *J* 2.6, 1.7, H2), 3.85 (3H, s, H8 or H16), 3.69 (3H, s, H8 or H16). ¹³C NMR (150 MHz, d₆-DMSO) δ_C 160.2 (C), 158.7 (C), 146.8 (C), 141.4 (C), 141.1 (C), 141.0 (C), 138.5 (CH), 138.2 (C), 137.0 (CH), 134.3 (C), 132.2 (CH), 130.3 (CH), 129.1 (CH), 128.5 (CH), 126.4 (CH), 124.3 (CH), 121.3 (CH), 119.9 (C), 118.1 (C), 116.7 (CH), 115.9 (CH), 115.1 (CH), 114.4 (CH), 113.4 (CH), 111.4 (C), 109.9 (CH), 55.6 (CH₃), 55.1 (CH₃), 47.4 (CH₂). HRMS (ESI) Calculated for C₃₁H₂₆N₃O₂S [M+H]⁺: 504.1746; found: 504.1744.

13.10 Synthetic Route Towards Sulfonium Salt **64** (Chapter 8)



Scheme 13.10: Synthesis of sulfonium salt **64**.

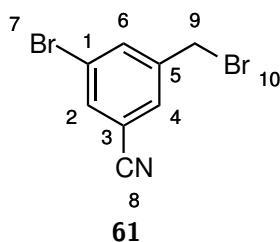
Reagents and conditions: (i) AIBN, NBS, chlorobenzene, reflux, 4 h; (ii) Phenylimidazole **46**, K_2CO_3 , DMF, 100 °C, 1 h; (iii) Thioether **4**, $Pd_2(dba)_3$, DPEphos, $KOtBu$, toluene, reflux, 2 h; (iv) NCS, TFOH, MeCN, rt, 2 h.



Scheme 13.11: Synthesis of reference compound **67**.

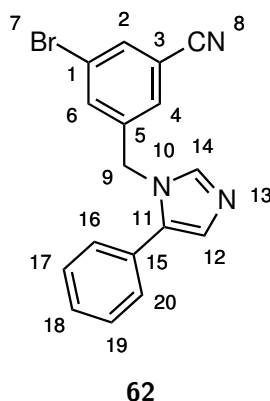
Reagents and conditions: (i) AIBN, NBS, chlorobenzene, reflux, 4 h; (ii) Phenylimidazole **46**, K_2CO_3 , DMF, 100 °C, 2 h.

3-Bromo-5-(bromomethyl)benzonitrile **61**



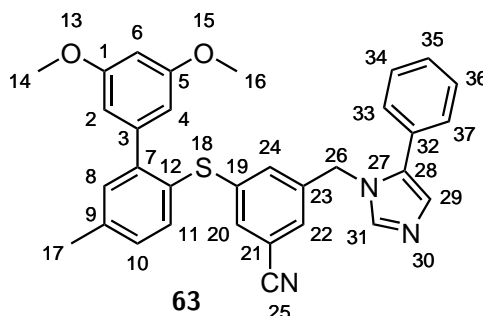
To a flame-dried three-neck round-bottom flask equipped with an argon inlet and condenser were added chlorobenzene (25.0 mL) and AIBN (167 mg, 1.02 mmol, 0.2 equiv.), followed by 3-bromo-5-methylbenzonitrile (1.00 g, 5.10 mmol, 1.0 equiv.) and NBS (998 mg, 5.61 mmol, 1.1 equiv.). The resulting solution was purged with argon before being plunged into a preheated block maintained at 125 °C and refluxed for 4 h. After cooling to room temperature, the mixture was diluted with DCM, washed with a 1 M aqueous Na₂S₂O₃ solution, dried over MgSO₄ and concentrated *in vacuo*. Flash column chromatography purification (0 → 8% Et₂O/PE) afforded the title compound as a white solid (672 mg, 48%), mp 108-110 °C. $\nu_{\text{max}}/\text{cm}^{-1}$ 2236, 1567, 1434, 1424, 1251, 1221. ¹H NMR (600 MHz, CDCl₃) δ_{H} 7.78 (1H, t, *J* 1.7, H6), 7.73 (1H, t, *J* 1.7, H2), 7.63 (1H, t, *J* 1.7, H4), 4.42 (2H, s, H9). ¹³C NMR (150 MHz, CDCl₃) δ_{C} 141.2 (C), 136.6 (CH), 134.6 (CH), 131.2 (CH), 123.9 (C), 116.9 (C), 114.7 (C), 30.1 (CH₂). HRMS (CI) Calculated for C₈H₉Br₂N₂ [M + NH₄⁺]: 290.9127; found: 290.9128.

3-Bromo-5-((5-phenyl-1*H*-imidazol-1-yl)methyl)benzonitrile **62**



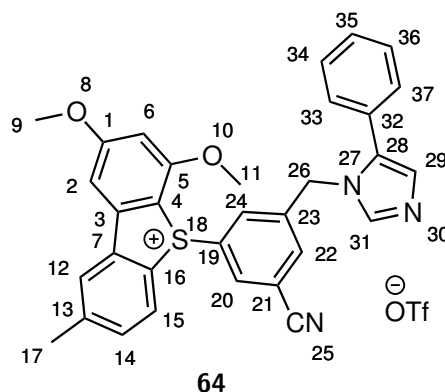
To a flame-dried three-neck round-bottom flask equipped with an argon inlet and condensers were added DMF (4.0 mL), phenylimidazole **46** (472 mg, 2.18 mmol, 2.0 equiv.), benzyl bromide **61** (300 mg, 1.09 mmol, 1.0 equiv.) and K_2CO_3 (377 mg, 2.73 mmol, 2.5 equiv.). The resulting solution was purged with argon before being plunged into a preheated block maintained at 100 °C and heated for 1 h. After cooling to room temperature, the mixture was diluted with DCM, washed with a saturated aqueous solution of LiCl, followed by H_2O , dried over $MgSO_4$ and concentrated *in vacuo*. Flash column chromatography purification (5 → 60% EtOAc/PE) afforded the title compound a yellow solid (267 mg, 72%), mp 148-150 °C. ν_{max}/cm^{-1} 3113, 3065, 2235, 1602, 1586, 1500, 1350. 1H NMR (600 MHz, $CDCl_3$) δ_H 7.78-7.77 (3H, m, H2, H16 and H20), 7.61 (1H, d, J 1.5, H14), 7.55 (1H, t, J 1.8, H6), 7.41 (1H, t, J 1.8, H4), 7.39 (2H, t, J 7.8, H17 and H19), 7.28-7.26 (1H, m, H18), 7.17 (1H, d, J 1.5, H12), 5.17 (2H, s, H9). ^{13}C NMR (150 MHz, $CDCl_3$) δ_C 143.8 (C), 139.9 (C), 137.7 (CH), 134.8 (CH), 134.6 (CH), 133.6 (C), 129.2 (CH), 128.8 (CH), 127.4 (CH), 125.1 (CH), 124.0 (C), 116.8 (C), 115.1 (C), 114.7 (CH), 49.6 (CH_2). HRMS (ESI) Calculated for $C_{17}H_{13}BrN_3$ $[M+H]^+$: 338.0293; found 338.0292.

3-((3',5'-Dimethoxy-5-methyl-[1,1'-biphenyl]-2-yl)thio)-5-((5-phenyl-1*H*-imidazol-1-yl)methyl)benzonitrile



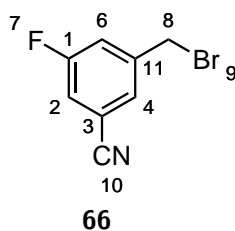
To a flame-dried three-neck round-bottom flask equipped with an argon inlet and condenser were added toluene (12.0 mL), Pd₂(dba)₃ (104 mg, 0.114 mmol, 0.1 equiv.) and DPEphos (123 mg, 0.228 mmol, 0.2 equiv.), followed by imidazole **62** (400 mg, 1.14 mmol, 1.0 equiv.), thioether **4** (735 mg, 1.63 mmol, 1.4 equiv.) and KO*t*Bu (183 mg, 1.63 mmol, 1.4 equiv.). The resulting mixture was purged with argon before being plunged into a preheated block maintained at 125 °C. It was refluxed for 2 h. After cooling to room temperature, it was filtered through a pad of Celite and concentrated *in vacuo*. Flash column chromatography purification (0 → 50% Et₂O/DCM) afforded the title compound as a yellow oil (53 mg, 17%). $\nu_{\max}/\text{cm}^{-1}$ 3310, 2957, 2931, 1635, 1585, 1542, 1454. ¹H NMR (600 MHz, CDCl₃) δ_{H} 7.77-7.76 (2H, m, H33 and H37), 7.53 (1H, d, *J* 1.4, H31), 7.41 (1H, d, *J* 8.2, H11), 7.39 (2H, tt, *J* 7.8, 2.4, H34 and H36), 7.28-7.25 (1H, m, H35), 7.20 (1H, d, *J* 2.1, H8), 7.17-7.15 (1H, dd, *J* 8.2, 2.1, H10), 7.15 (1H, t, *J* 1.8, H20), 7.11 (1H, t, *J* 1.8, H22), 7.09 (1H, d, *J* 1.4, H29), 6.98 (1H, t, *J* 1.8, H24), 6.40 (1H, t, *J* 2.3, H6), 6.33 (2H, d, *J* 2.3, H2 and H4), 5.03 (2H, s, H26), 3.71 (6H, s, H14 and H16), 2.37 (3H, s, H17). ¹³C NMR (150 MHz, CDCl₃) δ_{C} 160.3 (C), 145.9 (C), 143.4 (C), 142.6 (C), 142.4 (C), 140.2 (C), 138.1 (C), 137.7 (CH), 135.5 (CH), 133.8 (C), 132.1 (CH), 131.0 (CH), 130.6 (CH), 129.8 (CH), 128.8 (CH), 127.2 (CH), 127.0 (CH), 126.3 (C), 125.0 (CH), 117.9 (C), 114.7 (CH), 113.7 (C), 107.4 (CH), 99.6 (CH), 55.5 (CH₃), 49.9 (CH₂), 21.3 (CH₃). HRMS (ESI) Calculated for C₃₂H₂₈N₃O₂S [M+H]⁺: 518.1902; found 518.1909.

5-(3-Cyano-5-((5-phenyl-1*H*-imidazol-1-yl)methyl)phenyl)-2,4-dimethoxy-8-methyl-5*H*-dibenzo[*b,d*]thiophen-5-ium trifluoromethanesulfonate **64**



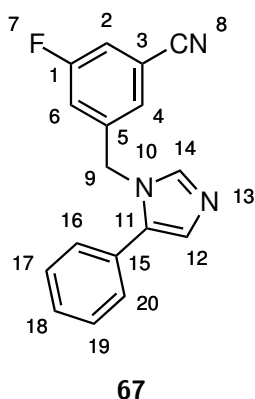
To a round-bottom flask were added MeCN (1.0 mL), thioether **63** (42.0 mg, 81.1 μmmol , 1.0 equiv.), NCS (10.8 mg, 81.1 μmmol , 1.0 equiv.) and TfOH (21.0 μL , 0.243 mmol, 3.0 equiv.). The reaction mixture was stirred at room temperature for 2 h. It was then concentrated *in vacuo*, diluted with DCM and washed with a 2 M NaOH solution. The organic layer was stirred vigorously with saturated NaOTf aqueous solution for 10 min, separated, dried over MgSO_4 and concentrated *in vacuo*. Flash column chromatography purification (0 \rightarrow 14% MeOH/DCM) afforded the title compound as an off-white solid (26.0 mg, 48%), mp 165-167 $^{\circ}\text{C}$ (dec). $\nu_{\text{max}}/\text{cm}^{-1}$ 3060, 2950, 2929, 1591, 1485, 1447, 1427. ^1H NMR (600 MHz, CDCl_3) δ_{H} 8.60 (1H, t, J 1.8, H24), 8.36 (1H, d, J 8.3, H15), 7.86 (1H, d, J 2.0, H12), 7.77-7.76 (2H, m, H33 and H37), 7.72 (1H, d, J 1.5, H31), 7.59 (1H, t, J 1.8, H22), 7.47 (1H, dd, J 8.3, 2.0, H14), 7.42 (1H, d, J 1.5, H29), 7.38 (2H, t, J 7.8, H34 and H36), 7.28-7.25 (1H, m, H35), 7.18 (1H, d, J 2.1, H6), 7.07 (1H, t, J 1.8, H20), 6.54 (1H, d, J 2.1, H2), 5.48 (1H, d, J 16.4, H26), 5.40 (1H, d, J 16.4, H26), 4.01 (3H, s, H9), 3.83 (3H, s, H11), 2.56 (3H, s, H17). ^{13}C NMR (150 MHz, CDCl_3) δ_{C} 168.2 (C), 158.8 (C), 146.6 (C), 143.0 (C), 142.4 (C), 142.3 (C), 139.0 (C), 137.7 (CH), 136.5 (CH), 135.1 (CH), 133.8 (CH), 133.3 (C), 130.2 (C), 129.8 (CH), 129.5 (CH), 128.8 (CH), 128.1 (C), 127.4 (CH), 125.0 (CH), 116.1 (C), 115.9 (C), 115.4 (CH), 106.1 (CH), 101.6 (C), 100.5 (CH), 57.2 (CH_3), 56.7 (CH_3), 49.4 (CH_2), 22.04 (CH_3). ^{19}F NMR (282 MHz, CDCl_3) δ_{F} -78.3. HRMS (ESI) Calculated for $\text{C}_{32}\text{H}_{26}\text{N}_3\text{O}_2\text{S}$ [$\text{M}]^{+}$: 516.1740; found: 516.1742.

3-(Bromomethyl)-5-fluorobenzonitrile **66**



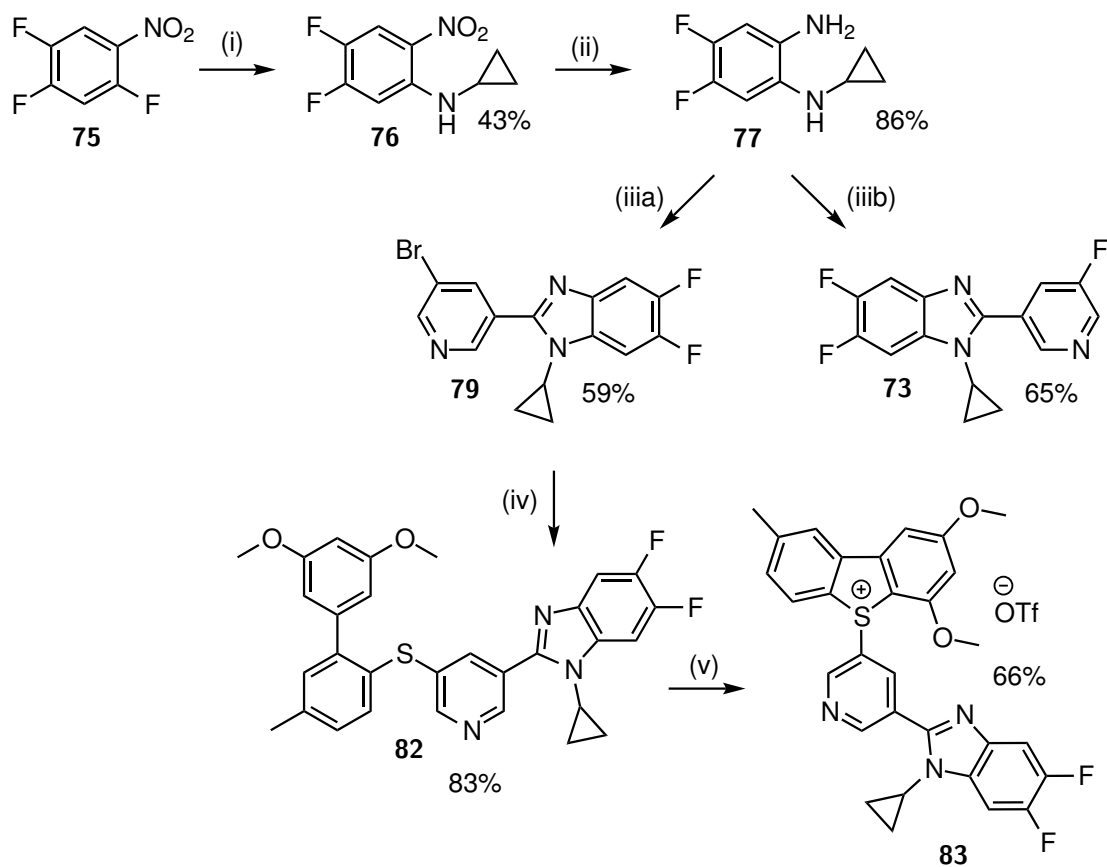
To a flame-dried three-neck round-bottom flask equipped with an argon inlet and condenser were added chlorobenzene (37.0 mL) and AIBN (49.0 mg, 0.30 mmol, 0.2 equiv.), followed by 3-fluoro-5-methylbenzonitrile (200 mg, 1.48 mmol, 1.0 equiv.) and NBS (290 mg, 1.63 mmol, 1.1 equiv.). The resulting solution was purged with argon before being plunged into a preheated block maintained at 125 °C. It was refluxed for 4 h. After cooling to room temperature, the mixture was diluted with DCM, washed with a 1 M aqueous Na₂S₂O₃ solution, dried over MgSO₄ and concentrated *in vacuo*. Flash column chromatography purification (0 → 12% Et₂O/PE) afforded the title compound as a shiny white solid (152 mg, 48%), mp 48-50 °C. $\nu_{\max}/\text{cm}^{-1}$ 3079, 2229, 1600, 1587, 1444, 1435, 1306. ¹H NMR (600 MHz, CDCl₃) δ_{H} 7.50 (1H, t, *J* 1.6, H4), 7.38 (1H, ddd, *J* 9.0, 2.5, 1.6, H6), 7.31 (1H, ddd, *J* 7.7, 2.5, 1.6, H2), 4.44 (2H, s, H8). ¹³C NMR (150 MHz, CDCl₃) δ_{C} 163.1 & 161.5 (d, *J* 250.5, C), 142.0 & 141.9 (d, *J* 8.3, C), 128.6 & 128.5 (d, *J* 3.2, CH), 121.2 & 121.1 (d, *J* 21.9, CH), 119.2 & 119.1 (d, *J* 24, CH), 117.2 & 117.1 (d, *J* 3.3, C), 114.5 & 114.4 (d, *J* 9.9, C), 30.3 & 30.2 (d, *J* 1.7, CH₂). ¹⁹F NMR (282 MHz, CDCl₃) δ_{F} -108.8. HRMS (CI) Calculated for C₈H₉BrFN₂ [M + NH₄⁺]: 230.9928; found: 230.9928.

3-Fluoro-5-((5-phenyl-1*H*-imidazol-1-yl)methyl)benzonitrile **67**



To a flame-dried three-neck round-bottom flask equipped with an argon inlet and condenser were added DMF (1.5 mL) and phenylimidazole **46** (205 mg, 0.947 mmol, 1.6 equiv.), followed by benzyl bromide **66** (123 mg, 0.575 mmol, 1.0 equiv.) and K_2CO_3 (144 mg, 1.04 mmol, 1.8 equiv.). The resulting solution was purged with argon before being plunged into a preheated block maintained at 100 °C and heated for 2 h. After cooling to room temperature, the mixture was diluted with DCM and washed with a saturated aqueous solution of LiCl, followed by H_2O , dried over $MgSO_4$ and concentrated *in vacuo*. Flash column chromatography purification (0 → 60% EtOAc/DCM) afforded the title compound as a yellow solid (80.0 mg, 50%), mp 135-137 °C. ν_{max}/cm^{-1} 3079, 3047, 3007, 1676, 1552, 1500, 1481. 1H NMR (600 MHz, $CDCl_3$) δ_H 7.77 (2H, m, H16 and H20), 7.62 (1H, d, J 1.5, H14), 7.39 (2H, tt, J 7.6, 3.6, H17 and H19), 7.35 (1H, dd, J 7.8, 1.9, H2), 7.31 (1H, d, J 1.9, H4), 7.27 (1H, tt, J 7.6, 3.6, H18), 7.18 (1H, d, J 1.5, H12), 7.11 (1H, dt, J 8.7, 1.9, H6), 5.20 (2H, s, H9). ^{13}C NMR (150 MHz, $CDCl_3$) δ_C 163.6 & 161.9 (d, J 252.2, C), 143.8 (C), 140.8 (d, J 7.1, C), 137.7 (CH), 133.6 (C), 128.8 (CH), 127.4 (CH), 126.4 (d, J 3.3, CH), 125.0 (CH), 119.4 & 119.2 (d, J 24.9, CH), 119.2 & 119.0 (d, J 22.0, CH), 117.0 (C), 115.0 & 114.9 (d, J 9.8, C), 114.7 (CH), 49.8 (CH_2). ^{19}F NMR (282 MHz, $CDCl_3$) δ_F -107.8. HRMS (ESI) Calculated for $C_{17}H_{13}FN_3$ $[M+H]^+$: 278.1094; found: 278.1091.

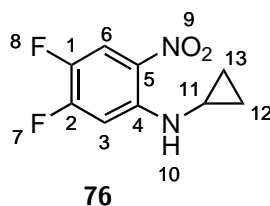
13.11 Synthetic Route Towards Sulfonium Salt **83** (Chapter 9)



Scheme 13.12: Synthesis of sulfonium salt **83** and cold reference compound **73**.

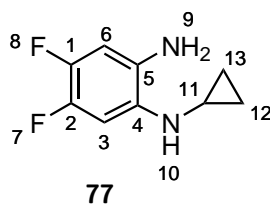
Reagents and conditions: (i) Cyclopropylamine, KF, K₂CO₃, MeCN, reflux, 1 h; (ii) Pd/C, H₂, MeOH, rt, 20 h; (iii a) 5-Bromonicotinaldehyde, Oxone[®], DMF/H₂O, rt, 1 h; (iii b) 5-Fluoronicotinaldehyde, Oxone[®], DMF/H₂O, rt, 1 h; (iv) Thioether **4**, Pd₂(dba)₃, DPEphos, KO^tBu, toluene, reflux, 2 h; (v) NCS (stock solution), TfOH, MeCN, rt, 30 min.

N-Cyclopropyl-4,5-difluoro-2-nitroaniline **76**



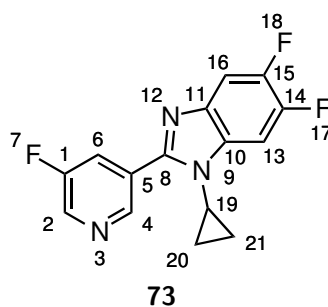
To a solution of KF (988 mg, 17.0 mmol, 1.5 equiv.), K₂CO₃ (1.56 g, 11.3 mmol, 1.0 equiv.) and 2,4,5-trifluoronitrobenzene (2.00 g, 11.3 mmol, 1.0 equiv.) in MeCN (5.0 mL) at reflux was added dropwise over 30 min a solution of cyclopropylamine (783 μL, 11.3 mmol, 1.0 equiv.) in MeCN (5.0 mL). The resulting deep-yellow suspension was refluxed for 1 h. After cooling to room temperature, the mixture was concentrated *in vacuo*. The residue was dissolved in DCM, washed with H₂O, brine, dried over MgSO₄ and concentrated *in vacuo*. Flash column chromatography purification (0 → 5% EtOAc/PE) afforded the title compound (fast eluting component) as a bright orange solid (1.03 g, 43%), mp 73-74 °C. $\nu_{\max}/\text{cm}^{-1}$ 3371, 3078, 3007, 1651, 1579, 1514, 1233. ¹H NMR (600 MHz, CDCl₃) δ_{H} 8.10 (1H, bs, H10), 8.04 (1H, dd, *J* 10.6, 8.3, H6), 7.10 (1H, dd, *J* 12.6, 7.0, H3), 2.57-2.53 (1H, m, H11), 0.97-0.94 (2H, m, H12 or H13), 0.69-0.67 (2H, m, H12 or H13). ¹³C NMR (150 MHz, CDCl₃) δ_{C} 157.0-155.2 (dd, *J* 257.0, 14.3, C), 144.9 & 144.8 (d, *J* 10.5, C), 142.2-140.5 (dd, *J* 240.9, 14.1, C) 126.8 & 126.7 (d, *J* 6.0, C), 115.1-114.9 (dd, *J* 21.5, 3.3, CH), 102.9 & 102.8 (d, *J* 22.5, CH), 24.9 (CH), 8.0 (CH₂). ¹⁹F NMR (282 MHz, CDCl₃) δ_{F} -122.1 & -122.2 (1F, d, *J* 23.4), -150.0 & -150.1 (1F, d, *J* 23.4). HRMS (CI) Calculated for C₉H₉F₂N₂O₂ [M+H]⁺: 215.0627; found: 215.0628.

*N*¹-Cyclopropyl-4,5-difluorobenzene-1,2-diamine **77**



To a flame-dried three-neck round-bottom flask equipped with an argon inlet were added 10 mol% Pd/C (72.0 mg, 0.667 mmol, 0.1 equiv.) and MeOH (35 mL), followed by nitrobenzene **76** (1.45 g, 6.77 mmol, 1.0 equiv.). The reaction vessel was thoroughly evacuated before H₂ balloon insertion and the resulting black suspension was stirred at room temperature for 20 h. It was then diluted with DCM, filtered through a pad of Celite and concentrated *in vacuo*. Flash column chromatography purification (0 → 50% EtOAc/PE) afforded the title compound as a red solid (1.07 g, 86%), mp 54-56 °C. $\nu_{\max}/\text{cm}^{-1}$ 3422, 3332, 3263, 2954, 1634, 1518, 1375. ¹H NMR (600 MHz, CDCl₃) δ_{H} 6.83 (1H, dd, *J* 12.4, 7.8, H6), 6.52 (1H, dd, *J* 11.2, 7.7, H3), 3.83 (1H, bs, H10), 3.17 (2H, bs, H9), 2.39 (1H, m, H11), 0.77-0.74 (2H, m, H12 or H13), 0.52-0.49 (2H, m, H12 or H13). ¹³C NMR (150 MHz, CDCl₃) δ_{C} 143.6-143.9 (dd, *J* 234.6, 13.2, C), 144.0-142.2 (dd, *J* 234.6, 13.1, C), 134.8-134.8 (dd, *J* 7.7, 2.1, C), 129.3-129.2 (dd, *J* 7.4, 2.3, C), 105.5 & 105.4 (d, *J* 20.3, CH), 101.8 & 101.7 (d, *J* 21.9, CH), 26.7 (CH), 7.2 (CH₂). ¹⁹F NMR (282 MHz, CDCl₃) δ_{F} -148.7 & -148.8 (1F, d, *J* 22.8), -151.9 & -152.0 (1F, d, *J* 22.8). HRMS (ESI) Calculated for C₉H₁₁F₂N₂ [M+H]⁺: 185.0890; found: 185.0887.

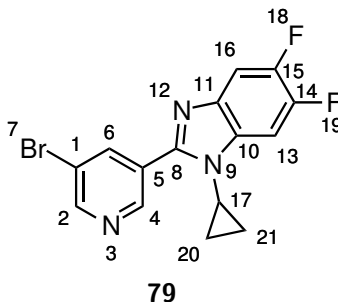
1-Cyclopropyl-5,6-difluoro-2-(5-fluoropyridin-3-yl)-1H-benzo[d]imidazole **73**



To a stirring solution of diamine **77** (130 mg, 0.706 mmol, 1.0 equiv.) in 97% DMF/H₂O were added 5-fluoronicotinaldehyde (97.0 mg, 0.775 mmol, 1.1 equiv.), followed by Oxone[®] (141 mg, 0.469 mmol, 0.65 equiv.). The resulting brown mixture was stirred at room temperature for 1 h. The reaction mixture was concentrated, diluted with EtOAc and H₂O, followed by addition of solid K₂CO₃ until the aqueous layer reached pH of \approx 9. The organic layer was separated, washed with H₂O and brine, dried over MgSO₄ and concentrated *in vacuo*. Flash column chromatography purification (0 \rightarrow 30% EtOAc/DCM) afforded the title compound as an orange solid (133 mg, 65%), mp 185-188 °C. $\nu_{\max}/\text{cm}^{-1}$ 3030, 1605, 1573, 1472, 1417. ¹H NMR (600 MHz, CDCl₃) δ_{H} 9.05 (1H, bs, H4), 8.62 (1H, d, *J* 2.7, H6), 8.02 (1H, ddd, *J* 8.8, 2.7, 1.7, H2), 7.58 (1H, dd, *J* 10.2, 7.3, H13 or H16), 7.42 (1H, dd, *J* 9.7, 7.0, H13 or H16), 3.58 (1H, tt, *J* 6.9, 3.8, H19), 1.27-1.24 (2H, m, H20 or H21), 0.83-0.80 (2H, m, H20 or H21). ¹³C NMR (150 MHz, CDCl₃) δ_{C} 160.0 & 158.3 (d, *J* 256.5, C), 151.1 (d, *J* 2.1, C), 149.7-149.3 (dd, *J* 48.0, 16.0, C), 148.0-147.7 (dd, *J* 48.0, 16.0, C), 145.6 & 145.5 (d, *J* 4.4, CH), 139.3 & 139.2 (d, *J* 22.5, CH), 137.9 & 137.8 (d, *J* 11.0, C), 132.7 & 132.6 (d, *J* 10.4, C), 127.9 & 127.8 (d, *J* 4.4, C), 123.3 & 123.2 (d, *J* 19.8, CH), 107.7 & 107.6 (d, *J* 18.6, CH), 99.3 & 99.2 (d, *J* 23.1, CH), 26.6 (CH₂), 9.2 (CH). ¹⁹F NMR (282 MHz, CDCl₃) δ_{F} -125.8 (1F, s), -139.4 & -139.5 (1F, d, *J* 20.6), -142.2 & -142.3 (1F, d, *J* 20.6). HRMS (CI) Calculated for C₁₅H₁₁F₃N₃ [M+H]⁺: 290.0900; found: 290.0899.

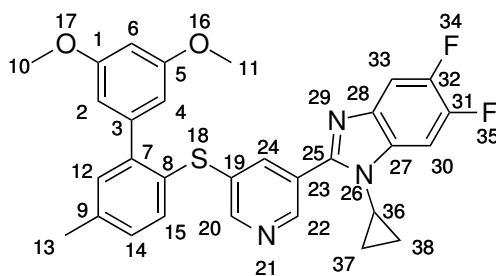
2-(5-Bromopyridin-3-yl)-1-cyclopropyl-5,6-difluoro-1H-benzo[d]imidazole

79



To a stirring solution of diamine **77** (1.07 g, 5.81 mmol, 1.0 equiv.) in 97% DMF/H₂O were added 5-bromonicotinaldehyde (1.19 g, 6.40 mmol, 1.1 equiv.), followed by Oxone[®] (1.16 g, 3.77 mmol, 0.65 equiv.). The resulting brown mixture was stirred at room temperature for 1 h. The reaction mixture was concentrated, diluted with EtOAc and H₂O and solid K₂CO₃ was added until the aqueous layer reached pH of \approx 9. The organic layer was separated and washed with H₂O and brine, dried over MgSO₄ and concentrated *in vacuo*. Flash column chromatography purification (0 \rightarrow 30% EtOAc/DCM) of the resulting yellow oil afforded the title compound as a light pink solid (1.20 g, 59%), mp 150-151 °C. $\nu_{\max}/\text{cm}^{-1}$ 3024, 1481, 1467, 1446, 1405, 1397. ¹H NMR (600 MHz, CDCl₃) δ_{H} 9.13 (1H, d, *J* 2.2, H4), 8.80 (1H, d, *J* 2.2, H2), 8.45 (1H, t, *J* 2.2, H6), 7.57 (1H, dd, *J* 10.2, 7.3, H13 or H16), 7.41 (1H, dd, *J* 9.7, 7.0, H13 or H16), 3.58 (1H, tt, *J* 6.8, 3.9, H17), 1.27-1.24 (2H, m, H20 or H21), 0.83-0.80 (2H, m, H20 or H21). ¹³C NMR (150 MHz, CDCl₃) δ_{C} 151.7 (CH), 151.0 (C), 149.7-149.3 (dd, *J* 23.6, 15.3, C), 148.0-147.6 (dd, *J* 22.4, 15.9, C), (CH), 138.9 (CH), 132.7 & 132.6 (d, *J* 10.4, C), 137.9 & 137.8 (d, *J* 12.1, C), 127.9 (C), 120.8 (C), 107.7 & 107.6 (d, *J* 19.8, CH), 99.3 & 99.1 (d, *J* 23.0, CH), 26.6 (CH), 9.17 (CH₂). ¹⁹F NMR (282 MHz, CDCl₃) δ_{F} -139.4 & -139.5 (1F, d, *J* 20.8), -142.2 & -142.3 (1F, d, *J* 20.8). HRMS (ESI) Calculated for C₁₅H₁₁BrF₂N₃ [M+H]⁺: 350.0104; found: 350.0109.

1-Cyclopropyl-2-(5-((3',5'-dimethoxy-5-methyl-[1,1'-biphenyl]-2-yl)thio)pyridin-3-yl)-5,6-difluoro-1*H*-benzo[*d*]imidazole 82

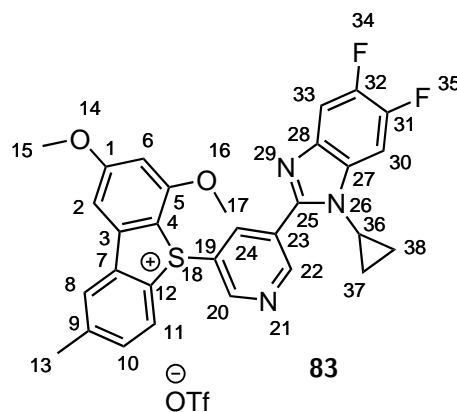


82

To a flame-dried three-neck round-bottom flask equipped with an argon inlet and condenser were added toluene (12.0 mL), Pd₂(dba)₃ (104 mg, 0.114 mmol, 0.1 equiv.) and DPEphos (123 mg, 0.228 mmol, 0.2 equiv.), followed by bromopyridine **79** (400 mg, 1.14 mmol, 1.0 equiv.), thioether **4** (735 mg, 1.63 mmol, 1.4 equiv.) and KO*t*Bu (183 mg, 1.63 mmol, 1.4 equiv.). The resulting mixture was purged with argon before being plunged into a preheated block maintained at 125 °C. The reaction mixture was refluxed for 2 h. After cooling to room temperature, the mixture was filtered through a pad of Celite and concentrated *in vacuo*. Flash column chromatography purification (0 → 50% Et₂O/DCM) of the resulting green oil afforded the title compound as a light orange solid (498 mg, 83%), mp 74-75 °C. ν_{\max} /cm⁻¹ 3080, 2932, 2837, 1590, 1478, 1466. ¹H NMR (600 MHz, CDCl₃) δ_{H} 8.91 (1H, d, *J* 2.0, H22), 8.41 (1H, d, *J* 2.2, H20), 7.94 (1H, t, *J* 2.2, H24), 7.54 (1H, dd, *J* 10.2, 7.3, H30 or H33), 7.40 (1H, d, *J* 7.9, H15), 7.37 (1H, d, *J* 9.8, 6.9, H30 or H33), 7.22 (1H, d, *J* 2.2, H12), 7.16 (1H, dd, *J* 7.9, 2.2, H14), 6.47 (2H, d, *J* 2.3, H2 and H4), 6.41 (1H, t, *J* 2.3, H6), 3.74 (6H, s, H10 and H11), 3.40 (1H, tt, *J* 6.9, 3.9, H36), 2.39 (3H, s, H13) 1.12-1.08 (2H, m, H37 or H38), 0.72-0.70 (2H, m, H37 or H38). ¹³C NMR (150 MHz, CDCl₃) δ_{C} 160.4 (C), 152.0 (C), 150.9 (CH), 149.5-149.1 (dd, *J* 19.5, 14.5, C), 147.8-147.5 (dd, *J* 18.1, 15.3, C), 147.0 (CH), 145.1 (CH), 142.5 (C), 139.1 (C), 137.9 & 137.8 (d, *J* 9.8, C), 136.9 (CH), 135.1 (C), 134.3 (CH), 132.6 (d, *J* 10.4, C), 131.9 (CH), 129.5 (CH), 129.4 (C), 127.7 (C), 126.5 (C), 107.6 (CH), 107.6 & 107.4 (d, *J* 19.7, CH), 99.7 (CH), 99.1 & 99.0 (d, *J* 23.0, CH), 55.5 (CH₃), 26.5 (CH), 21.2 (CH₃), 9.0 (CH₂). ¹⁹F NMR (282 MHz, CDCl₃) δ_{F} -140.0 & -140.1 (1F, d, *J* 21.0), -142.6 & -142.7 (1F, d, *J* 21.0). HRMS (ESI) Calculated for C₃₀H₂₆F₂N₃O₂S [M+H]⁺:

530.1714; found: 530.1709.

5-(5-(1-Cyclopropyl-5,6-difluoro-1*H*-benzo[*d*]imidazol-2-yl)pyridin-3-yl)-2,4-dimethoxy-8-methyl-5*H*-dibenzo[*b*,*d*]thiophen-5-ium trifluoromethanesulfonate **83**

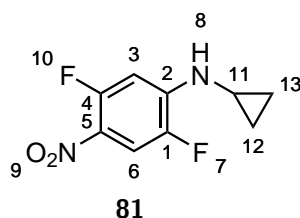


To a round-bottom flask were added thioether **82** (50 mg, 0.0944 mmol, 1.0 equiv.), NCS (12.6 mg, 0.0944 mmol, 1.0 equiv.) in MeCN (2.0 mL), followed by TfOH (25.0 μ L, 0.285 mmol, 3.0 equiv.). The reaction mixture was stirred at room temperature for 30 min. The reaction mixture was concentrated *in vacuo* and the resulting yellow residue dissolved in DCM, washed with a 2 M NaOH solution, then H₂O, dried over MgSO₄ and concentrated *in vacuo*. Flash column chromatography purification (0 \rightarrow 10% MeOH/DCM) afforded the title compound as a light yellow solid (42.0 mg, 66%), mp 138-140 $^{\circ}$ C. $\nu_{\max}/\text{cm}^{-1}$ 3057, 2931, 1591, 1468, 1411. ¹H NMR (600 MHz, CDCl₃) δ_{H} 9.38 (1H, d, *J* 2.1, H22), 9.30 (1H, t, *J* 2.1, H24), 8.39 (1H, d, *J* 8.3, H11), 8.21 (1H, d, *J* 2.1, H20), 8.01 (1H, d, *J* 2.0, H8), 7.54 (1H, dd, *J* 10.1, 7.1, H30 or H33), 7.47-7.42 (2H, m, H30 or H33 and H10), 7.36 (1H, d, *J* 2.1, H2), 6.58 (1H, d, *J* 2.1, H6), 4.07 (3H, s, H15), 3.97 (1H, tt, *J* 6.9, 3.8, H36), 3.91 (3H, s, H17), 2.56 (3H, s, H13), 1.44-1.39 (1H, m, H37 or H38), 1.34-1.29 (1H, m, H37 or H38), 0.81-0.77 (1H, m, H37 or H38), 0.65-0.60 (1H, m, H37 or H38). ¹³C NMR (150 MHz, CDCl₃) δ_{C} 168.2 (C), 158.6 (C), 154.4 (CH), 149.8-147.8 (2C) 148.1 (CH), 146.2 (C), 142.8 (C), 139.5 (CH), 138.8 (C), 137.8 & 137.7 (d, *J* 11.0, C), 133.2 (CH), 132.9 & 132.8 (d, *J* 11.0, C), 129.6 (CH), 129.3 (C), 128.5 (C), 125.4 (C), 125.2 (CH), 121.9 (C), 107.6 & 107.5 (d, *J* 19.7, CH), 106.2 (C), 101.4 (CH), 100.7 (CH), 99.7 & 99.5 (d, *J* 23.0, CH), 57.2 (CH₃), 57.0 (CH₃), 26.6 (CH), 21.9 (CH₃), 9.5 (CH₂), 8.9 (CH₂). ¹⁹F NMR (282 MHz, CDCl₃) δ_{F} -78.4, -138.5 & -138.6 (1F, d, *J* 20.3), -141.8 & -141.9 (1F, d, *J* 20.3). HRMS (CI) Calculated for C₃₀H₂₆F₂N₃O₂S [M]⁺:

528.1552; found: 528.1553.

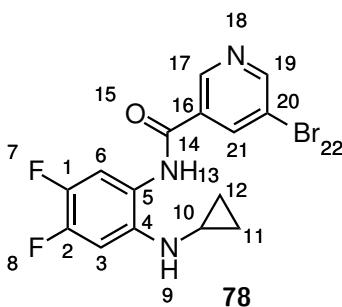
13.12 Compounds 81, 78 and 80 (Chapter 9)

N-Cyclopropyl-2,5-difluoro-4-nitroaniline 81



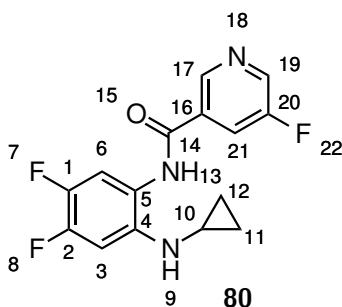
A regioisomer of **76** was isolated during flash column chromatography purification (slow eluting component) as a bright yellow solid. ^1H NMR (600 MHz, CDCl_3) δ_{H} 7.79 (1H, dd, J 11.1, 6.2, H6), 6.80 (1H, dd, J 13.3, 7.1, H3), 5.11 (1H, bs, H8), 2.56-2.52 (1H, m, H11), 0.94-0.91 (2H, m, H12 or H13), 0.67-0.64 (2H, m, H12 or H13). ^{13}C NMR (150 MHz, CDCl_3) δ_{C} 155.8 & 154.1 (d, J 261.6, C), 145.7 & 144.1 (d, J 238.5, C), 144.5 & 144.4 (d, J 25.2, C), 125.1 & 125.0 (d, J 6.7, C), 112.1 & 112.0 (d, J 26.0, CH), 100.2 & 100.0 (d, J 23.8, CH), 24.5 (CH), 7.69 (CH_2). ^{19}F NMR (282 MHz, CDCl_3) δ_{F} -116.8 & -116.9 (1F, d, J 13.0), -140.2 & -140.3 (1F, d, J 13.0). HRMS (ESI) Calculated for $\text{C}_9\text{H}_9\text{F}_2\text{N}_2\text{O}_2$ $[\text{M}+\text{H}]^+$: 215.0627; found: 215.0616.

5-Bromo-*N*-(2-(cyclopropylamino)-4,5-difluorophenyl)nicotinamide **78**



To a stirring solution of diamine **77** (300 mg, 1.63 mmol, 1.0 equiv.) in DCM (8 mL) were added 5-bromonicotinic acid (362 mg, 1.79 mmol, 1.1 equiv.), HATU (685 mg, 1.80 mmol, 1.1 equiv.), HOBT (242 mg, 1.79 mmol, 1.1 equiv.) and DIPEA (1.14 mL, 6.55 mmol, 4.0 equiv.). The resulting dark red solution was stirred at room temperature for 2 h. It was then diluted with DCM, washed with H₂O and brine, dried over MgSO₄ and concentrated *in vacuo*. Flash column chromatography purification (0 → 30% Et₂O/DCM) afforded the title compound as an off-white solid (391 mg, 65%), mp 183-185 °C (dec). $\nu_{\max}/\text{cm}^{-1}$ 3265, 3021, 1643, 1518, 1421. ¹H NMR (600 MHz, CDCl₃) δ_{H} 8.98 (1H, d, *J* 2.1, H17), 8.87 (1H, d, *J* 2.1, H19), 8.37 (1H, t, *J* 2.1, H21), 7.54 (1H, bs, H13), 7.30 (1H, dd, *J* 11.2, 8.6, H3 or H6), 7.04 (1H, dd, *J* 11.8, 7.8, H3 or H6), 4.20 (1H, bs, H9), 2.45 (1H, m, H10), 0.80-0.78 (2H, m, H11 and H12), 0.53-0.50 (2H, m, H11 and H12). ¹³C NMR (150 MHz, CDCl₃) δ_{C} 162.9 (C), 154.2 (CH), 154.0 (C), 148.9 (CH), 140.2 & 140.1 (d, *J*, 6.0, C), 138.3 (CH), 130.9 (CH), 121.4 (CH), 118.2 & 118.1 (d, *J* 6.6, C), 118.0 (C), 114.6-114.5 (dd, *J* 19.0, 1.1, CH), 103.6-103.5 (dd, *J* 20.0, 1.7, CH), 25.8 (CH), 7.51 (CH₂). ¹⁹F NMR (282 MHz, CDCl₃) δ_{F} -137.4 & -137.5 (d, *J* 23.0), -149.3 & -149.4 (d, *J* 23.0). Calculated for C₁₅H₁₃BrF₂N₃O [M+H]⁺: 368.0210; found: 368.0203.

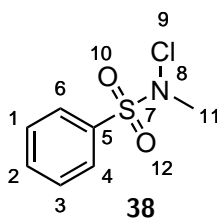
***N*-(2-(Cyclopropylamino)-4,5-difluorophenyl)-5-fluoronicotinamide 80**



To a stirring solution of diamine **77** (70.0 mg, 0.380 mmol, 1.0 equiv.) in DCM (2.0 mL) were added 5-fluoronicotinic acid (59.0 mg, 0.418 mmol, 1.1 equiv.), HATU (160 mg, 0.421 mmol, 1.1 equiv.), HOBT (57.0 mg, 0.422 mmol, 1.1 equiv.) and DIPEA (265 μ L, 1.52 mmol, 4.0 equiv.). The resulting black solution was stirred at room temperature for 17 h. The reaction mixture was then diluted with DCM, washed with H₂O and brine, dried over MgSO₄ and concentrated *in vacuo*. Flash column chromatography purification (0 \rightarrow 30% Et₂O/DCM) afforded the title compound as an off-white solid (76.0 mg, 65%), 145-147 $^{\circ}$ C. $\nu_{\text{max}}/\text{cm}^{-1}$ 3266, 1647, 1526, 1512, 1425. ¹H NMR (600 MHz, CDCl₃) δ_{H} 8.90 (1H, bs, H17), 8.68 (1H, d, *J* 2.7, H19), 7.97 (1H, dd, *J* 8.5, 2.2, H21), 7.57 (1H, bs, H13), 7.33 (1H, dd, *J* 11.1, 7.9, H3 or H6), 7.04 (1H, dd, *J* 12.5, 7.6, H3 or H6), 4.20 (1H, bs, H9), 2.46 (1H, m, H10), 0.81-0.79 (2H, m, H11 and H12), 0.53-0.51 (2H, m, H11 and H12). ¹³C NMR (150 MHz, CDCl₃) δ_{C} 162.9 (C), 160.4 & 158.7 (d, *J* 262, C), 143.3 (d, *J* 3.9, CH), 141.9 & 141.8 (d, *J* 22.5, CH), 140.1 (C), 140.0 (dd, *J* 2.8, 1.1, C), 131.2 (d, *J* 3.9, C), 122.8 & 122.6 (d, *J* 18.8, CH), 118.3 (C), 114.5 & 114.4 (d, *J* 21.6, CH), 103.7 & 103.5 (d, *J* 21.6, CH), 25.8 (CH), 7.5 (CH₂). ¹⁹F NMR (282 MHz, CDCl₃) δ_{F} -124.9, -138.9 & -139.0 (d, *J* 23.0), -139.6 & -139.7 (d, *J* 23.0). HRMS (ESI) Calculated for C₁₅H₁₃F₃N₃O [M+H]⁺: 308.1011; found: 308.0644.

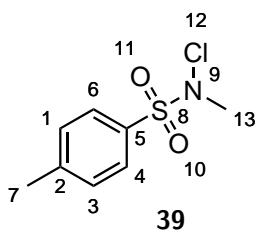
13.13 *N*-Chlorosulfonamides as Reagents for Cyclisation

N-Chloro-*N*-methylbenzenesulfonamide **38**



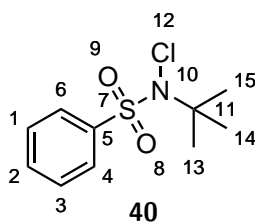
To a stirring solution of technical grade calcium hypochlorite (65 ww%, 167 mg, 0.762 mmol, 1.3 equiv.) and alumina (300 mg, 2.94 mmol, 5.0 equiv.) in CHCl_3 (1.5 mL) at 40 °C was added *N*-methylbenzenesulfonamide (100 mg, 0.584 mmol, 1.0 equiv.). The resulting suspension was stirred at 40 °C for 2 h. After cooling to room temperature, the reaction mixture was diluted with CHCl_3 , filtered and concentrated *in vacuo*. Flash column chromatography purification (0 → 40% $\text{Et}_2\text{O}/\text{PE}$) afforded the title compound as a white solid (112 mg, 93%). Data in agreement with literature¹⁴⁹. ^1H NMR (600 MHz, CDCl_3) δ_{H} 7.96 (2H, dd, 8.3, 1.3, H4 and H6), 7.74 (1H, tt, *J* 7.6, 1.3, H2), 7.63 (2H, dd, *J* 8.3, 7.6, H1 and H3), 3.12 (3H, s, H11). ^{13}C NMR (150 MHz, CDCl_3) δ_{C} 134.5 (CH), 131.6 (C), 130.0 (CH), 129.2 (CH), 45.5 (CH_3).

N-Chloro-*N*,4-dimethylbenzenesulfonamide



To a stirring solution of technical grade calcium hypochlorite (65 ww%, 772 mg, 3.51 mmol, 1.3 equiv.) and alumina (1.40 g, 13.7 mmol, 5.0 equiv.) in CHCl_3 (7.0 mL) at 40 °C was added *N*,4-dimethylbenzenesulfonamide (500 mg, 2.70 mmol, 1.0 equiv.). The resulting suspension was stirred at 40 °C for 2 h. After cooling to room temperature, the reaction mixture was diluted with CHCl_3 , filtered and concentrated *in vacuo*. Flash column chromatography purification (50% $\text{Et}_2\text{O}/\text{PE}$) afforded the title compound as a white solid (512 mg, 88%). Data in agreement with literature¹⁴⁸. ^1H NMR (600 MHz, CDCl_3) δ_{H} 7.84 (2H, d, J 8.3, H4 and H6), 7.41 (2H, d, J 8.3, H1 and H3), 3.11 (3H, s, H7), 2.49 (3H, s, H13). ^{13}C NMR (150 MHz, CDCl_3) δ_{C} 145.7 (C), 130.0 (CH), 129.8 (CH), 128.6 (C), 45.5 (CH_3), 21.9 (CH_3).

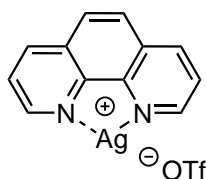
N-(*tert*-Butyl)-*N*-chlorobenzenesulfonamide **40**



To a stirring solution of technical grade calcium hypochlorite (65 ww%, 403 mg, 1.83 mmol, 1.3 equiv.) and alumina (719 mg, 7.05 mmol, 5.0 equiv.) in CHCl_3 (3.5 mL) at 40 °C was added *N*-(*tert*-butyl)benzenesulfonamide (300 mg, 1.41 mmol, 1.0 equiv.). The resulting suspension was stirred at 40 °C for 2 h. After cooling to room temperature, the reaction mixture was diluted with CHCl_3 , filtered and concentrated *in vacuo*. Flash column chromatography purification (50% $\text{Et}_2\text{O}/\text{PE}$) afforded the title compound as a colourless oil (326 mg, 93%). Data in agreement with literature¹⁴⁸. ^1H NMR (600 MHz, CDCl_3) δ_{H} 7.99 (2H, dd, J 8.5, 1.3, H4 and H6), 7.65 (1H, tt, J 7.8, 1.3, H2), 7.55 (2H, dd, J 8.5, 7.8, H1 and H3), 1.40 (9H, s, H13, H14 and H15). ^{13}C NMR (150 MHz, CDCl_3) δ_{C} 138.5 (C), 133.7 (CH), 129.0 (CH), 129.0 (CH), 68.3 (C), 29.3 (CH_3).

13.14 Miscellaneous Compounds

(1,10-Phenanthroline)silver trifluoromethanesulfonate



To a round-bottom flask were added MeOH (7.0 mL), 10-phenanthroline (200 mg, 1.11 mmol, 1.0 equiv.) and a solution of AgOTf (285 mg, 1.11 mmol, 1.0 equiv.) H₂O (7.0 mL). The resulting suspension was stirred for 15 min at room temperature. The title compound was isolated by filtration, washed with cold MeOH and dried over P₂O₅ overnight (286 mg, 55%).

tert-Butyl hypochlorite

To an ice-cooled commercial bleach solution (< 5% chlorine content, 40 mL) in a round-bottom flask were added *t*-butanol (176 μ L, 18.4 mmol, 1.0 equiv.) and glacial acetic acid (104 μ L, 18.4 mmol, 1.0 equiv.). The reaction mixture was stirred in darkness at 0 °C for 3 min. The mixture was washed with a 10% solution of K₂CO₃, H₂O and brine. The resulting yellow oil was stored over CaCl₂ in the freezer for a short period of time.

13.15 Calibration Curve for Sulfonium Salt 7

This calibration curve was prepared in order to determine the concentration of sulfonium salt **7** in cyclisation reactions performed in Chapter 5, Table 5.1 (page 66).

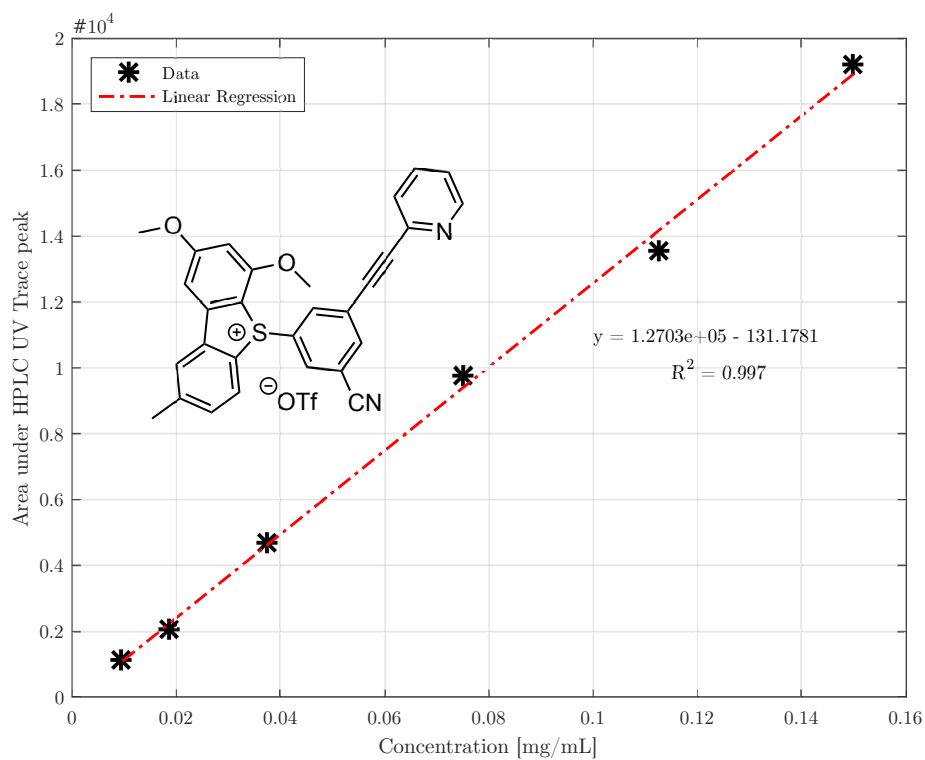


Figure 13.1: Calibration curve for sulfonium salt **7**.

References

- [1] Gambhir, S. S. *Nat. Rev. Cancer* **2002**, *2*, 683–693.
- [2] Miller, P. W.; Long, N. J.; Vilar, R.; Gee, A. D. *Angew. Chem. Int. Ed. Engl.* **2008**, *47*, 8998–9033.
- [3] Vaquero, J. J.; Kinahan, P. *Annu. Rev. Biomed. Eng.* **2015**, *17*, 385–414.
- [4] Sander, K.; Gendron, T.; Yiannaki, E.; Cybulska, K.; Kalber, T. L.; Lythgoe, M. F.; Årstad, E. *Sci. Rep.* **2015**, *5*, 9941.
- [5] Keinänen, O.; Li, X.-G.; Chenna, N. K.; Lumen, D.; Ott, J.; Molthoff, C. F. M.; Sarparanta, M.; Helariutta, K.; Vuorinen, T.; Windhorst, A. D.; Airaksinen, A. J. *ACS Med. Chem. Lett.* **2016**, *7*, 62–66.
- [6] Preshlock, S.; Tredwell, M.; Gouverneur, V. *Chem. Rev.* **2016**, *116*, 719–766.
- [7] Budisa, N.; Kubyshkin, V.; Schulze-Makuch, D. *Life* **2014**, *4*, 374–385.
- [8] O'Hagan, D. *J. Fluor. Chem.* **2010**, *131*, 1071–1081.
- [9] Zhou, Y.; Wang, J.; Gu, Z.; Wang, S.; Zhu, W.; Aceña, J. L.; Soloshonok, V. A.; Izawa, K.; Liu, H. *Chem. Rev.* **2016**, *116*, 422–518.
- [10] Jacobson, O.; Kiesewetter, D. O.; Chen, X. *Bioconjug. Chem.* **2015**, *26*, 1–18.
- [11] Alauddin, M. M. *Am. J. Nucl. Med. Mol. Imaging* **2012**, *2*, 55–76.
- [12] Cole, E. L.; Stewart, M. N.; Littich, R.; Hoareau, R.; Scott, P. J. H. *Curr. Top. Med. Chem.* **2014**, *14*, 875–900.
- [13] Kilbourn, M. R. *Nucl. Med. Biol.* **2013**, *40*, 956–958.
- [14] Kurli, M.; Chin, K.; Finger, P. T. *Br. J. Ophthalmol.* **2008**, *92*, 479–482.

- [15] Nguyen, N. C.; Akduman, I.; Osman, M. M. *J. Radiol. Nurs.* **2008**, *27*, 61–69.
- [16] Agarwal, A.; Marcus, C.; Xiao, J.; Nene, P.; Kachnic, L. A.; Subramaniam, R. M. *Am. J. Roentgenol.* **2014**, *203*, 1109–1119.
- [17] O'Brien, J. T.; Firbank, M. J.; Davison, C.; Barnett, N.; Bamford, C.; Donaldson, C.; Olsen, K.; Herholz, K.; Williams, D.; Lloyd, J. *J. Nucl. Med.* **2014**, *55*, 1959–1965.
- [18] Poston, K. L.; Eidelberg, D. *PET Clin.* **2010**, *5*, 55–64.
- [19] Pinilla, I.; Rodríguez-Vigil, B.; Gómez-León, N. *Clin. Med. Oncol.* **2008**, *2*, 181–198.
- [20] Jadvar, H.; Parker, J. A. *Clinical PET and PET/CT*; Springer-Verlag: London, 2005; p 64.
- [21] Ametamey, S. M.; Honer, M.; Schubiger, P. A. *Chem. Rev.* **2008**, *108*, 1501–16.
- [22] Herrmann, K., Nieweg, O. E., Povoski, S. P., Eds. *Radioguided Surgery*; Springer International Publishing: Cham, 2016.
- [23] Emran, A. M., Ed. *New Trends in Radiopharmaceutical Synthesis, Quality Assurance, and Regulatory Control*; Springer US: Boston, MA, 1991.
- [24] Dong, M. W. *Modern HPLC for Practicing Scientists*; John Wiley & Sons, Inc.: Hoboken, NJ, USA, 2006.
- [25] Bird, I. M. *BMJ* **1989**, *299*, 783–787.
- [26] Chen, Y.; Mehok, A. R.; Mant, C. T.; Hodges, R. S. *J. Chromatogr. A* **2004**, *1043*, 9–18.
- [27] Lindegren, S.; Jensen, H.; Jacobsson, L. *J. Chromatogr. A* **2014**, *1337*, 128–132.
- [28] Veltkamp, A. *J. Chromatogr. B Biomed. Sci. Appl.* **1990**, *531*, 101–129.
- [29] Parasuraman R. Balamurugan, S. Muralidharan, S. Jayaraj Kumar, K. Vijayan, V, S. A. *Pharm. Methods* **2014**, *5*, 47–55.

- [30] Ho, C. S.; Lam, C. W. K.; Chan, M. H. M.; Cheung, R. C. K.; Law, L. K.; Lit, L. C. W.; Ng, K. F.; Suen, M. W. M.; Tai, H. L. *Clin. Biochem. Rev.* **2003**, *24*, 3–12.
- [31] Brooks, A. F.; Topczewski, J. J.; Ichiishi, N.; Sanford, M. S.; Scott, P. J. H. *Chem. Sci.* **2014**, *5*, 4545–4553.
- [32] van der Born, D.; Pees, A.; Poot, A. J.; Orru, R. V. A.; Windhorst, A. D.; Vugts, D. J. *Chem. Soc. Rev.* **2017**, *46*, 4709–4773.
- [33] Hamacher, K.; Coenen, H. H.; Stöcklin, G. *J. Nucl. Med.* **1986**, *27*, 235–238.
- [34] Kalgutkar, A. S.; Jones, R.; Sawant, A. *RSC Publ.*; 2010; pp 210–274.
- [35] Ward, S. E.; Beswick, P. *Expert Opin. Drug Discov.* **2014**, *9*, 995–1003.
- [36] Firnau, G.; Chirakal, R.; Garnett, E. S. *J. Nucl. Med.* **1984**, *25*, 1228–1233.
- [37] Cacace, F.; Giacomello, P.; Wolf, A. P. *J. Am. Chem. Soc.* **1980**, *102*, 3511–3515.
- [38] Pretze, M.; Wängler, C.; Wängler, B. *Biomed Res. Int.* **2014**, *2014*, 1–12.
- [39] de Vries, E. F.; Luurtsema, G.; Brüssermann, M.; Elsinga, P. H.; Vaalburg, W. *Appl. Radiat. Isot.* **1999**, *51*, 389–394.
- [40] Lu, S.; Pike, V. W. *J. Fluor. Chem.* **2010**, *131*, 1032–1038.
- [41] Shiue, C. Y.; Salvadori, P. A.; Wolf, A. P.; Fowler, J. S.; MacGregor, R. R. *J. Nucl. Med.* **1982**, *23*, 899–903.
- [42] Teare, H.; Robins, E. G.; Kirjavainen, A.; Forsback, S.; Sandford, G.; Solin, O.; Luthra, S. K.; Gouverneur, V. *Angew. Chemie Int. Ed.* **2010**, *49*, 6821–6824.
- [43] Teare, H.; Robins, E. G.; Kirjavainen, A.; Forsback, S.; Sandford, G.; Solin, O.; Luthra, S. K.; Gouverneur, V. *Angew. Chemie Int. Ed.* **2010**, *49*, 6821–6824.
- [44] Neumann, C. N.; Hooker, J. M.; Ritter, T. *Nature* **2016**, *534*, 369–373.
- [45] Richter, S.; Wuest, F. *Molecules* **2014**, *19*, 20536–20556.

- [46] Glaser, M.; Årstad, E. *Bioconjug. Chem.* **2007**, *18*, 989–993.
- [47] Chatterjee, N.; Goswami, A. *Eur. J. Org. Chem.* **2017**, *2017*, 3023–3032.
- [48] Olofsson, B. *Top. Curr. Chem.*; 2015; Vol. 373; pp 135–166.
- [49] Bielawski, M.; Zhu, M.; Olofsson, B. *Adv. Synth. Catal.* **2007**, *349*, 2610–2618.
- [50] Bielawski, M.; Aili, D.; Olofsson, B. *J. Org. Chem.* **2008**, *73*, 4602–4607.
- [51] Merritt, E. A.; Olofsson, B. *Angew. Chemie Int. Ed.* **2009**, *48*, 9052–9070.
- [52] Pike, V. W.; Aigbirhio, F. I. *J. Chem. Soc. Chem. Commun.* **1995**, 2215–2216.
- [53] Yusubov, M. S.; Svitich, D. Y.; Larkina, M. S.; Zhdankin, V. V. *Arkivoc* **2013**, *2013*, 364–395.
- [54] Chun, J.-H.; Lu, S.; Lee, Y.-S.; Pike, V. W. *J. Org. Chem.* **2010**, *75*, 3332–3338.
- [55] Gail, R.; Hocke, C.; Coenen, H. H. *J. Label. Compd. Radiopharm.* **1993**, *40*, 50–52.
- [56] Coenen, H. H. *Ernst Schering Res. Found. Workshop* **2007**, 15–50.
- [57] Ross, T. L.; Ermert, J.; Hocke, C.; Coenen, H. H. *J. Am. Chem. Soc.* **2007**, *129*, 8018–8025.
- [58] Telu, S.; Chun, J.-H.; Siméon, F. G.; Lu, S.; Pike, V. W. *Org. Biomol. Chem.* **2011**, *9*, 6629.
- [59] Irving, H.; Reid, R. W. *J. Chem. Soc.* **1960**, 2078.
- [60] Moon, B. S.; Kil, H. S.; Park, J. H.; Kim, J. S.; Park, J.; Chi, D. Y.; Lee, B. C.; Kim, S. E. *Org. Biomol. Chem.* **2011**, *9*, 8346.
- [61] Massaweh, G.; Schirmacher, E.; la Fougere, C.; Kovacevic, M.; Wängler, C.; Jolly, D.; Gravel, P.; Reader, A. J.; Thiel, A.; Schirmacher, R. *Nucl. Med. Biol.* **2009**, *36*, 721–727.
- [62] Rotstein, B. H.; Stephenson, N. A.; Vasdev, N.; Liang, S. H. *Nat. Commun.* **2014**, *5*.

- [63] Ye, C.; Twamley, B.; Shreeve, J. M. *Org. Lett.* **2005**, *7*, 3961–3964.
- [64] Rotstein, B. H.; Wang, L.; Liu, R. Y.; Patteson, J.; Kwan, E. E.; Vasdev, N.; Liang, S. H. *Chem. Sci.* **2016**, *7*, 4407–4417.
- [65] Stephenson, N. A.; Holland, J. P.; Kassenbrock, A.; Yokell, D. L.; Livni, E.; Liang, S. H.; Vasdev, N. *J. Nucl. Med.* **2015**, *56*, 489–492.
- [66] Angelini, G.; Speranza, M.; Wolf, A.; Shiue, C.-Y. *J. Fluor. Chem.* **1985**, *27*, 177–191.
- [67] Maeda, M.; Fukumura, T.; Kojima, M. *Int. J. Radiat. Appl. Instrumentation. Part A. Appl. Radiat. Isot.* **1987**, *38*, 307–310.
- [68] Mu, L.; Fischer, C. R.; Holland, J. P.; Becaud, J.; Schubiger, P. A.; Schibli, R.; Ametamey, S. M.; Graham, K.; Stellfeld, T.; Dinkelborg, L. M.; Lehmann, L. *Eur. J. Org. Chem.* **2012**, *2012*, 889–892.
- [69] Lee, E.; Kamlet, A. S.; Powers, D. C.; Neumann, C. N.; Boursalian, G. B.; Furuya, T.; Choi, D. C.; Hooker, J. M.; Ritter, T. *Science (80-.)*. **2011**, *334*, 639–642.
- [70] Kamlet, A. S.; Neumann, C. N.; Lee, E.; Carlin, S. M.; Moseley, C. K.; Stephenson, N.; Hooker, J. M.; Ritter, T. *PLoS One* **2013**, *8*.
- [71] Qiao, J.; Lam, P. *Synthesis (Stuttg)*. **2011**, *2011*, 829–856.
- [72] Ye, Y.; Sanford, M. S. *J. Am. Chem. Soc.* **2013**, *135*, 4648–4651.
- [73] Tredwell, M.; Preshlock, S. M.; Taylor, N. J.; Gruber, S.; Huiban, M.; Passchier, J.; Mercier, J.; Génicot, C.; Gouverneur, V. *Angew. Chemie - Int. Ed.* **2014**, *53*, 7751–7755.
- [74] Nanni, C.; Fanti, S.; Rubello, D. *J. Nucl. Med.* **2007**, *48*, 1577–1579.
- [75] Ichiishi, N.; Canty, A. J.; Yates, B. F.; Sanford, M. S. *Org. Lett.* **2013**, *15*, 5134–5137.
- [76] Ichiishi, N.; Brooks, A. F.; Topczewski, J. J.; Rodnick, M. E.; Sanford, M. S.; Scott, P. J. H. *Org. Lett.* **2014**, *16*, 3224–3227.

- [77] Brooks, A. F.; Topczewski, J. J.; Ichiishi, N.; Sanford, M. S.; Scott, P. *Chem. Sci.* **2014**, *2014*.
- [78] Petersen, I. N.; Kristensen, J. L.; Herth, M. M. *Eur. J. Org. Chem.* **2017**, *2017*, 453–458.
- [79] Crivello, J. V.; Lam, J. H. W. *J. Org. Chem.* **1978**, *43*, 3055–3058.
- [80] Itoh, T.; Mase, T. *J. Org. Chem.* **2006**, *71*, 2203–2206.
- [81] Haryono, A.; Miyatake, K.; Natori, J.; Tsuchida, E. *Macromolecules* **1999**, *32*, 3146–3149.
- [82] Vasu, D.; Yorimitsu, H.; Osuka, A. *Angew. Chemie Int. Ed.* **2015**, *54*, 7162–7166.
- [83] Smith, L. H. S.; Coote, S. C.; Sneddon, H. F.; Procter, D. J. *Angew. Chemie Int. Ed.* **2010**, *49*, 5832–5844.
- [84] Chen, C. H.; Reynolds, G. A.; Van Allan, J. A. *J. Org. Chem.* **1977**, *42*, 2777–2778.
- [85] Tuleen, D. L.; Stephens, T. *J. Org. Chem.* **1969**, *34*, 31–35.
- [86] Meldrum, B. S. *J. Nutr.* **2000**, *130*, 1007S–15S.
- [87] Newell, K. A. *Future Med. Chem.* **2013**, *5*, 1471–1474.
- [88] Putney, J. W.; Tomita, T. *Adv. Biol. Regul.* **2012**, *52*, 152–164.
- [89] Marino, M. J.; Valenti, O.; Conn, P. J. *Drugs Aging* **2003**, *20*, 377–397.
- [90] Notenboom, R. G. E. *Brain* **2005**, *129*, 96–107.
- [91] Brownell, A.-L.; Kuruppu, D.; Kil, K.-E.; Jokivarsi, K.; Poutiainen, P.; Zhu, A.; Maxwell, M. *J. Neuroinflammation* **2015**, *12*, 217.
- [92] Choi, K. Y.; Chang, K.; Pickel, J. M.; Badger, J. D.; Roche, K. W. *Proc. Natl. Acad. Sci.* **2011**, *108*, 15219–15224.
- [93] Hamill, T. G. *et al. Synapse* **2005**, *56*, 205–216.

- [94] Wong, D. F.; Waterhouse, R.; Kuwabara, H.; Kim, J.; Brasic, J. R.; Chamroonrat, W.; Stabins, M.; Holt, D. P.; Dannals, R. F.; Hamill, T. G.; Mozley, P. D. *J. Nucl. Med.* **2013**, *54*, 388–396.
- [95] Felts, A. S. *et al. J. Med. Chem.* **2017**, *60*, 5072–5085.
- [96] Wang, J.-Q.; Tueckmantel, W.; Zhu, A.; Pellegrino, D.; Brownell, A.-L. *Synapse* **2007**, *61*, 951–961.
- [97] Schopfer, U.; Schlapbach, A. *Tetrahedron* **2001**, *57*, 3069–3073.
- [98] Carney, J. M.; Donoghue, P. J.; Wuest, W. M.; Wiest, O.; Helquist, P. *Org. Lett.* **2008**, *10*, 3903–3906.
- [99] Gaspard-Iloughmane, H.; Le Roux, C. *Eur. J. Org. Chem.* **2004**, *2004*, 2517–2532.
- [100] Garrigues, B.; Gonzaga, F.; Robert, H.; Dubac, J. *J. Org. Chem.* **1997**, *62*, 4880–4882.
- [101] Ondet, P.; Lemièrre, G.; Duñach, E. *Eur. J. Org. Chem.* **2017**, *2017*, 761–780.
- [102] Leonard, N. M.; Wieland, L. C.; Mohan, R. S. *Tetrahedron* **2002**, *58*, 8373–8397.
- [103] Salnikov, G. E.; Genaev, A. M.; Vasiliev, V. G.; Shubin, V. G. *Org. Biomol. Chem.* **2012**, *10*, 2282–8.
- [104] Olah, G. A.; Wang, Q.; Sandford, G.; Surya Prakash, G. K. *J. Org. Chem.* **1993**, *58*, 3194–3195.
- [105] Dalziel, J. R.; Aubke, F. *Inorg. Chem.* **1973**, *12*, 2707–2711.
- [106] Prakash, G. K. S.; Mathew, T.; Hoole, D.; Esteves, P. M.; Wang, Q.; Rasul, G.; Olah, G. A. *J. Am. Chem. Soc.* **2004**, *126*, 15770–6.
- [107] Eckert, F.; Leito, I.; Kaljurand, I.; Kütt, A.; Klamt, A.; Diedenhofen, M. *J. Comput. Chem.* **2009**, *30*, 799–810.

- [108] Pastoriza, C.; Antelo, J. M.; Crugeiras, J. *J. Phys. Org. Chem.* **2014**, *27*, 952–959.
- [109] Lengyel, I.; Cesare, V.; Stephani, R. *Synth. Commun.* **1998**, *28*, 1891–1896.
- [110] Gowda, B. T.; Mary, M. C. *Indian J. Chem.* **2001**, *40A*, 1196–1202.
- [111] Nwaukwa, S. O.; Keehn, P. M. *Synth. Commun.* **2006**,
- [112] Firouzabadi, H.; Iranpoor, N.; Karimi, B. *Synlett* **1999**, *1999*, 413–414.
- [113] Kaushik, N. K.; Kaushik, N.; Attri, P.; Kumar, N.; Kim, C. H.; Verma, A. K.; Choi, E. H. *Molecules* **2013**, *18*, 6620–62.
- [114] Bandini, M. *Org. Biomol. Chem.* **2013**, *11*, 5206.
- [115] Palego, L.; Betti, L.; Rossi, A.; Giannaccini, G. *J. Amino Acids* **2016**, *2016*, 1–13.
- [116] Guastella, A. R.; Michelhaugh, S. K.; Klinger, N. V.; Kupsky, W. J.; Polin, L. A.; Muzik, O.; Juhász, C.; Mittal, S. *Mol. Imaging* **2016**, *15*, 1–11.
- [117] Chugani, D. C. *Biomark. Med.* **2011**, *5*, 567–575.
- [118] Kannan, L.; Vogrin, S.; Bailey, C.; Maixner, W.; Harvey, A. S. *Brain* **2016**, *139*, 2653–2667.
- [119] Diksic, M.; Nagahiro, S.; Sourkes, T. L.; Yamamoto, Y. L. *J. Cereb. Blood Flow Metab.* **1990**, *10*, 1–12.
- [120] Diksic, M.; Nagahiro, S.; Chaly, T.; Sourkes, T. L.; Yamamoto, Y. L.; Feindel, W. *J. Neurochem.* **1991**, *56*, 153–162.
- [121] Chugani, H. T.; Chugani, D. C. *Epilepsy Curr.* **2005**, *5*, 201–206.
- [122] Dailey, J. W.; Reigel, C. E.; Mishra, P. K.; Jobe, P. C. *Epilepsy Res.* **1989**, *3*, 3–17.
- [123] Statnick, M. A.; Dailey, J. W.; Jobe, P. C.; Browning, R. A. *Epilepsia* **1996**, *37*, 311–321.

- [124] Kumar, A.; Asano, E.; Chugani, H. T. *Biomark. Med.* **2011**, *5*, 577–584.
- [125] Peters, J. C. *Tryptophan Nutrition and Metabolism: An Overview*; 1991; pp 345–358.
- [126] Dounay, A. B.; Tuttle, J. B.; Verhoest, P. R. *J. Med. Chem.* **2015**, *58*, 8762–8782.
- [127] Fox, J. M.; Sage, L. K.; Huang, L.; Barber, J.; Klonowski, K. D.; Mellor, A. L.; Tompkins, S. M.; Tripp, R. A. *J. Gen. Virol.* **2013**, *94*, 1451–1461.
- [128] Opitz, C. A.; Wick, W.; Steinman, L.; Platten, M. *Cell. Mol. Life Sci.* **2007**, *64*, 2542–2563.
- [129] Bosnyak, E.; Kamson, D. O.; Guastella, A. R.; Varadarajan, K.; Robbinette, N. L.; Kupsky, W. J.; Muzik, O.; Michelhaugh, S. K.; Mittal, S.; Juhasz, C. *Neuro. Oncol.* **2015**, *17*, 1284–1292.
- [130] Platten, M.; Wick, W.; Van den Eynde, B. J. *Cancer Res.* **2012**, *72*, 5435–5440.
- [131] Campbell, B. M.; Charych, E.; Lee, A. W.; Möller, T. *Front. Neurosci.* **2014**, *8*.
- [132] Xin, Y.; Cai, H. *Mol. Imaging Biol.* **2017**, *19*, 589–598.
- [133] Michelhaugh, S. K.; Muzik, O.; Guastella, A. R.; Klinger, N. V.; Polin, L. A.; Cai, H.; Xin, Y.; Mangner, T. J.; Zhang, S.; Juhász, C.; Mittal, S. *J. Nucl. Med.* **2017**, *58*, 208–213.
- [134] Giglio, B. C.; Fei, H.; Wang, M.; Wang, H.; He, L.; Feng, H.; Wu, Z.; Lu, H.; Li, Z. *Theranostics* **2017**, *7*, 1524–1530.
- [135] Sono, M.; Roach, M. P.; Coulter, E. D.; Dawson, J. H. *Chem. Rev.* **1996**, *96*, 2841–2888.
- [136] Goetz, A. E.; Garg, N. K. *Nat. Chem.* **2012**, *5*, 54–60.
- [137] Baumann, M.; Baxendale, I. R. *Beilstein J. Org. Chem.* **2013**, *9*, 2265–2319.

- [138] Pryde, D. C.; Dalvie, D.; Hu, Q.; Jones, P.; Obach, R. S.; Tran, T. D. *J. Med. Chem.* **2010**, *53*, 8441–8460.
- [139] Dolle, F. *Ernst Schering Res. Found. Workshop* **2007**, 113–157.
- [140] Dolci, L.; Dolle, F.; Jubeau, S.; Vaufrey, F.; Crouzel, C. *J. Label. Compd. Radiopharm.* **1999**, *42*, 975–985.
- [141] Chen, Y.; Pullambhatla, M.; Foss, C. A.; Byun, Y.; Nimmagadda, S.; Senthamizhchelvan, S.; Sgouros, G.; Mease, R. C.; Pomper, M. G. *Clin. Cancer Res.* **2011**, *17*, 7645–7653.
- [142] Baur, B.; Solbach, C.; Andreolli, E.; Winter, G.; Machulla, H.-J.; Reske, S. *Pharmaceuticals* **2014**, *7*, 517–529.
- [143] Tosoian, J. J.; Gorin, M. A.; Rowe, S. P.; Andreas, D.; Szabo, Z.; Pienta, K. J.; Pomper, M. G.; Lotan, T. L.; Ross, A. E. *Clin. Genitourin. Cancer* **2017**, *15*, e65–e68.
- [144] Bouvet, V.; Wuest, M.; Jans, H.-S.; Janzen, N.; Genady, A. R.; Valliant, J. F.; Benard, F.; Wuest, F. *EJNMMI Res.* **2016**, *6*, 40.
- [145] Karramkam, M.; Hinnen, F.; Vaufrey, F.; Dollé, F. *J. Label. Compd. Radiopharm.* **2003**, *46*, 979–992.
- [146] Beer, H.-F.; Frey, L.; Häberli, M.; Schubiger, P. *Nucl. Med. Biol.* **1995**, *22*, 999–1004.
- [147] Brugarolas, P.; Freifelder, R.; Cheng, S.-H.; DeJesus, O. *Chem. Commun.* **2016**, *52*, 7150–7152.
- [148] Heuger, G.; Göttlich, R. *Beilstein J. Org. Chem.* **2015**, *11*, 1226–1234.
- [149] Rodriguez, R. A.; Pan, C.-m.; Yabe, Y.; Kawamata, Y.; Eastgate, M. D.; Baran, P. S. *J. Am. Chem. Soc.* **2014**, *136*, 6908–6911.
- [150] Samanta, R. C.; Yamamoto, H. *Eur. J. Org. Chem.* **2015**, *21*, 11976–11979.
- [151] Maddox, S. M.; Nalbandian, C. J.; Smith, D. E.; Gustafson, J. L. *Org. Lett.* **2015**, *17*, 1042–1045.

- [152] Atlas, S. A. *J. Manag. Care Pharm.* **2007**, *13*, 9–20.
- [153] Tomaschitz, A.; Pilz, S.; Ritz, E.; Obermayer-Pietsch, B.; Pieber, T. R. *Nat. Rev. Endocrinol.* **2010**, *6*, 83–93.
- [154] Mattsson, C.; Young, W. F. *Nat. Clin. Pract. Nephrol.* **2006**, *2*, 198–208.
- [155] Monticone, S.; Burrello, J.; Tizzani, D.; Bertello, C.; Viola, A.; Buffolo, F.; Gabetti, L.; Mengozzi, G.; Williams, T. A.; Rabbia, F.; Veglio, F.; Mulatero, P. *J. Am. Coll. Cardiol.* **2017**, *69*, 1811–1820.
- [156] White, P. C. *Mol. Cell. Endocrinol.* **2004**, *217*, 81–87.
- [157] Strushkevich, N.; Gilep, A. A.; Shen, L.; Arrowsmith, C. H.; Edwards, A. M.; Usanov, S. A.; Park, H.-W. *Mol. Endocrinol.* **2013**, *27*, 315–324.
- [158] Zhang, G.-x.; Wang, B.-j.; Ouyang, J.-z.; Deng, X.-y.; Ma, X.; Li, H.-z.; Wu, Z.; Liu, S.-l.; Xu, H.; Zhang, X. *Hypertens. Res.* **2010**, *33*, 478–84.
- [159] Shojaati, K.; Causevic, M.; Kadereit, B.; Dick, B.; Imobersteg, J.; Schneider, H.; Beinder, E.; Kashiwagi, M.; Frey, B. M.; Frey, F. J.; Mohaupt, M. G. *Kidney Int.* **2004**, *66*, 2322–2328.
- [160] Hahner, S.; Stuermer, A.; Kreissl, M.; Reiners, C.; Fassnacht, M.; Haen-scheid, H.; Beuschlein, F.; Zink, M.; Lang, K.; Allolio, B.; Schirbel, A. *J. Clin. Endocrinol. Metab.* **2008**, *93*, 2358–2365.
- [161] Meredith, E. L. *et al. ACS Med. Chem. Lett.* **2013**, *4*, 1203–1207.
- [162] Roumen, L.; Peeters, J. W.; Emmen, J. M. A.; Beugels, I. P. E.; Custers, E. M. G.; de Gooyer, M.; Plate, R.; Pieterse, K.; Hilbers, P. A. J.; Smits, J. F. M.; Vekemans, J. A. J.; Leysen, D.; Ottenheijm, H. C. J.; Janssen, H. M.; Hermans, J. J. R. *J. Med. Chem.* **2010**, *53*, 1712–25.
- [163] Powlson, A. S.; Gurnell, M.; Brown, M. J. *Curr. Opin. Endocrinol. Diabetes Obes.* **2015**, *22*, 150–156.
- [164] Daunt, N. *RadioGraphics* **2005**, *25*, S143–S158.

- [165] Bergström, M.; Juhlin, C.; Bonasera, T. A.; Sundin, A.; Rastad, J.; Åkerström, G.; Långström, B. *J. Nucl. Med.* **2000**, *41*, 275–282.
- [166] Minn, H.; Salonen, A.; Friberg, J.; Roivainen, A.; Viljanen, T.; Långsjö, J.; Salmi, J.; Välimäki, M.; Nägren, K.; Nuutila, P. *J. Nucl. Med.* **2004**, *45*, 972–9.
- [167] Wadsak, W.; Mitterhauser, M. *J. Label. Compd. Radiopharm.* **2003**, *46*, 379–388.
- [168] Ettliger, D. E.; Wadsak, W.; Mien, L.-K.; Machek, M.; Wabnegger, L.; Rendl, G.; Karanikas, G.; Viernstein, H.; Kletter, K.; Dudczak, R.; Mitterhauser, M. *Eur. J. Nucl. Med. Mol. Imaging* **2006**, *33*, 928–931.
- [169] Erlandsson, M.; Karimi, F.; Lindhe, Ö.; Långström, B. *Nucl. Med. Biol.* **2009**, *36*, 435–445.
- [170] Hu, Q.; Yin, L.; Hartmann, R. W. *J. Med. Chem.* **2014**, *57*, 5011–5022.
- [171] Schumacher, C. D.; Steele, R. E.; Brunner, H. R. *J. Hypertens.* **2013**, *31*, 2085–2093.
- [172] Hansch, C.; Leo, A.; Taft, R. W. *Chem. Rev.* **1991**, *91*, 165–195.
- [173] Swain, C. G.; Kaiser, L. E. *J. Am. Chem. Soc.* **1958**, *80*, 4089–4092.
- [174] Muller, T.; Vaccher, C.; Vaccher, M.-p.; Flouquet, N. *Synth. Commun.* **1998**, *28*, 2343–2354.
- [175] Hoyt, S. B. *et al. ACS Med. Chem. Lett.* **2015**, *6*, 573–578.